

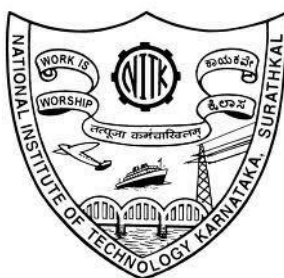
DESIGN, SYNTHESIS AND
INVESTIGATION ON OPTOELECTRONIC
PROPERTIES OF THIOPHENE BASED
HETEROCYCLES

Thesis

Submitted in partial fulfilment of the requirements for the degree of
DOCTOR OF PHILOSOPHY

by

VIPRABHA K



DEPARTMENT OF CHEMISTRY
NATIONAL INSTITUTE OF TECHNOLOGY KARNATAKA,
SURATHKAL, MANGALURU – 575025

August, 2020

DECLARATION

by the Ph.D. Research Scholar

I hereby declare that the Research Thesis entitled “**Design, synthesis and investigation on optoelectronic properties of thiophene based heterocycles**” which is being submitted to the National Institute of Technology Karnataka, Surathkal in partial fulfilment of the requirements for the award of the Degree of Doctor of Philosophy in Chemistry is a *bonafide report of the research work carried out by me*. The material contained in this Research Thesis has not been submitted to any University or Institution for the award of any degree.

Viprabha K

Register No. 155056CY15F07

Department of Chemistry

Place: NITK-Surathkal

Date:

CERTIFICATE

This is to *certify* that the Research Thesis entitled “**Design, synthesis and investigation on optoelectronic properties of thiophene based heterocycles**” submitted by Ms. Viprabha K (Register No: 155056CY15F07) as the record of the research work carried out by her, is *accepted as the Research Thesis submission* in partial fulfilment of the requirements for the award of degree of Doctor of Philosophy.

Dr. Udaya Kumar Dalimba

Research Guide

Date:

Chairman – DRPC

Date:

No language can express the power, beauty, heroism, and majesty of a mother's love. It shrinks not where man cowers, and grows stronger where man faints, and over the wastes of worldly fortunes sends the radiance of its quenchless fidelity like a star in heaven.

---Edwin Hubbell Chapin

This thesis is dedicated to my beloved mother

ACKNOWLEDGEMENT

I owe my deepest gratitude to the Almighty for giving me the strength and patience to work throughout these years.

I acknowledge the people who are the pillars of my life, my parents, for instilling in me the virtues of perseverance and commitment and relentlessly encouraging me to strive for excellence.

I owe a debt of gratitude to my research supervisor, Dr. Udaya Kumar D., Associate Professor, Department of Chemistry, NITK, Surathkal, for giving me an opportunity to pursue my research work under his valuable guidance, from whom I have learnt how to be humble and patient.

I express my thanks to NITK Surathkal, for providing the research fellowship and the laboratory facilities for my research work.

My sincere gratitude to the RPAC members, Prof. B. Ramachandra Bhat, Department of Chemistry and Dr. H.S. Nagaraja, Department of Physics for their timely assessment and providing thoughtful suggestions during the progress of my work.

I thank the present Head of the Department, Prof. Arun M. Isloor, and former Head of the Department Prof. D. Krishna Bhat for providing the laboratory facilities. I am also thankful to Prof. A. Nithyananda Shetty, Prof. A. V. Adhikari, Prof. A. Chitharanjan Hegde, Prof. B. Ramchandra Bhat, Dr., Darshak R. Trivedi, Dr. Sib Sankar Mal, Dr. Saikat Dutta and Dr. Debasree Chakraborty for their encouragement and moral support. My special thanks to Dr. P.B. Beneesh for the fruitful discussions and valuable suggestions.

My heartfelt thanks to Prof. Keloth Chandrasekharan, NIT Calicut, for providing facility for NLO studies and for his valuable suggestions. I also thank Mr. Nikhil P P, for his assistance in carrying out Z-scan studies, without them the present work would not have been possible.

My special thanks to Prof. Narayanan Unni, NIIST Trivandrum, for providing facility for OLED fabrication. I also thank Mr. Vibhu Darshan for his help during the device fabrication.

I am very much thankful to Dr. Oruganti Srinivas and Mrs. Abhilasha from Dr. Reddy's Institute of Life Sciences for providing the analytical support.

I sincerely thank my former lab members, Dr. Murali M.G., Dr. Nikhila Ghokale, Dr. Nagabhushana and Dr. Ramprasad J., for their active co-operation and for rebuilding my confidence at each and every stage of my research work. A special thanks to my research colleague Dr. Rajkumar Reddyrajula for constant help, support and all the fun we had in the last four years.

The saying “A real friend is the one who walks in when the rest of the world walks out” holds true and it’s my fortune to gratefully acknowledge the support of my friends, Susheela, Akshatha R Shetty and Aranganathan for their support and generous care throughout the research tenure. They were always beside me during the happy and hard moments to push me and motivate me, without whom the learning curve would have been very much steeper.

I extend my sincere thanks to my close friends Praveen Mishra, Harsha, Meenaketan and Dilip with whom I have shared moments of deep anxiety but also of big excitement. Special thanks are extended to Mr. Makesh Mohan for DFT studies and Mrs. Srikala Makesh for motivating me. I extend my deep sense of gratitude to my junior, Mr. Sathish C.G. for inspiring me to think new ideas and giving me all positive vibes.

It will not be complete without mentioning my gratitude to the non-teaching staff members of Chemistry Department Mrs. Shamila Nandini, Ms. Vikitha, Mrs. Rashmi, Mr. Prashanth, Mr. Pradeep, Mr. Harish, Mrs. Sharmila, Mrs. Deepa, Mr. Santhosh, Mr. Gopal and Mr. Vaman Shetty for their timely help during my research.

Last, but not the least, a very special word of thanks goes for my sisters who have nurtured my education, my brother in laws, my niece and nephew whom I thank for putting up with my idiosyncrasies and for providing such a rich source of conversation, education and entertainment. Finally, with all respect, I would like to acknowledge my grandmother for showering infinite love and wisdom and teaching me the value of life.

This thesis would not have been possible without the inspiration and support of a number of wonderful individuals — my thanks and appreciation to all of them who are scattered around the country for being part of this journey and making this possible.

VIPRABHA K

ABSTRACT

The use of π -conjugated semiconducting materials in flexible and large-area optoelectronic devices is proliferated worldwide owing to the easy structural modifications and solution processability possible, leading to the change in optoelectronic properties. Most of the applications such as flexible displays and solid-state lighting sources based on organic light-emitting diodes (OLEDs) and nonlinear optical (NLO) devices are still in the developing stage due to the lack of ideal materials that exhibit the processability and an ability to interface with other materials. The research is continuing as ever to develop and characterize materials with large and fast optical responses which can satisfy different technological necessities. Furthermore, a definite correlation between the linear/nonlinear optical mechanism and the contribution of structure and nature of some thiophene based heterocycle is yet to be clearly interpreted.

In this context, the present research work is focused on the design and synthesis of new class of thiophene based donor-acceptor (D-A) heterocycles for optoelectronic applications. A total of eighteen D-A type organic compounds were designed with various design strategies. They were successfully synthesized following appropriate synthetic protocols and characterized using different spectral analyses. The structure-property relationships of the synthesized compounds were established by the optical absorption (UV-Vis), electrochemical (CV) and theoretical (DFT) studies. The third order NLO property i.e., the "effective two-photon absorption" of the compounds was confirmed by single-beam Z-scan analysis. The compounds **VK3**, **VK8**, **VK10**, **VK12**, **VK13**, **VK14**, **VK15** and **VK17** exhibit high nonlinear absorption coefficient (β_{eff}) and a strong optical limiting behaviour. The preliminary studies on the electroluminescent properties of **VK15** show that the molecule **VK15** emits green light with low threshold voltage.

Keywords: Thiophene; Imidazo [2,1-*b*][1,3,4] thiadiazole; Pyridine; HOMO-LUMO energy; Density functional calculations; Z-scan; Nonlinear optics; OLED; Structure-property relationship.

CONTENTS

CHAPTER 1 – INTRODUCTION

1.1 INTRODUCTION TO π -CONJUGATED SYSTEMS	1
1.1.1 π -conjugated polymers	3
1.1.2 π -conjugated small molecules	4
1.2 CONDUCTION IN CONJUGATED SYSTEM.....	4
1.3 DONOR-ACCEPTOR (D-A) π -CONJUGATED SMALL MOLECULES	5
1.4 BAND GAP ENGINEERING OF π -CONJUGATED SYSTEM.....	7
1.5 NONLINEAR OPTICS	9
1.5.1 Theoretical formulation	10
1.5.2 Second order nonlinearity	11
1.5.3 Third order nonlinearity	11
1.5.3.1 Nonlinear absorption (NLA).....	11
1.5.3.2 Nonlinear refraction (NLR)	15
1.5.4 Optical limiting (OL)	15
1.5.5 Nonlinear optical analysis.....	17
1.5.5.1 Z-scan.....	17
1.5.6 Conjugated materials for NLO.....	17
1.6 ORGANIC LIGHT EMITTING DIODES (OLEDs)	18
1.6.1 Fundamentals of OLEDs.....	18
1.6.1.1 Basic device physics: Architecture and working principle.....	18
1.6.1.2 Important device parameters.....	20
1.7 LITERATURE REVIEW	22
1.7.1 Salient features of the literature review	35
1.8 SCOPE AND OBJECTIVES	36
1.9 MOLECULAR DESIGN OF NEW D-A TYPE CONJUGATED MATERIALS	38

1.10 THESIS FRAMEWORK	44
CHAPTER 2 – EXPERIMENTAL SECTION	
2.1 EXPERIMENTAL	45
2.1.1 Materials and methods	45
2.1.2 Synthesis of molecules (VK1–VK3) of series–1.....	46
2.1.2.1 Synthesis	46
2.1.2.2 The detailed experimental procedure.....	47
2.1.3 Synthesis of molecules (VK4–VK6) of series–2.....	50
2.1.3.1 Synthesis	50
2.1.3.2 The detailed experimental procedure.....	51
2.1.4 Synthesis of oligomers (VK7–VK10) of series–3.....	53
2.1.4.1 Synthesis	53
2.1.4.2 The detailed experimental procedure.....	56
2.1.5 Synthesis of compounds (VK11–VK14) of series–4	62
2.1.5.1 Synthesis	62
2.1.5.2 The detailed experimental procedure.....	64
2.1.6 Synthesis of molecules (VK15–VK18) of series–5.....	67
2.1.6.1 Synthesis	67
2.1.6.2 The detailed experimental procedure.....	70
2.2 CHARACTERIZATION DETAILS	75
2.2.1 NMR spectroscopy.....	75
2.2.2 Mass spectrometry	76
2.2.3 Elemental analysis	76
2.2.4 Photophysical studies.....	76
2.2.4.1 UV-Vis spectroscopy	77
2.2.4.2 Fluorescence spectroscopy.....	77

2.2.5 Electrochemical studies	78
2.2.5.1 Materials, methods and instrumentation	78
2.2.5.2 Equations used for calculating the HOMO/LUMO energies.....	79
2.2.6 Theoretical calculations	79
2.2.6.1 Simulations	80
2.2.7 Thermal analysis	80
2.2.8 Z–scan analysis	80
2.2.8.1 Z–scan experimental set up.....	81
2.2.8.2 Equations used for the theoretical fitting of the experimental results	82
CHAPTER 3 – RESULTS AND DISCUSSION	
3.1 EFFECTS OF SUBSTITUENTS ON THE ENRICHMENT OF THE OPTICAL LIMITING ACTION OF NOVEL IMIDAZO[2,1- <i>b</i>][1,3,4]THIADIAZOLE FUSED THIOPHENE BASED SMALL MOLECULES (VK1–VK3).....	85
3.1.1 Structural elucidation of intermediates and final compounds.....	86
3.1.2 Photophysical studies.....	92
3.1.3 Electrochemical studies	93
3.1.4 Theoretical studies	94
3.1.5 Thermal properties	97
3.1.6 Third–order NLO properties	98
3.1.6.1 Nonlinear absorption studies.....	98
3.1.6.2 Optical limiting studies	99
3.1.6.3 Nonlinear refraction studies	100
3.1.7 The important findings from the experimental data	101
3.2 AN INVESTIGATION ON PHOTOPHYSICAL AND THIRD–ORDER NONLINEAR OPTICAL PROPERTIES OF NOVEL THERMALLY–STABLE THIOPHENE–IMIDAZO [2,1- <i>b</i>][1,3,4] THIADIAZOLE BASED AZOMETHINES (VK4–VK6).....	102

3.2.1 Structural elucidation of the intermediates and final compounds.....	102
3.2.2 Photophysical studies.....	108
3.2.3 Electrochemical studies	109
3.2.4 Theoretical studies	111
3.2.5 Thermal properties	112
3.2.6 Third-order NLO properties	113
3.2.6.1 Nonlinear absorption studies.....	113
3.2.6.2 Optical limiting studies	113
3.2.6.3 Nonlinear refraction studies.....	114
3.2.7 The important findings from the experimental data	116
3.3 IMPACT OF DONOR-ACCEPTOR ALTERNATION ON OPTICAL POWER LIMITING BEHAVIOR OF H-SHAPED THIOPHENE-IMIDAZO[2,1- <i>b</i>][1,3,4]THIADIAZOLE FLANKED CONJUGATED OLIGOMERS (VK7-VK10)	117
3.3.1 Structural elucidation of the intermediates and final compounds.....	117
3.3.2 Photophysical studies.....	129
3.3.3 Electrochemical studies	130
3.3.4 Theoretical studies	131
3.3.5 Thermal properties	134
3.3.6 Third-order NLO properties	134
3.3.6.1 Nonlinear absorption studies.....	134
3.3.6.2 Optical limiting studies	136
3.3.6.3 Nonlinear refraction studies.....	137
3.3.7 The important findings from the experimental data	140
3.4 EXPLORATION OF EXCITED STATE ASSISTED TWO-PHOTON ABSORPTION PROPERTY OF D-A-D TYPE THIOPHENE-PYRIDINE DERIVATIVES (VK11-VK14)	141

3.4.1 Structural elucidation of the intermediates and final compounds.....	141
3.4.2 Photophysical studies.....	152
3.4.3 Electrochemical studies	154
3.4.4 Theoretical studies	155
3.4.5 Thermal properties	159
3.4.6 Third order NLO properties	160
3.4.6.1 Nonlinear absorption studies.....	160
3.4.6.2 Optical limiting studies	161
3.4.7 The important findings from the experimental data	164
3.5 BUTTERFLY-SHAPED THIOPHENE-PYRIDINE HYBRIDS (VK15–VK18): GREEN ELECTROLUMINESCENCE AND LARGE THIRD-ORDER OPTICAL NONLINEARITIES	165
3.5.1 Structural elucidation of the intermediates and final compounds.....	165
3.5.2 Photophysical studies.....	172
3.5.3 Electrochemical studies	175
3.5.4 Theoretical studies	177
3.5.5 Thermal properties	180
3.5.6 Third–order NLO properties	181
3.5.6.1 Nonlinear absorption studies.....	181
3.5.6.2 Optical limiting studies	183
3.5.6.3 Nonlinear refraction studies	184
3.5.7 Electroluminescence properties	187
3.5.8 The important findings from the experimental data	189
CHAPTER 4 – SUMMARY AND CONCLUSIONS	
4.1 SUMMARY	191
4.2 CONCLUSIONS.....	192

4.3 SCOPE FOR FURTHER WORK.....	193
APPENDIX 1.....	195
REFERENCES.....	205
LIST OF PUBLICATIONS	223
CONFERENCES ATTENDED	224
BIODATA.....	225

NOMENCLATURE

LIST OF ABBREVIATIONS

^{13}C NMR	Carbon 13 nuclear magnetic resonance
^1H NMR	Proton nuclear magnetic resonance
7CB	4'-Heptyl-4-biphenylcarbonitrile
AIBN	Azobisisobutyronitrile
Alq3	Tris-(8-hydroxyquinoline)aluminum
B3LYP	Becke's three-parameter hybrid functional with Lee-Yang-Parr's gradient-corrected correlation functional
BLA	Bond length alternation
c.d.	Current density
$\text{C}_2\text{H}_5\text{OH}$	Ethanol
CA	Closed aperture
CH_3CN	Acetonitrile
CH_3OH	Methanol
CHCl_3	Chloroform
CPs	Conducting polymers
CV	Cyclic voltammetry
D-A	Donor-acceptor
DCM	Dichloromethane
DFG	Difference frequency generation
DFT	Density functional theory
dI/dz	Nonlinear propagation
DMF	N,N-dimethylformamide
$\text{DMSO-}d_6$	Deuterated dimethyl sulfoxide
DSC	Differential scanning calorimetry
EBL	Electron blocking layer
EDOT	3,4-ethylenedioxythiophene

E _g	Optical band gap
EIL	Electron injecting layer
EL	Electroluminescence
EML	Emissive layer
EQE	External Quantum Efficiency
ESA	Excited-state absorption
ESI-MS	Electrospray ionization-mass
ETL	Electron transporting layer
FIrpic	Bis[2-(4,6-difluorophenyl)pyridinato C2,N](picolinato)iridium(III)
FWHM	Full width half maximum
HBL	Hole blocking layer
HCl	Hydrochloric acid
HIL	Hole injecting layer
HOMO	Highest occupied molecular orbital
HTL	Hole transporting layer
HTMs	Hole-transporting materials
ICPs	Intrinsically conducting polymers
ICT	Intramolecular charge transfer
IEFPCM	Integral equation formalism variant
im $\chi^{(3)}$	Imaginary part of third order nonlinear susceptibility
IQE	Internal quantum efficiency
ITD	Imidazo[2,1- <i>b</i>][1,3,4]thiadiazole
ITO	Indium tin oxide
J-V-L	Current density-voltage-luminance
K ₂ CO ₃	Potassium carbonate
LiF	Lithium fluoride
LT	Limiting threshold
LUMO	Lowest unoccupied molecular orbital

MALDI TOF–MS	Matrix-assisted laser desorption/ionization-time of flight–mass
MOT	Molecular orbital theory
Na ₂ CO ₃	Sodium carbonate
Na ₂ SO ₄	Sodium sulphate
NaBH ₄	Sodium borohydride
NaH	Sodium hydride
NaOC ₂ H ₅	Sodium ethoxide
NaOH	Sodium hydroxide
NBS	N-bromosuccinimide
NH ₄ Cl	Ammonium chloride
NLA	Nonlinear absorption
NLO	Nonlinear optics
NLR	Nonlinear refraction
NLS	Nonlinear scattering
NMP	N–methyl–2–pyrrolidone
NMR	Nuclear magnetic resonance
NPB	N,N'-bis(naphthalen-1-yl)-N,N'-bis(phenyl)benzidine
OA	Open aperture
OFET	Organic field effect transistor
OL	Optical limiting
OLED	Organic light emitting diode
OPV	Organic photovoltaic
PCM	Polarizable continuum model
pet ether	Petroleum ether
PHOLED	Phosphorescent OLED
POCl ₃	Phosphorous oxychloride
PPh ₃ HBr	Triphenylphosphine hydrobromide
PTZ	Phenothiazine
QD	Quantum dot

Φ_F	Quantum yield
RB	Round bottomed
RGB	Red-green-blue
RISC	Reverse inter system crossing
RSA	Reverse saturable absorption
RT	Room temperature
SA	Saturable absorption
SCE	Saturated calomel electrode
SCF	Self-consistent field
SFG	Sum frequency generation
SHG	Second harmonic generation
SOCl ₂	Thionyl chloride
$T(z)$	Normalized transmittance
TADF	Thermally activated delayed fluorescence
TBAPC	Tetrabutylammonium perchlorate
T _d	Decomposition temperature
TD-DFT	Time-dependent density functional theory
T _g	Glass transition temperature
TGA	Thermogravimetric analysis
THG	Third harmonic generation
Th-ITD	Thiophene- imidazo[2,1- <i>b</i>][1,3,4]thiadiazole
TLC	Thin layer chromatography
TMS	Tetramethyl silane
TPA	Two photon absorption
TPBi	2,2',2''-(1,3,5-Benzinetriyl)-tris(1-phenyl-1-H-benzimidazole
tztz	Thiazolo[5,4- <i>d</i>]thiazole
UV-Vis	Ultraviolet-visible
$\alpha(I)$	Linear absorption coefficient
β_{eff}	Effective TPA coefficient

η_{CE}	Current efficiency
η_{EQE}	External quantum efficiency
η_{LE}	Luminous efficiency
η_{PE}	Power efficiency
η_{Pmax}	Maximum power efficiency
λ_{max}	Maximum absorption wavelength
$\chi^{(2)}$	Second-order nonlinear optical susceptibility
$\chi^{(3)}$	Third-order nonlinear optical susceptibility

SYMBOLS AND UNIT

%	Percent
>	Greater than
\geq	Greater than or equal to
°C	Degree Celsius
Ag	Silver
Al	Aluminium
Au	Gold
Ca	Calcium
g	Gram
h	Hours
Hz	Hertz
M	Molar
m/z	Mass to charge ratio
MHz	Megahertz
min	Minutes
mL	Millilitre
mmol	Millimole
ppm	Parts per million
sec	Seconds

δ	Delta
η	Eta
θ	Theta

CHAPTER 1

INTRODUCTION

1.1 INTRODUCTION TO π -CONJUGATED SYSTEMS

The commencement of research work in conducting polymers (CPs) or, more precisely, intrinsically conducting polymers (ICPs) roots back to the 1960s, when Pohl, Katon, and their co-workers synthesized and characterized the semiconducting polymers for the first time. The discovery of highly conducting polysulfurnitride (SN)_x was a dynamic step towards CPs as they are known today (Stenger-Smith 1998). However, the remarkable breakthrough in the entire field of π -conjugated organic materials was commenced nearly 40 years back when the ground-breaking discovery of profound increase in the electrical conductivity in polyacetylene was achieved upon I₂ vapor doping by Alan Heeger, Alan MacDiarmid, and Hideki Shirakawa in 1977 (Chiang et al. 1977, Shirakawa et al. 1977). In 2000, the work was further reinforced with awarding the Nobel Prize in chemistry to these pioneers “*for the discovery and development of electrically conductive polymers*”. As a result, a variety of π -conjugated materials (polymers, oligomers or small molecules) based on aromatic precursors such as p-phenylenevinylene, thiophene, triphenylamine, carbazole, fluorene and their derivatives (Junkers et al. 2012; McCullough 1998; Roncali 1992; Sahin et al. 2011; Skotheim et al. 2007) have been developed (**Figure 1.1**) and their photophysical and electrochemical properties have also been intensively studied in the subsequent years. Moreover, the semiconducting/ metallic conducting properties, a broad range of optical absorption, charge mobility and charge storage properties of these conjugated materials enabled the practical usage of these systems in the field of organic electronics and photonics, such as organic photovoltaics (OPVs) (Brabec et al. 2001), OLEDs (Kraft et al. 1993), nonlinear optics (Prasad and Williams 1991), sensors (McQuade et al. 2000), thin film transistors (Halls et al. 1995), electrochromic devices (Invernale et al. 2009), and they are also used as electrical transporters or battery electrodes (Liang et al. 2012).

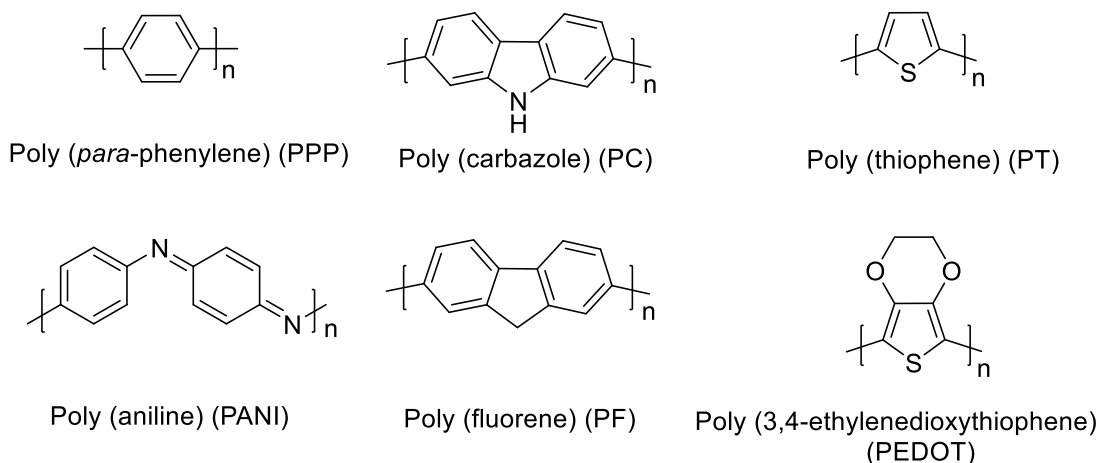


Figure 1.1 Some important conjugated polymers.

Conjugated materials (polymers/molecules) are organic materials consisting of alternate single and double bonds along the molecular chain, comprised mainly of carbon, hydrogen and heteroatoms such as oxygen, nitrogen and sulfur (**Figure 1.1**). The overlap of π -orbitals in such systems leads to the extended and delocalized conjugation which originates conductivity in the system. These conjugated materials possessing the optical, electronic, magnetic and electrical properties of a metal, have been fascinating numerous researchers all over the world due to their practical application in modern technology. These metallic characteristics of CPs turn them into the category of so-called '*synthetic metals*'.

Moreover, the low cost of synthesis, tunability and mechanical flexibility of π -conjugated organic materials establishes considerable interest when compared to the traditional inorganic-based electronic materials such as silicon (Kelley et al. 2004). Unlike the synthesis of inorganic materials, which usually involves high temperatures ($T \geq 500^\circ\text{C}$) (Pell et al. 2004), the conjugated materials can be easily synthesized through robust organic reactions such as condensation reactions, green synthesis, one-pot multicomponent reactions, Palladium-catalysed cross-coupling reactions and so on (Cheng et al. 2009; Demeter et al. 2014), which are cost-effective. The inorganic-based materials are mostly brittle and hard, while the conjugated materials, on the other hand, are mechanically flexible in nature, and the modern organic synthetic methods allow facile functionalization of the conjugated system which can readily tune their photophysical and electronic properties, making the conjugated materials a mainstay of our technological existence (Forrest 2004; Gibson et al. 2012).

1.1.1 π -conjugated polymers

In this system the π -orbitals are extended throughout the entire conjugated backbone in the polymer chain which enable sufficient optical absorption in the ultraviolet-visible (UV-Vis) region and facilitate the intramolecular charge-transfer (ICT) (Farchioni and Grosso 2013; Nalwa 1997). These polymers are often functionalized with solubilizing agents, namely, hydrocarbon chains that not only improve the solution processability but also enhances the intermolecular interaction in the solid state (Allard et al. 2008).

The performance of polymer-based materials depends on the molecular weight and distribution of molecular weight, which is called the dispersity (D). The high molecular weight polymers have longer conjugation which broadens the absorption and enhances the charge transporting ability. Moreover, polymers with lower D value have fewer surface defects and smooth morphologies, which is desirable for high efficacy devices (Facchetti 2011). The inherent drawback of conjugated polymer systems is their low solubility in common organic solvents, low crystallinity and the sample purity that lead to the improper charge transport which ultimately diminishes the materials performance (Martin and Diederich 1999). However, high viscosity of the conjugated polymers yields good quality thin-films with uniform and smooth surface, which improves the device performance (Facchetti 2011).

A number of π -conjugated polymers have been designed and synthesized from electron rich systems like poly(3-hexylthiophene) (P3HT), electron deficient systems such as poly(benzobisimidazobenzophenanthroline) (PBBL) as well as donor (D)-acceptor (A) type polymers like poly(N,N'-dialkylperylene-dicarboximide-dithiophene) (PDIR-T2). Some of them are shown in **Figure 1.2**.

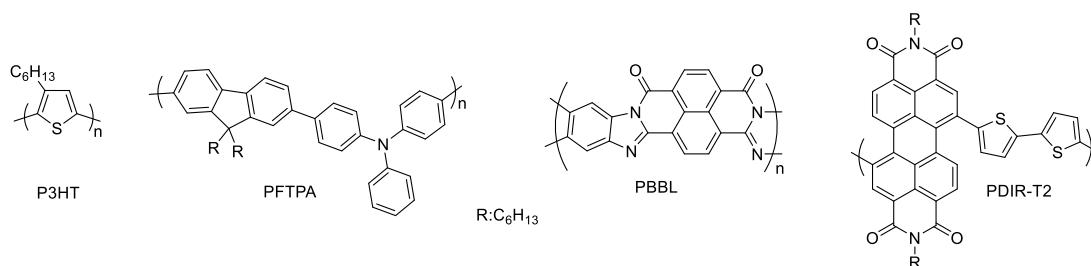


Figure 1.2 Chemical structures of P3HT, PFTPA, PBBL and PDIR-T2.

1.1.2 π -conjugated small molecules

The organic π -conjugated small molecules also have greatly been extended in the optoelectronic field since couple of decades. A wide chemical functionality and simple modifications in synthetic route can tune optical, morphological, electrical and electrochemical properties. Also, proper selection of alkyl groups improves the solubility of the system (Mishra and Bauerle 2012). The purification of organic materials is very essential since the impurities develop charge-carrier traps, which reduces the performance of the device. Small molecule organic materials can be purified by traditional crystallization technique or column chromatography, that are not applicable to purify high molecular weight polymers. Further, high crystallinity can be achieved in small molecule materials by simple solution-grown crystallization and vacuum deposition techniques which facilitates the intermolecular charge-transport efficiently, and hence, enhances the performance of electronic materials. The small molecules have similar design principle as that of polymers where electron deficient, electron rich and D-A moieties play crucial role to fine tune their optoelectronic properties. There are numerous reports on π -conjugated small molecules in the literature, some of them are shown in **Figure 1.3**.

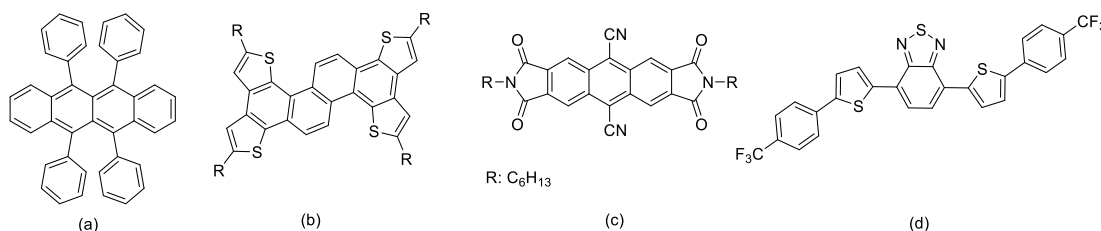


Figure 1.3 Molecular structures of (a) Rubrene, (b) electron-rich, (c) electron-deficient and (d) D-A π -conjugated small molecules.

1.2 CONDUCTION IN CONJUGATED SYSTEM

The molecular orbital theory (MOT) becomes more prominent in the case of molecules where two or more π -bonds interact with one another. The π -molecular orbitals are used to describe the energies and locations of π -electrons in conjugated systems. The π -molecular orbitals usually include the frontier molecular orbitals, which are the highest occupied molecular orbital (HOMO), corresponding to fully occupied π -band and the lowest unoccupied molecular orbital (LUMO), corresponding to empty π^* -band. The HOMO and the LUMO energy levels analogous to the

conduction band and the valence band of inorganic semiconductors. The difference in the energy levels between the HOMO and the LUMO is called the band gap (E_g) (**Figure 1.4**). The mechanism of conduction is explained by band theory, according to which the half-filled valence band forms a continuous delocalized π -system, is responsible for the conductivity in the material. In the case of conjugated polymers, the conductivity could be enhanced by the process called *doping*, which involves either oxidation (removal of electrons) or reduction (addition of electrons) of polymeric system. The mechanism of conductivity in these polymers is based on the movement of charged defects within the conjugated framework. These charge carries/defects, either positive (p-type) or negative (n-type), are the products of oxidation or reduction of the polymer, respectively.

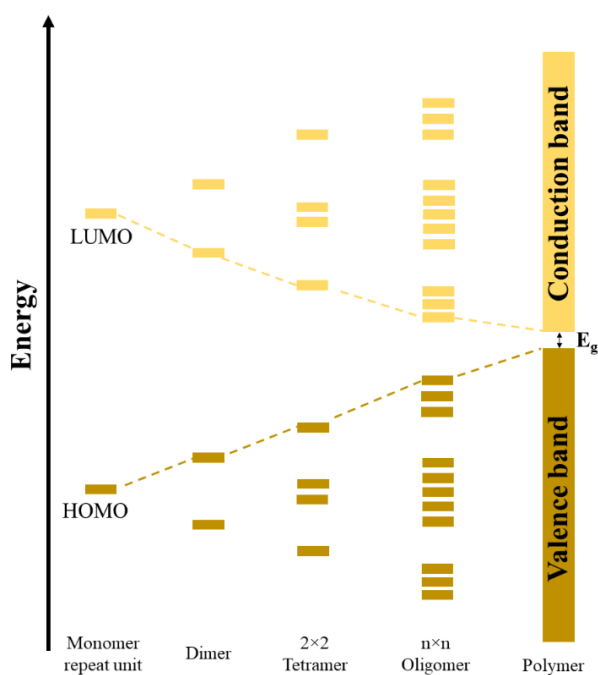


Figure 1.4 Schematic of band formation from molecular repeat unit to π -conjugated polymer.

1.3 DONOR-ACCEPTOR (D-A) π -CONJUGATED SMALL MOLECULES

The ease of synthesis, structural diversity, tunability and fascinating optoelectronic properties of carbon and heteroatom based conjugated materials have attracted particular interest in the field of material science. However, for achieving high performing devices, the conjugated materials should possess certain physical and chemical properties such as broader solar absorption, low band gap, efficient

photoinduced charge transfer and separation, low oxidation potential and ambipolar charge transport with high mobilities (Nielsen et al. 2013). Therefore, in order to attain desired requirements, modification in the HOMO and the LUMO energy levels is of great importance.

The D–A approach, wherein the electron rich/donor (D) and the electron deficient/acceptor (A) substituents are arranged alternatively along the conjugated backbone, has attracted intense attention in the past couple of decades (Havinga et al. 1993). When compared to the conjugated materials consisting of all the donor units, D–A conjugated materials with the alternate D and A units absorb solar energy at longer wavelengths. The interaction between a strong electron-donor and a strong electron-acceptor gives rise to an increased double bond character between these units, since they can accommodate the charges that are associated with such a mesomerism ($DA \leftrightarrow D^+A^-$). As a result, a significant enhancement of ICT could be seen in such D–A systems which extends the conjugation length, leading to a prolonged absorption and a higher absorption coefficient. If the energy of the HOMO level of D and the LUMO level of A moiety is relatively close, there exists a strong intramolecular orbital mixing between the D and A units, which considerably lowers the LUMO level and raises the HOMO level, resulting a low energy gap (Balan et al. 2008; Zotti et al. 1999) as depicted in **Figure 1.5**. Hence, in a conjugated molecule with an alternating sequence of appropriate D and A units, the hybridization of energy levels of the D and the A moieties can induce an unusually low HOMO–LUMO separation, resulting a reduction in its E_g (Brocks and Tol 1996). Due to this feature, the D–A conjugated materials are being spotlighted since couple of decades for their application in many optoelectronic and electronic devices such as OLEDs, OSCs and OFETs.

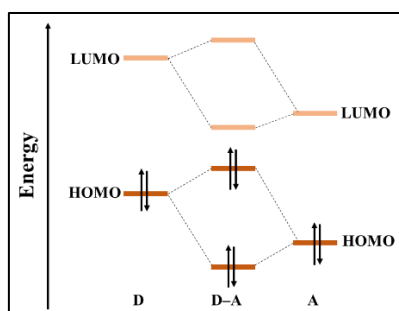


Figure 1.5 Interaction of molecular orbitals of D/A moieties leading to a D–A unit with low HOMO–LUMO separation (H. A.M. Mullekom 2000).

In D–A systems, the introduction of strong electron-donor groups raises the HOMO levels, while the introduction of strong electron-withdrawing groups lowers the LUMO levels, which results in the narrow HOMO–LUMO energy gap (Ajayaghosh 2003). Thus, key design criterion is the selection of proper electron-donor and acceptor units to achieve desired HOMO and LUMO levels beneficial for the development of organic optoelectronic materials. Additionally, the presence of strong electron-donors and acceptors increases the delocalization of π -electrons, making the material highly polarizable which causes remarkable optical nonlinearities in such system. Due to these benefits, they are also considered as potential candidates in the area of nonlinear optics (Albota et al. 1998; Huang et al. 2012).

Although, the D–A conjugated materials have developed rapidly and became popular in the couple of decades, they are still the focus of intensive research. There is still a considerable room for the rational design and synthesis of new D–A type materials. For an instance, the most widely used electron donating moieties are thiophene, carbazole, triphenylamine, phenothiazine and fluorene, and the most commonly used electron accepting groups are 1,3,4-oxadiazole, cyanovinylene, perylene diimides, 2,1,3-benzothiadiazole and pyridine, which involve various functionalization and different substitution patterns. These substituents play a vital role in “bandgap engineering” of organic molecules to fine-tune their optoelectronic properties.

1.4 BAND GAP ENGINEERING OF π -CONJUGATED SYSTEM

The control of HOMO–LUMO gap by structural modification is the key factor to design low E_g conjugated materials, which governs the optical, electronic and conducting properties of the conjugated materials. In order to cover the visible and other parts of the spectrum effectively, flexible tuning and precise control of the E_g is necessary. The E_g of conjugated aromatic materials is determined by several factors. Some of the factors on which the E_g is dependent on are: bond length alternation (BLA), which contributes by a quantity E_{BLA} to the magnitude of E_g ; resonance effect, due to which the π -electrons confine within the aromatic ring. As a result, their delocalization along the whole conjugated chain is prevented. This effect, thus, contributes by a quantity E_{Res} . Another major factor contributing to E_g is the rotational disorder around interannular single bonds. A mean dihedral angle θ between the consecutive units limits

the delocalization of π -electrons along the conjugated backbone and hence, increases the E_g by a quantity E_θ . The introduction of electron-releasing or electron-accepting substituents is the most direct way to modulate the HOMO and LUMO levels, and hence, their difference, of a conjugated system. This contribution is represented by a term E_{Sub} (Roncali 2007). However, when assembling individual molecules or polymer chains into a material, intermolecular interactions (E_{Int}) also contribute to the magnitude of E_g .

Thus, $E_g = E_{BLA} + E_{Res} + E_{Sub} + E_\theta + E_{Int}$

The individual factors those play an important role in the synthesis of low band gap conjugated system are (Roncali 2007):

Resonance energy: The torsion angle existing due to steric interactions between adjacent phenyl rings and the rotational freedom around single bonds can be suppressed by introducing double bonds between the aromatic rings, which allows the conjugated system to adopt a planar structure. Also, double bonds lead to a decrease of the overall aromaticity of the system which further reduces the gap.

Rigidification of the conjugated system: Covalent rigidification of π -conjugated systems i.e., covalent fastening of elemental units (bithiophene, dithienylethylene, terthiophene or dithienylhexatriene) leads to fully-planar conjugated structures with significantly lower E_g values than the parent open-chain compounds, which is largely from a decrease in the BLA but is limited by the remaining possible inter-ring rotations in the conjugated backbone.

Electron-releasing groups: Introduction of electron-donating groups to a conjugated system produces an increase of the HOMO level, which usually reduces the E_g to a considerable extent. For example, the inductive effect of simple alkyl groups decreases the oxidation potential of the thiophene ring by approximately 0.20 V. On the other hand, linear alkyl chains of sufficient length (typically 6–9 carbons) indirectly contribute to reduce the E_g by enhancing the long-range order in the polymer.

Electron-withdrawing groups: Introduction of acceptor groups such as nitro, carboxy or cyano at the appropriate position in the π -conjugated system induces a large increase in the oxidation potential. This represents the most immediate way to tune the LUMO energy level of a conjugated system.

Increasing the quinoid character: The most direct way to increase the quinoid character of the neutral polyaromatic chain involves the fusion of the aromatic ring of polyaromatic chain with an aromatic system with higher resonance energy (E_{Res}). Since the aromatic sextet tends to localize in the system of highest E_{Res} , it follows that the aromatic ring of polyaromatic chain tends to dearomatize to adopt a quinoid structure. The quinoidal form has higher ground state energy than the aromatic form and in turn, forms a smaller energy band gap. Additionally, the quinoid form enables π -electrons to delocalize more effectively in aromatic rings and increases planarity in the polymer backbone (Son et al. 2011).

Alternating donor-acceptor groups: The basic idea of D-A concept is that conjugated systems involving a regular alternation of D and A groups should lead to a broadening of the valence and conduction bands and thus E_g reduction.

Apart from the intrinsic properties of a single polymer chain, intermolecular interaction between polymer single chains such as π - π stacking in the solid state also contributes to reduce the E_g of conjugated polymers. A closely packed and ordered structure of polymer chains promotes a planar structure in the polymer backbone, facilitating π -electron delocalization and hence, the reduction of E_g .

Since D-A π -conjugated materials possess distinct advantages like lightweight, good film forming property, relatively low manufacturing cost, bio-compatibility, moderate to high conductivity and easy tunability of desired properties, they are broadly used as active components in optoelectronic/ photonic devices such as OPVs, OLEDs, OFETs and NLO. Amongst the various applications reported for D-A π -conjugated materials, their usage in NLO and OLED attained considerable interest in recent years. The following section essentially discusses the theoretical formalisms of the cause and effect relationships that exist in the domain of NLO, the materials exhibiting optical nonlinearity and their device level applications. The section also involves a brief account on construction and working principle of OLEDs and the importance of conjugated materials in OLEDs.

1.5 NONLINEAR OPTICS

The contributions of NLO to the entirety of science and especially to our daily affairs, are praiseworthy. So far almost nine Nobel prizes awarded in physics and

chemistry owe credit to NLO (Garmire 2013). NLO is regarded as the branch of optics which deals with high intensity light-matter interactions and various optical phenomena occurring as a result of such interactions. This field has been at its height since 1961, after the invention of the laser by Theodore Maiman in 1960 (Bloembergen 1984; Maiman 1960) followed by the observation of second harmonic generation (SHG) by Franken and co-workers in quartz, a year later. Later on, NLO contributed in diversifying laser, light-material interaction and information technology. Nonlinear optical phenomena can be observed from the extreme ultra-violet to the deep infrared wavelengths and can even be used to produce terahertz radiation. Various organic and inorganic systems such as polymers, dyes, semiconductors, liquid crystals, nanoparticles, nanocrystals, nanocomposites, gases, plasma, etc., are being investigated for several NLO applications. NLO phenomena such as SHG, third harmonic generation (THG), and sum and difference frequency generation enhanced the range and diversity of lasers (Bloembergen 1984; Garmire 2013). Most of the NLO applications are still in their infancy owing to the lack of ideal materials displaying ease in processability and an ability to interface with other materials. Researchers in NLO are keenly in search of ideal materials with requisite specifications so as to furnish the need of optical industry and research.

1.5.1 Theoretical formulation

Electromagnetic waves interact with materials, mainly through the outer electrons to generate electric dipoles which lead to macroscopic polarization in the matter. For the low intensity electromagnetic radiations, the induced polarization is directly proportional to the applied electric field.

Under normal light, polarization, P can be assumed as:

$$P = \epsilon_0 \chi E \dots \dots \dots 1.1$$

where ϵ_0 is the permittivity of free space, E is the applied electric field and χ is the electric susceptibility of the material.

Under intense light-matter interaction, higher order powers of electric fields also contribute in the above Equation 1.1 (Sutherland 2003) and can be expressed as:

$$P = \epsilon_0 \left(\chi^{(1)} E + \chi^{(2)} EE + \chi^{(3)} EEE + \dots \dots \dots \right) \dots \dots \dots 1.2$$

where $\chi^{(1)}$, $\chi^{(2)}$ and $\chi^{(3)}$ are first-order, second-order and third-order susceptibility tensors. Generally, $\chi^{(n)}$ is n^{th} order susceptibility tensor of rank $n+1$. Each susceptibility tensor leads to different processes, for example, second-order susceptibility tensor governs sum and difference frequency generations, SHG, parametric amplification, etc., while third-order nonlinear susceptibility tensor governs THG, two-photon absorption (TPA), optical Kerr effect, optical phase conjugation, etc (Boyd 2003; Shen 1984; Sutherland 2003).

1.5.2 Second order nonlinearity

The nonlinear optical phenomena associated with second-order nonlinear optical susceptibility ($\chi^{(2)}$) have a variety of applications in laser technologies. $\chi^{(2)}$ lacks in materials, which have a centre of symmetry. The major phenomenon includes SHG, sum and difference frequency generation and parametric amplification. The SHG is the first and foremost demonstrated nonlinear optical phenomenon, where two photons of same frequency combine to form a single photon of double the frequency. For example, a wavelength of 532 nm is produced out of 1064 nm in Nd: YAG laser system using Potassium Dihydrogen Phosphate crystal. SHG has applications in high-resolution optical microscopy. In the process of sum frequency generation (SFG), two photons of frequencies ω_1 and ω_2 combine to form a photon of frequency ω_3 which is the sum of the input frequencies. In difference frequency generation (DFG) the generated frequency is the difference of that of the input waves. Both SFG and DFG are really useful in producing new tunable frequencies at new wavelengths in lasers.

1.5.3 Third order nonlinearity

The third-order nonlinear optical susceptibility ($\chi^{(3)}$) is responsible for various third-order nonlinear optical phenomena. Though $\chi^{(3)}$ is a general phenomenon, it strongly depends on the material property and input intensity. The real part of $\chi^{(3)}$ is directly related to nonlinear refraction (NLR) and the imaginary part is related to nonlinear absorption (NLA). Some of the major phenomena associated to $\chi^{(3)}$ are discussed below.

1.5.3.1 Nonlinear absorption (NLA)

In light-matter interaction, if the intensity of the light is sufficiently strong, NLA may occur. NLA either result in an increase in transmittance (saturable absorption (SA)) or decrease in transmittance (reverse saturable absorption (RSA)) on increasing the

intensity of the input light. Moreover, it could also be possible for a switching behavior from SA to RSA or RSA to SA or a combined effect of both SA and RSA on increasing the intensity. The NLA mechanism is strongly dependent on the nature of the material and the intensity of laser light. Some of the major mechanisms which come under NLA are discussed below:

(i) Saturable absorption (SA)

SA is a NLA mechanism which normally occurs at sufficiently high input intensity where output transmittance increases with increasing intensity. Materials which exhibit intense electronic absorption can act as saturable absorbers. As a result of intense absorption at the excitation wavelength, the ground state population is depleted significantly and finally leads to the saturation of absorption. In SA material, the absorption cross section for ground state (σ_g) is higher than that of the excited state (σ_e) (**Figure 1.6**).

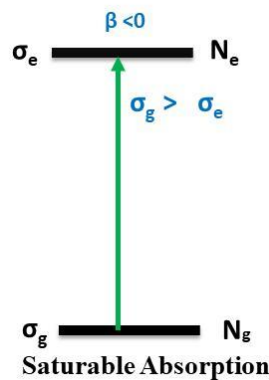


Figure 1.6 Schematic representation of SA in two level system.

Thus, the intensity-dependent linear absorption coefficient ($\alpha(I)$) is given by:

$$\alpha(I) = \alpha_0 \frac{1}{1 + \frac{I}{I_s}} \dots\dots\dots 1.3$$

where $I_s = h\nu/\tau\sigma$, is the saturation intensity, at which $\alpha(I)$ becomes half of α_0 ; α_0 is the ground state linear absorption coefficient.

(ii) Two photon absorption (TPA)

TPA is a NLA mechanism, where two photons from the incident field are absorbed simultaneously by an electron in the ground state (N_g) which later excites to

the next level (N_e) through the virtual state. Schematic representation of energy levels involved in TPA is shown in **Figure 1.7**.

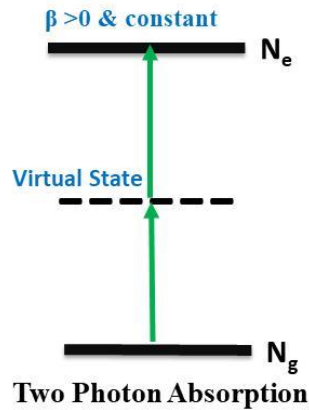


Figure 1.7 Schematic representation of TPA in two level system.

In the case of TPA, the rate of change of beam intensity on propagating through a nonlinear medium is given by:

$$\frac{dI}{dz} = -\alpha_0 I - \beta I^2 \dots\dots\dots 1.4$$

where α_0 is the linear absorption coefficient and β is the TPA coefficient. The unit of β is $m W^{-1}$.

Suppose the linear absorption of the system is negligible, the second term (TPA) in the Equation 1.4 dominates, and Equation 1.4 becomes:

$$\frac{dI}{dz} = -\beta I^2 \dots\dots\dots 1.5$$

Then, the solution becomes:

$$I_z = \frac{I_0}{1 + \beta I_0 z} \dots\dots\dots 1.6$$

where I_0 is the incident intensity.

(iii) Reverse saturable absorption (RSA)

Consider a system with multiple energy levels, in which the electrons can be excited to higher levels on irradiating with a suitable laser beam. On interacting with high intense light, system is raised to the first excited level and it can be subsequently excited to higher levels by absorbing more photons, which results in a decrease in net transmittance and the phenomenon is termed as RSA. The RSA may arise from various

processes such as TPA, excited state absorption (ESA), nonlinear scattering etc. Compared to TPA, in ESA, the promotion of an electron to a higher level happens via absorption of photons from a lower excited state. The transition from second to the third level is possible through the absorption of one photon according to the frequency of the laser beam and the nature of the material, provided σ_{e1} is significantly greater than σ_g . The schematic representation of RSA is shown in **Figure 1.8**.

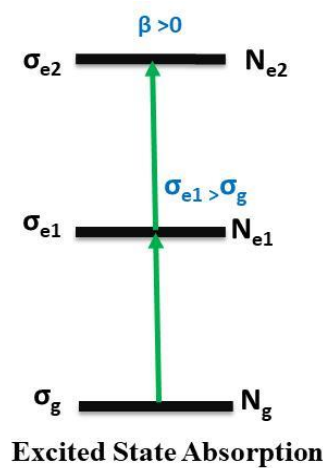


Figure 1.8 Schematic representation of RSA, including both TPA and ESA in multi-level system.

Considering the steady state condition, the spatial rate of change of laser intensity along the direction of propagation can be expressed as:

$$\frac{dI}{dz} = -\alpha_0 I - \beta_{eff} I^2 \dots\dots\dots 1.7$$

where, β_{eff} is the effective TPA coefficient, including both TPA and ESA.

(iv) Free carrier absorption

When a semiconducting material interacts with high intensity light, charge carriers (electrons or holes) are formed and these carriers can be excited to higher levels in the conduction band by absorbing photons. The excitation to higher levels takes place with the assistance of photons and is known as free carrier absorption, which is similar to ESA in molecular systems. Consider the free carrier absorption due to the absorption of a single photon, the change in intensity is given by:

$$\frac{dI}{dz} = -(\alpha + \sigma N) I \dots\dots\dots 1.8$$

where σ is the free carrier absorption cross section and N is the number of electron-hole pairs per unit volume.

1.5.3.2 Nonlinear refraction (NLR)

When a Gaussian profiled beam propagates through the medium, besides NLA it can also undergo phase distortions. The spatial and temporal characteristics of a propagating beam depend largely on the material property and the intensity of light. The nonlinear refractive index of the medium is given by:

$$n = n_0 + n_2 I \dots\dots\dots 1.9$$

Here n_0 is the linear refractive index, I is the intensity of the light and n_2 is the nonlinear refractive index coefficient and it can be either positive or negative. If the value of $n_2 > 0$, the material is of self-focusing behavior, where the material itself can act as a positive lens and try to converge the beam. In a positive n_2 material, the net refractive index is higher than n_0 . If the value of $n_2 < 0$, the material is of self-defocussing nature and the system tries to diverge (negative lens) the beam. In such a case the net refractive index is smaller than n_0 . The third-order NLR plays a crucial role in self-phase modulation, mode-locking, wave-mixing, photo refractivity, phase conjugation, spatial solitons, nonlinear waveguides and interfaces, and optical bistability.

1.5.4 Optical limiting (OL)

Controlling the intensity of light in a stable and foreseeable way is the most fundamental innovation in photonic technology, which has wide applications in the field of optical communications and optical computing (Chen 2001; Hernandez et al. 2000; Sutherland 1989). Optical limiting is the phenomenon of decrease in the transmittance of a nonlinear material on increasing the intensity of the incident optical beam. A perfect optical limiter is the one which exhibits constant transmittance at low input fluence and reduced transmittance at high input fluence. Optical limiters can be exploited in applications such as pulse shaping, pulse smoothing, pulse compression, laser pulse regulation, mode locking, etc. However, their main application is to safeguard the sensors, detectors and human eyes from the high intense light (Anand et al. 2011). From 1960 onwards optical limiters have been developed for protecting optical sensors against laser light induced damages. B- or P- doped silicon single crystals were reported as the first material exhibiting optical limiting property by

Geusic et al. of Bell labs in 1967 (Geusic et al. 1967). The first optical limiter was demonstrated by Soileau and co-workers (Soileau 1980) in 1980 using CS₂ solutions to suppress 1064 nm laser pulses via self-focusing method.

In dynamic optical limiters, certain feedback devices are used to control the intensity of transmittance light and they are with some limitations like lower speed and high complexity whereas, in passive optical limiters the process of limiting is very fast and less complex. In a passive optical limiter, the material itself does all the functions of a sensor, which monitors the input light intensity, the processor, which activates a modulator and finally the modulator, which limits the intensity of the light. Optical limiters made out of NLO materials are passive optical limiters.

The optical limiting data are extracted from the graphs of normalized transmittance obtained from NLA analysis against input fluence. From the graph, the onsets of limiting action (the value of input fluence at which the intensity of output transmittance starts decreasing) and the limiting threshold (LT) values (the value of input fluence at which the intensity of output pulse becomes 50% of the initial value) can be determined, which are very much essential to study the optical limiting action of materials. The characteristics of a passive optical limiter are shown in **Figure 1.9**.

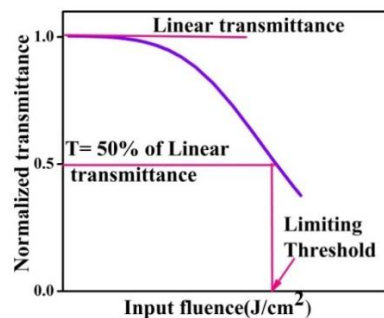


Figure 1.9 Transmittance features of a passive optical limiter.

OL property of a material can be characterized by its coefficients of NLA and NLR, since both are responsible for the nonlinear variations in the intensity as it propagates through the medium. The essential qualities of optical limiters include high damage threshold, wide dynamic range, low optical limiting threshold value, fast optical response and good chemical and mechanical stability. The mechanisms which contribute to the optical limiting behavior of a material are ESA, TPA, thermal

defocusing, thermal scattering, photorefraction, NLR, induced scattering *etc.*, (Tutt and Boggess 1993).

1.5.5 Nonlinear optical analysis

Various techniques are introduced to examine the nonlinear optical properties of materials, such as degenerate four-wave mixing technique, four-wave mixing technique, optical Kerr gate technique, optical power limiter technique and Z-scan analysis. Different nonlinear light-matter interactions make use of the above-mentioned techniques and hence, values of nonlinear parameters extracted are different in each technique. Among the above-mentioned experimental techniques, Z-scan, introduced by Sheik Bahae and his co-workers in 1990 (Sheik-Bahae et al. 1990), is widely used technique for the measurement of third-order nonlinear parameters.

1.5.5.1 Z-scan

The Z-scan technique is simple and sensitive for determining the third-order nonlinear optical parameters. Both the magnitude and the sign of NLA and NLR coefficients can be figured out from the experiment.

1.5.6 Conjugated materials for NLO

A variety of materials are being investigated for third-order optical nonlinearity after its discovery. In 1991, Cheng et al. reported the nature of π -conjugated bond in a series of benzene and stilbene derivatives towards nonlinearity (Cheng et al. 1991). The three main basic requirements for organic materials to exhibit NLO property are (i) polarizability (electrons need to be greatly perturbed from their equilibrium positions), (ii) acentric crystal packing and (iii) asymmetric charge distribution (incorporation of D–A molecules). Further, the materials must possess (a) large oscillator strength for electronic transitions from the ground state to the excited state, (b) excited states close in energy to the ground state and (c) a large difference between the ground and excited state dipole moments. As D–A π -systems allow charge transfer between electron donating and electron withdrawing moieties, many of them are studied for NLO properties and device applications. So far, many conjugated organic molecules are recognized as the key components due to their ease and low cost of synthesis, high laser damage thresholds, large optical nonlinearity and short response time (Dalton et al. 2009; Liu et al. 2015; Rajeshirke et al. 2018; Thakare et al. 2017). The existence of π -conjugation between suitable D and A units in conjugated molecules enables interesting

feature of ICT via interaction between D and A groups in organic materials (Karuppanan and Kalainathan 2018). Further, variations in D and A groups facilitate the modifications in electronic structures which in turn alters the molecular polarizability, electronic and nonlinear optical properties (Quade et al. 2000; Murali et al. 2012). Thus, the organic materials with strong π -conjugated system and alternating sequence of D–A units are found to exhibit remarkable third order nonlinearity (Audebert et al. 2003; Bredas et al. 1994; Karuppanan and Kalainathan 2018), which make them promising in the fields such as optical computing, optical switching and electro–optic modulation (Kanis et al. 1994; Prasad and Williams 1991; Williams 1983).

1.6 ORGANIC LIGHT EMITTING DIODES (OLEDs)

The OLEDs made of organic semiconducting materials, are solid-state lighting sources. Ever since their discovery (Tang and VanSlyke 1987), OLEDs have kept receiving great attentions in both academia and private industry due to their superior properties such as simplicity of fabrication, potentially lower cost, higher color contrast, high brightness and power efficiency, mechanical flexibility and light weight compared to the conventional inorganic semiconductors. These unique qualities of OLEDs make them perfect candidates for next-generation solid state lighting and display technologies. OLEDs are now being used in consumer electronic industry as emissive materials in modern day electronic devices such as digital cameras, televisions, tablets, smart watches and phones.

1.6.1 Fundamentals of OLEDs

1.6.1.1 Basic device physics: Architecture and working principle

In an OLED, the recombination of injected electrons and holes in an electroluminescent active organic layer generates the light. A very basic device structure needs only one organic layer. The device structure is shown in **Figure 1.10 (a)**. In the basic device structure, transparent indium tin oxide (ITO) is typically used as an anode, a low-work-function metal such as calcium (Ca) or aluminium (Al) is used as a cathode and the active organic layer is sandwiched between the electrodes where the emission of light takes place. The active material can be either small molecule or polymer. When a voltage is applied to the device, charge carriers are injected into the active organic layer from the electrodes, namely holes from the anode and electrons

from the cathode (Brutting et al. 2001). Injected charges further move into organic layer and recombine to form an exciton. The excitons formed at the active layer further diffuses to undergo radiative emission, which is shown in **Figure 1.10 (a)**. However, in order to overcome the discrepancies like mismatching of energy levels among the functional layers and charge leakage through the organic materials in single, two- and three-layered devices, a commonly adopted structure is a stack of multi-layer organic heterostructures in almost all OLED devices.

In general, highly efficient OLEDs, developing at present, consist of many layers with different functionalities. The typical multilayer device comprises of (1) the anode: ITO, pre-deposited on a glass substrate, (2) hole injecting layer (HIL), (3) hole transporting layer (HTL), (4) electron blocking layer (EBL), (5) emissive layer (EML), (6) hole blocking layer (HBL), (7) electron transporting layer (ETL), (8) electron injecting layer (EIL) and a low work function cathode (Al, Ca or Mg). The holes are injected from a high-work-function metal (anode, ITO) into the HOMO of HIL, while the electrons are injected from a low-work-function metal (cathode, Al, Ca or Mg) into LUMO of EIL. The HIL and EIL, which are typically organic semiconductors containing strong electron donors and acceptors, act as “Ohmic” buffer layers to facilitate hole and electron injection from the anode and cathode, respectively. Further, the holes and electrons are transported via the HTL and ETL, which are typically weak electron donors and acceptors, respectively, serve as media for transporting holes and electrons to the HOMO and LUMO level of EML. Holes and electrons recombine at the light-emitting layer to form excitons, which can decay radiatively (electroluminescence) or non-radiatively. Before the holes and electrons reach the EML, they have to pass EBL and HBL (optional), respectively. These blocking layers prevent the leakage of opposite charges from EML to HTL or ETL and confine the excitons within the EML. The recombination region depends on the magnitude of the injection barriers and the relative mobilities of holes and electrons, while the color of the emitted light is governed by the HOMO–LUMO energy difference of the organic material. To enhance radiative recombination, the emitting layer is typically a dopant-host matrix in which the dopant, present in various concentrations, is a highly fluorescent or phosphorescent organic compound, and the host is an organic compound

or mixture capable of transporting both holes and electrons (Reineke et al. 2013). A schematic of multilayer OLED structure is shown in the **Figure 1.10 (b)**.

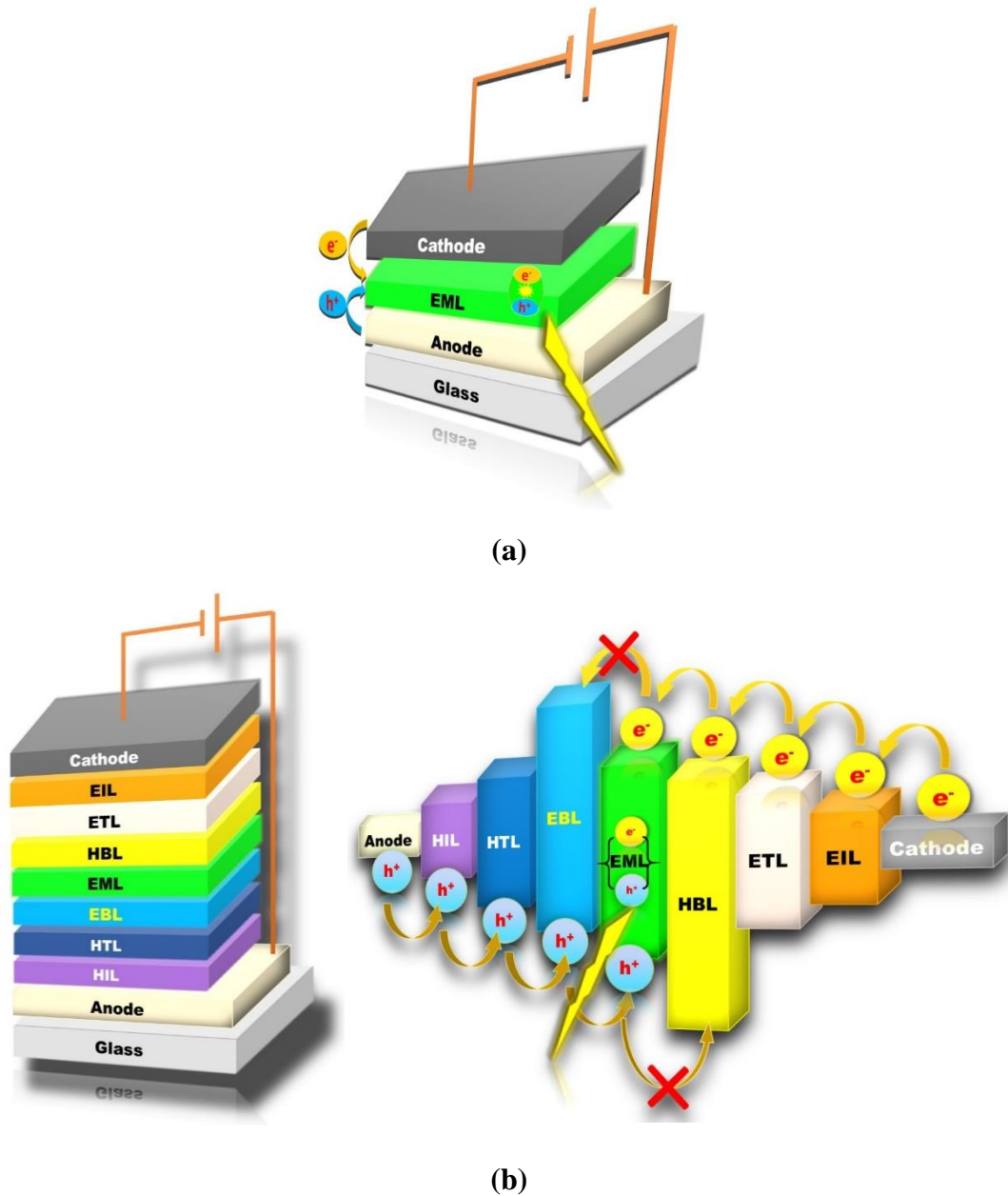


Figure 1.10 (a) OLED single layer structure, (b) OLED multilayer structure with energy level diagram explaining electroluminescence mechanism.

1.6.1.2 Important device parameters

(i) Luminance (L)

This describes the amount of light that is emitted from an area of 1 m^2 per a given solid angle.

(ii) External Quantum Efficiency (EQE)

The ratio of number of photons emitted in the forward direction of a device to the number of electrons injected into the diode. i.e.,

$$EQE\% = \frac{\eta_{ph}}{\eta_e} \times 100$$

where, η_{ph} is the total number of photons emitted from the device and η_e is the total number of electrons injected into the device.

EQE is also defined as:

$$EQE = \gamma \times \eta_{int} \times \eta_{QY} \times \eta_{ext}$$

where, γ = charge injection efficiency, is the ratio of number of charges that recombine to the total number of charges injected into the device. η_{int} = internal quantum efficiency (IQE), is the amount of luminescent exciton recombination to the total number of excitons recombined within the device. η_{QY} = quantum yield, is a measure of number of photons emitted from a luminescent material to the number of photons absorbed by it. η_{ext} = extraction efficiency or out coupling efficiency, is the ratio of number of photons collected at the surface of a device to the total number of photons generated within the device.

(iii) Current Efficiency (η_{CE})

It is the ratio of forward luminance, L to the applied current density, J . It is expressed in units of mA/cm².

$$\eta_{CE} = \frac{L}{J}$$

(iv) Luminous efficiency (η_{LE})

It is the ratio of luminous flux ϕ_v to the radiant flux ϕ and it is expressed in units of lumens per watt (lm/W).

$$\eta_{LE} = \frac{\phi_v}{\phi}$$

(v) Power efficiency (η_{PE})

It is the measure of the amount of light flux produced by a source at a given input power, is also expressed in units of lm/W.

In order to improve the light output, lifetime and efficiency of OLEDs, innovations on multiple fronts are still needed. The best method to extract the light generated by the OLED, the advancement in design and synthesis of materials and device architectures to achieve high efficiency and stability remain as key challenges. Moreover, reduction of cost is another major factor which need to be taken into account when comes to the commercialization.

To address these issues, the best way is understanding the structure-property relationship between the molecular structure of conjugated system and its electroluminescent properties. For efficient charge injection and transportation, close alignment of the energy levels (HOMO/ LUMO) of conjugated materials and the work function of the metal electrodes is necessary. In this regard, many approaches have been attempted to improve the charge injection/transport (Parker et al. 1994 and Son et al. 1995). Recently, alongside the development of device configuration, growing interest has been focused on finding materials with D–A combinations, aiming for new materials to develop more efficient OLEDs.

The following section gives a brief account on the literature report on important D–A type conjugated materials carrying different types of D and A moieties. Further, it also highlights the effect of various D/A units on optical and electrochemical properties of the materials.

1.7 LITERATURE REVIEW

Part A: This section covers a brief literature report on different kinds of D–A type conjugated small molecules and the influence of structure on third-order NLO properties of the molecules.

Gu et al. 2014 studied the linear and NLO properties of four 1,8-naphthalimide hydrazones (**1.1a–1.1d**) possessing different electron-donating groups. Their TPA behavior with femtosecond laser pulses at 800 nm and ESA behavior with nanosecond laser pulses at 532 nm were investigated. Different from TPA behavior, compound **1.1b** showed the best NLA properties at 532 nm and its β_{eff} and $\chi^{(3)}$ were up to 1.41×10^{-10} m W^{-1} and 4.65×10^{-12} esu, respectively, due to its D–A conjugation and the absence of linear absorption at 532 nm.

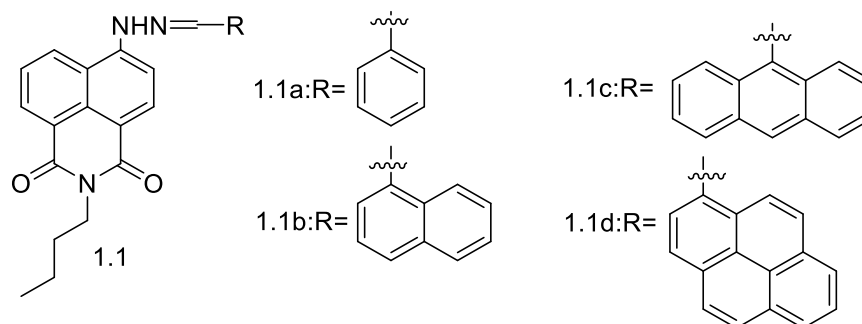


Figure 1.11

A novel D- π -A- π -D type thiophene-pyrimidine derivative, 2,2'-thiophene-4,6-bis (4-N,N-diethylbenzene ethenyl) pyrimidine (**1.2**), was synthesized via Knoevenagel and Suzuki coupling reactions by Zhang et al. 2014. Detailed experiments on third-order NLO properties revealed that the thiophene-pyrimidine derivative showed strong third-order NLO response and large TPA cross section in high polar solvents. The β_{eff} and remarkable value of $\chi^{(3)}$ were 0.451 cm GW^{-1} and $1.45 \times 10^{-8} \text{ esu}$, respectively.

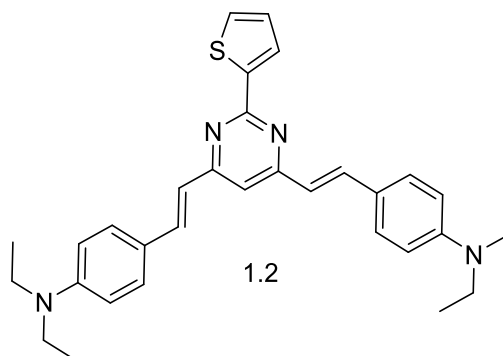


Figure 1.12

Jia et al. 2017 reported the third-order NLO properties of quinacridone (QA)-based materials (**1.3a1–1.3c1**, **1.3a2–1.3c2**, **1.3d**). Introduction of dicyanoethylene groups to the quinacridone core not only successfully modified the structures and photoelectric properties of the chromophores, but also led to the superior third-order NLO properties. The chromophore **1.3b2** exhibited a maximum $\chi^{(3)}$ of $15.456 \times 10^{-13} \text{ esu}$, which was 5 times higher than that of mono-modified QA and also, the β_{eff} value was $30.071 \times 10^{-11} \text{ m W}^{-1}$. The results suggested that quinacridone-based materials have good photo-thermal stability and large third-order NLO properties, which are very promising for integrated NLO devices.

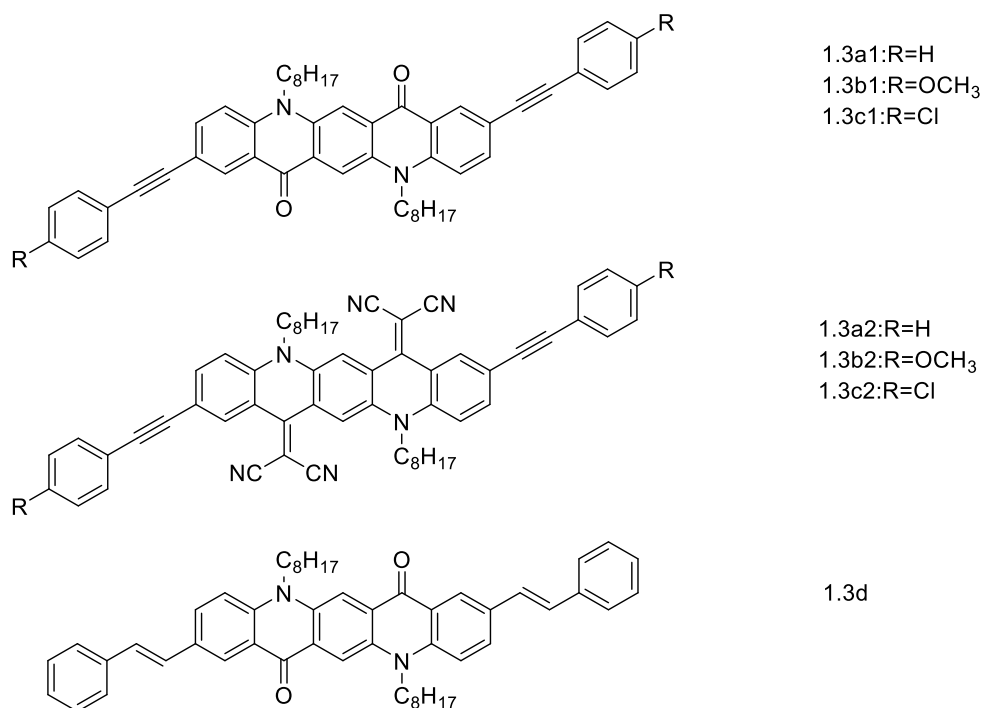


Figure 1.13

Xu et al. 2017 designed and synthesized mono- and di-4-N,N-bis(4-methoxyphenyl)aniline-substituted anthraquinone derivatives **1.4a** and **1.4b**. The third-order NLO studies of the synthesized molecules revealed that the symmetric D–A–D type molecule, di-methoxy triphenylamine-substituted anthraquinone (**1.4b**) showed a larger β_{eff} and TPA cross section compared to asymmetric D– π –A type molecule, mono methoxy triphenylamine-substituted anthraquinone (**1.4a**). The β_{eff} obtained by the open Z-scan curves increased from $2.04 \times 10^{-12} \text{ cm W}^{-1}$ to $3.91 \times 10^{-12} \text{ cm W}^{-1}$ when second triphenylamine unit was introduced to the core moiety.

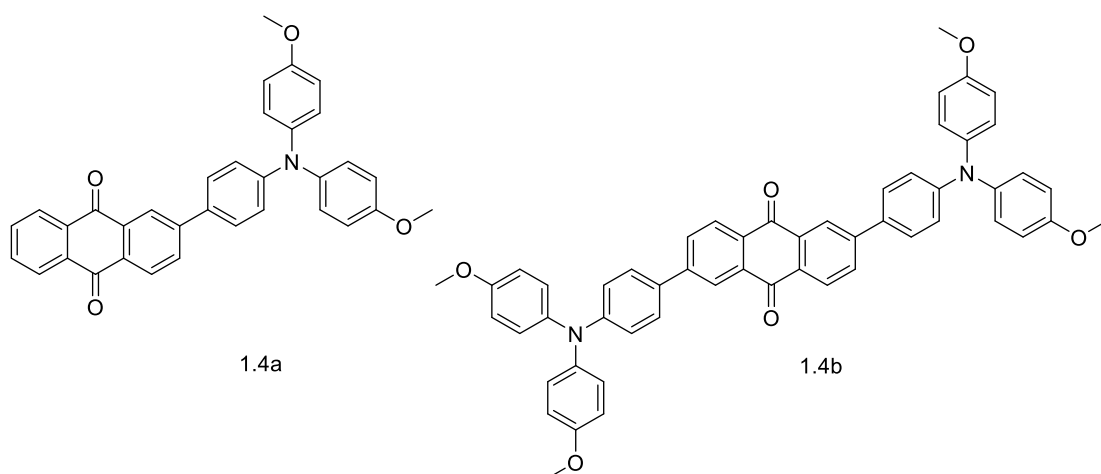


Figure 1.14

Anandan et al. 2018 designed, synthesized and characterized two thiophene derivatives **1.5a** and **1.5b**. The optical limiting properties were studied using Z-scan under nanosecond laser excitation at 532 nm with an input energy of 100 μJ . The molecules showed TPA process. The effective delocalization of electrons in dialdehyde (**1.5b**) led to a maximum β_{eff} value of $2.9 \times 10^{-11} \text{ m W}^{-1}$.

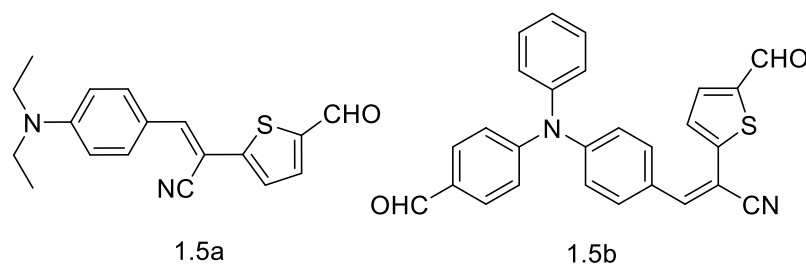


Figure 1.15

Gowda et al. 2018 synthesized 3,4-ethylenedioxythiophene (EDOT) based bent-core shaped mesogens (**1.6a** and **1.6b**) bearing terminal alkyl chains. The presence of extended delocalized π -electron conjugations in the mesogens resulted in large optical nonlinear properties. The mesogens showed effective TPA when measured under excitation by nanosecond laser pulses at 532 nm. In bent-core mesogens (**1.6a** and **1.6b**), the acetylene linking group acted as a conjugating spacer between the central heteroaromatic EDOT ring and the phenyl group with flexible alkoxy chain entities, which further enhanced the nonlinearities. With extended delocalized π -electronic conjugation, the compound **1.6a** showed RSA with β_{eff} of $5.6 \times 10^{-11} \text{ m W}^{-1}$.

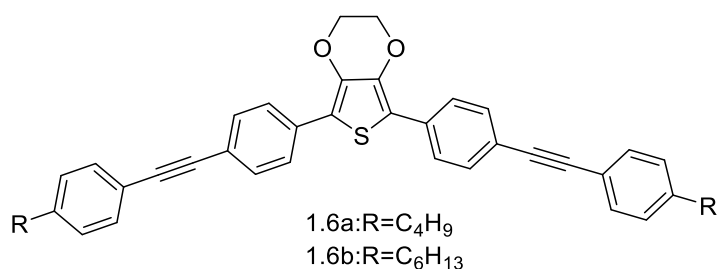


Figure 1.16

Jia et al. 2018 synthesized a series of quinazolinone-based materials (**1.7a–1.7f**) and their third-order nonlinear optical properties were investigated using Z-scan measurement. The results showed that the introduction of phenylacetylene groups on the planar structure reduced the π - π intermolecular stacking of parent ring. And the formation of push-pull structure by connecting phenylacetylene groups to

quinazolinone backbone decreased the energy gap of entire molecule. A good NLO response was obtained for all the molecules. Out of all the six molecules, the molecule **1.7b** showed an excellent β_{eff} of $0.471 \times 10^{-11} \text{ m W}^{-1}$ and $\chi^{(3)}$ value of $1.184 \times 10^{-13} \text{ esu}$.

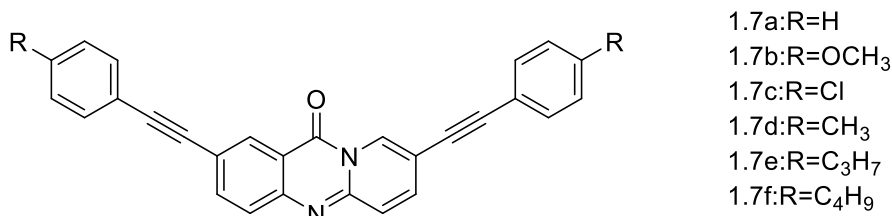


Figure 1.17

Wu et al. 2018 synthesized three novel D–A type phenanthridine derivatives (**1.8a**, **1.8b** and **1.8c**) and their third-order NLO properties were systematically determined by open/closed aperture Z-scan methods using tunable femtosecond laser. The results revealed that **1.8b** possessed largest TPA coefficient ($\beta_{eff}=0.349 \text{ cm GW}^{-1}$) and cross sections ($s=1669.306 \text{ GM}$) compared to the others. The highly delocalized π -electronic configuration and superior intrinsic planarity made **1.8b** a potential candidate for third-order NLO materials in the near infrared region.

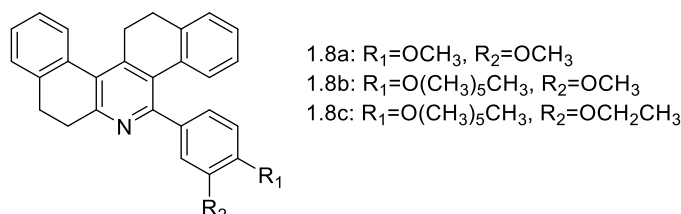


Figure 1.18

Avhad et al. 2019 synthesized three push-pull rhodanine-arylamine based D– π –A dyes (**1.9a–1.9c**) and studied the effect of donor on electronic, linear and NLO properties. The dyes **1.9a**, **1.9b** and **1.9c** possessed a vinyl spacer conjugated with triphenylamine, julolidine and carbazole donors, respectively, with a methoxy group and rhodanine-3-acetic acid. The dyes **1.9a** and **1.9c** showed RSA with positive β_{eff} and reasonable values of $\chi^{(3)}$. The β_{eff} and $\chi^{(3)}$ values of **1.9a** and **1.9c** were $3.718 \times 10^{-12} \text{ m W}^{-1}$ and $1.8766 \times 10^{-13} \text{ esu}$, and $3.133 \times 10^{-12} \text{ m W}^{-1}$ and $1.1758 \times 10^{-13} \text{ esu}$, respectively.

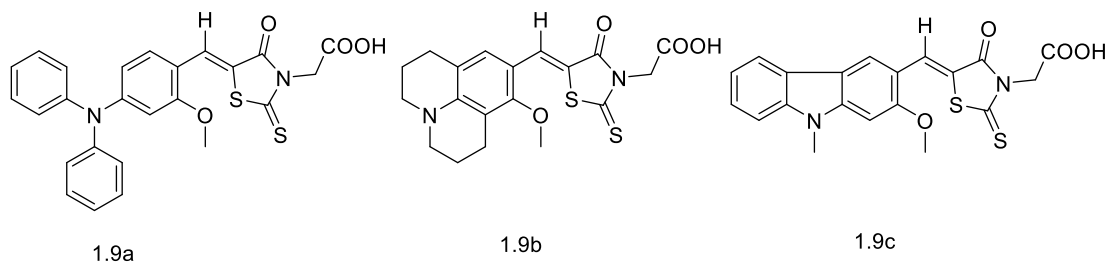


Figure 1.19

Three novel N-heteroacene molecules (**1.10a**, **1.10b** and **1.10c**) based on tetraazachrysene units as cores were designed and synthesized by Li et al. 2019. The TPA studies were carried out using open and closed aperture Z-scan technique. The molecule **1.10c** showed a significant enhancement in the TPA cross section with magnitudes as high as ~ 700 GM ($1 \text{ GM} = 1 \times 10^{-50} \text{ cm}^4 \text{ s/photon}$) when excited with 800 nm light. Due to the weak electron-donating ability of (triisopropylsilyl)acetylene segment, **1.10a** exhibited negligible third-order NLO properties, while **1.10b** and **1.10c** exhibited β_{eff} of 0.43×10^{-12} and $0.51 \times 10^{-12} \text{ cm W}^{-1}$, respectively.

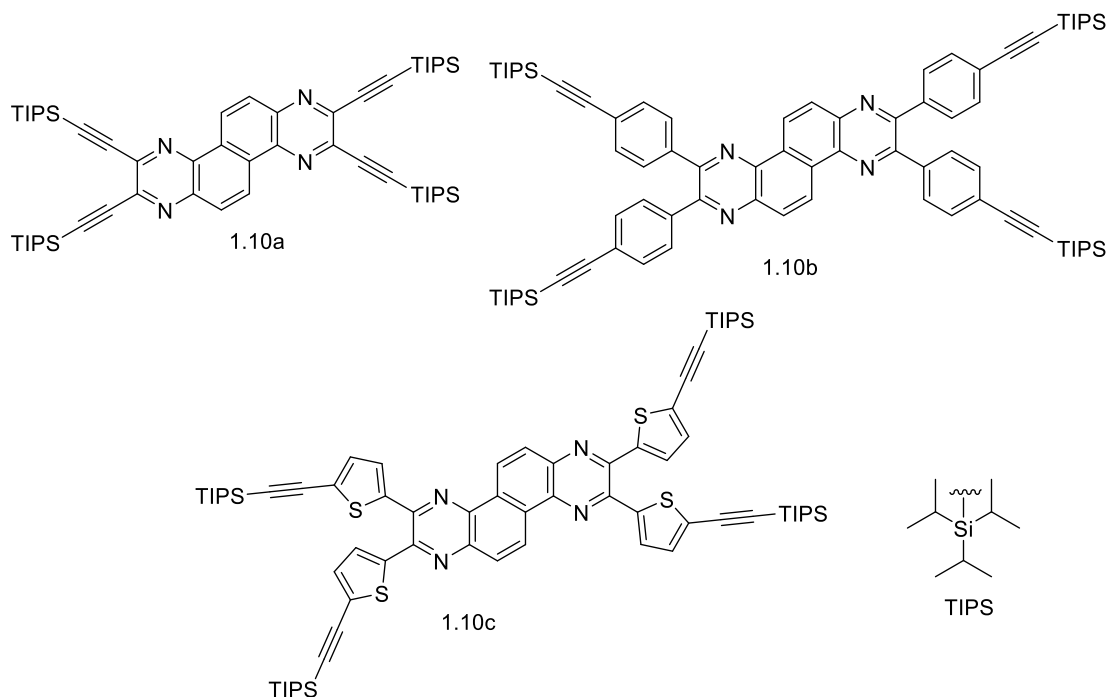


Figure 1.20

Xu et al. 2019 synthesized two thiophene containing pyrene derivatives **1.11a** and **1.11b**, and investigated the third order NLO properties using femtosecond Z-scan at 532 nm. The measured NLA of two compounds was related to the TPA mechanism.

The molecule **1.11b** exhibited higher β_{eff} value due to the extended conjugation when compared to the other molecule, **1.11a** and was determined to be $3.45 \times 10^{-13} \text{ m W}^{-1}$.

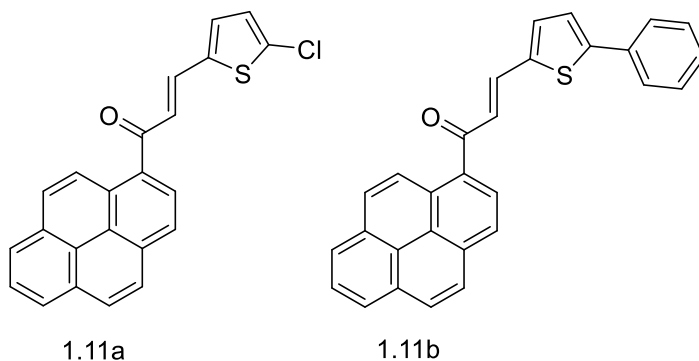


Figure 1.21

Zheng et al. 2019 synthesized quinazolinone based compounds (**1.12a–1.12d**) containing triphenylamine moiety for the application of third-order NLO. The NLO properties evaluated by the Z-scan technique showed that the introduction of a benzene ring as a π -bridge reduced the transmission energy of electrons from the ground state to the excited state and the added methoxy in TPA moiety promoted the ICT and improved the third-order NLO properties of molecules. With enlarged π -conjugation and additional electron donating groups, the compound **1.12d** exhibited excellent third-order NLO responses with the β_{eff} of $3.692 \times 10^{-11} \text{ m W}^{-1}$ and $\chi^{(3)}$ of $9.295 \times 10^{-13} \text{ esu}$.

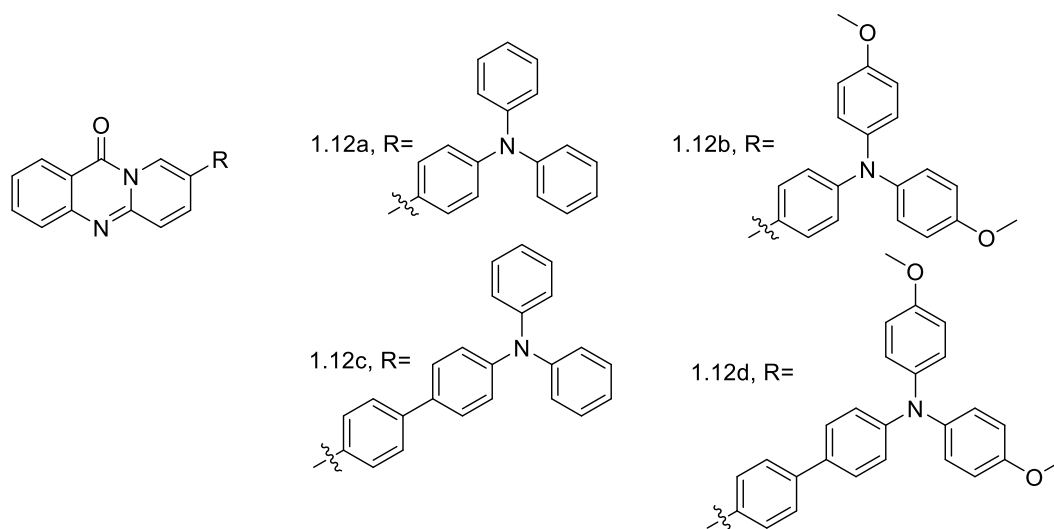
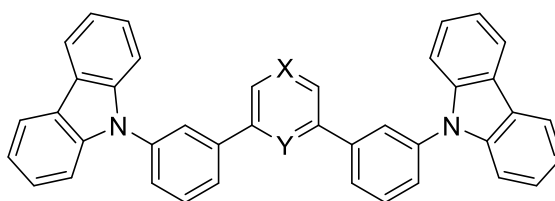


Figure 1.22

Part B: This section covers a brief literature review on different kinds of star shaped D–A type conjugated small molecules and the effect of structure on OLED device parameters.

Su et al. 2008 designed and synthesized unique bipolar host materials (**1.1.3a** and **1.1.3b**) combining carbazole as electron donor with high triplet energy and pyridine as electron acceptor with high electron affinity. Bis[2-(4,6-difluorophenyl)pyridinato-C2,N](picolinato)iridium(III) (FIrpic)-based blue phosphorescent OLEDs (PHOLEDs) fabricated using the present bipolar molecules as host materials showed a record EQE of 24% and a η_{PE} of 46 lm W⁻¹ with reduced efficiency roll-off at a high driving current as a result of good confinement of the triplet excitons on the guest molecules and improved carrier balance injected into in the emissive layer. The findings suggested a new route to further improve the performance of PHOLEDs, especially at a high driving current.



1.13a : X=CH, Y=N
 1.13b : X=N, Y=CH

Figure 1.23

Yuan et al. 2008 synthesized and characterized amorphous 2,4,6-trisubstituted pyridines, containing two triphenylamine and one carbazole moieties (**1.14b**) or three peripheral carbazole moieties (**1.14a**) and studied their photophysical, electrochemical and thermal properties. The results showed that the molecules possess good thermal stability, emit intense blue light and the HOMO/LUMO levels match with those of N,N'-bis(naphthalen-1-yl)-N,N'-bis(phenyl)benzidine (NPB). The results showed that the materials could be of potential candidate in optoelectronics.

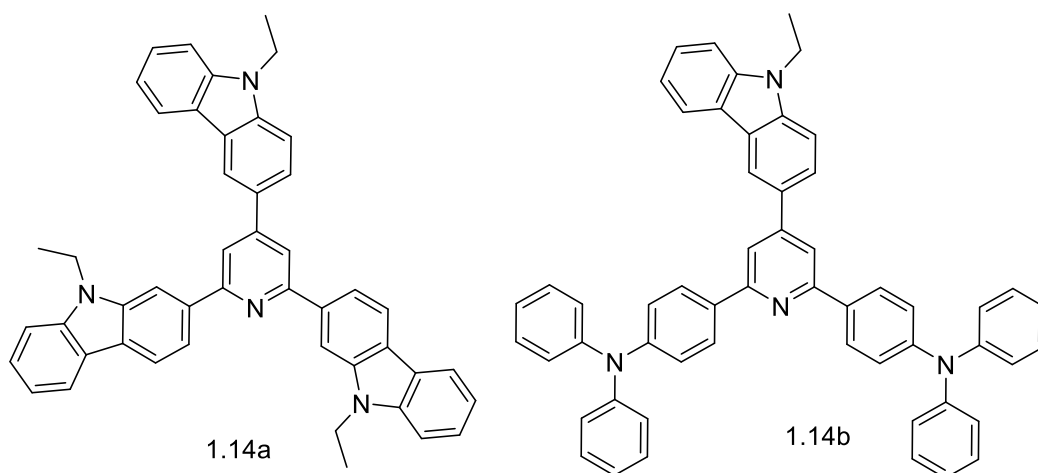


Figure 1.24

Li et al. 2010 reported two multiaryl substituted pyridine derivatives (**1.15a** and **1.15b**) for applications in non-doped deep blue OLEDs as ETL. The low LUMO energy levels for the two pyridine derivatives implied no barrier and facilitated electron injection from the cathode to the organic layer. The devices based on the new compounds exhibited a maximum η_{CE} of above 2.1 cd A^{-1} .

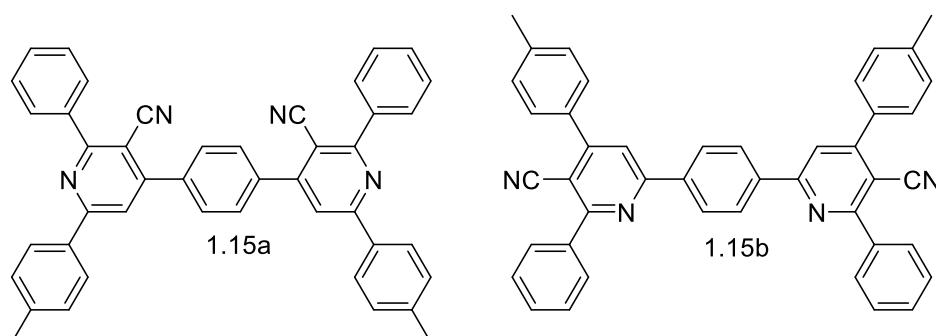


Figure 1.25

Su et al. 2012 synthesized a series of star shaped host materials comprising arylene cores, such as benzene (**1.16a**), pyridine (**1.16b**) and pyrimidine (**1.16c**) for red-green-blue (RGB) PHOLEDs. ICT leading to bathochromic shift in the photoluminescent spectrum and reduced E_g was achieved in molecules with heterocyclic cores of pyridine (**1.16b**) and pyrimidine (**1.16c**) in comparison with molecule with benzene core (**1.16a**). In addition, reduced LUMO level, lower singlet-triplet excited state energy, smaller singlet-triplet energy difference and improved bipolarity were achieved with heterocyclic cores of pyridine and pyrimidine instead of benzene.

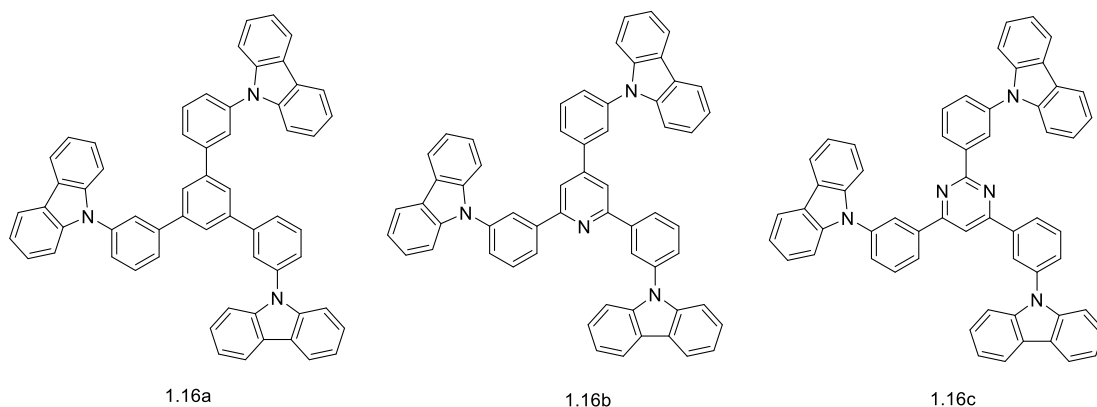


Figure 1.26

You et al. 2012 synthesized and characterized a series of cyano substituted pyridine derivatives (**1.17a–1.17e**). In addition to the electron transporting properties of pyridine derivatives, they also showed light emitting as well as bipolar transporting properties when incorporated with large π -systems. Besides that, introduction of triphenylamine groups endowed it with hole transporting characteristics. The devices based on these materials showed low turn on and driving voltages, high power efficiency and mild efficiency roll-off.

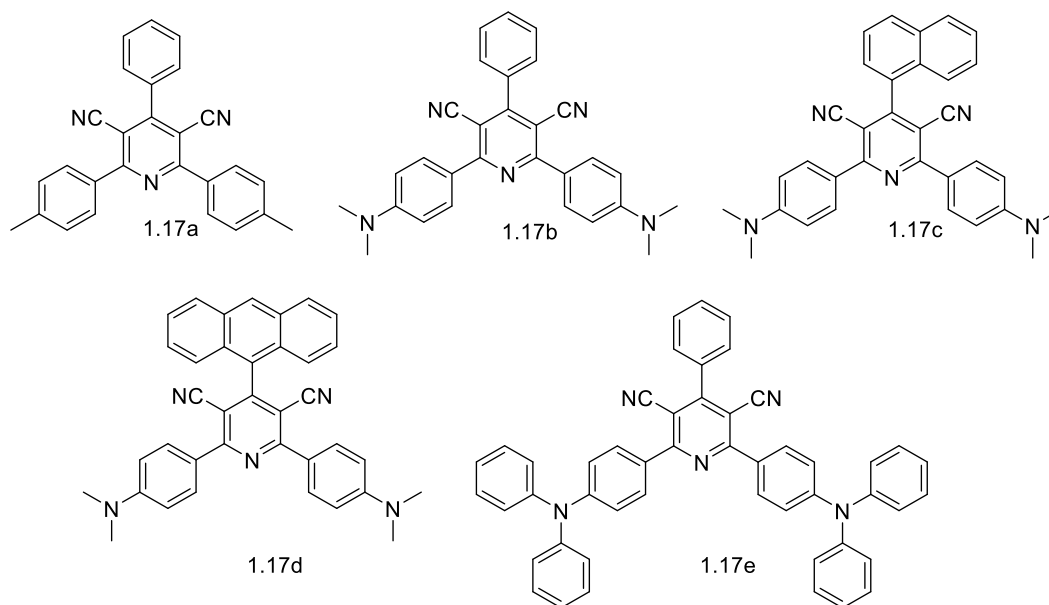


Figure 1.27

Jeong et al. 2013 synthesized two triphenylamine substituted benzimidazole derivatives (**1.18a** and **1.18b**) for use as efficient deep-blue emitters in non-doped fluorescent OLEDs. The device based on **1.18a** showed higher current density (c.d.)

(5.12 mA cm^{-2}) than that based on **1.18b** (3.13 mA cm^{-2}). As the packing densities in the solid-state result in different c.d., the structurally less bulky **1.18a** showed higher c.d. than that of the device with structurally bulkier **1.18b**. But the device fabricated using **1.18b** exhibited a high EQE of 4.67% compared to the device based on **1.18a** (3.05%). The increased steric bulkiness of **1.18b** limited the molecular packing which suppressed the exciton quenching and led to high device performance that that of **1.18a**.

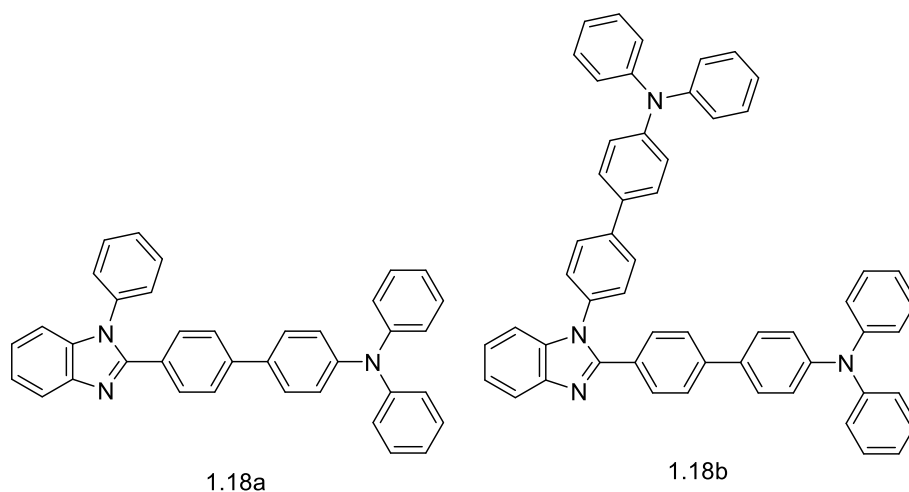


Figure 1.28

Zhan et al. 2013 synthesized pyrene-functionalized triphenylamine derivatives (**1.19a–1.19c**) by alternate Heck and Wittig reactions. The increase in the number of carbazole–vinylene conjugated bridges increased the nonplanarity of the molecules which resulted in blue-shifts of the absorption and emission maxima. Further, the compounds **1.19a**, **1.19b** and **1.19c** were employed as the emitters as well as the hole-transporting materials (HTMs) in electroluminescent devices. Due to the less number of carbazole–vinylene units the device based on **1.19a** exhibited good performance with a low turn-on voltage of 2.8 V, a maximum luminance of $29,880 \text{ cd m}^{-2}$ at 9.5 V, a high η_{CE} of 3.34 cd A^{-1} , a high η_{PE} of 2.67 lm W^{-1} and resulted in green emission which suggested the use of **1.19a** as potential material in non-doped green OLEDs.

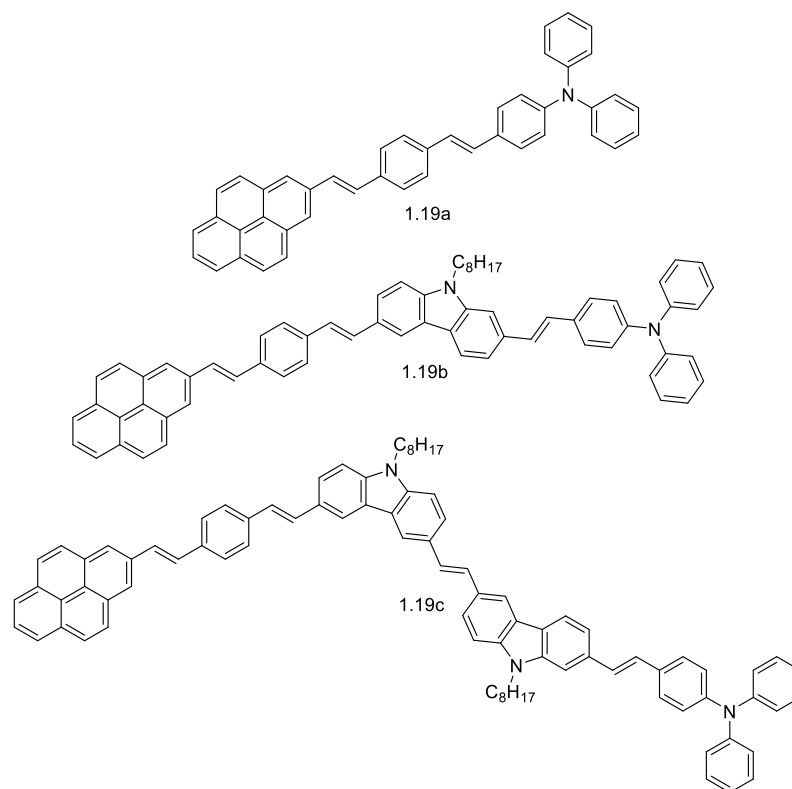


Figure 1.29

Liu et al. 2015 designed and synthesized thermally activated delayed fluorescence (TADF) emitter containing carbazole as electron donor unit and pyridine-3,5-dicarbonitrile as electron acceptor unit (**1.20**). With the extremely small singlet-triplet splitting and high PL quantum yield, material acted as efficient blue TADF emitter. The optimized OLED based on this material exhibited maximum η_{CE} , η_{PE} and EQE of 47.7 cd A^{-1} , 42.8 lm W^{-1} and 21.2%, respectively.

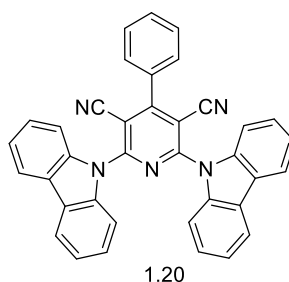


Figure 1.30

Karthik et al. 2016 synthesized carbazole and benzimidazole based organic luminescent materials (**1.21a–1.21e**) in which thiophene and phenyl moieties were used as spacers. The thiophene containing dyes exhibited red-shifted absorption and low

oxidation potential than that of the phenyl analogs due to the effective electron distribution and high electron density in the former. Moreover, the devices containing thiophene-based dyes showed relatively low turn-on voltage, attributed to the favorable alignment of energy levels, which facilitated balanced charge transport. Also, thiophene-based dye, **1.21e**, exhibited better performance in the series with EQE as high as 1.5%, η_{CE} of 0.7 cd A^{-1} , η_{PE} of 6.8 lm W^{-1} at 100 cd m^{-2} with low turn-on voltage.

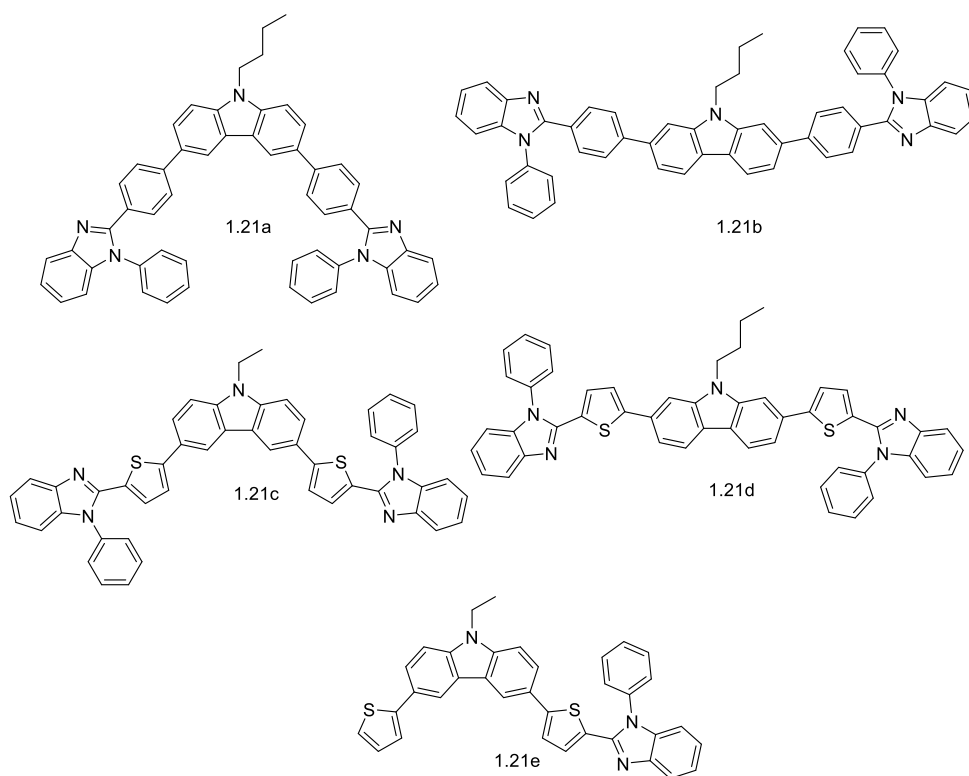


Figure 1.31

Cunha et al. 2018 designed and synthesized triphenylamine substituted quinacridone based small molecule (**1.22**) for solution processed OLEDs. The methoxy triphenylamine as end capping group provided propeller shaped conformation which hindered the intermolecular π - π stacking and aggregation in thin film and hence, suppressed the concentration quenching. The OLEDs based on **1.22** as dopant in host material tris-(8-hydroxyquinoline)aluminum (Alq₃) showed a turn on voltage of $\sim 6.4 \text{ V}$, a maximum luminescence of $\sim 800 \text{ cd m}^{-2}$, a maximum η_{CE} and EQE of 0.42 cdA^{-1} and 0.2%, respectively.

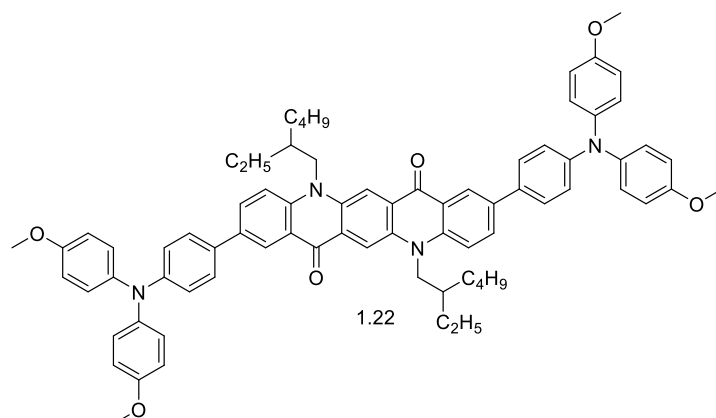


Figure 1.32

Marghad et al. 2019 synthesized new TADF molecule (**1.23**) containing 4,6-bis-phenyl phenothiazine as donor units and 2-thiophene-1,3,5-triazine as acceptor unit. The device utilizing **1.23** as active emissive layer exhibited green-yellowish emission with a turn-on voltage of 4.6 V, a maximum η_{CE} of 35.47 cd A⁻¹, a η_{PE} of 11.1 lm W⁻¹, a maximum luminance up to 10,370 cd m⁻² and a maximum EQE of 9.4%. The enhanced performance was attributed to an efficient TADF process enabling the effective up conversion of the triplets to the singlets *via* reverse inter system crossing (RISC).

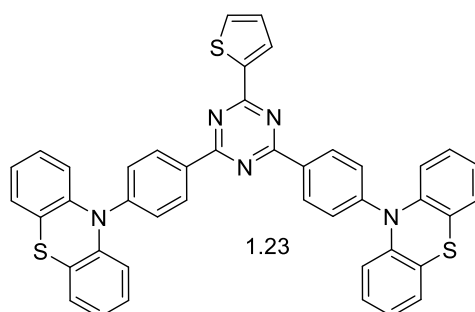


Figure 1.33

1.7.1 Salient features of the literature review

- The D–A system with planar structure provides improved ICT, polarizability and enhanced optical nonlinearity.
- A molecule possessing rigid-cyclic ring system exhibits excellent optical limiting behavior.
- The HOMO–LUMO energy levels of organic molecules must match to the work function of the respective semiconductor.

- Star-shaped molecules possess good thermal stability, high purity, good thin film formation, good solution processability and outstanding device performance.
- There is still a good scope for variation of donor moiety, π -spacer and electron acceptor group which can ameliorate the optical nonlinearity/ device performance.
- There is still a considerable room for the development of star-shaped molecules which can improve the efficacy of the OLED.

1.8 SCOPE AND OBJECTIVES

A thorough literature review provides the scientific community with both general and in-depth information on structure-property relationships of the organic conjugated molecules/polymers, which play an important role in synthesizing novel materials with unique properties. In this context, several organic conjugated molecules/polymers have been synthesized from a different range of conjugated aromatic systems. The conjugated molecules with rigid structural skeleton are being explored because of their promising optoelectronic properties. Some of the problems associated with high molecular weight polymers such as solubility, sample purity etc. could be improved in case of conjugated molecules. Further functional modification could be easily carried out with conjugated molecules so as to achieve desired properties required for device applications. In comparison to the conjugated polymers, conjugated molecules possess some critical advantages such as, (1) well-defined molecular structures lead to their synthetic reproducibility with high purity which is vital to obtain repeatable device performance; (2) crystalline features of molecules favor the long range order in the solid state and benefit the charge carrier transport; (3) the devices can be readily fabricated by both solution-processable and vacuum-deposited techniques (Collins et al. 2017). Among different molecular combinations studied, conjugated system containing both electron donor and acceptor units arranged alternatively along the conjugated molecular chain are demonstrated to be the most auspicious materials for optoelectronic devices.

The presence of electron donor and acceptor group in the organic molecules increases the charge transfer through π -electron delocalization, which increases the molecular polarizability, making the organic materials superior to inorganics both in

the speed of response and in the magnitude of the third-order effect. Thus, recently, these push-pull π -systems with large optical nonlinearity and polarizability have received extensive attention in emerging electronic and photonic technologies like optical computing, optical limiters for sensors and eye protection, telecommunication etc. Though significant advances have already been established in this field, there is still a scope for improving the third order NLA and hence, the limiting action of the molecules. In this regard, search for efficient NLO materials is grossing much interest in recent years.

In this perception and based on the literature review, the following objectives have been proposed for the present research work.

1. To design new D–A type thiophene containing conjugated compounds.
2. To synthesize the designed compounds using standard multistep organic synthetic protocols.
3. To characterize the intermediates and new compounds using spectroscopic methods viz. $^1\text{H-NMR}$, $^{13}\text{C-NMR}$ and mass spectral techniques followed by elemental analysis.
4. To study the linear optical properties of the synthesized D–A conjugated compounds using UV-Vis absorption and fluorescence emission spectroscopic methods.
5. To study the electrochemical properties of the synthesized D–A conjugated compounds using cyclic voltammetry (CV).
6. To discuss the electronic distribution in HOMO-LUMO energy levels using density functional theory (DFT).
7. To investigate the third order NLO properties of the synthesized compounds using Z-scan technique.
8. To discuss the structure-property relationship by comparing the results obtained in the optical, electrochemical and other studies of the conjugated compounds with their chemical structure.

Following the literatures and keeping the above objectives in view, five series of thiophene based conjugated materials have been designed.

1.9 MOLECULAR DESIGN OF NEW D-A TYPE CONJUGATED MATERIALS

A detailed literature survey reveals that the synthesis of intermediate-sized conjugated molecules or oligomers with extended conjugation can provide the desirable qualities of both polymers and small molecules. There has been a dramatic surge in design, synthetic development of conjugated molecules and also, in terms of device efficiency in recent years. Plenty of materials with various D–A combinations such as D–A–D, A–D–A, D– π –A and star-shaped architectures have been reported with excellent optoelectronic performances. Among them, D–A–D module is emerged as one of the most successful and promising modules explored in optoelectronic and photonic industry (Raynor et al. 2015). Tuning of frontier molecular orbital plays vital role in achieving desired properties in such π –systems. There are four primary ways to modify the frontier orbital energies: (i) enlarging the π –conjugation; (ii) incorporating planar fused aromatic ring systems so as to increase the planarity of the system; (iii) incorporating strong donor/acceptor functional units alternatively and (iv) incorporation of polarizable double bonds.

Most of the reported D–A conjugated materials contain simple organic compounds such as thiophene, carbazole, triphenylamine, phenothiazine, fluorene etc., as powerful electron donors and 1,3,4-oxadiazole, pyridine, cyanovinylene, perylene diimides, 2,1,3-benzothiadiazole, thiadiazole, thiazolo[5,4-*d*]thiazole etc, as electron accepting groups. However, thiophene based π –conjugated systems have progressively supplanted other classes of systems in a variety of plastic electronic technologies. The unique combination of efficient electron transfer, structural versatility, environmental stability, a moderate band gap and ease of functionalization of thiophene provides an indispensable role for the thiophene based materials in organic optoelectronic fields such as OSCs, OLEDs, sensors, OFETs and NLO (Perepichka and Perepichka 2009; Skabara 2009). Accordingly, in the present study, it is planned to design and synthesize five new series of thiophene based D–A–D type conjugated compounds. Out of five series, molecules of **series–1** to **series–3** carry thiophene as electron donor and imidazo[2,1-*b*][1,3,4]thiadiazole (ITD) as electron acceptor group along with π –linkers and other supporting electron donor and acceptor groups, while compounds of **series–4** and **series–5** comprise thiophene as donor and pyridine as acceptor moiety along with π –linkers and other supporting electron donor groups.

(i) Design of molecules (VK1–VK3) of series–1

ITD ring is a fused, partially planar and rigid aromatic heterocyclic system with extended π -conjugation, consisting of two heteroaromatic rings, *viz.*, imidazole and [1,3,4]thiadiazole fused together with a bridgehead nitrogen atom (Khazi et al. 2011). The biological activities of ITD derivatives have been extensively studied but there is no research work reported on optoelectronic/photovoltaic results achieved since its discovery. Therefore, in this series three new D–A–D type organic molecules were designed, wherein ITD is an electron acceptor unit and thiophene/ phenyl moieties are electron donor units that produce a D–A–D configuration. The thiophene–ITD (Th–ITD) core structure comprises three different groups *viz.*, thiophene–2–acetonitrile (VK1), phenylacetonitrile (VK2) and rhodanine–3–acetic acid (VK3). The design strategy for the molecules VK1–VK3 is depicted in Figure 1.34.

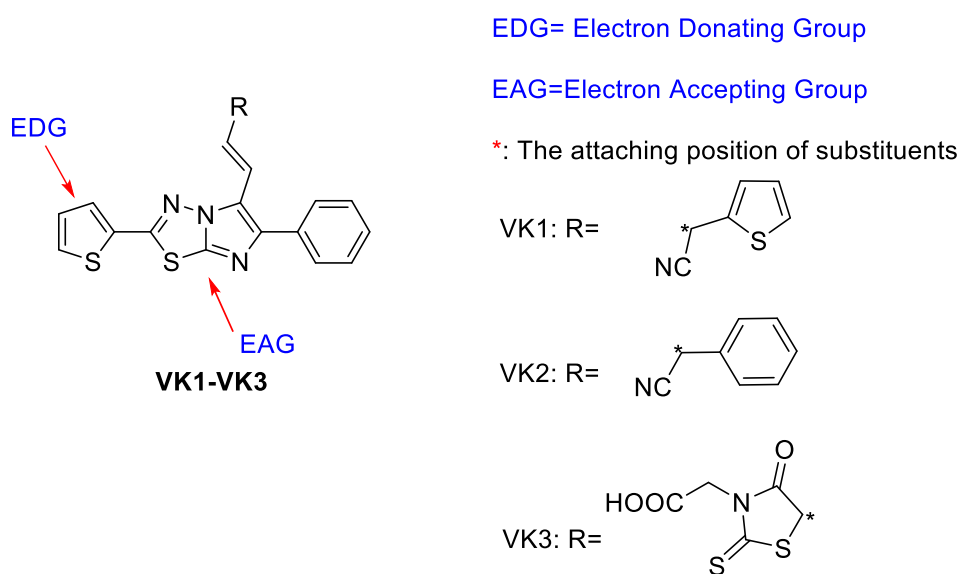


Figure 1.34

(ii) Design of molecules (VK4–VK6) of series–2

In this series three new class of azomethines were designed wherein thiophene and ITD remain as the invariable donor and acceptor moieties, and three different π -conjugated systems *viz.*, pyrene (VK4), anthracene (VK5) and triphenylamine (VK6) are bonded with the thiophene–ITD core unit via azomethine linkage as π -extenders. The design strategy for the molecules VK4–VK6 is shown in Figure 1.35.

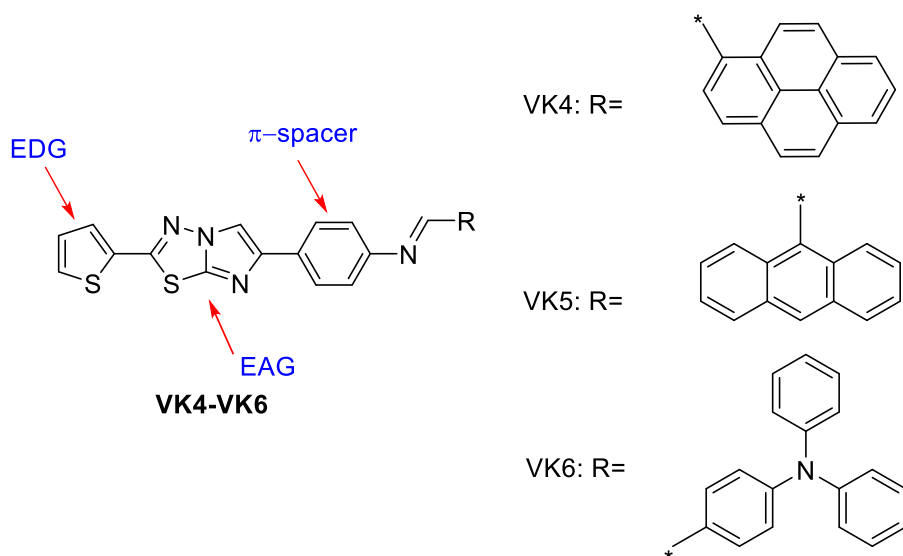


Figure 1.35

(iii) Design of oligomers (VK7–VK10) of series–3

Despite the numerous studies on impact of electron donors on optoelectronic properties, there is a paucity of work on the effect of strong electron acceptors on the performance of D–A type materials. The one acceptor, that has immense applications in optoelectronic industry is 1,3,4-oxadiazole (Cristiano et al. 2005). Lately, 2,5-diaryl-1,3,4-oxadiazoles have been explored as versatile electron transporting materials in optoelectronic field due to their electron-deficient nature, resistance to oxidative degradation, high thermal and hydrolytic stability. Further, they help in extending the conjugation when substituted in D–A type systems (Hughes and Bryce 2005; Li et al. 2014). In addition, the organic molecules with the fused heterocycles have gained much interest as these molecules could increase the performance when applied in optoelectronics. For an instance, thiazolo[5,4-*d*]thiazole (tztz), a rigid, fused heterocyclic system having the coplanar structure with electron-withdrawing nitrogen atoms forming an imine (C=N-) backbone, also acts as an efficient electron acceptor (Cheng et al. 2013; Nazim et al. 2013). The small molecules comprising tztz as an electron acceptor unit with either D–A–D or A–D–A structure are utilized as potent optoelectronic/ photovoltaic materials in the recent past (Cheng et al. 2013; Dutta et al. 2012; Lee et al. 2011; Peng et al. 2005; Shi et al. 2012). However, the structure–property relationship of such molecules is yet to be understood. Hence, it is planned to design a series of four H-shaped conjugated oligomers with thiophene (VK7),

thiophene–1,3,4–oxadiazole–thiophene (**VK8**), tztz (**VK9**) and phenyl–tztz–phenyl (**VK10**) units as central cores, respectively and the Th–ITD moiety at the periphery. The design strategy for the oligomers **VK7–VK10** is depicted in **Figure 1.36**.

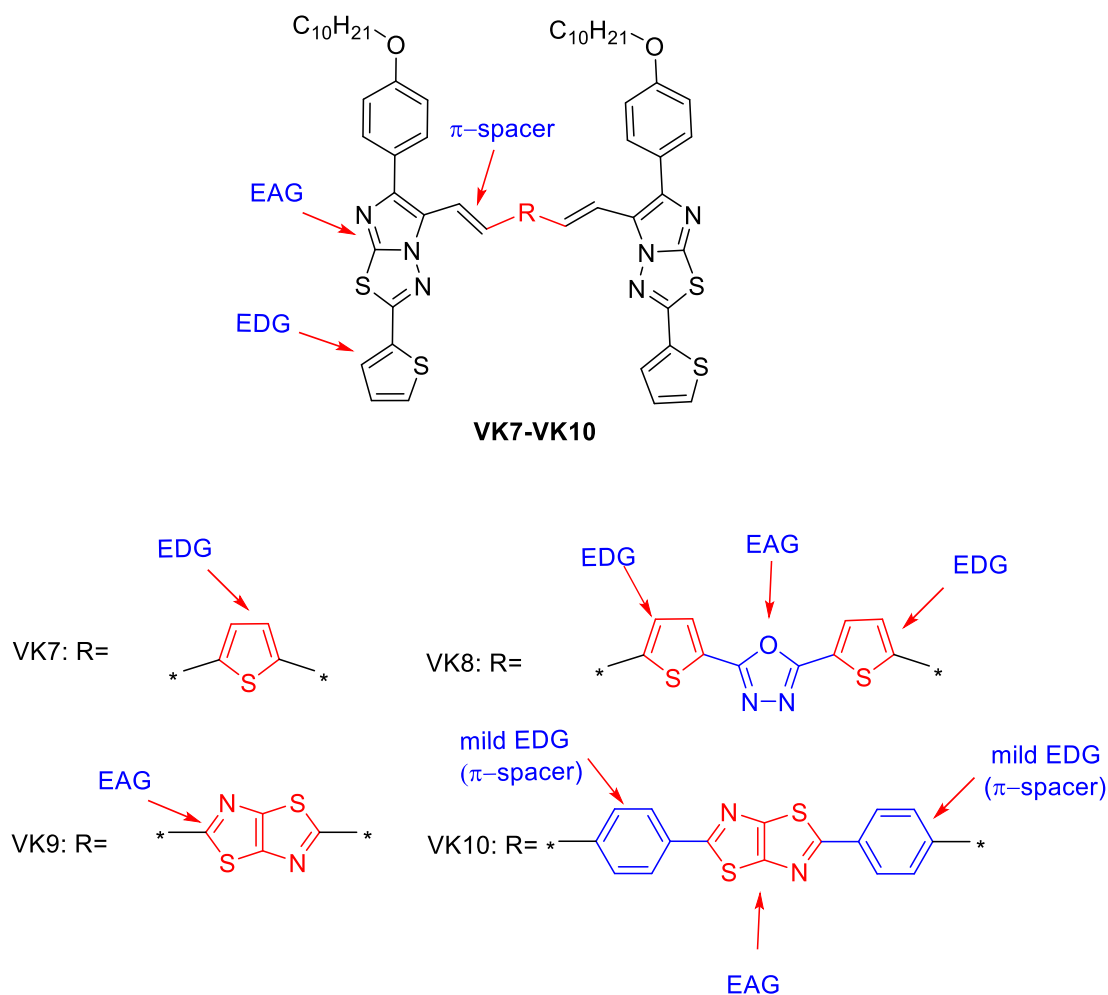


Figure 1.36

(iv) Design of compounds (VK11–VK14) of series–4

To synthesize organic materials with larger TPA or ESA cross sections and to scale up the applications, various design strategies such as D– π –A, D–A–D and A–D–A have been established by many research groups (Albota et al. 1998; Reinhardt et al. 1998). In addition, proper selection of D and A building blocks, distance between D and A moieties, suitable π –linkers to connect D and A units and the symmetry of the molecule play key roles in fine tuning the optical nonlinearity of the system (Xu et al. 2017).

Among the various electron acceptors, pyridine ring is found to be a well-known electron deficient and a highly electron withdrawing moiety. The electro-optical properties of pyridine derivatives can be tuned by substitution of pyridine at different positions and also, by coordination of different guest units to the nitrogen atom of the pyridine group (Vellis et al. 2008). The high thermal stability, chemical stability and good electron-transporting abilities of pyridine make pyridine to have significant role in optoelectronic industry (Liaw et al. 2009).

Given that, in the present work, a new class of trigonal-shaped molecules and polymers with D–A–D structural arrangement were designed with 2,4,6-trisubstituted pyridine (served as electron acceptor) and thiophene (served as electron donor) backbone with thiophene acetonitrile (**VK11**), phenyl acetonitrile (**VK12**, **VK14**) and thiophene (**VK13**) units as side groups. The design strategy for the compounds **VK11**–**VK14** is shown in **Figure 1.37**.

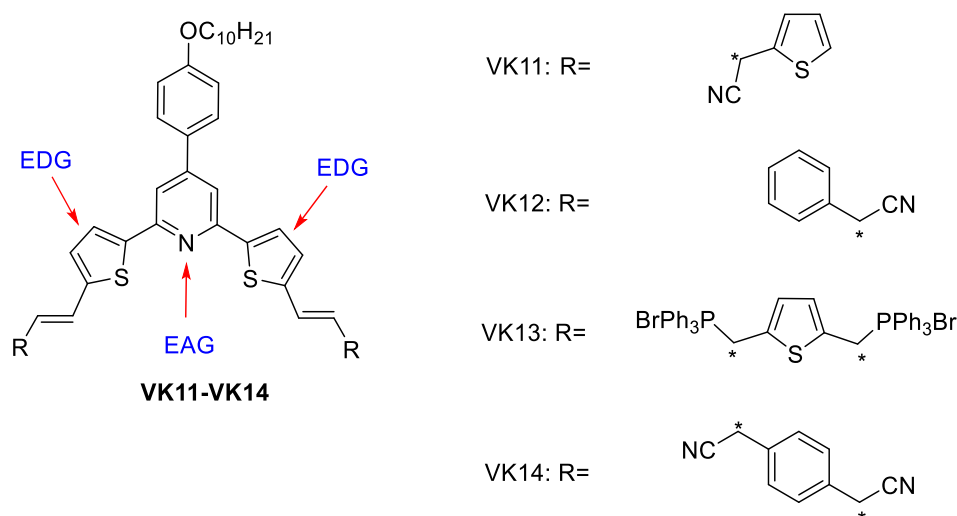


Figure 1.37

(v) Design of molecules (**VK15**–**VK18**) of series–5

Similar to thiophene, another excellent electron donor is propeller shaped triphenylamine moiety, possessing a continuous conjugation between the central nitrogen atom and peripheral phenyl groups (Jana and Ghorai 2012). In addition, it has a high triplet energy of 3.04 eV and possesses good hole transporting property (Jiang et al. 2009; Sonntag et al. 2005; Tong et al. 2007). The compounds containing carbazole, another electron donating group, also have attracted much attention due to their good charge-transport function, high thermal stability, solubility, moderately high

oxidation potential and extended glassy state (Liaw et al. 2009; Yook and Lee 2014). In this series, two sets of four, symmetric, novel star-shaped molecules (**VK15–VK18**) were designed. In one set (**VK15** and **VK16**) the central pyridine core (served as electron acceptor) was connected to terminal triphenylamine (**VK15**)/carbazole (**VK16**) moieties (served as electron donors) through thiophene (served as π -linker), which provided a D– π –A– π –D structural configuration to the system, whereas, in another set (**VK17** and **VK18**), the central triphenylamine (**VK17**)/carbazole (**VK18**) moiety was connected to the peripheral thiophene–pyridine–thiophene unit (D–A– π) to provide D–A– π –D– π –A–D configuration. The design strategy for the compounds **VK15–VK18** is shown in **Figure 1.38**.

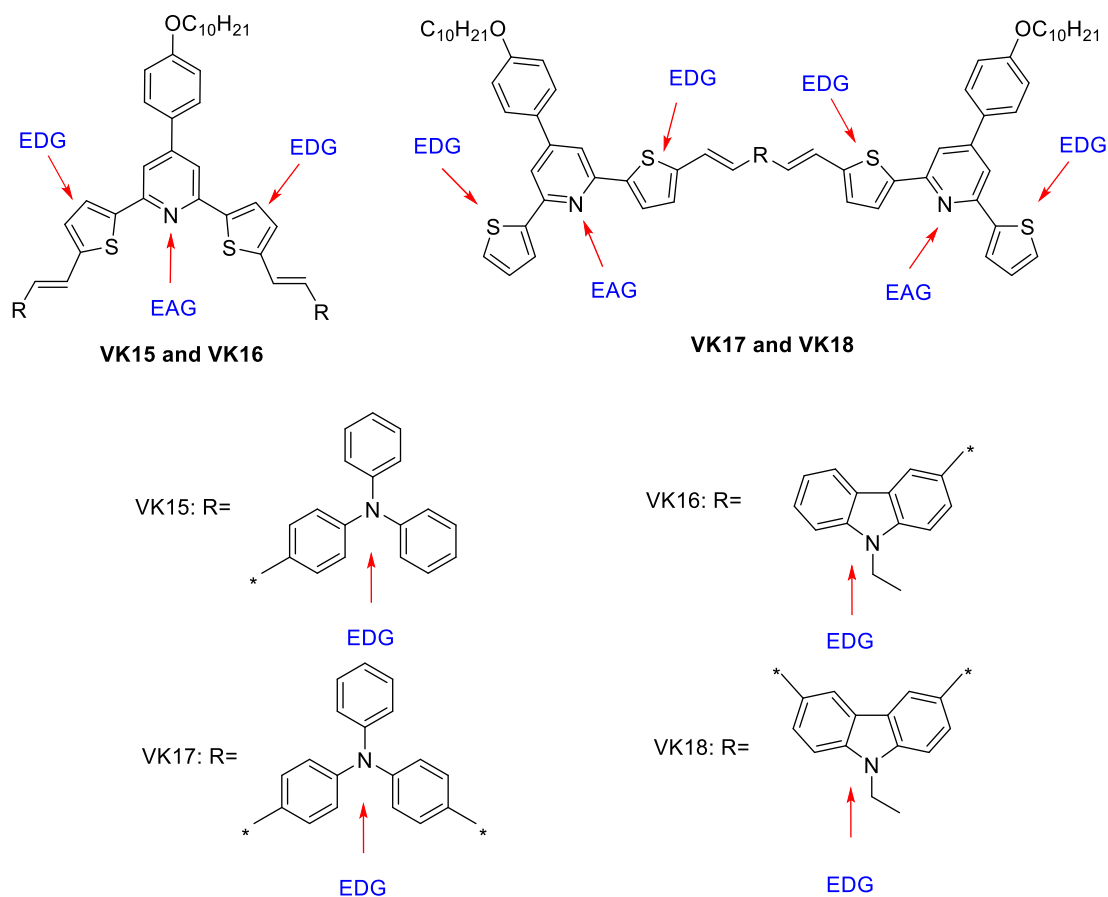


Figure 1.38

1.10 THESIS FRAMEWORK

The present research work has been presented in the thesis in four chapters, details of each are given below:

Chapter 1 introduces the conjugated polymers/molecules, D–A approach, followed by a brief account on NLO, its theory and various processes involved with it. It also gives a brief description on OLED, its working principle and parameters to characterize the device. The chapter also includes a brief literature review pertaining to the work carried out. The scope and objectives of the research work are presented in this chapter and finally, it consists of the design strategy for five new series comprising sixteen D–A–D type conjugated molecules and two D–A–D type conjugated polymers.

Chapter 2 is on the experimental section which includes: the materials and methods used in the work, experimental procedure, synthetic scheme of compounds and a brief description on characterization techniques used. This chapter also includes important equations used in the work.

Chapter 3 presents the results and discussion of five series of compounds which includes: spectral elucidation of all the intermediates and final compounds; the photophysical and electrochemical studies; theoretical calculations; thermal properties and the third-order NLO properties of the final compounds. It also discusses the OLED device fabrication and performance of **VK15** as a proof of concept and also throws light upon the important findings from the experimental data.

Chapter 4 summarizes the present research work and lists the conclusions. It also includes the scope for further work.

CHAPTER 2

EXPERIMENTAL SECTION

2.1 EXPERIMENTAL

In accordance with the design strategy of five series of D–A–D conjugated systems discussed in the previous chapter, the compounds were synthesized utilizing appropriate multistep synthetic protocols. The detailed experimental procedure for the synthesis of newly designed compounds and the characterization details of the intermediates and the final compounds are discussed herein.

2.1.1 Materials and methods

All the reagents and the starting materials were procured from commercial suppliers and used as received unless specially stated. The chemicals used were thiophene-2-carboxylic acid (Sigma Aldrich, 99%), thiosemicarbazide (Alfa Aesar, 98%), phenacyl bromide (Spectrochem, 99%), thiophene-2-acetonitrile (Sigma Aldrich, 97%), phenylacetonitrile (Spectrochem, 98%), rhodanine-3-acetic acid (Alfa Aesar, 98%), 4-nitrophenacyl bromide (Spectrochem, 95%), iron powder-325 mesh (Sigma Aldrich, 97%), 1-pyrenecarboxaldehyde (Sigma Aldrich, 99%), 9-anthracenecarboxaldehyde (Sigma Aldrich, 97%) and 4-(diphenylamino)benzaldehyde (Alfa Aesar, 98%), 4-hydroxyphenacyl chloride (Spectrochem, 95%), potassium carbonate (K_2CO_3) (Loba Chemie, 99%), 1-bromodecane (Sigma Aldrich, 98%), 2,5-dimethylthiophene (Sigma Aldrich, 98%), 5-methyl-2-thiophenecarboxylic acid (Sigma Aldrich, 99%), N-bromosuccinimide (NBS) (Loba Chemie, 98%), Azobisisobutyronitrile (AIBN) (Spectrochem, 98%), triphenylphosphine (Sigma Aldrich, 99%), thionyl chloride ($SOCl_2$) (Loba Chemie, 99%), hydrazine hydrate (Loba Chemie, 99%), dithiooxamide (Sigma Aldrich, 97%), 2-acetylthiophene (Avra Synthesis Pvt. Ltd, 95%), 4-hydroxybenzaldehyde (Loba Chemie, 98%), ammonium acetate (Merck, 97%), 1,4-phenylenediacetonitrile (Alfa Aesar, 97%), sodium borohydride ($NaBH_4$) (Spectrochem, 96%), triphenylphosphine hydrobromide ($PPh_3.HBr$) (Sigma Aldrich, 97%), 9H-carbazole (Loba Chemie, 95%), 1-bromoethane (Sigma Aldrich, 98%), sodium hydride (NaH) (Sigma Aldrich, 60% dispersion in mineral oil) and bis(4-formylphenyl)phenylamine (Sigma Aldrich, 95%). All the solvents were of analytical grade and dried prior to the usage. All the reactions were carried out under inert conditions in round bottomed (RB) flask and the progress of the reaction was monitored using thin layer chromatography (TLC) technique which was performed on pre-coated aluminium sheets with 60 F254 silica gel (Merck KGaA). The

developed TLCs were observed under a short/long wavelength UV–Vis lamp. All the synthesized intermediates as well as final compounds were purified either by column chromatography or by recrystallization using suitable solvent system.

2.1.2 Synthesis of molecules (VK1–VK3) of series–1

2.1.2.1 Synthesis

The molecular structures and the synthetic route for **VK1–VK3** are shown in **Figure 2.1** and **Scheme 2.1**, respectively. The synthesis of molecules **VK1–VK3** includes four steps. In the first step, the intermediate **3** was synthesized *via* a reaction between the commercially available thiophene-2-carboxylic acid and thiosemicarbazide in the presence of phosphorous oxychloride (POCl_3). The intermediate **4** was synthesized by the reaction between the intermediate **3** and phenacyl bromide followed by cyclization, which was then subjected to Vilsmeier–Haack formylation to obtain the intermediate **5**. In the final step, the precursor **5** was subjected to the well-known Knoevenagel condensation reaction with active methylene compounds, *viz.*, thiophene-2-acetonitrile, phenylacetonitrile and rhodanine-3-acetic acid, to achieve the target compounds **VK1**, **VK2** and **VK3**, respectively.

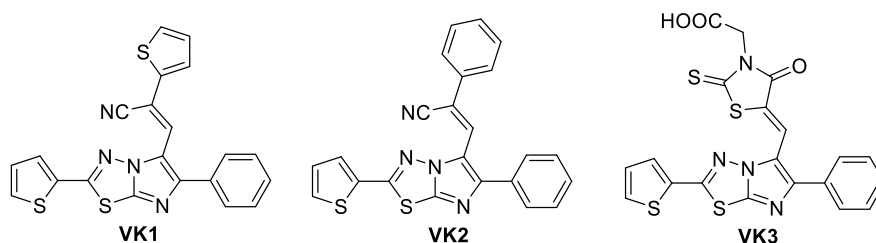
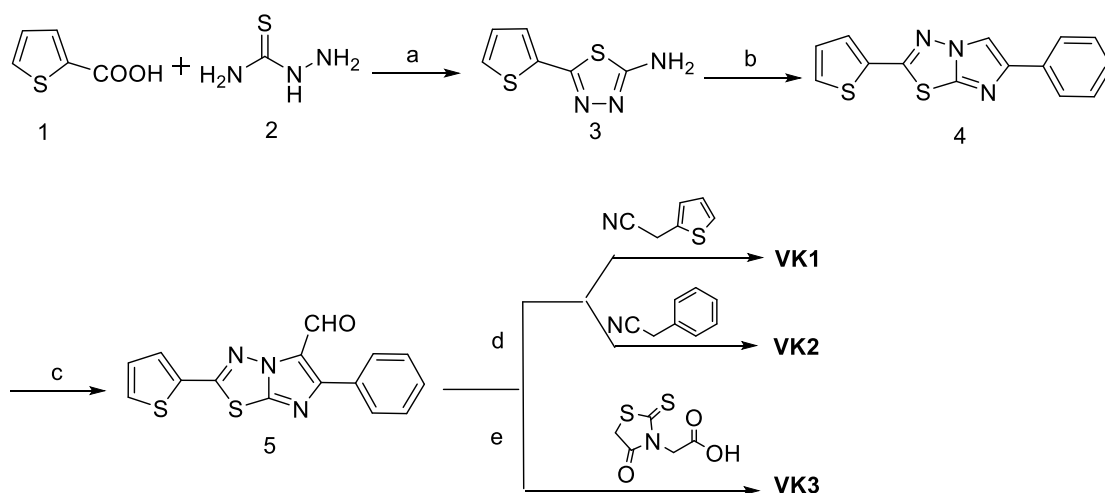


Figure 2.1 Molecular structures of **VK1**, **VK2** and **VK3**.



Scheme 2.1. Synthetic route for molecules **VK1–VK3**. Reagents and reaction conditions: (a) POCl₃, 75°C, 2 h, yield: 94%; (b) Phenacyl bromide, ethanol, 85–90°C, 24 h, yield: 89%; (c) POCl₃, DMF 60–65°C, 6 h, yield: 86%; (d) NaOC₂H₅, C₂H₅OH, RT, yield: 73–76%; (e) Piperidine, 80–85°C, 8 h, yield: 70%.

2.1.2.2 The detailed experimental procedure

Synthesis of 5-(thiophen-2-yl)-1,3,4-thiadiazol-2-amine (3)

Thiophene-2-carboxylic acid (**1**) (9.0 g, 70.23 mmol) and thiosemicarbazide (**2**) (6.4 g, 70.23 mmol) were taken in a clean RB flask, followed by the addition of POCl₃ (10.0 mL). The mixture was heated for 2 h; then, the mixture was cooled down to room temperature (RT) and quenched using ice cold water. It was then basified with a 20% sodium hydroxide (NaOH) solution, and the obtained solid was filtered and dried. The crude product was purified by column chromatography (60–120 mesh silica) using dichloromethane (DCM) as an eluent to obtain intermediate **3** as a white colored solid (12.08 g, yield: 94%). ESI-MS (*m/z*) calcd. for C₆H₅N₃S₂: 182.99, found: 184.0 [M+H]⁺; ¹H NMR (400 MHz, DMSO-*d*₆) δ (ppm): 7.60 (d, *J* = 5.2 Hz, 1H, Ar-H), 7.42 (s, 2H, Ar-NH₂), 7.38 (d, *J* = 4.4 Hz, 1H, Ar-H), 7.11–7.09 (m, 1H, Ar-H); ¹³C NMR (100 MHz, DMSO-*d*₆) δ (ppm): 168.5, 151.0, 133.7, 128.4, 128.2, 128.0; Anal. calcd. for C₆H₅N₃S₂: C, 39.33; H, 2.75; N, 22.93; S, 34.99; found: C, 39.29; H, 2.78; N, 22.89; S, 34.97.

Synthesis of 6-phenyl-2-(thiophen-2-yl)imidazo[2,1-b][1,3,4]thiadiazole (4)

To a solution of intermediate **3** (6.0 g, 32.74 mmol) in ethanol (C₂H₅OH) (20 mL), phenacyl bromide (7.8 g, 39.29 mmol) was added, followed by refluxing for 24h.

Excess C₂H₅OH was removed under reduced pressure, and the resulting solid was suspended in water and refluxed for 4 h. After this, the product was neutralized with 10% sodium carbonate (Na₂CO₃). The obtained solid product was filtered, dried and purified by column chromatography using a mixture of petroleum ether (pet ether): ethyl acetate (8: 2, v/v) as an eluent to achieve intermediate **4** as a brown colored solid (8.25 g, yield: 89%). ESI-MS (*m/z*) calcd. for C₁₄H₉N₃S₂: 283.02, found: 284.00 [M+H]⁺; ¹H NMR (400 MHz, CDCl₃) δ (ppm): 8.01 (s, 1H, Ar-H), 7.99 (d, *J* = 8.0 Hz, 1H, Ar-H), 7.82 (d, *J* = 8.0 Hz, 2H, Ar-H), 7.61–7.40 (m, 4H, Ar-H), 7.33–7.14 (m, 1H, Ar-H); ¹³C NMR (100 MHz, CDCl₃) δ (ppm): 155.8, 146.1, 144.6, 133.1, 132.3, 129.9, 129.2, 128.8, 128.1, 127.8, 125.1, 109.4; Anal. calcd. for C₁₄H₉N₃S₂: C, 59.34; H, 3.20; N, 14.83; S, 22.63; found: C, 59.25; H, 3.31; N, 14.76; S, 22.71.

Synthesis of 6-phenyl-2-(thiophen-2-yl)imidazo[2,1-*b*][1,3,4]thiadiazole-5-carbaldehyde (5)

Freshly distilled N,N-dimethylformamide (DMF) (2.18 mL, 28.26 mmol) was taken in a two-necked RB flask and cooled down from 0 to –5°C. To this, POCl₃ (2.64 mL, 28.26 mmol) was added drop-wise followed by stirring for 15 min to obtain the Vilsmeier salt. The solution of intermediate **4** (4.0 g, 14.13 mmol) in DMF was added to the formed Vilsmeier salt, and the mixture was heated at 65°C for 6 h; after this, the mixture was quenched using ice cold water. The obtained solid was filtered, dried and purified by column chromatography using a mixture of ethyl acetate and pet ether (3:7, v/v) as an eluent to obtain intermediate **5** as a yellow solid (3.78 g, yield: 86%). ESI-MS (*m/z*) calcd. for C₁₅H₉N₃OS₂: 311.02, found: 312.00 [M+H]⁺; ¹H NMR (400 MHz, CDCl₃) δ (ppm): 10.11 (s, 1H, –CHO), 7.92–7.90 (m, 2H, Ar-H), 7.66–7.60 (m, 2H, Ar-H), 7.54–7.45 (m, 3H, Ar-H), 7.19–7.17 (m, 1H, Ar-H); ¹³C NMR (100 MHz, CDCl₃) δ (ppm): 177.4, 163.0, 157.8, 155.9, 149.9, 132.2, 131.6, 130.9, 130.0, 129.1, 128.8, 125.1, 124.2; Anal. calcd. for C₁₅H₉N₃OS₂: C, 57.86; H, 2.91; N, 13.50; S, 20.59; found: C, 57.79; H, 2.82; N, 13.62; S, 20.67.

Synthesis of (E)-3-(6-phenyl-2-(thiophen-2-yl)imidazo[2,1-*b*][1,3,4]thiadiazol-5-yl)-2-(thiophen-2-yl)acrylonitrile (VK1)

To a freshly prepared solution of sodium ethoxide (NaOC₂H₅) (89.3 mg, 8.11 mmol), thiophene-2-acetonitrile (0.40 mL, 3.85 mmol) was added slowly under stirring.

After 15 min of stirring, intermediate **5** (1.0 g, 3.21 mmol) was added and the reaction mixture was stirred at RT for 5 h. The precipitated solid was obtained by filtration, washed with C₂H₅OH and purified by column chromatography using a mixture of pet ether: ethyl acetate (9: 1, v/v) as an eluent to obtain **VK1** as a yellow solid (0.97 g, yield: 73%). ESI-MS (*m/z*) calcd. for C₂₁H₁₂N₄S₃: 416.02, found: 417.10 [M+H]⁺; ¹H NMR (400 MHz, CDCl₃) δ (ppm): 7.74–7.71 (m, 2H, Ar-H), 7.64–7.63 (m, 1H, Ar-H), 7.56 (d, *J* = 4.0 Hz, 1H, Ar-H), 7.51–7.47 (m, 2H, Ar-H), 7.44–7.41 (m, 3H, Ar-H), 7.34–7.33 (m, 1H, Ar-H), 7.16 (d, *J* = 8.0 Hz, 1H, Ar-H), 7.11 (d, *J* = 8.0 Hz, 1H, Ar-H); ¹³C NMR (100 MHz, CDCl₃) δ (ppm): 155.4, 149.0, 147.3, 139.3, 130.5, 129.5, 128.9, 128.7, 128.3, 128.2, 128.1, 127.4, 126.6, 119.0, 116.3, 107.6; Anal. calcd. for C₂₁H₁₂N₄S₃: C, 60.55; H, 2.90; N, 13.45; S, 23.09; found: C, 60.61; H, 2.98; N, 13.36; S, 23.01.

Synthesis of (Z)-2-phenyl-3-(6-phenyl-2-(thiophen-2-yl)imidazo[2,1-b][1,3,4]thiadiazol-5-yl)acrylonitrile (VK2)

Molecule **VK2** was synthesized following the above-mentioned procedure for **VK1**, using the precursors phenylacetonitrile (0.44 mL, 3.85 mmol) and intermediate **5** (1.0 g, 3.21 mmol) (yellow solid, 1.00 g, yield: 76%). ESI-MS (*m/z*) calcd. for C₂₃H₁₄N₄S₂: 410.07, found: 411.10 [M+H]⁺; ¹H NMR (400 MHz, CDCl₃) δ (ppm): 7.72 (d, *J* = 8.0 Hz, 4H, Ar-H), 7.64–7.63 (m, 1H, Ar-H), 7.58–7.55 (m, 2H, Ar-H), 7.49–7.38 (m, 6H, Ar-H), 7.17–7.14 (m, 1H, Ar-H); ¹³C NMR (100 MHz, CDCl₃) δ (ppm): 155.3, 149.0, 147.2, 134.2, 133.6, 132.3, 130.4, 129.4, 129.3, 129.1, 128.9, 128.6, 128.2, 128.1, 126.2, 126.1, 119.5, 117.2, 113.5; Anal. calcd. for C₂₃H₁₄N₄S₂: C, 67.29; H, 3.44; N, 13.65; S, 15.62; found: C, 67.35; H, 3.53; N, 13.55; S, 15.51.

Synthesis of (E)-2-(4-oxo-5-((6-phenyl-2-(thiophen-2-yl)imidazo[2,1-b][1,3,4]thiadiazol-5-yl)methylene)-2-thioxothiazolidin-3-yl)acetic acid (VK3)

A mixture of intermediate **5** (1.0g, 3.21 mmol) and rhodanine-3-acetic acid (0.61 g, 3.21 mmol) was taken in acetonitrile (CH₃CN) (10 mL). Piperidine (0.5 mL) was added to the mixture followed by refluxing for 8 h. After this, the solvent was evaporated and to the obtained residue, distilled water (20 mL) was added followed by neutralization using 10% hydrochloric acid (HCl). The suspended solid was filtered, dried and purified by column chromatography using a mixture of pet ether: ethyl acetate

(6: 4, v/v) as an eluent to obtain **VK3** as an orange solid (1.08 g, yield: 70%). ^1H NMR (400 MHz, $\text{DMSO}-d_6$) δ (ppm): 13.00 (s, 1H, $-\text{COOH}$), 8.03–8.02 (m, 1H, Ar–H), 7.96–7.95 (m, 1H, Ar–H), 7.76 (s, 1H, Ar–H), 7.69–7.67 (m, 2H, Ar–H), 7.58–7.49 (m, 3H, Ar–H), 7.31–7.29 (m, 1H, Ar–H), 4.70 (s, 1H, $-\text{CH}_2$). ^{13}C NMR (100 MHz, $\text{DMSO}-d_6$) δ (ppm): 194.7, 167.9, 167.4, 157.8, 153.3, 149.7, 144.5, 133.2, 132.3, 131.4, 129.9, 129.6, 129.5, 129.2, 119.4, 119.1, 118.3, 45.7; Anal. calcd. for $\text{C}_{20}\text{H}_{12}\text{N}_4\text{O}_3\text{S}_4$: C, 49.57; H, 2.50; N, 11.56; S, 26.46; found: C, 49.46; H, 2.58; N, 11.64; S, 26.38.

2.1.3 Synthesis of molecules (VK4–VK6) of series–2

2.1.3.1 Synthesis

The molecular structures and the synthetic pathways of three new molecules **VK4–VK6** are shown in **Figure 2.2** and **Scheme 2.2**, respectively. The intermediate **3**, synthesized in Series–1, was cyclized with 4-nitro phenacyl bromide to obtain intermediate **6**. Further, the intermediate **7** was synthesized by the reduction of intermediate **6** in the presence of iron powder. Finally, Schiff base condensation reactions of intermediate **7** with pyrene-1-carbaldehyde, anthracene-9-carbaldehyde and 4-(diphenylamino)benzaldehyde resulted in final compounds **VK4**, **VK5** and **VK6**, respectively.

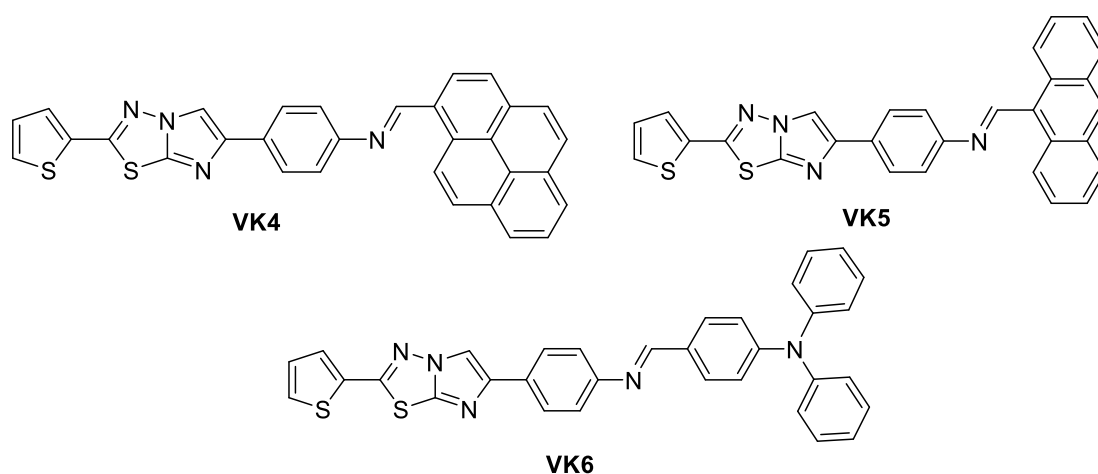
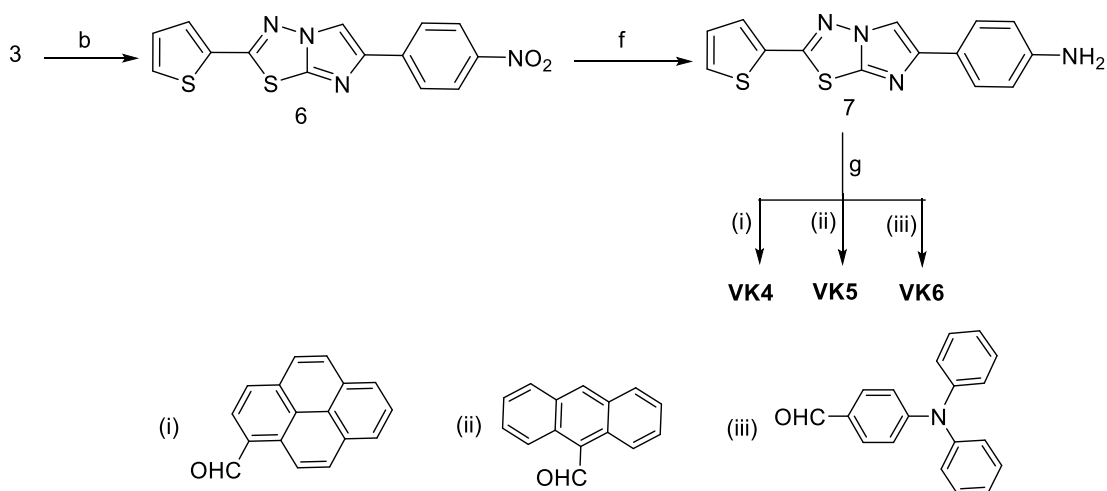


Figure 2.2 Molecular structures of **VK4**, **VK5** and **VK6**.



Scheme 2.2 Synthetic pathways of **VK4–VK6**. Reagents and reaction conditions: (b) 4-nitro phenacyl bromide, C₂H₅OH, 85–90°C, 24 h, yield: 82%; (f) Iron powder, NH₄Cl, CH₃OH, 60–65°C, 5 h, yield: 73%; (g) Substituted aldehydes, acetic acid, C₂H₅OH, RT, 12 h, yield: 72–82%.

2.1.3.2 The detailed experimental procedure

Synthesis of 6-(4-nitrophenyl)-2-(thiophen-2-yl)imidazo[2,1-b][1,3,4]thiadiazole (6)

The intermediate **6** was synthesized following the procedure for intermediate **4** using the precursors intermediate **3** (3.0 g, 16.37 mmol) and 4-nitro phenacyl bromide (4.8 g, 19.64 mmol) (a yellow solid, 4.40 g, yield: 82%). ESI-MS (*m/z*) calcd. for C₁₄H₈N₄O₂S₂: 328.01, found: 329.0 [M+H]⁺; Anal. calcd. for C₁₄H₈N₄O₂S₂: C, 51.21; H, 2.46; N, 17.06; S, 19.53; found: C, 51.10; H, 2.47; N, 17.01; S, 19.55.

Synthesis of 4-(2-(thiophen-2-yl)imidazo[2,1-b][1,3,4]thiadiazol-6-yl)aniline (7)

A mixture of intermediate **6** (3 g, 9.03 mmol), iron powder (2.5 g, 45.68 mmol) and ammonium chloride (NH₄Cl) (15 mL) was refluxed in methanol (CH₃OH) (10 mL) for 5 h. Later, it was filtered using celite and the filtrate was extracted using ethyl acetate. The solvent was evaporated by vacuum and the obtained solid was purified by column chromatography using a mixture of pet ether/ ethyl acetate (6:4) as mobile solvent to get **7** as yellow crystals (1.99 g, yield: 73%). ESI-MS (*m/z*) calcd. for C₁₄H₁₀N₄S₂: 298.38, found: 299.00 [M+H]⁺; ¹H NMR (400 MHz, CDCl₃) δ (ppm): 7.87 (s, 1H, Ar-H), 7.63 (d, *J* = 8.0 Hz, 2H, Ar-H), 7.53–7.51 (m, 2H, Ar-H), 7.16–7.13 (m, 1H, Ar-H), 6.74 (d, *J* = 8.0 Hz, 2H, Ar-H), 3.76 (s, 2H, –NH₂); ¹³C NMR (100 MHz, DMSO-*d*₆) δ (ppm): 154.7, 147.1, 146.1, 144.2, 132.7, 129.4, 128.7, 128.0,

126.3, 124.4, 115.2, 107.9; Anal. calcd. for C₁₄H₁₀N₄S₂: C, 56.36; H, 3.38; N, 18.78; S, 21.49; found: C, 56.17; H, 3.40; N, 18.69; S, 21.40.

Synthesis of (E)-N-(pyren-1-ylmethylene)-4-(2-(thiophen-2-yl)imidazo[2,1-b][1,3,4]thiadiazol-6-yl)aniline (VK4)

A mixture of intermediate **7** (0.5 g, 1.67 mmol) and pyrene-1-carbaldehyde (0.38 g, 1.67 mmol) was taken in dry C₂H₅OH (5 mL), a catalytic amount of acetic acid was added and stirred at RT for 12 h. The obtained solid was filtered, washed with cold C₂H₅OH and recrystallized from a mixture of CH₃OH and chloroform (CHCl₃) (1:1) to get compound **VK4** as yellow crystals (0.67 g, yield: 79%). ESI-MS (*m/z*) calcd. for C₃₁H₁₈N₄S₂: 510.10, found: 511.50 [M+H]⁺; ¹H NMR (400 MHz, CDCl₃) δ (ppm): 9.55 (s, 1H, Ar-H), 9.06–9.04 (m, 1H, Ar-H), 8.78–8.76 (m, 1H, Ar-H), 8.27–8.23 (m, 4H, Ar-H), 8.17–8.12 (m, 2H, Ar-H), 8.09–8.03 (m, 2H, Ar-H), 7.95–7.93 (m, 2H, Ar-H), 7.55–8.03 (m, 4H, Ar-H), 7.16 (d, *J* = 8.0 Hz, 1H, Ar-H); ¹³C NMR (100 MHz, CDCl₃) δ (ppm): 157.3, 151.0, 145.4, 143.7, 132.4, 131.5, 130.7, 130.2, 129.5, 128.6, 128.0, 128.0, 127.5, 127.0, 126.4, 125.8, 125.2, 125.1, 124.9, 124.9, 124.0, 123.9, 123.6, 121.5, 120.6, 108.2. Anal. calcd. for C₃₁H₁₈N₄S₂: C, 72.92; H, 3.55; N, 10.97; S, 12.56; found: C, 72.80; H, 3.51; N, 10.80; S, 12.58.

(E)-N-(anthracen-9-ylmethylene)-4-(2-(thiophen-2-yl)imidazo[2,1-b][1,3,4]thiadiazol-6-yl)aniline (VK5)

The above-mentioned procedure for **VK4** was followed to get molecule **VK5**, by reacting intermediate **7** (0.5 g, 1.67 mmol) with anthracene-9-carbaldehyde (yellow solid, 0.34 g, 1.67 mmol) (0.58 g, yield: 72%). ESI-MS (*m/z*) calcd. for C₂₉H₁₈N₄S₂: 486.10, found: 487.10 [M+H]⁺; ¹H NMR (400 MHz, CDCl₃) δ (ppm): 9.70 (s, 1H, Ar-H), 8.73–8.71 (m, 2H, Ar-H), 8.51 (s, 1H, Ar-H), 8.01–7.89 (m, 5H, Ar-H), 7.54–7.43 (m, 8H, Ar-H), 7.11–7.09 (m, 1H, Ar-H); ¹³C NMR (100 MHz, CDCl₃) δ (ppm): 158.3, 145.3, 130.3, 129.7, 129.7, 128.7, 128.0, 127.0, 126.3, 125.0, 124.4, 123.8, 120.6, 108.3. Anal. calcd. for C₂₉H₁₈N₄S₂: C, 71.58; H, 3.73; N, 11.51; S, 13.18; found: C, 71.52; H, 3.75; N, 11.26; S, 13.09.

(E)-N,N-diphenyl-4-(((4-(2-(thiophen-2-yl)imidazo[2,1-b][1,3,4]thiadiazol-6-yl)phenyl)imino)methyl)aniline (VK6)

Molecule **VK6** was synthesized following the procedure mentioned for **VK4**, by reacting intermediate **7** (0.5 g, 1.67 mmol) with 4-(diphenylamino)benzaldehyde (yellow solid, 0.45 g, 1.67 mmol) (0.76 g, yield: 82 %). ESI-MS (m/z) calcd. for $C_{33}H_{23}N_5S_2$: 553.14, found: 554.20 $[M+H]^+$; 1H NMR (400 MHz, $CDCl_3$) δ (ppm): 8.35 (s, 1H, Ar-H), 7.94 (s, 1H, Ar-H), 7.78 (d, $J = 8$ Hz, 2H, Ar-H), 7.68 (d, $J = 8.4$ Hz, 2H, Ar-H), 7.48 (s, 2H, Ar-H), 7.25–7.19 (m, 6H, Ar-H), 7.09–7.01 (m, 9H, Ar-H); ^{13}C NMR (100 MHz, $CDCl_3$) δ (ppm): 158.1, 150.7, 149.8, 145.9, 130.2, 128.9, 128.6, 128.4, 127.9, 127.0, 124.8, 124.4, 123.0, 120.5, 120.4, 108.1. Anal. calcd. for $C_{33}H_{23}N_5S_2$: C, 71.58; H, 4.19; N, 12.65; S, 11.58; found: C, 71.55; H, 4.20; N, 12.59; S, 11.53.

2.1.4 Synthesis of oligomers (VK7–VK10) of series-3

2.1.4.1 Synthesis

The thiophene substituted moiety, intermediate **8**, obtained by the cyclization of intermediate **3** with 4-hydroxy phenacyl chloride, was alkylated to yield intermediate **9**. In the alkylation step, the decyl chain was selected as alkylating agent to improve the solubility in different organic solvents. Later, intermediate **9** was formylated via well-known Vilsmeier-Haack reaction to achieve intermediate **10**. On the other hand, three different Wittig salts (intermediates **13**, **19** and **24**) with different conjugations were synthesized using multistep synthetic protocol as mentioned in **Scheme 2.3**. Finally, the intermediate **10** was reacted with dithiooxamide and the Wittig salts **13**, **19** and **24** to yield **VK9**, **VK7**, **VK8** and **VK10**, respectively. The chemical structures of **VK7–VK10** are shown in **Figure 2.3** and the synthetic pathway is depicted in **Scheme 2.3**.

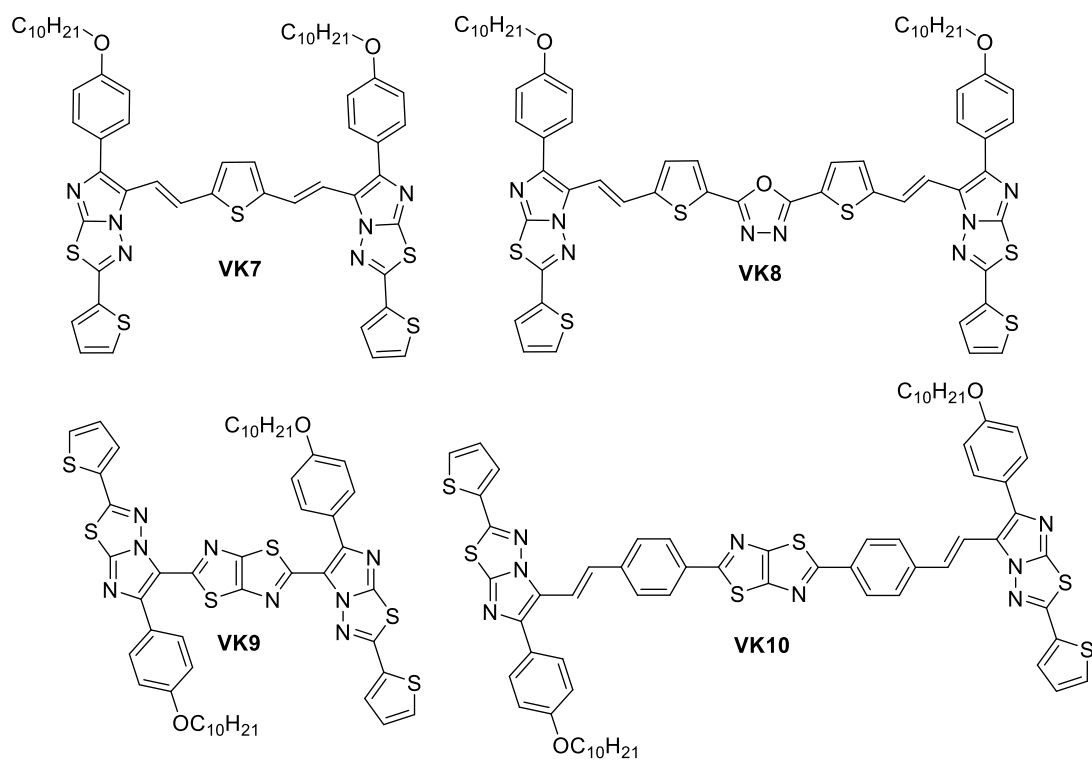
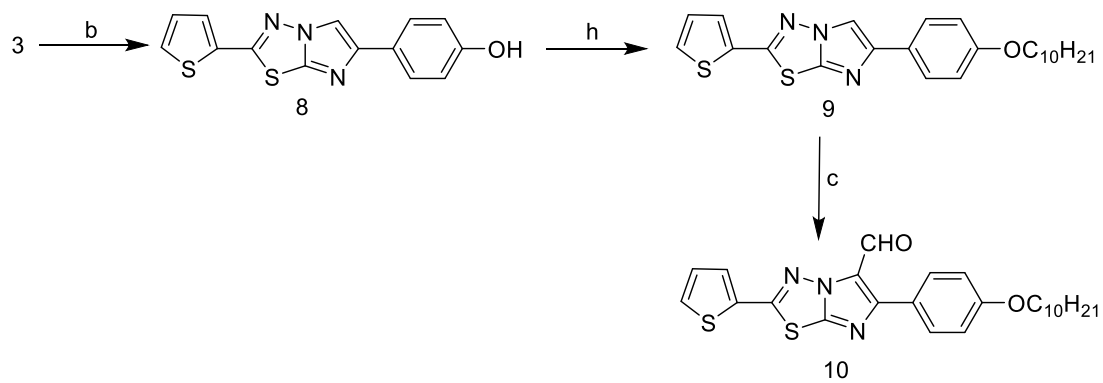
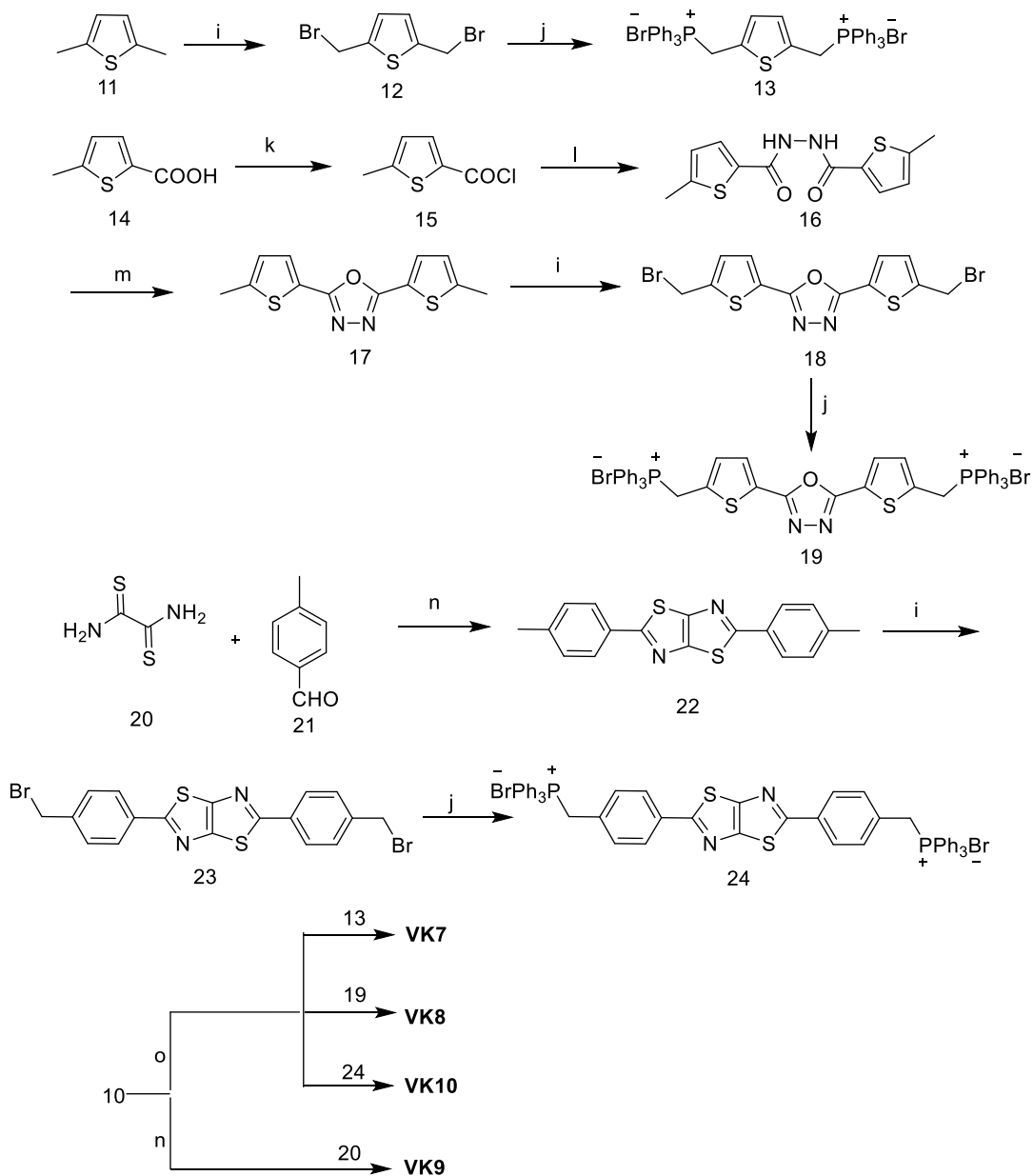


Figure 2.3 Chemical structures of four oligomers **VK7**, **VK8**, **VK9** and **VK10**.





Scheme 2.3 Synthetic pathways for the oligomers **VK7–VK10**. Reagents and reaction conditions: (b) 4-hydroxy phenacyl chloride, C_2H_5OH , $80^\circ C$, 24 h, yield: 89%; (h) 1–Bromodecane, K_2CO_3 , DMF, RT– $85^\circ C$, 12 h, yield: 91%; (i) NBS, AIBN, Benzene, $75^\circ C$, 2 h, yield: 64–74%; (j) Triphenylphosphine, DMF, $85^\circ C$, 12 h, yield: 78–90%; (k) $SOCl_2$, $0^\circ C$ –RT, 4 h, yield: 94%; (l) Hydrazine hydrate, triethylamine, NMP, RT, 8 h, yield: 94%; (m) $POCl_3$, $75^\circ C$, 3 h, yield: 78%; (n) DMF, $160^\circ C$, 5 h, yield: 41–55%; (o) C_2H_5ONa , $CHCl_3$, C_2H_5OH , RT, 12 h, yield: 82–85%.

2.1.4.2 The detailed experimental procedure

Synthesis of 2-(thiophen-2-yl)imidazo[2,1-b][1,3,4]thiadiazol-6-ol (8)

The intermediate **8** was synthesized following the procedure for intermediate **4** using intermediate **3** (3.0 g, 16.37 mmol) and 4-hydroxy phenacyl bromide (4.8 g, 19.64 mmol) (off-white solid, 7.27 g, yield: 89%). ESI-MS (m/z) calcd. for $C_{14}H_9N_3OS_2$: 299.02, found: 300.00 $[M+H]^+$; 1H NMR (400 MHz, DMSO- d_6) δ (ppm): 9.51 (s, 1H, -OH), 8.49 (s, 1H, Ar-H), 7.91–7.89 (m, 1H, Ar-H), 7.83–7.82 (m, 1H, Ar-H), 7.66 (d, $J = 8.0$ Hz, 2H, Ar-H), 7.26–7.24 (m, 1H, Ar-H), 6.78 (d, $J = 8.0$ Hz, 2H, Ar-H); ^{13}C NMR (100 MHz, DMSO- d_6) δ (ppm): 157.5, 155.3, 146.2, 143.9, 132.0, 131.5, 130.8, 129.1, 126.5, 125.0, 115.9, 109.4; Anal. calcd. for $C_{14}H_9N_3OS_2$: C, 56.17; H, 3.03; N, 14.04; S, 21.42; found: C, 56.02; H, 3.15; N, 14.16; S, 21.47.

Synthesis of 6-(decyloxy)-2-(thiophen-2-yl)imidazo[2,1-b][1,3,4]thiadiazole (9)

The intermediate **8** (4 g, 13.36 mmol) and anhydrous K_2CO_3 (5.53 g, 40.08 mmol) were added to DMF (20 mL) and the mixture was stirred at RT for 0.5 h. Later, 1-bromodecane (4.15 mL, 20.04 mmol) was added slowly to the above mixture and heated at 80°C for 12 h. The reaction mixture was quenched using cold distilled water. The obtained solid was filtered and purified using column chromatography using a mixture of pet ether/ethyl acetate (9:1, v/v) as eluent to get **9** as a yellow solid (5.34 g, yield: 91%). ESI-MS (m/z) calcd. for $C_{24}H_{29}N_3OS_2$: 439.18, found: 440.10 $[M+H]^+$; 1H NMR (400 MHz, $CDCl_3$) δ (ppm): 7.91 (s, 1H, Ar-H), 7.73 (d, $J = 8.0$ Hz, 2H, Ar-H), 7.54–7.52 (m, 2H, Ar-H), 7.15–7.13 (m, 1H, Ar-H), 6.94 (d, $J = 8.0$ Hz, 2H, Ar-H), 3.98 (t, $J = 6.8$ Hz, 2H, -OCH₂), 1.81–1.27 (m, 16H, -CH₂), 0.87 (t, $J = 7.2$ Hz, 3H, -CH₃); ^{13}C NMR (100 MHz, $CDCl_3$) δ (ppm): 158.9, 155.1, 146.4, 144.3, 132.5, 129.6, 128.9, 128.0, 126.3, 126.0, 114.7, 108.4, 68.0, 31.8, 29.5, 29.5, 29.4, 29.3, 29.2, 26.0, 22.6, 14.1; Anal. calcd. for $C_{24}H_{29}N_3OS_2$: C, 65.57; H, 6.65; N, 9.56; S, 14.58; found: C, 65.49; H, 6.67; N, 9.52; S, 14.64.

Synthesis of 6-(decyloxy)-2-(thiophen-2-yl)imidazo[2,1-b][1,3,4]thiadiazole-5-carbaldehyde (10)

The intermediate **10** was synthesized following the procedure mentioned for intermediate **5** using a freshly distilled DMF (1.05 mL, 13.64 mmol), $POCl_3$ (1.27 mL, 13.64 mmol) and intermediate **9** (3 g, 6.82 mmol) (a yellow solid, 2.74 g, yield: 86%).

ESI-MS (m/z) calcd. for $C_{25}H_{29}N_3O_2S_2$: 467.17, found: 468.10 $[M+H]^+$; 1H NMR (400 MHz, $CDCl_3$) δ (ppm): 10.09 (s, 1H, -CHO), 7.88 (d, $J = 8.0$ Hz, 2H, Ar-H), 7.64–7.59 (m, 2H, Ar-H), 7.18–7.16 (m, 1H, Ar-H), 7.01 (d, $J = 9.2$ Hz, 2H, Ar-H), 4.02 (t, $J = 6.8$ Hz, 2H, $-OCH_2$), 1.81–1.27 (m, 16H, $-CH_2-$), 0.87 (t, $J = 7.2$ Hz, 3H, $-CH_3$); ^{13}C NMR (100 MHz, $CDCl_3$) δ (ppm): 177.3, 160.7, 157.4, 155.8, 149.8, 131.6, 130.7, 130.4, 129.8, 128.1, 124.4, 123.6, 114.7, 68.1, 31.8, 29.5, 29.3, 29.1, 26.0, 22.6, 14.1; Anal. calcd. for $C_{25}H_{29}N_3O_2S_2$: C, 64.21; H, 6.25; N, 8.99; S, 13.71; found: C, 64.30; H, 6.19; N, 8.92; S, 13.78.

Synthesis of 2,5-bis(bromomethyl)thiophene (12)

To a solution of 2,5-dimethylthiophene (**11**) (1.01 mL, 8.91 mmol) in benzene (10 mL), NBS (3.33 g, 18.71 mmol) and AIBN (0.292 g, 1.78 mmol) were added and the mixture was refluxed for 2 h. The excess of solvent was evaporated under reduced pressure to yield a viscous fluid, to which distilled water (25 mL) was added to remove the excess of NBS; the product formed was extracted with ethyl acetate and dried using sodium sulphate (Na_2SO_4). Then, the ethyl acetate was evaporated to get **12** as brown oily liquid, which was used as such without further purification (1.75 g, yield: 74%). Anal. calcd. for $C_6H_6Br_2S$: C, 26.69; H, 2.24; S, 11.87; found: C, 26.75; H, 2.17; S, 11.79.

Synthesis of (thiophene-2,5-diylbis(methylene))bis(triphenylphosphonium) bromide (13)

The intermediate **12** (0.5 g, 1.86 mmol) and triphenylphosphine (1.07 g, 4.10 mmol) were mixed in anhydrous DMF (5 mL) and the mixture was refluxed for 12 h. Later, the mixture was cooled down to RT and slowly poured into ethyl acetate (25 mL) to obtain a solid product, which was filtered, washed with ethyl acetate and dried to get **13** as a brown colored solid (1.31 g, yield: 89%). 1H NMR (400 MHz, $CDCl_3$) δ (ppm): 7.76–7.59 (m, 30H, Ar-H), 6.70 (s, 2H, Ar-H), 5.53 (d, $J = 12.0$ Hz, 4H, Ar- CH_2-); ^{13}C NMR (100 MHz, $CDCl_3$) δ (ppm): 135.3, 134.1, 131.7, 130.1, 129.3, 117.6, 116.7; Anal. calcd. for $C_{42}H_{36}Br_2P_2S$: C, 63.49; H, 4.57; S, 4.03; found: C, 63.38; H, 4.53; S, 4.11.

Synthesis of 5-methylthiophene-2-carbonyl chloride (15)

5-methyl thiophene-2-carboxylic acid (**14**) (5 g, 35.21 mmol) was taken in a dry RB flask, to this SOCl₂ (2.54 mL, 35.21 mmol) was added slowly followed by the addition of DMF (0.2 mL). The stirring was performed at RT for 4 h. The excess SOCl₂ was removed under reduced pressure to obtain a colorless oily liquid **15**, which was used as such for the next step (5.28 g, yield: 94%). Anal. calcd. for C₆H₅ClOS: C, 44.87; H, 3.14; S, 19.96; found: C, 44.95; H, 3.19; S, 19.82.

Synthesis of 5-methyl-N'-(5-methylthiophene-2-carbonyl)thiophene-2-carbohydrazide (16)

To the solution of **15** (5 g, 31.13 mmol) in N-methyl-2-pyrrolidone (NMP), triethylamine (8 mL, 36.16 mmol) and hydrazine hydrate (~1.0 mL, 15.56 mmol) were added slowly at 0°C and the mixture was stirred at RT for 8 h. It was quenched using cold distilled water to precipitate the crude product, which was purified by column chromatography using a mixture of DCM/CH₃OH (9:1, v/v) as mobile solvent to get intermediate **16** as a white solid (8.22 g, yield: 94%). ESI-MS (*m/z*) calcd. for C₁₂H₁₂N₂O₂S₂: 280.03, found: 281.00 [M+H]⁺; ¹H NMR (400 MHz, DMSO-*d*₆) δ (ppm): 10.34 (s, 2H, -NH), 7.64 (d, *J* = 4.0 Hz, 2H, Ar-H), 6.88 (s, 2H, Ar-H), 2.48 (s, 6H, -CH₃); ¹³C NMR (100 MHz, DMSO-*d*₆) δ (ppm): 161.3, 146.1, 135.1, 129.7, 127.1, 15.6; Anal. calcd. for C₁₂H₁₂N₂O₂S₂: C, 51.41; H, 4.31; N, 9.99; S, 22.87; found: C, 51.50; H, 4.35; N, 9.88; S, 22.95.

Synthesis of 2,5-bis(5-methylthiophen-2-yl)-1,3,4-oxadiazole (17)

The intermediate **16** (2 g, 7.13 mmol) in POCl₃ (8 mL) was refluxed for 4 h. Later, the mixture was cooled down to RT and quenched using ice cold water to precipitate the crude product. The product was filtered and purified by column chromatography using a mixture of pet ether/ethyl acetate (7:3, v/v) as mobile solvent to get intermediate **17** as a brown solid (1.45 g, yield: 78%). ESI-MS (*m/z*) calcd. for C₁₂H₁₀N₂OS₂: 262.02, found: 263.00 [M+H]⁺; ¹H NMR (400 MHz, DMSO-*d*₆) δ (ppm): 7.65 (s, 2H, Ar-H), 6.99 (s, 2H, Ar-H), 2.52 (s, 6H, -CH₃); ¹³C NMR (100 MHz, DMSO-*d*₆) δ (ppm): 159.8, 146.1, 131.0, 127.7, 121.9, 15.5; Anal. calcd. for C₁₂H₁₀N₂OS₂: C, 54.94; H, 3.84; N, 10.68; S, 24.44; found: C, 54.86; H, 3.90; N, 10.63; S, 24.53.

Synthesis of 2,5-bis(5-(bromomethyl)thiophen-2-yl)-1,3,4-oxadiazole (18)

A mixture of **17** (1 g, 3.81 mmol), NBS (1.42 g, 8.00 mmol) and AIBN (0.125 g, 0.76 mmol), was refluxed in benzene (10 mL) for 2 h. The excess of solvent was evaporated to get brown colored fluid, to which distilled water (25 mL) was added and stirred at RT for 0.5 h. The obtained solid product was filtered and recrystallized using a mixture of ethyl acetate/CHCl₃ (1:1) to obtain intermediate **18** as a brown colored solid (1.08 g, yield: 68%). ¹H NMR (400 MHz, DMSO-*d*₆) δ (ppm): 7.73 (d, *J* = 4.0 Hz, 2H, Ar-H), 7.38 (d, *J* = 4.0 Hz, 2H, Ar-H), 5.13 (s, 4H, -CH₂Br); ¹³C NMR (100 MHz, DMSO-*d*₆) δ (ppm): 160.0, 146.7, 130.8, 130.4, 125.2, 27.4; Anal. calcd. for C₁₂H₈Br₂N₂OS₂: C, 34.31; H, 1.92; N, 6.67; S, 15.26; found: C, 34.40; H, 1.86; N, 6.74; S, 15.18.

Synthesis of 2,5-bis(5-((bromotriphenylphosphoranyl)methyl)thiophen-2-yl)-1,3,4-oxadiazole (19)

The intermediate **19** was synthesized following the procedure mentioned for intermediate **13** using intermediate **18** (0.5 g, 1.19 mmol) and triphenylphosphine (0.68 g, 2.61 mmol) (brown solid, 1.01 g, yield: 90%). ¹H NMR (400 MHz, DMSO-*d*₆) δ (ppm): 7.93–7.68 (m, 30H, Ar-H), 7.14 (s, 4H, Ar-H), 5.29 (d, *J* = 16 Hz, 4H, Ar-CH₂-); ¹³C NMR (100 MHz, DMSO-*d*₆) δ (ppm): 162.7, 159.5, 135.9, 134.3, 132.5, 130.9, 125.3, 118.2, 117.3, 36.2; Anal. calcd. for C₄₈H₃₈Br₂N₂OP₂S₂: C, 61.03; H, 4.05; N, 2.97; S, 6.79; found: C, 61.12; H, 4.16; N, 2.86; S, 6.65.

*Synthesis of 2,5-di-*p*-tolylthiazolo[5,4-*d*]thiazole (22)*

Dithiooxamide (**20**) (1.0 g, 8.32 mmol) and *p*-tolualdehyde (**21**) (2 g, 16.64 mmol) were dissolved in dry DMF (15 mL). The mixture was refluxed for 6 h, which later, was cooled to RT while intermediate **22** started crystallizing out. The crystals were separated by filtration and purified by column chromatography using a mixture of pet ether/ ethyl acetate (9:1, v/v) to get compound **22** as yellow crystals (2.95 g, yield: 55%). ESI-MS (*m/z*) calcd. for C₁₈H₁₄N₂S₂: 322.06, found: 323.00 [M+H]⁺; ¹H NMR (400 MHz, DMSO-*d*₆) δ (ppm): 7.91 (d, *J* = 8.0 Hz, 4H, Ar-H), 7.36 (d, *J* = 8.0 Hz, 4H, Ar-H), 2.37 (s, 6H, -CH₃); Anal. calcd. for C₁₈H₁₄N₂S₂: C, 67.05; H, 4.38; N, 8.69; S, 19.89; found: C, 67.14; H, 4.32; N, 8.58; S, 19.97.

*Synthesis of 2,5-bis(4-(bromomethyl)phenyl)thiazolo[5,4-*d*]thiazole (23)*

The intermediate **23** was synthesized following the procedure of intermediate **18** using intermediate **22** (0.6 g, 1.86 mmol), NBS (0.695 g, 3.90 mmol) and AIBN (0.061 g, 0.37 mmol) (yellow solid, 0.57 g, yield: 64%). ¹H NMR (400 MHz, CDCl₃) δ (ppm): 7.89 (d, *J* = 8.0 Hz, 2H, Ar-H), 7.69 (d, *J* = 8.4 Hz, 2H, Ar-H), 7.51–7.49 (m, 3H, Ar-H), 7.29 (d, *J* = 8.0 Hz, 1H, Ar-H), 4.53 (s, 4H, Ar-CH₂Br); Anal. calcd. for C₁₈H₁₂Br₂N₂S₂: C, 45.02; H, 2.52; N, 5.83; S, 13.35; found: C, 45.13; H, 2.44; N, 5.89; S, 13.42.

Synthesis of 2,5-bis(4-((bromotriphenylphosphoranyl) methyl) phenyl) thiazolo[5,4-*d*]thiazole (24)

The intermediate **24** was synthesized following the procedure of intermediate **19** using intermediate **23** (0.5 g, 1.04 mmol) and triphenylphosphine (0.60 g, 2.29 mmol) (brown solid, 0.81 g, yield: 78%). ¹H NMR (400 MHz, DMSO-*d*₆) δ (ppm): 7.93–7.89 (m, 10H, Ar-H), 7.76–7.68 (m, 23H, Ar-H), 7.36 (d, *J* = 8.0 Hz, 1H, Ar-H), 7.14 (d, *J* = 8.0 Hz, 4H, Ar-H), 5.29 (d, *J* = 16.0 Hz, 4H, Ar-CH₂-); ¹³C NMR (100 MHz, DMSO-*d*₆) δ (ppm): 168.4, 151.0, 135.6, 134.5, 134.4, 133.3, 132.3, 130.7, 130.6, 126.9, 118.4, 117.6; Anal. calcd. for C₅₄H₄₂Br₂N₂P₂S₂: C, 64.55; H, 4.21; N, 2.79; S, 6.38; found: C, 64.48; H, 4.16; N, 2.83; S, 6.44.

2,5-bis((*E*)-2-(6-(4-(decyloxy)phenyl)-2-(thiophen-2-yl)imidazo[2,1-*b*][1,3,4]thiadiazol-5-yl)vinyl)thiophene (VK7)

The intermediates **13** (0.5 g, 0.52 mmol) and **10** (0.49 g, 1.05 mmol) were dissolved in a mixture of CHCl₃ and C₂H₅OH (1:1), to which, a freshly prepared solution of C₂H₅ONa (89.3 mg, 8.11 mmol in 3 mL of ethanol) was added drop wise in argon atmosphere and the mixture was stirred at RT for 12 h. The excess of solvent was removed under reduced pressure and the residue was purified by column chromatography using a mixture of pet ether/ethyl acetate (8:2, v/v) to get the compound **VK7** as an orange colored solid (0.52 g, yield: 83%). MALDI-TOF-MS (*m/z*) calcd. for C₅₆H₆₂N₆O₂S₅: 1011.452, found: 1012.346 [M+H]⁺; ¹H NMR (400 MHz, CDCl₃) δ (ppm): 7.89 (s, 1H, Ar-H), 7.85 (s, 1H, Ar-H), 7.68 (d, *J* = 8.0 Hz, 4H, Ar-H), 7.60–7.56 (m, 4H, Ar-H), 7.19–7.16 (m, 2H, Ar-H), 7.11 (s, 1H, Ar-H), 7.07 (s, 1H, Ar-H), 7.05–7.03 (m, 6H, Ar-H), 4.03 (t, *J* = 8.0 Hz, 4H, -OCH₂), 1.86–1.81 (m, 4H, -CH₂-), 1.79–1.47 (m, 7H, -CH₂-), 1.34–1.28 (m, 21H, -CH₂-), 0.88 (t, *J* =

8.0 Hz, 6H, -CH₃); ¹³C NMR (100 MHz, CDCl₃) δ (ppm): 159.0, 154.8, 145.2, 145.1, 142.2, 132.6, 129.7, 129.4, 129.0, 128.0, 127.1, 126.7, 121.7, 121.5, 114.8, 113.7, 68.1, 31.9, 29.6, 29.5, 29.4, 29.3, 26.1, 22.6, 14.1; Anal. calcd. for C₅₆H₆₂N₆O₂S₅: C, 66.50; H, 6.18; N, 8.31; S, 15.85; found: C, 66.58; H, 6.09; N, 8.43; S, 15.97.

2,5-bis(5-((E)-2-(6-(4-(decyloxy)phenyl)-2-(thiophen-2-yl)imidazo[2,1-b][1,3,4]thiadiazol-5-yl)vinyl)thiophen-2-yl)-1,3,4-oxadiazole (VK8)

The compound **VK8** was synthesized following the same procedure for **VK7** using intermediate **19** (0.5 g, 0.63 mmol) and intermediate **10** (0.59 g, 1.26 mmol) (orange solid, 0.52 g, yield: 85%). MALDI-TOF-MS (*m/z*) calcd. for C₆₂H₆₄N₈O₃S₆: 1160.343, found: 1159.100 [M]⁺; ¹H NMR (400 MHz, CDCl₃) δ (ppm): 7.89 (s, 1H, Ar-H), 7.85 (s, 2H, Ar-H), 7.80–7.60 (m, 3H, Ar-H), 7.57–7.48 (m, 2H, Ar-H), 7.42–7.39 (m, 3H, Ar-H), 7.22–7.15 (m, 3H, Ar-H), 7.14–7.00 (m, 3H, Ar-H), 6.96–6.93 (m, 2H, Ar-H), 6.89–6.78 (m, 2H, Ar-H), 6.75–6.72 (m, 1H, Ar-H), 4.06 (t, *J* = 8.0 Hz, 2H, -OCH₂), 3.95 (t, *J* = 8.0 Hz, 2H, -OCH₂), 1.86–1.83 (m, 4H, -CH₂-), 1.76–1.58 (m, 5H, -CH₂-), 1.50–1.42 (m, 4H, -CH₂-), 1.30–1.27 (m, 19H, -CH₂-), 0.88 (t, *J* = 8.0 Hz, 6H, -CH₃); ¹³C NMR (100 MHz, CDCl₃) δ (ppm): 160.0, 159.9, 158.9, 154.6, 148.3, 145.8, 144.8, 132.5, 128.5, 127.8, 126.8, 126.3, 124.7, 121.1, 119.7, 118.0, 116.6, 114.9, 114.5, 68.1, 31.8, 29.5, 29.3, 29.2, 26.0, 22.6, 14.0; Anal. calcd. for C₆₂H₆₄N₈O₃S₆: C, 64.11; H, 5.55; N, 9.65; S, 16.56; found: C, 64.23; H, 5.42; N, 9.58; S, 16.67.

Synthesis of 2,5-bis(6-(4-(decyloxy)phenyl)-2-(thiophen-2-yl)imidazo[2,1-b][1,3,4]thiadiazol-5-yl)thiazolo[5,4-d]thiazole (VK9)

The oligomer **VK9** was synthesized following the procedure for intermediate **22** using the precursors intermediate **10** (0.5 g, 1.06 mmol) and intermediate **20** (0.064 g, 0.53 mmol) (yellow crystals, 0.44 g, yield: 41%). MALDI-TOF-MS (*m/z*) calcd. for C₅₂H₅₆N₈O₂S₆: 1016.285, found: 1016.989 [M+H]⁺; ¹H NMR (400 MHz, CDCl₃) δ (ppm): 7.96 (d, *J* = 8.0 Hz, 4H, Ar-H), 7.65 (d, *J* = 4.0 Hz, 2H, Ar-H), 7.60 (d, *J* = 8.0 Hz, 2H, Ar-H), 7.20–7.18 (m, 2H, Ar-H), 6.99 (d, *J* = 8.0 Hz, 4H, Ar-H), 4.03 (t, *J* = 8.0 Hz, 4H, -OCH₂), 1.84–1.80 (m, 5H, -CH₂-), 1.50–1.46 (m, 4H, -CH₂-), 1.38–1.28 (m, 23H, -CH₂-), 0.87 (t, *J* = 8.0 Hz, 6H, -CH₃); ¹³C NMR (100 MHz, CDCl₃) δ (ppm): 159.7, 156.2, 155.8, 147.2, 145.4, 132.2, 130.4, 130.2, 129.4, 129.2, 128.1, 125.7,

118.7, 114.2, 68.0, 31.8, 29.5, 29.4, 29.2, 26.0, 22.6, 14.0; Anal. calcd. for C₅₂H₅₆N₈O₂S₆: C, 61.39; H, 5.55; N, 11.01; S, 18.91; found: C, 61.48; H, 5.51; N, 11.13; S, 18.86.

Synthesis of 2,5-bis(4-((E)-2-(6-(4-(decyloxy)phenyl)-2-(thiophen-2-yl)imidazo[2,1-b][1,3,4]thiadiazol-5-yl)vinyl)phenyl)thiazolo[5,4-d]thiazole (VK10)

The compound **VK10** was synthesized following the procedure mentioned for **VK7**, using intermediates **24** (yellow solid, 0.5 g, 0.497 mmol) and **10** (0.46 g, 0.995 mmol) (0.49 g, yield: 82%). MALDI-TOF-MS (*m/z*) calcd. for C₆₈H₆₈N₈O₂S₆: 1221.706, found: 1222.723 [M+H]⁺; ¹H NMR (400 MHz, CDCl₃) δ (ppm): 7.97 (d, *J* = 8.0 Hz, 4H, Ar-H), 7.83 (s, 1H, Ar-H), 7.79 (s, 1H, Ar-H), 7.68 (d, *J* = 8.0 Hz, 4H, Ar-H), 7.60–7.58 (m, 7H, Ar-H), 7.38 (s, 3H, Ar-H), 7.20–7.18 (m, 2H, Ar-H), 7.04 (d, *J* = 8.0 Hz, 4H, Ar-H), 4.04 (t, *J* = 8.0 Hz, 4H, -OCH₂), 1.87–1.80 (m, 4H, -CH₂-), 1.52–1.46 (m, 5H, -CH₂-), 1.31–1.25 (m, 23H, -CH₂-), 0.89 (t, *J* = 8.0 Hz, 6H, -CH₃); ¹³C NMR (100 MHz, CDCl₃) δ (ppm): 159.1, 145.4, 132.6, 129.6, 129.5, 128.9, 128.8, 128.4, 128.0, 126.8, 126.6, 126.2, 125.8, 121.8, 115.6, 114.7, 114.4, 68.1, 31.8, 29.6, 29.5, 29.3, 29.2, 26.0, 22.6, 14.0; Anal. calcd. for C₆₈H₆₈N₈O₂S₆: C, 66.85; H, 5.61; N, 9.17; S, 15.75; found: C, 66.93; H, 5.70; N, 9.06; S, 15.68.

2.1.5 Synthesis of compounds (VK11–VK14) of series-4

2.1.5.1 Synthesis

The synthetic route for **VK11–VK14** are depicted in **Scheme 2.4** and their structures are shown in **Figure 2.4**. In the first step, the green synthesis of intermediate **27** involves one-pot multicomponent reaction under solvent-free (neat) condition via microwave irradiation. The intermediate **27** was alkylated in the next step to improve the solubility in different organic solvents using 1-bromodecane, to yield intermediate **28**. Then, the intermediate **28** was formylated via Vilsmeier Haack reaction to obtain intermediate **29**. Finally, the intermediate **29** was subjected to well-known Knoevenagel condensation and Wittig condensation reactions with active methylene compounds *viz.*, thiophene-2-acetonitrile, phenylacetonitrile, 1,4-phenylenediacetonitrile and Wittig salt **13** (series-3) to obtain the target compounds **VK11**, **VK12**, **VK14** and **VK13**, respectively.

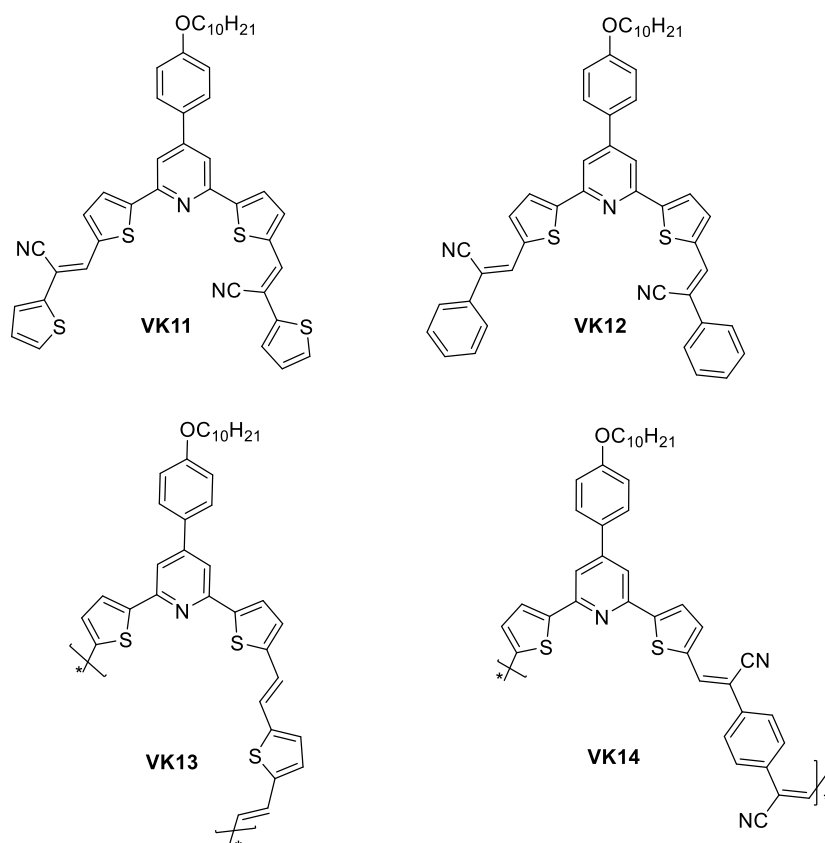
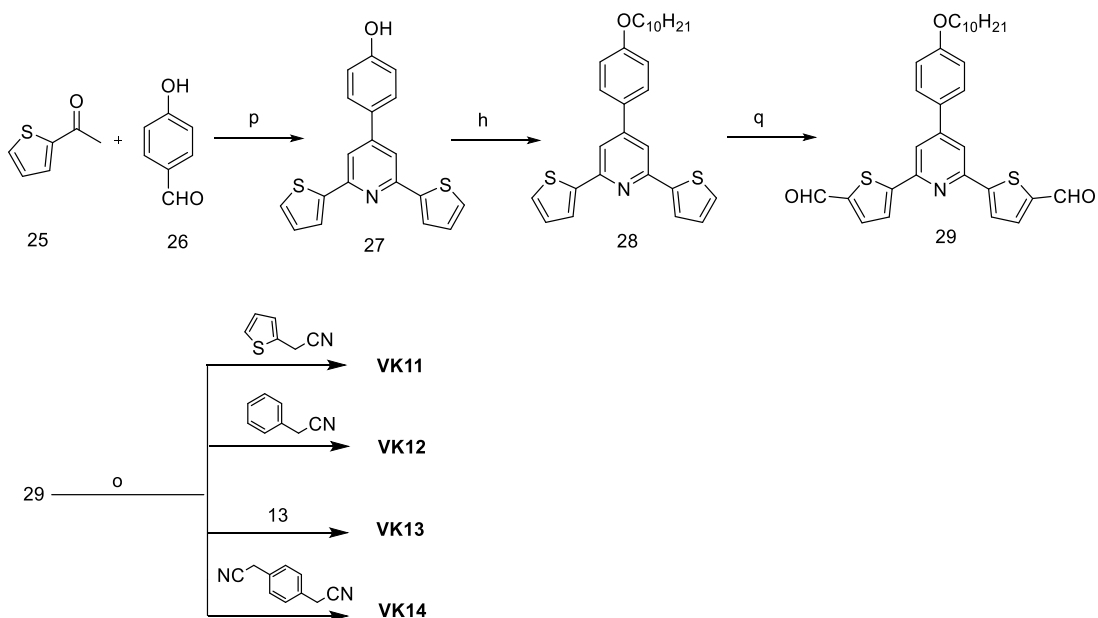


Figure 2.4 Chemical structures of VK11, VK12, VK13 and VK14.



Scheme 2.4 Synthetic route for VK11–VK14. Reagents and reaction conditions: (p) ammonium acetate, microwave, 400 W, 120°C, 0.5 h, yield: 68%; (q) POCl₃, DMF, 90–95°C, 48 h, yield: 49%.

2.1.5.2 The detailed experimental procedure

Synthesis of 4-(4-(hydroxy)phenyl)-2,6-di(thiophen-2-yl)pyridine (27)

In a single-necked RB flask, 2-acetylthiophene (**25**) (8.84 mL, 81.88 mmol), 4-hydroxybenzaldehyde (**26**) (5.0 g, 40.94 mmol) and ammonium acetate (63.12 g, 818.86 mmol) were taken. The mixture was subjected to microwave irradiation (400 W) at 120°C for 0.5 h, then the residue was quenched using ice-water (60 mL) and the obtained solid was filtered. The solid was washed several times with ice cold distilled water to remove unreacted ammonium acetate and purified by column chromatography using a mixture of pet ether/ethyl acetate (8:2, v/v) as mobile solvent to get intermediate **27** as a white solid (9.32 g, yield: 68%). ESI-MS (m/z) calcd. for $C_{19}H_{13}NOS_2$: 335.04 found: 336.21 $[M+H]^+$; 1H NMR (400 MHz, $CDCl_3$) δ (ppm): 7.72 (s, 2H, Ar-H), 7.65–7.60 (m, 4H, Ar-H), 7.44 (d, $J = 8.0$ Hz, 2H, Ar-H), 7.17–7.14 (m, 2H, Ar-H), 6.97 (d, $J = 8.4$ Hz, 2H, Ar-H), 5.31 (s, 1H, -OH); ^{13}C NMR (100 MHz, $CDCl_3$) δ (ppm): 156.6, 152.5, 149.5, 144.9, 130.9, 128.4, 127.9, 127.7, 124.7, 116.0, 114.6; Anal. calcd. for $C_{19}H_{13}NOS_2$: C, 68.03; H, 3.91; N, 4.18; S, 19.12; found: C, 67.86; H, 4.17; N, 3.97; S, 19.66.

Synthesis of 4-(4-(decyloxy)phenyl)-2,6-di(thiophen-2-yl)pyridine (28)

The intermediate **28** was synthesized following the procedure for intermediate **9** (series-3), using intermediate **27** (4.00 g, 11.92 mmol), K_2CO_3 (4.94 g, 35.77 mmol) and 1-bromodecane (3.77 mL, 17.88 mmol) (off-white solid, 5.10 g, yield: 90%). ESI-MS (m/z) calcd. for $C_{29}H_{33}NOS_2$: 475.20 found: 476.34 $[M+H]^+$; 1H NMR (400 MHz, $CDCl_3$) δ (ppm): 7.72 (s, 2H, Ar-H), 7.67–7.65 (m, 4H, Ar-H), 7.44 (d, $J = 4.0$ Hz, 2H, Ar-H), 7.17–7.14 (m, 2H, Ar-H), 7.04 (d, $J = 8$ Hz, 2H, Ar-H), 4.04 (t, $J = 8.0$ Hz, -OCH₂), 1.88–1.81 (m, 2H, -CH₂-), 1.52–1.49 (m, 2H, -CH₂-), 1.37–1.29 (m, 12H, -CH₂-), 0.92 (t, $J = 8.0$ Hz, -CH₃); ^{13}C NMR (100 MHz, $CDCl_3$) δ (ppm): 160.1, 152.5, 149.6, 145.0, 130.3, 128.1, 127.9, 127.6, 124.7, 115.0, 114.4, 68.1, 31.9, 29.6, 29.4, 29.4, 29.2, 26.0, 22.7, 14.1; Anal. calcd. for $C_{29}H_{33}NOS_2$: C, 73.22; H, 6.99; N, 2.94; S, 13.48; found: C, 73.88; H, 6.18; N, 2.55; S, 13.87.

Synthesis of 5,5'-(4-(4-(decyloxy)phenyl)pyridine-2,6-diyl)bis(thiophene-2-carbaldehyde) (29)

Freshly distilled DMF (11.66 mL, 151.35 mmol) was taken in a dry two-necked RB flask and cooled to 0 to -5°C . To this, POCl_3 (14.10 mL, 151.35 mmol) was added drop wise and stirred for 30 min to get Vilsmeier salt. Then, solution of **28** (4.0 g, 8.40 mmol) in DMF (10 mL) was added to the formed Vilsmeier salt and the mixture was refluxed at 95°C for 48 h. The reaction mass was quenched using ice-cold water and subsequently, basified using NaOH solution (5 M). The precipitated solid was collected by filtration and the crude product was purified by column chromatography using a mixture of pet ether/ethyl acetate (8:2, v/v) as eluent to obtain **29** as a yellow solid (2.2 g, yield: 49%). ESI-MS (m/z) calcd. for $\text{C}_{31}\text{H}_{33}\text{NO}_3\text{S}_2$: 531.19 found: 532.43 $[\text{M}+\text{H}]^+$; ^1H NMR (400 MHz, CDCl_3) δ (ppm): 9.88 (s, 2H, $-\text{CHO}$), 7.72–7.69 (m, 6H, Ar-H), 7.57 (d, $J = 8.8$ Hz, 2H, Ar-H), 6.99 (d, $J = 8.4$ Hz, 2H, Ar-H), 4.00 (t, $J = 6.8$ Hz, $-\text{OCH}_2$), 1.84–1.77 (m, 2H, $-\text{CH}_2-$), 1.48–1.43 (m, 2H, $-\text{CH}_2-$), 1.32–1.26 (m, 12H, $-\text{CH}_2-$), 0.86 (t, $J = 6.8$ Hz, $-\text{CH}_3$); ^{13}C NMR (100 MHz, CDCl_3) δ (ppm): 183.0, 160.6, 153.1, 151.3, 150.2, 144.4, 136.5, 129.0, 128.1, 125.5, 116.5, 115.1, 68.2, 31.8, 29.5, 29.3, 29.2, 29.1, 25.9, 22.6, 14.0; Anal. calcd. for $\text{C}_{31}\text{H}_{33}\text{NO}_3\text{S}_2$: C, 70.02; H, 6.26; N, 2.63; S, 12.06; found: C, 70.47; H, 6.52; N, 2.09; S, 12.17.

Synthesis of (2E,2'E)-3,3'-((4-(4-(decyloxy)phenyl)pyridine-2,6-diyl)bis(thiophene-5,2-diyl))bis(2 (thiophen-2-yl)acrylonitrile) (VK11)

The molecule **VK11** was synthesized following the procedure for the oligomer **VK7** (series-3), using $\text{C}_2\text{H}_5\text{ONa}$ (89.3 mg, 8.11 mmol), thiophene-2-acetonitrile (0.12 mL, 1.18 mmol) and intermediate **29** (0.3 g, 0.56 mmol) (yellow solid, 0.29 g, yield: 71%). MALDI-TOF-MS (m/z) calcd. for $\text{C}_{43}\text{H}_{39}\text{N}_3\text{OS}_4$: 741.20 found: 742.194 $[\text{M}+\text{H}]^+$; ^1H NMR (400 MHz, CDCl_3) δ (ppm): 7.77–7.76 (m, 2H, Ar-H), 7.73–7.72 (m, 4H, Ar-H), 7.67 (d, $J = 8.8$ Hz, 2H, Ar-H), 7.48 (s, 2H, Ar-H), 7.38–7.37 (m, 2H, Ar-H), 7.32–7.30 (m, 2H, Ar-H), 7.09–7.07 (m, 2H, Ar-H), 7.04 (d, $J = 8.8$ Hz, 2H, Ar-H), 4.04 (t, $J = 6.4$ Hz, 2H, $-\text{OCH}_2$), 1.79–1.75 (m, 2H, $-\text{CH}_2-$), 1.49–1.47 (m, 2H, $-\text{CH}_2-$), 1.28–1.25 (m, 12H, $-\text{CH}_2-$), 0.88 (t, $J = 6.8$ Hz, 3H, $-\text{CH}_3$); ^{13}C NMR (100 MHz, CDCl_3) δ (ppm): 160.4, 151.5, 149.7, 148.2, 138.9, 134.8, 132.3, 131.6, 130.1, 129.5, 128.7, 127.1, 125.6, 116.9, 115.8, 115.1, 103.3, 68.2, 38.7, 31.8, 29.6, 29.5, 29.3,

29.2, 28.9, 26.0, 22.6, 14.0; Anal. calcd. for C₄₃H₃₉N₃OS₄: C, 69.60; H, 5.30; N, 5.66; S, 17.28; found: C, 69.42; H, 5.71; N, 5.52; S, 17.33.

Synthesis of (2Z,2'Z)-3,3'-((4-(4-(decyloxy)phenyl)pyridine-2,6-diyl)bis(thiophene-5,2-diyl))bis(2-phenylacrylonitrile) (VK12)

The compound **VK12** was synthesized following the above-mentioned procedure for **VK11**, using the precursors **29** (0.3 g, 0.56 mmol) and phenylacetonitrile (0.13 mL, 1.18 mmol) (yellow solid, 0.27 g, yield: 68%). MALDI-TOF-MS (*m/z*) calcd. for C₄₇H₄₃N₃OS₂: 729.28 found: 730.221 [M+H]⁺; ¹H NMR (400 MHz, CDCl₃) δ (ppm): 7.79 (s, 2H, Ar-H), 7.75 (s, 2H, Ar-H), 7.69–7.67 (m, 6H, Ar-H), 7.47–7.44 (m, 4H, Ar-H), 7.40–7.37 (m, 4H, Ar-H), 7.05 (d, *J* = 8.8 Hz, 2H, Ar-H), 6.99 (s, 2H, Ar-H), 4.04 (t, *J* = 6.4 Hz, 2H, –OCH₂), 1.77–1.75 (m, 2H, –CH₂–), 1.50–1.47 (m, 2H, –CH₂–), 1.30–1.25 (m, 12H, –CH₂–), 0.88 (t, *J* = 6.8 Hz, 3H, –CH₃); ¹³C NMR (100 MHz, CDCl₃) δ (ppm): 160.4, 151.7, 148.3, 139.4, 133.9, 133.8, 132.6, 129.6, 129.1, 129.0, 128.2, 125.8, 125.7, 118.1, 115.7, 115.1, 108.5, 68.2, 31.8, 29.5, 29.4, 29.3, 29.2, 26.0, 22.6, 14.0; Anal. calcd. for C₄₇H₄₃N₃OS₂: C, 77.33; H, 5.94; N, 5.76; S, 8.78; found: C, 77.17; H, 5.76; N, 5.89; S, 8.92.

Synthesis of poly [(E)-4-(4-(decyloxy)phenyl)-2-(thiophen-2-yl)-6-(5-(2-(5-vinylthiophen-2-yl)vinyl)thiophen-2-yl)pyridine] (VK13)

The polymer **VK13** was synthesized following the above-mentioned procedure for **VK11**, using C₂H₅ONa (89.3 mg, 8.11 mmol in 3 mL of ethanol), intermediates **29** (0.3 g, 0.56 mmol) and **13** (0.49 g, 0.62 mmol). The reaction mixture was poured slowly into 50 mL CH₃OH and the precipitated polymer **VK13** was filtered. Thus, obtained polymer was re-dissolved in CHCl₃ and precipitated in CH₃OH several times. The obtained orange colored solid polymer **VK13** after filtration was vacuum dried. Mw = 4241, PD = 1.22; ¹H NMR (400 MHz, CDCl₃) δ (ppm): 7.94–7.81 (m, 3H, Ar-H), 7.77–7.68 (m, 2H, Ar-H), 7.60–7.52 (m, 4H, Ar-H), 7.42–7.38 (m, 3H, Ar-H), 7.17–7.15 (m, 1H, Ar-H), 7.06–7.04 (m, 3H, Ar-H), 6.94–6.91 (m, 2H, Ar-H), 4.04 (t, *J* = 6.8 Hz, 2H, –OCH₂), 1.79–1.77 (m, 2H, –CH₂–), 1.43–1.29 (m, 14H, –CH₂–), 0.89 (t, *J* = 6.4 Hz, 3H, –CH₃); ¹³C NMR (100 MHz, CDCl₃) δ (ppm): 132.1, 132.0, 131.9, 128.5, 128.3, 128.1, 115.1, 68.2, 31.8, 29.5, 29.2, 26.0, 22.6, 14.0; Anal. calcd. for C₄₃H₄₅NOS₄: C, 71.72; H, 6.30; N, 1.95; S, 17.81; found: C, 71.89; H, 6.16; N, 1.72; S, 17.63.

Synthesis of poly [(Z)-2-(4-(1-cyanovinyl)phenyl)-3-(5-(4-(4-(decyloxy)phenyl)-6-(thiophen-2-yl)pyridin-2-yl)thiophen-2-yl)acrylonitrile] (VK14)

The polymer **VK14** was synthesized following the procedure for polymer **VK13**, using the precursors **29** (0.3 g, 0.56 mmol) and 1,4-phenylenediacetonitrile (0.096 g, 0.62 mmol). Mw = 10426, PD = 4.34; ¹H NMR (400 MHz, CDCl₃) δ (ppm): 7.63–7.39 (m, 7H, Ar–H), 7.20–6.99 (m, 15H, Ar–H), 4.00 (t, *J* = 6.8 Hz, 2H, –OCH₂), 1.80 (m, 2H, –CH₂–), 1.29–1.24 (m, 14H, –CH₂–), 0.88 (t, *J* = 6.8 Hz, 3H, –CH₃); ¹³C NMR (100 MHz, CDCl₃) δ (ppm): 128.1, 125.8, 115.0, 68.1, 31.8, 29.5, 26.0, 22.6, 14.0; Anal. calcd. for C₄₉H₄₇N₃OS₂: C, 77.64; H, 6.25; N, 5.54; S, 8.46; found: C, 77.82; H, 6.46; N, 5.32; S, 8.79.

2.1.6 Synthesis of molecules (VK15–VK18) of series–5

2.1.6.1 Synthesis

The synthesis of molecules **VK15–VK18** is depicted in **Scheme 2.5** and their chemical structures are shown in **Figure 2.5**. The intermediate **28** (series–4) was formylated to obtain intermediates **29** (series–4) and **30**. The reduction of intermediates **30** and **29** yielded the intermediates **31** and **32**, respectively, which were later converted into their corresponding Wittig salts **33** and **34**. Finally, the Wittig reaction of intermediate **34** with 4-formyltriphenylamine (**39**) and intermediate **37** produced final molecules **VK15** and **VK16**, respectively, while the Wittig reaction of intermediate **33** with bis(4-formylphenyl)phenylamine (**40**) and intermediate **38** produced final molecules **VK17** and **VK18**, respectively.

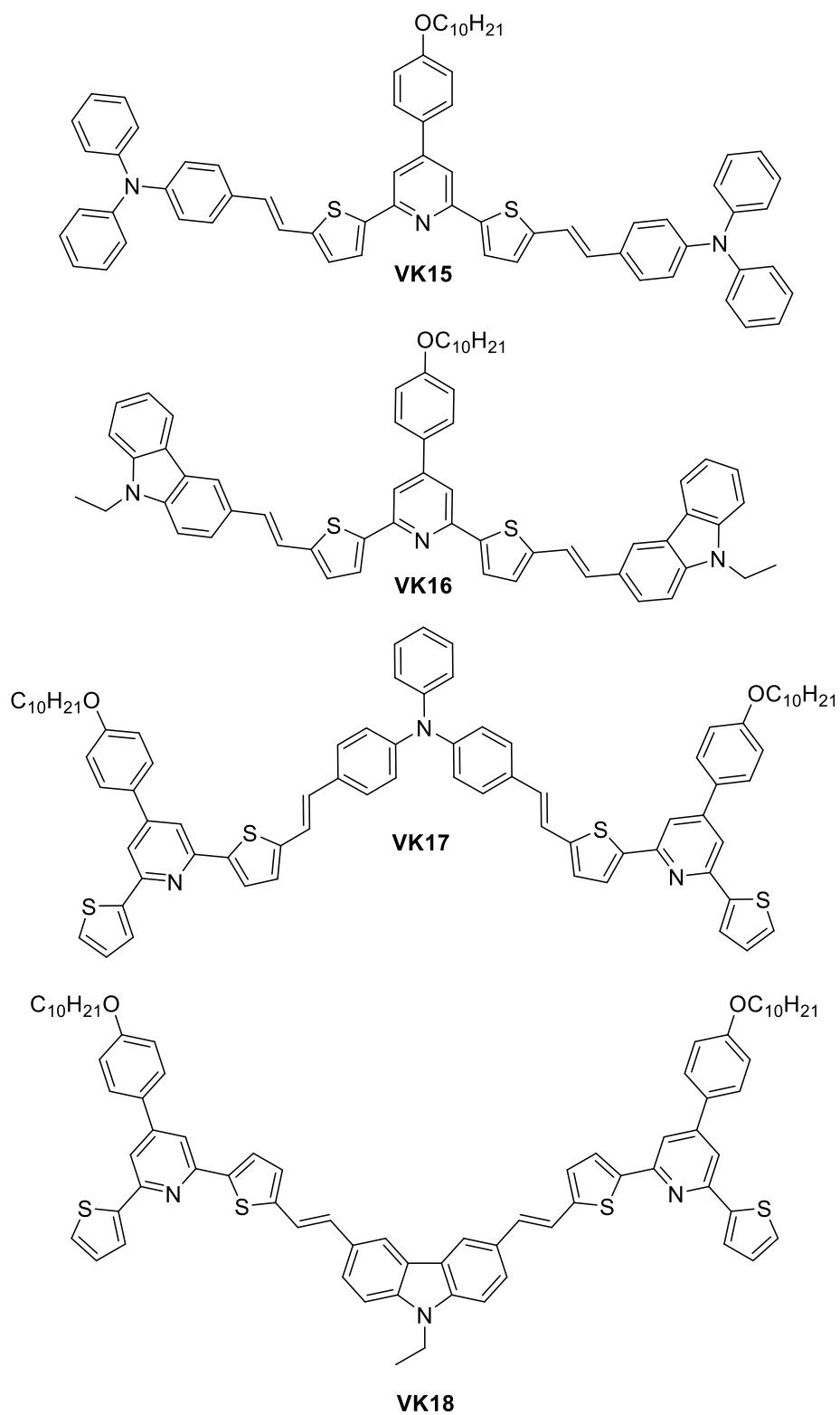
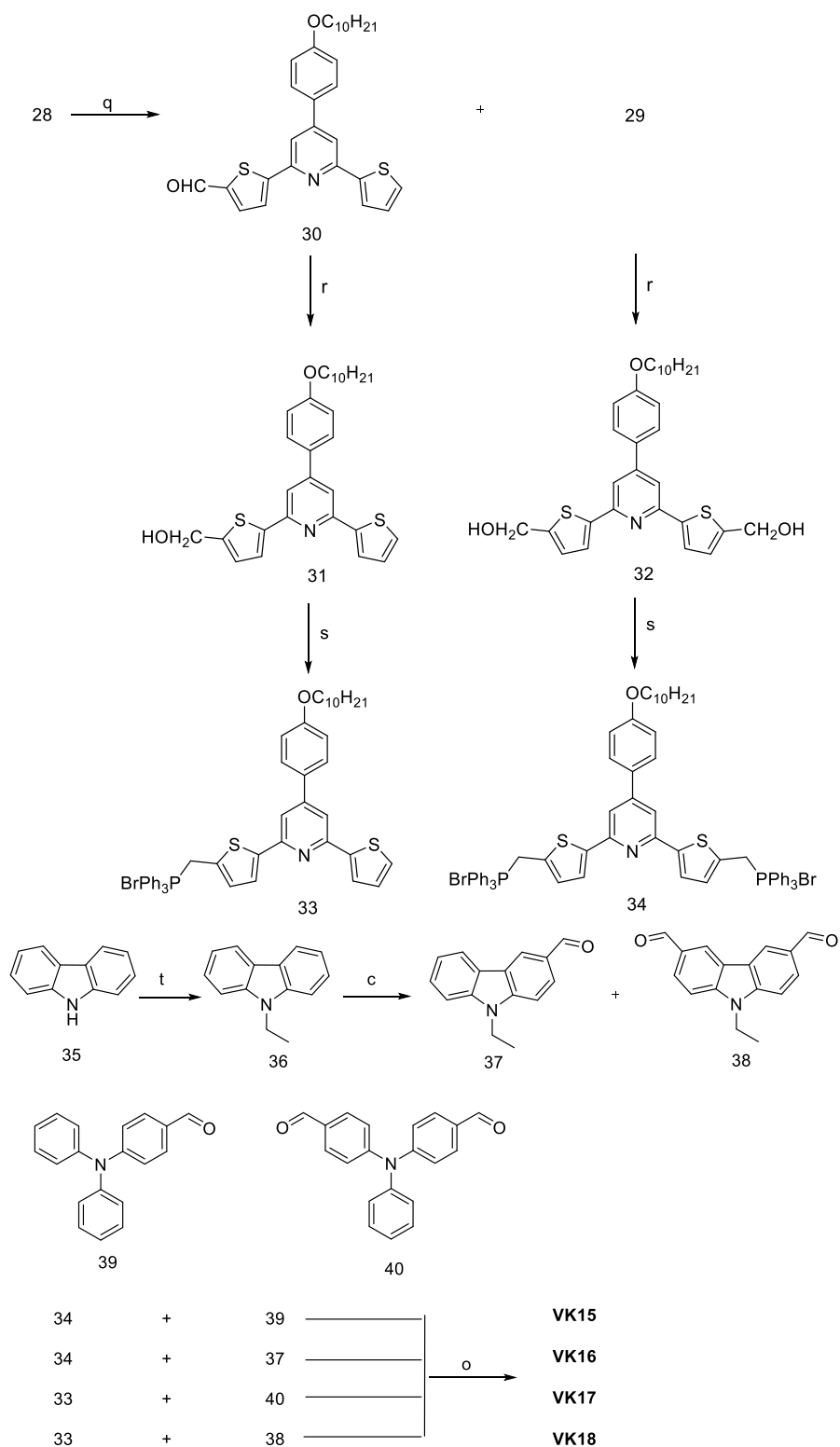


Figure 2.5 Chemical structures of **VK15**, **VK16**, **VK17** and **VK18**.



Scheme 2.5 Synthetic pathways of **VK15**, **VK16**, **VK17** and **VK18**. Reagents and reaction conditions: (r) NaBH₄, CH₃OH, RT, 12 h, yield: 90–92%; (s) PPh₃HBr, CHCl₃, 60°C, 3 h, yield: 93–94%; (t) NaH, C₂H₅Br, DMF, RT, 12 h, yield: 82%.

2.1.6.2 The detailed experimental procedure

Synthesis of 5-(4-(4-(decyloxy)phenyl)-6-(thiophen-2-yl)pyridin-2-yl)thiophene-2-carbaldehyde (30)

The intermediate **30** was obtained in the synthesis of intermediate **29** (series-4) and was separated in the purification step by column chromatography using a mixture of pet ether/ethyl acetate (9:1 v/v) as eluent (yellow solid, 1.1 g, yield: 26%). ESI-MS (m/z) calcd. for $C_{30}H_{33}NO_2S_2$: 503.20 found: 504.37 $[M+H]^+$; 1H NMR (400 MHz, $CDCl_3$) δ (ppm): 9.96 (s, 1H, -CHO), 7.79–7.71 (m, 5H, Ar-H), 7.66 (d, $J = 8.0$ Hz, 2H, Ar-H), 7.46 (d, $J = 4.0$ Hz, 1H, Ar-H), 7.17–7.15 (m, 1H, Ar-H), 7.05 (d, $J = 8.0$ Hz, 2H, Ar-H), 4.04 (t, $J = 6.8$ Hz, 2H, -OCH₂), 1.87–1.83 (m, 2H, -CH₂-), 1.53–1.49 (m, 2H, -CH₂-), 1.31–1.28 (m, 12H, -CH₂-), 0.91 (t, $J = 6.4$ Hz, 3H, -CH₃); ^{13}C NMR (100 MHz, $CDCl_3$) δ (ppm): 183.2, 160.4, 154.2, 152.9, 151.0, 149.9, 144.3, 144.1, 136.7, 129.8, 128.1, 128.0, 125.1, 126.0, 115.9, 115.2, 115.1, 68.2, 31.8, 29.5, 29.3, 30.0, 29.2, 26.0, 22.6, 14.0; Anal. calcd. for $C_{30}H_{33}NO_2S_2$: C, 71.53; H, 6.60; N, 2.78; S, 12.73; found: C, 70.99; H, 6.87; N, 2.03; S, 12.27.

Synthesis of (5-(4-(4-(decyloxy)phenyl)-6-(thiophen-2-yl)pyridin-2-yl)thiophen-2-yl)methanol (31)

In a clean and dry RB flask, a solution of **30** (1.00 g, 1.98 mmol) in CH_3OH (10 mL) was prepared. To this solution, $NaBH_4$ (0.15 g, 3.97 mmol) was added and the mixture was stirred at RT for 4 h. After the completion of the reaction, the solution was quenched using ice-cold water, the obtained solid was filtered, washed with excess of distilled water, dried and purified by column chromatography using a mixture of pet ether/ethyl acetate (7:3, v/v) as eluent to obtain intermediate **31** as white solid (0.92 g, yield: 92%). 1H NMR (400 MHz, $CDCl_3$) δ (ppm): 7.75 (s, 1H, Ar-H), 7.67–7.58 (m, 5H, Ar-H), 7.52 (d, $J = 4.0$ Hz, 1H, Ar-H), 7.39 (d, $J = 4.0$ Hz, 1H, Ar-H), 7.12–7.10 (m, 1H, Ar-H), 7.01–6.99 (m, 2H, Ar-H), 4.84 (s, 2H, -CH₂OH), 3.99 (t, $J = 6.8$ Hz, 2H, -OCH₂), 1.99 (s, 1H, -CH₂OH), 1.82–1.79 (m, 2H, -CH₂-), 1.47–1.45 (m, 2H, -CH₂-), 1.28 (m, 12H, -CH₂-), 0.87 (t, $J = 6.4$ Hz, 3H, -CH₃); ^{13}C NMR (100 MHz, $CDCl_3$) δ (ppm): 160.3, 152.5, 152.2, 149.4, 144.8, 144.5, 130.3, 127.7, 127.5, 126.2, 124.7, 124.4, 115.1, 114.3, 114.2, 68.2, 60.3, 31.8, 29.5, 29.3, 26.0, 22.5, 14.0; Anal. calcd. for $C_{30}H_{35}NO_2S_2$: C, 71.25; H, 6.98; N, 2.77; S, 12.68; found: C, 71.98; H, 6.32; N, 2.89; S, 12.41.

Synthesis of ((4-(4-(decyloxy)phenyl)pyridine-2,6-diyl)bis(thiophene-5,2-diyl))dimethanol (32)

The intermediate **32** was synthesized following the procedure for intermediate **31**, using intermediate **29** (2.00 g, 3.76 mmol) and NaBH₄ (0.56 g, 15.04 mmol) (white solid, 1.82 g, yield: 90%). ESI-MS (*m/z*) calcd. for C₃₁H₃₇NO₃S₂: 535.22 found: 536.44 [M+H]⁺; ¹H NMR (400 MHz, CDCl₃) δ (ppm): 7.58 (d, *J* = 8.8 Hz, 2H, Ar-H), 7.54 (s, 2H, Ar-H), 7.50 (d, *J* = 4.0 Hz, 2H, Ar-H), 7.00–6.97 (m, 4H, Ar-H), 4.83 (s, 4H, –CH₂OH), 4.01 (t, *J* = 6.8 Hz, 2H, –OCH₂), 2.50 (s, 2H, –CH₂OH), 1.86–1.79 (m, 2H, –CH₂–), 1.51–1.46 (m, 2H, –CH₂–), 1.36–1.31 (m, 12H, –CH₂–), 0.91 (t, *J* = 7.2 Hz, 3H, –CH₃); ¹³C NMR (100 MHz, CDCl₃) δ (ppm): 160.1, 152.2, 149.3, 146.3, 144.7, 130.2, 128.0, 126.0, 124.4, 115.0, 114.1, 68.2, 60.3, 31.8, 29.5, 29.4, 29.3, 29.2, 26.0, 22.6, 14.1; Anal. calcd. for C₃₁H₃₇NO₃S₂: C, 69.50; H, 6.96; N, 2.61; S, 11.97; found: C, 69.08; H, 6.50; N, 2.93; S, 12.08.

Synthesis of 2-(5-((bromotriphenyl-λ⁵-phosphanyl)methyl)thiophen-2-yl)-4-(4-(decyloxy)phenyl)-6-(thiophen-2-yl)pyridine (33)

A mixture of intermediate **31** (0.7 g, 1.38 mmol) and PPh₃.HBr (0.57 g, 1.66 mmol) was taken in CHCl₃ (10 mL) and refluxed at 60°C for 3 h. Then, the solvent was removed under reduced pressure and diethyl ether (5 mL) was added to solidify the product. Thus, obtained intermediate **33** as yellow solid was used as such for the next step (1.08 g, yield: 94%). ¹H NMR (400 MHz, CDCl₃) δ (ppm): 7.86–7.79 (m, 10H, Ar-H), 7.71–7.69 (m, 6H, Ar-H), 7.61–7.56 (m, 3H, Ar-H), 7.52–7.50 (m, 2H, Ar-H), 7.44–7.43 (m, 1H, Ar-H), 7.22 (s, 1H, Ar-H), 7.14–7.12 (m, 1H, Ar-H), 7.00 (d, *J* = 8.4 Hz, 2H, Ar-H), 5.82 (d, *J* = 12.0 Hz, 2H, Ar-CH₂–), 4.02 (t, *J* = 6.8 Hz, 2H, –OCH₂), 1.84–1.79 (m, 2H, –CH₂–), 1.49–1.47 (m, 2H, –CH₂–), 1.29 (m, 12H, –CH₂–), 0.89 (t, *J* = 6.8 Hz, 3H, –CH₃); ¹³C NMR (100 MHz, CDCl₃) δ (ppm): 160.6, 151.5, 151.3, 150.8, 136.6, 135.2, 134.5, 134.4, 133.5, 130.5, 130.4, 130.2, 129.1, 128.4, 128.3, 126.4, 125.6, 118.1, 117.1, 116.8, 115.1, 68.3, 59.4, 31.8, 29.6, 29.3, 29.2, 28.3, 27.5, 25.9, 22.7, 14.0; Anal. calcd. for C₄₈H₄₉BrNOPS₂: C, 69.38; H, 5.94; N, 1.69; S, 7.72; found: C, 69.14; H, 5.56; N, 1.91; S, 7.85.

Synthesis of 2,6-bis(5-((bromotriphenyl-λ⁵-phosphanyl)methyl)thiophen-2-yl)-4-(4-(decyloxy)phenyl)pyridine (34)

The intermediate **34** was synthesized following the above-mentioned procedure for intermediate **33** using intermediate **32** (1.0 g, 1.86 mmol) and PPh₃.HBr (0.76 g, 2.23 mmol) (yellow solid, 2.05 g, yield: 93%). ¹H NMR (400 MHz, CDCl₃) δ (ppm): 7.87–7.77 (m, 17H, Ar–H), 7.72–7.64 (m, 12H, Ar–H), 7.45–7.40 (m, 4H, Ar–H), 7.20–7.18 (m, 2H, Ar–H), 7.07 (s, 2H, Ar–H), 6.88 (d, *J* = 8.0 Hz, 2H, Ar–H), 5.94 (d, *J* = 16.0 Hz, 4H, Ar–CH₂), 3.96 (t, *J* = 6.8 Hz, 2H, –OCH₂), 1.84–1.79 (m, 2H, –CH₂–), 1.47–1.29 (m, 14H, –CH₂), 0.88 (t, *J* = 6.4 Hz, 3H, –CH₃); ¹³C NMR (100 MHz, CDCl₃) δ (ppm): 160.6, 150.2, 149.9, 143.1, 135.0, 134.6, 134.5, 133.0, 131.0, 130.2, 130.1, 128.3, 126.9, 118.0, 114.9, 68.2, 59.3, 31.8, 29.5, 29.4, 29.2, 27.1, 26.7, 26.0, 22.6, 14.0; Anal. calcd. for C₆₇H₆₅Br₂NOP₂S₂: C, 67.85; H, 5.52; N, 1.18; S, 5.41; found: C, 67.67; H, 5.32; N, 1.58; S, 5.97.

Synthesis of 9-ethyl-9H-carbazole (36)

To a solution of 9H-carbazole (**35**) (2.0 g, 11.96 mmol) in DMF (15 mL), NaH (0.86 g, 35.88 mmol) was added portion wise under argon at 0°C and the reaction mixture was stirred at RT for 30 min. Later, 1-bromoethane (1.07 mL, 14.35 mmol) was added drop-wise and the reaction mixture was stirred at RT for 6 h. After the completion of the reaction, the resulted solution was quenched using ice cold water, then the solid product obtained was filtered and the crude product was purified using column chromatography with pet ether as eluent to get intermediate **36** as white solid (2.93 g, yield: 82%). ¹H NMR (400 MHz, CDCl₃) δ (ppm): 8.17 (d, *J* = 8.0 Hz, 2H, Ar–H), 7.54–7.51 (m, 2H, Ar–H), 7.46–7.44 (m, 2H, Ar–H), 7.31–7.28 (m, 2H, Ar–H), 4.38 (q, *J* = 7.2 Hz, 2H, –NCH₂), 1.46 (t, *J* = 7.2 Hz, 3H, –CH₃); ¹³C NMR (100 MHz, CDCl₃) δ (ppm): 139.9, 125.6, 122.9, 120.4, 118.7, 108.4, 37.4, 13.7; Anal. calcd. for C₁₄H₁₃N: C, 86.12; H, 6.71; N, 7.17; found: C, 86.28; H, 6.36; N, 7.27.

Synthesis of 9-ethyl-9H-carbazole-3-carbaldehyde (37)

The intermediate **37** was synthesized following the procedure mentioned for intermediate **5** using the precursors POCl₃ (3.81 mL, 40.96 mmol), DMF (3.15 mL, 40.96 mmol) and intermediate **36** (2.0 g, 10.24 mmol) (off-white solid, 1.12 g, yield: 49%). ¹H NMR (400 MHz, CDCl₃) δ (ppm): 10.05 (s, 1H, –CHO), 8.55 (s, 1H, Ar–H), 8.11 (d, *J* = 8.4 Hz, 1H, Ar–H), 7.97 (d, *J* = 8.8 Hz, 1H, Ar–H), 7.53–7.49 (m, 1H, Ar–H), 7.42–7.39 (m, 2H, Ar–H), 7.32–7.28 (m, 1H, Ar–H), 4.32 (q, *J* = 7.2 Hz, 2H, –

NCH₂), 1.42 (t, $J = 7.2$ Hz, 3H, –CH₃); ¹³C NMR (100 MHz, CDCl₃) δ (ppm): 191.7, 143.5, 140.6, 128.5, 127.1, 126.7, 123.9, 123.1, 123.0, 120.7, 120.2, 109.1, 108.6, 37.8, 13.7; Anal. calcd. for C₁₅H₁₃NO: C, 80.69; H, 5.87; N, 6.27; found: C, 80.31; H, 5.76; N, 6.38.

Synthesis of 9-ethyl-9H-carbazole-3,6-dicarbaldehyde (38)

The intermediate **38** was obtained in the synthesis of intermediate **37** and was separated in the purification step by column chromatography using a mixture of pet ether/ethyl acetate (7:3 v/v) as eluent (yellow solid, 0.98 g, yield: 38%). ¹H NMR (400 MHz, CDCl₃) δ (ppm): 10.16 (s, 2H, –CHO), 8.69 (s, 2H, Ar–H), 8.11 (d, $J = 8.0$ Hz, 2H, Ar–H), 7.58 (d, $J = 8.0$ Hz, 2H, Ar–H), 7.53–7.49 (m, 1H, Ar–H), 7.42–7.39 (m, 2H, Ar–H), 7.32–7.28 (m, 1H, Ar–H), 4.48 (q, $J = 7.2$ Hz, 2H, –NCH₂), 1.53 (t, $J = 7.2$ Hz, 3H, –CH₃); ¹³C NMR (100 MHz, CDCl₃) δ (ppm): 191.6, 144.2, 129.5, 127.8, 127.0, 124.0, 123.1, 120.7, 109.4, 109.1, 108.6, 37.9, 13.8; Anal. calcd. for C₁₆H₁₃NO₂: C, 76.48; H, 5.21; N, 5.57; found: C, 76.62; H, 5.33; N, 5.21.

Synthesis of 4,4'-((1E,1'E)-((4-(4-(decyloxy)phenyl)pyridine-2,6-diyl)bis(thiophene-5,2-diyl))bis(ethene-2,1-diyl))bis(N,N-diphenylaniline) (VK15)

The molecule **VK15** was synthesized following the procedure for the oligomer **VK7** (Series–3), using the precursors 4-formyltriphenylamine (**39**) (0.14 g, 0.50 mmol) and intermediate **29** (0.30 g, 0.25 mmol) (a yellow solid, 0.163 g, yield: 63%). MALDI–TOF–MS (m/z) calcd. for C₆₉H₆₃N₃OS₂: 1013.44 found: 1013.849 [M+H]⁺; ¹H NMR (400 MHz, CDCl₃) δ (ppm): 7.65 (d, $J = 8.0$ Hz, 2H, Ar–H), 7.61 (s, 2H, Ar–H), 7.58 (d, $J = 4.0$ Hz, 2H, Ar–H), 7.38 (d, $J = 8.0$ Hz, 4H, Ar–H), 7.29–7.25 (m, 10H, Ar–H), 7.15–7.11 (m, 9H, Ar–H), 7.06–7.02 (m, 13H, Ar–H), 4.02 (t, $J = 6.8$ Hz, 2H, –OCH₂), 1.86–1.81 (m, 2H, –CH₂–), 1.51–1.47 (m, 2H, –CH₂–), 1.28–1.25 (m, 12H, –CH₂–), 0.88 (t, $J = 6.4$ Hz, 3H, –CH₃); ¹³C NMR (100 MHz, CDCl₃) δ (ppm): 160.2, 152.4, 149.3, 147.5, 145.4, 143.0, 131.0, 130.5, 129.3, 128.7, 128.1, 127.3, 126.6, 125.3, 124.6, 123.4, 123.1, 120.3, 115.1, 114.2, 68.2, 31.9, 29.7, 29.6, 29.6, 29.4, 29.3, 29.2, 26.0, 22.7, 14.1; Anal. calcd. for C₆₉H₆₃N₃OS₂: C, 81.70; H, 6.26; N, 4.14; S, 6.32; found: C, 81.65; H, 6.17; N, 4.23; S, 6.44.

Synthesis of 3,3'-((1E,1'E)-((4-(4-(decyloxy)phenyl)pyridine-2,6-diyl)bis(thiophene-5,2-diyl))bis(ethene-2,1-diyl))bis(9-ethyl-9H-carbazole) (VK16)

The molecule **VK16** was synthesized following the procedure for **VK15**, using the precursors intermediate **37** (0.113 g, 0.50 mmol) and intermediate **29** (0.30 g, 0.25 mmol) (a yellow solid, 0.137 g, yield: 59%). MALDI-TOF-MS (m/z) calcd. for $C_{61}H_{59}N_3OS_2$: 913.41 found: 913.652 $[M+H]^+$; 1H NMR (400 MHz, $CDCl_3$) δ (ppm): 8.26 (s, 2H, Ar-H), 8.15 (d, $J = 8.0$ Hz, 2H, Ar-H), 7.70–7.66 (m, 4H, Ar-H), 7.63–7.62 (m, 4H, Ar-H), 7.51–7.47 (m, 2H, Ar-H), 7.43–7.39 (m, 4H, Ar-H), 7.37–7.31 (m, 4H, Ar-H), 7.28–7.25 (m, 2H, Ar-H), 7.10 (d, $J = 4.0$ Hz, 2H, Ar-H), 7.04 (d, $J = 8.0$ Hz, 2H, Ar-H), 4.38 (q, $J = 7.2$ Hz, 4H, $-NCH_2$), 4.03 (t, $J = 6.4$ Hz, 2H, $-OCH_2$), 1.85–1.81 (m, 2H, $-CH_2-$), 1.50–1.48 (m, 2H, $-CH_2-$), 1.46 (t, $J = 7.0$ Hz, 3H, $-CH_3$), 1.29–1.25 (m, 12H, $-CH_2-$), 0.89 (t, $J = 6.8$ Hz, 3H, $-CH_3$); ^{13}C NMR (100 MHz, $CDCl_3$) δ (ppm): 160.1, 152.5, 149.2, 145.9, 142.7, 140.4, 139.8, 130.6, 130.3, 128.2, 126.2, 125.8, 125.3, 124.4, 123.4, 123.0, 120.5, 119.4, 119.1, 118.8, 115.0, 114.1, 108.7, 108.6, 68.2, 37.7, 31.9, 29.7, 29.6, 29.3, 29.2, 26.0, 22.7, 14.1, 13.9; Anal. calcd. for $C_{61}H_{59}N_3OS_2$: C, 80.14; H, 6.50; N, 4.60; S, 7.01; found: C, 80.31; H, 6.37; N, 4.77; S, 7.22.

Synthesis of 4-((E)-2-(5-(4-(4-(decyloxy)phenyl)-6-(thiophen-2-yl)pyridin-2-yl)thiophen-2-yl)vinyl)-N-(4-((E)-2-(5-(4-(4-(decyloxy)phenyl)-6-(thiophen-2-yl)pyridin-2-yl)thiophen-2-yl)vinyl)phenyl)-N-phenylaniline (VK17)

The molecule **VK17** was synthesized following the procedure for **VK15**, using the precursors bis(4-formylphenyl)phenylamine (**40**) (0.054 g, 0.18 mmol) and intermediate **30** (0.30 g, 0.36 mmol) (a yellow solid, 0.136 g, yield: 61%). MALDI-TOF-MS (m/z) calcd. for $C_{80}H_{81}N_3O_2S_4$: 1243.52 found: 1243.866 $[M+H]^+$; 1H NMR (400 MHz, $CDCl_3$) δ (ppm): 7.71–7.69 (m, 3H, Ar-H), 7.67–7.64 (m, 7H, Ar-H), 7.60–7.59 (m, 2H, Ar-H), 7.44–7.30 (m, 8H, Ar-H), 7.21–7.13 (m, 8H, Ar-H), 7.10–7.00 (m, 11H, Ar-H), 4.03 (t, $J = 6.8$ Hz, 4H, $-OCH_2$), 1.86–1.89 (m, 4H, $-CH_2-$), 1.52–1.45 (m, 4H, $-CH_2-$), 1.29–1.25 (m, 24H, $-CH_2-$), 0.88 (t, $J = 6.4$ Hz, 6H, $-CH_3$); ^{13}C NMR (100 MHz, $CDCl_3$) δ (ppm): 160.2, 153.0, 152.5, 149.5, 147.0, 145.4, 145.0, 143.1, 131.5, 131.3, 130.5, 129.8, 128.2, 127.9, 127.6, 127.3, 125.3, 124.7, 123.9, 115.1, 114.4, 68.2, 31.9, 29.7, 29.6, 29.4, 29.3, 29.2, 26.0, 22.7, 14.1; Anal. calcd. for $C_{80}H_{81}N_3O_2S_4$: C, 77.19; H, 6.56; N, 3.38; S, 10.30; found: C, 77.38; H, 6.67; N, 3.44; S, 10.09.

Synthesis of 3,6-bis((E)-2-(5-(4-(4-(decyloxy)phenyl)-6-(thiophen-2-yl)pyridin-2-yl)thiophen-2-yl)vinyl)-9-ethyl-9H-carbazole (VK18)

The molecule **VK18** was synthesized following the procedure for **VK15**, using the precursors intermediate **38** (0.046 g, 0.18 mmol) and intermediate **30** (0.30 g, 0.36 mmol) (a yellow solid, 0.121 g, yield: 56%). MALDI-TOF-MS (m/z) calcd. for $C_{76}H_{79}N_3O_2S_4$: 1193.51 found: 1193.815 $[M+H]^+$; 1H NMR (400 MHz, $CDCl_3$) δ (ppm): 7.73–7.62 (m, 12H, Ar-H), 7.57–7.41 (m, 8H, Ar-H), 7.30–7.29 (m, 3H, Ar-H), 7.17–7.15 (m, 2H, Ar-H), 7.12–7.10 (m, 2H, Ar-H), 7.05–7.03 (m, 4H, Ar-H), 6.98–6.96 (m, 1H, Ar-H), 4.39 (q, $J = 7.2$ Hz, $-NCH_2$), 4.03 (t, $J = 6.8$ Hz, $-OCH_2$), 1.85–1.80 (m, 4H, $-CH_2-$), 1.50–1.48 (m, 4H, $-CH_2-$), 1.45 (t, $J = 7.0$ Hz, 3H, $-CH_3$), 1.28–1.25 (m, 24H, $-CH_2-$), 0.88 (t, $J = 6.4$ Hz, 6H, $-CH_3$); ^{13}C NMR (100 MHz, $CDCl_3$) δ (ppm): 160.2, 152.4, 149.4, 145.8, 145.1, 142.6, 140.2, 130.5, 128.2, 128.1, 127.9, 127.6, 125.4, 124.7, 123.4, 115.0, 114.3, 108.9, 68.2, 31.9, 29.6, 29.4, 29.3, 29.2, 26.0, 22.7, 14.1; Anal. calcd. for $C_{76}H_{79}N_3O_2S_4$: C, 76.41; H, 6.67; N, 3.52; S, 10.73; found: C, 76.62; H, 6.51; N, 3.32; S, 10.90.

2.2 CHARACTERIZATION DETAILS

The spectroscopic techniques such as nuclear magnetic resonance (NMR): proton nuclear magnetic resonance (1H NMR) and carbon 13 nuclear magnetic resonance (^{13}C NMR); mass spectral analysis and elemental analysis were used to elucidate the structures of synthesized intermediates and final compounds. The UV-Vis and fluorescence spectroscopies were used to study the photophysical properties of the final compounds, whereas the CV was used to study the electrochemical properties. The DFT and time-dependent DFT (TD-DFT) were carried out for the theoretical calculations and the thermogravimetric analysis (TGA) was used to analyse the thermal properties of the compounds. The Z-scan technique was followed to study the third-order NLO properties of the compounds. Brief details of the characterization techniques are given below.

2.2.1 NMR spectroscopy

The NMR spectroscopy is one of the most powerful and widely used techniques in chemical research which gives the information about the number of magnetically distinct atoms of the type being used. The NMR spectroscopy was used in the present study for investigating the content, the purity and the molecular structures of the

synthesized intermediates and final compounds. From the ^1H NMR, the number of each of the distinct type of hydrogen nuclei and the nature of the immediate environment of each type of protons present in the synthesized intermediates and final compounds was determined. Similar type of information was obtained from ^{13}C NMR as well. The ^1H NMR of the intermediates and final compounds were recorded using a Bruker 400 MHz NMR spectrometer using tetramethyl silane (TMS) as the internal reference and deuterated dimethyl sulfoxide ($\text{DMSO-}d_6$)/ CHCl_3 as the solvent. The ^{13}C NMR spectra of the compounds were recorded using a Bruker 100 MHz NMR spectrometer.

2.2.2 Mass spectrometry

This analytical tool was used to quantify the compounds, and to further elucidate the structure and the chemical properties of the synthesized compounds. The specific mass-to-charge ratio (m/z) (with or without fragmentation) and relative abundance of each ion type was obtained from the mass spectrometer which was used to calculate the exact molecular weight of the synthesized intermediates and final compounds. The electrospray ionization–mass (ESI–MS) of the intermediates and final compounds were recorded using a Waters micro mass Q-Tofmicro mass spectrometer and the matrix-assisted laser desorption/ionization-time of flight–mass (MALDI TOF–MS) of the final compounds was recorded using an Autoflex speed MALDI TOF-MS mass spectrometer.

2.2.3 Elemental analysis

This was used to determine the type of element present and the number of each element present in the compound. In particular, the CHNS analysis was carried out to determine the mass fractions of carbon (C), hydrogen (H), nitrogen (N) and sulfur (S) of the synthesized intermediates and final compounds. The elemental analyses were performed on a flash EA-112 CHNS analyser (Thermo electron corporation).

2.2.4 Photophysical studies

Most of the organic molecules/polymers containing π or non–bonding (n) electrons are transparent in UV and visible region (180–800 nm) in the electromagnetic spectrum. As a result, optical methods are found to be one of the most widely used methods to derive valuable information about the structures of such organic materials. As the study of interaction of materials with light is very much useful for their optical

characterization, the UV–Vis absorption and the fluorescence emission spectroscopic techniques are found to be two well-known tools to study the material properties.

2.2.4.1 UV-Vis spectroscopy

The UV-Vis absorption spectroscopy basically deals with the electronic transitions from the ground state or the HOMO to the excited state or the LUMO of the material. The lower the gap between the HOMO and the LUMO, the longer the wavelength of light it can absorb. Therefore, the UV–Vis spectroscopy was used to detect the extent of conjugation in the synthesized compounds and also, to investigate the effect of double bonds on the absorption wavelength of the compounds **VK1–VK18**. The UV–Vis spectral data of final compounds were collected from Analytik jena SPECORD S600 spectrometer. All the spectra were recorded in solution state using CHCl_3 as the solvent (1×10^{-5} M) at RT.

2.2.4.2 Fluorescence spectroscopy

The fluorescence emission spectroscopy involves the excitation of analyte by irradiation at a certain wavelength and the emission of radiation of a different wavelength from the excited state to the ground state. When the molecule absorbs a light of suitable wavelength, it excites to one of the many vibrational levels in one of the excited electronic states, for instance, the first excited singlet state, S_1 . The relaxation of the molecule from S_1 can occur via several processes. Fluorescence is one of them. The intensity and the wavelength of emitted light determines the suitability of the material for the application in optoelectronics. Therefore, the fluorescence spectroscopy was used to study the emission properties of the synthesized compounds **VK1–VK18**. The photoluminescence (PL) spectra were recorded using a Fluoromax Horiba Jobin Yuan spectrometer and a Jasco FP 6200 spectrometer. All the spectra were recorded in solution state using CHCl_3 as solvent (1×10^{-5} M) at RT. The emission spectra of **VK1–VK18** were obtained under excitation at their corresponding maximum absorption wavelength (λ_{max}).

From the results of optical studies, the important parameters such as absorption and emission region in the electromagnetic spectrum and the optical band gap (E_g) of **VK1–VK18** were evaluated, which are key factors for selecting the materials as active materials in photovoltaic/ optoelectronic/ photonic applications.

2.2.5 Electrochemical studies

As the electrochemistry relates the flow of electrons to the chemical changes, the electrochemical study involves the understanding of basic electronic structures of organic materials. It describes their oxidation and reduction potentials, which are highly useful in determining their HOMO–LUMO energy levels and charge carrying properties. The CV is a popular and powerful electrochemical technique, generally employed to investigate the oxidation and the reduction processes of molecular species and is also utilized to estimate the HOMO and LUMO energy levels of the molecules (Li et al. 1999). In the basic CV experiment, for the applied potential (E) to the working electrode, resulting current (I) is measured. The oxidation potentials of the molecular species are investigated by sweeping them anodically (positive bias) while the reduction potentials are investigated by sweeping cathodically (negative bias). The data plotted as a graph of E versus I is referred as a cyclic voltammogram.

In the present work, the CV studies were carried out to determine the oxidation potentials and hence, to evaluate the HOMO/LUMO energy levels of the compounds **VK1–VK18**, which are very much essential in molecular design and controlling the band gap; and also, for the proper selection of electrodes in optoelectronic devices.

2.2.5.1 Materials, methods and instrumentation

All the solvents were degassed before the usage. The solvents and the chemicals used were: anhydrous CHCl_3 (Loba Chemie, 99.8%), CH_3CN (Merck, 99.8%), ferrocene (Sigma Aldrich, 98%) and tetrabutylammonium perchlorate (TBAPC) (Sigma Aldrich, 98%). The CV measurements of the compounds were carried out using an IVIUM (Vertex-V55610) electrochemical workstation with three-electrode system wherein, the compounds were dissolved in CHCl_3 and drop casted on a glassy carbon electrode, which was used as a working electrode; moreover, a platinum (Pt) wire was used as a counter electrode, a saturated calomel electrode (SCE) was used as a reference electrode, and the electrolyte used was a 0.1 M solution of TBAPC in CH_3CN . The experiment was performed at a scan rate of 100 mV s^{-1} and all the measurements were calibrated using ferrocene/ferrocenium (Fc/Fc^+) system, which was used as an internal standard.

2.2.5.2 Equations used for calculating the HOMO/LUMO energies

Considering the onset of oxidation potential, the energy of HOMO level (E_{HOMO}) was calculated using the **Equation 2.1** (Leeuw et al. 1997),

$$E_{HOMO} = -[E_{onset}^{ox} + 4.8eV - E_{FOC}] \dots\dots\dots(2.1)$$

where, E_{onset}^{ox} and E_{FOC} are the onset oxidation potentials of the samples and ferrocene ($E_{FOC} = 0.27$ V vs SCE (**Figure 2.6**)), respectively, and -4.8 eV is the HOMO energy level of ferrocene against vacuum.

The energy of LUMO level was obtained from electrochemically measured HOMO energy and spectroscopically determined band gap, using the **Equation 2.2** (Wang et al. 2014):

$$E_{LUMO} = E_{HOMO} + E_g \dots\dots\dots(2.2)$$

where, $E_g = 1240/\lambda$, λ = point of intersection between the absorption and emission spectra.

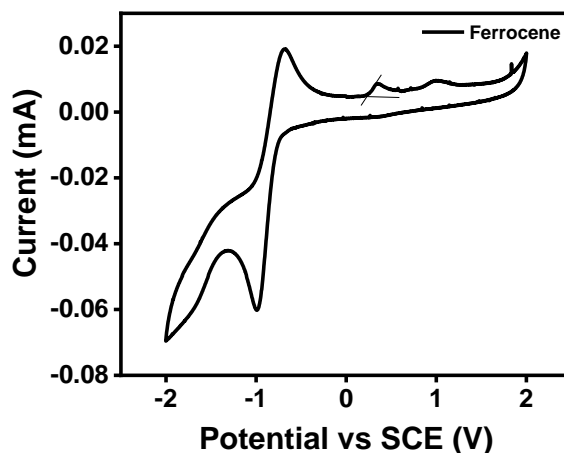


Figure 2.6 Cyclic voltammogram of ferrocene recorded in CH_3CN solution.

2.2.6 Theoretical calculations

In order to predict the ground and the excited state properties as well as to understand the spatial arrangement and the distribution of electrons in the molecules, DFT and TD-DFT are two widely used theoretical methods. These computational studies help to rationalize the relationship between the molecular structure and device performance (Martsinovich and Troisi 2011). They are also useful in designing new organic materials for achieving enhanced device performances.

2.2.6.1 Simulations

All the calculations were performed using a Gaussian 09 software. The ground state calculations were performed using the DFT, wherein, the molecular geometry was first optimized at vacuum using Becke's three-parameter hybrid functional with Lee-Yang-Parr's gradient-corrected correlation functional (B3LYP) (Becke 1993; Lee et al. 1988) with the 6-311+G(d, p) basis set (Hariharan and Pople 1973; Hehre et al. 2003). The frontier molecular orbitals (HOMO and LUMO) were obtained using the Avogadro software (Version 1.2.0) (Hanwell et al. 2012). The self-consistent field (SCF) convergence thresholds for minimizing energies of both ground and first excited state optimization was set at 10^{-6} . The ground state geometry, obtained at gas phase, was further optimized in the solvent medium, for which the excited state calculations were carried out by TD-DFT using same basis set at the same level of calculation as that used for optimizing ground state. The self-consistent reaction field based on the polarizable continuum model (PCM) using the integral equation formalism variant (IEFPCM) was used to study the solvent effect on the energy parameters (Mohan et al. 2019). The TD-DFT calculations were done for vertical excitations up to first 10 excited states in CHCl_3 as the solvent to generate simulated absorption spectra.

2.2.7 Thermal analysis

For the material to use as a potent candidate in optoelectronic devices, it should be thermally stable. The TGA is used to determine the thermal stability of the material which measures the amount of weight change of the material as a function of temperature. It mainly provides the information about the phase transitions and the thermal decompositions of the materials. The TGA of the final compounds **VK1–VK18** were carried out using the Seiko Instruments (TGA/DTA Exstar 6300), Japan, at the heating rate of $10^\circ\text{C min}^{-1}$ under argon atmosphere to study the thermal stabilities of **VK1–VK18**.

2.2.8 Z-scan analysis

To investigate the application of **VK1–VK18** in optoelectronics, NLO studies were performed by Z-scan technique under nano second excitation (Sheik-Bahae et al. 1990). Using this technique both NLA and NLR parameters were measured, which finally provided the $\chi^{(3)}$ value. The NLA and optical limiting parameters were obtained via the open aperture (OA) Z-scan analysis whereas the NLR parameters were obtained

via the closed aperture (CA) Z-scan analysis. In the OA Z-scan analysis the optical transmittance of the sample was recorded as a function of input intensity. The schematic representation of the Z-scan set up is shown in **Figure 2.7**. The sample solutions were made to translate across the focus of a convex lens (focal length: 150 mm) in the direction of laser beam (z axis: from -z to +z) in predetermined steps using a translational stage that was controlled by a computer program.

The maximum intensity of the samples was observed at the focus which decreased equally on either side of the focus. The output transmittance from the sample at each position was collected by a detector and then plotted against the position of the samples. The NLA properties of the samples were measured by numerically fitting the obtained data to the theoretical model. To obtain the NLR parameters using the CA Z-scan, a small aperture was placed in front of the signal detector. Thus, the obtained transmittance was affected by both the NLA as well as the NLR and susceptible to phase distortion. The division of the CA output from the OA output resulted in the pure NLR part. All the experiments were carried out in the “single shot” mode. Sufficient time intervals were provided between successive pulses to avoid accumulative thermal effects in the sample. The NLO studies were performed using a Q-switched Nd-YAG laser Quanta Ray INDI-40 (Austin, USA) (7 ns pulse width) working at the wavelength of 532 nm with the frequency of 10 Hz. The linear transmittance of all the molecules was fixed between 50–85% at the excitation wavelength when taken in a 1 mm cuvette.

2.2.8.1 Z-scan experimental set up

A frequency doubled Q switched Nd:YAG laser (Quanta-Ray INDI-40) operating at 532 nm wavelength, 7 ns pulse width and 10 Hz repeating rate excitation source was used for the Z-scan experiment. Using a beam splitter, the laser beam was split into reference beam and the sample beam, which was passed through the sample taken in a 1 mm thick quartz cuvette through a convex lens of focal length 150 mm. The sample cuvette was placed on a computer controlled translational stage and was moved along the direction of laser beam in z-direction from +z to -z about 20 mm on the either side of the focus of the lens in predetermined steps (1000 microns). The convex lens was adjusted in such a way that the laser beam provides maximum energy to the sample at the focus which then equally decreases on the either side of the focus. The beam waist at the focus and Rayleigh range of the beam were estimated to be 17.56

μm and 1.82 mm, respectively. During CA scan, an aperture of 3 mm diameter was placed in the front of detector. Both the reference beam and the transmitted beam from the sample were detected using two identical pyroelectric detectors (RjP-735, laser Probe Inc, USA) and were collected in the energy meter (Rj-7620, Laser Probe, Inc, USA). Since the sample thickness was much smaller than Rayleigh range, the experiment was carried out by adopting thin sample approximation method (Sheik-Bahae et al. 1990).

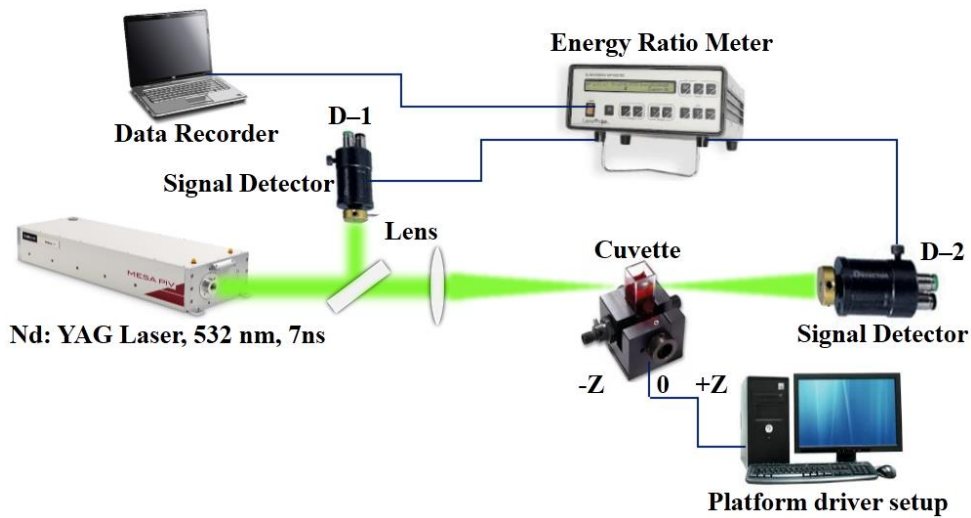


Figure 2.7 Schematic representation of Z-scan experimental setup.

2.2.8.2 Equations used for the theoretical fitting of the experimental results

Following the intensity dependent absorption coefficient ($\alpha(I)$) for the ESA assisted TPA (associated with SA), OA Z-scan recordings were theoretically fitted using **Equation 2.3** to determine the nonlinear absorption coefficient (β_{eff}) and is written as follows:(Couris et al. 1995)

$$\alpha(I) = \frac{\alpha_0}{1 + I/I_s} + \beta_{eff} I \dots \dots \dots (2.3)$$

where, α_0 is the linear absorption coefficient, I is the incident laser intensity, I_s is the saturation intensity, β_{eff} is the effective TPA coefficient associated to the RSA response (Divyasree et al. 2018).

The rate of change in the intensity of a beam as it passes through a medium i.e., pulse propagation equation to calculate β_{eff} is provided as follows:

$$\frac{dI}{dz} = - \left(\frac{\alpha_o}{1 + \frac{I}{I_s}} \right) I - \beta_{\text{eff}} I^2 \dots\dots\dots(2.4)$$

where, z is the propagation distance within the sample. The first term in **Equation 2.4** expresses the SA and the next term indicates the effective TPA part.

The normalized transmittance derived from **Equations 2.3** and **2.4** is presented by the following equation:

$$T(z) = \frac{1}{\sqrt{\pi q_0(z)}} \int_{-\infty}^{\infty} \ln \left[1 + q_0(z) e^{-\tau^2} \right] d\tau \dots\dots\dots(2.5)$$

where, $q_0(z) = \beta_{\text{eff}} I_0 L_{\text{eff}} / \left(1 + \frac{z^2}{z_0^2} \right)$ and $L_{\text{eff}} = \left(1 - e^{-\alpha_o L} \right) / \alpha_o$

L_{eff} is the effective sample length, L is the sample length, α_o is the unsaturated linear absorption coefficient, z is the position of the sample, $z_o = \pi \omega_o^2 / \lambda$ is the Raleigh range, ω_o is the beam waist radius at the focal point and λ is the wavelength of laser beam.

The imaginary part of third order nonlinear susceptibility ($\chi^{(3)}$) is presented by the following equation:

$$\text{Im } \chi^{(3)} = \frac{n_o^2 \epsilon_o c \lambda \beta_{\text{eff}}}{2\pi} \dots\dots\dots(2.6)$$

where, n_o is the linear refractive index, c is the speed of light and ϵ_o is the permittivity of free space.

The normalized transmittance (T) under the CA condition is presented by the equation (Sheik-Bahae et al. 1990):

$$T(z, \Delta\Phi_o) = 1 + \frac{4 \left(\frac{z}{z_o} \right)}{\left(\left(\frac{z}{z_o} \right)^2 + 1 \right) \left(\left(\frac{z}{z_o} \right)^2 + 9 \right)} \Delta\Phi_o \dots\dots\dots(2.7)$$

where, T is the normalized transmittance, $\Delta\Phi_o$ is the on-axis nonlinear phase shift at the focus, $z=0$.

Therefore, the nonlinear refractive index (η_2) is calculated presented by the following equation:

$$n_2 (esu) = \frac{cn_0 \lambda \Delta \Phi_o}{80\pi^2 I_o L_{eff}} \dots\dots\dots(2.8)$$

The real $\chi^{(3)}$ is related to η_2 by the relation (in electrostatic unit):

$$Real \chi^{(3)} = 2n_o^2 \epsilon_o c n_2 \dots\dots\dots(2.9)$$

where n_o^2 is the linear refractive index, c velocity of light, ϵ_o is the permittivity of free space.

CHAPTER 3

RESULTS AND DISCUSSION

3.1 EFFECTS OF SUBSTITUENTS ON THE ENRICHMENT OF THE OPTICAL LIMITING ACTION OF NOVEL IMIDAZO[2,1-*b*][1,3,4]THIADIAZOLE FUSED THIOPHENE BASED SMALL MOLECULES (VK1–VK3)

The structure-property relationship signifies that the optoelectronic property of the molecule can be improved on increasing the D and A strengths and also, by increasing the conjugation length. In addition to the molecular engineering of the core moiety, the recent focus is on the development of different types of substituents, as they are essential for the proper electron transfer and to fine-tune the HOMO and LUMO energy levels, which exert immense impact on the ICT from the D to A fragments. The introduction of substituted acrylonitrile groups as side groups/ substituents lowers the LUMO level and also increases the electrochemical stability of the conjugated material, which is desirable to achieve high-performance optoelectronic devices (Mikroyannidis et al. 2009). Also, the molecules with substituted acrylonitrile groups exhibited promising performances on their usage in various organic electronics such as organic field effect transistors (OFETs), OLEDs and OPVs (Hindson et al. 2010; Iwan et al. 2012; Petrus et al. 2013) (Moussalem et al. 2014; Petrus et al. 2014). Similarly, rhodanine-3-acetic acid, is a well-known common electron acceptor among the numerous electron acceptors used in various optoelectronic fields such as dye sensitized solar cells (Modelli et al. 2010; Wan et al. 2017) and NLO (Fernandes et al. 2018). The presence of rhodanine-3-acetic acid induces better electrochemical and optical properties and it also impacts on the ICT of the π -system.

The introduction of olefinic bond as π -linker between the aromatic rings leads to the reduction in steric hindrance, improvement in planarity, extends the π -conjugation (Jebnoui et al. 2018) and modulates the electrochemical properties such as light emitting property, charge transfer ability, *etc.*, (Hwang and Chen 2002; Qing et al. 2015; Roncali 1997; Song et al. 1999). Hence, in the present work, three different groups *viz.*, thiophene-2-acetonitrile (**VK1**), phenylacetonitrile (**VK2**) and rhodanine-3-acetic acid (**VK3**) were chosen as substituents which were connected to the Th-ITD core through olefinic bond via Knoevenagel condensation reaction. Herein, the effect of structural modifications of the substituents on the optical and electrochemical

properties is discussed with the expectation that it would produce good performance when used in optoelectronic devices.

3.1.1 Structural elucidation of intermediates and final compounds

In the first step, three aromatic protons at δ 7.61–7.09 ppm of thiophene and two protons at δ 7.42 ppm of amine group attached to thiadiazole unit present in the ^1H NMR spectrum of intermediate **3** confirm its structure. Also, in the ^{13}C NMR spectrum of intermediate **3**, all the signals at higher frequency region (δ 168.5–120 ppm) confirm its structure. Further, the mass spectrum shows a molecular ion peak at m/z 184.00, corresponding to $[\text{M}+\text{H}]$ of intermediate **3**, which clearly confirms the structure. The disappearance of two $-\text{NH}_2$ protons and formation of six aromatic protons corresponding to thiophene, phenyl and ITD at δ 8.00–7.14 ppm in the ^1H NMR spectrum of intermediate **4** clearly confirm its formation. The structure of the compound is also supported by its ^{13}C NMR spectrum, which is further confirmed by its mass spectrum, which shows a molecular ion peak at m/z 284.00 corresponding to $[\text{M}+\text{H}]$ of intermediate **4**. The singlet signal of $-\text{CHO}$ at δ 10 ppm and at δ 177.4 ppm in the ^1H and ^{13}C NMR spectrum of **5**, respectively, confirm the formylation of **4**. The molecular ion peak at m/z 312.00 corresponding to $[\text{M}+\text{H}]$ of **5** in its mass spectrum further supports the structure. In the final step, the disappearance of singlet signal of $-\text{CHO}$ at δ 10 ppm and appearance of peak due to olefinic and other aromatic protons at the downfield region in the ^1H NMR spectra of **VK1–VK3** confirm the formation of final compounds and also, the broad singlet signal at δ 13.00 ppm of $-\text{COOH}$ group and sharp singlet signal at δ 4.70 ppm accounting for the two methylene protons ($-\text{N}-\text{CH}_2$) of rhodanine-3-acetic acid in the ^1H NMR spectrum of **VK3** further validates the formation of **VK3**. The disappearance of peak corresponding to aldehydic carbon at δ 177.4 ppm and appearance of new signals due to aromatic and vinylic carbons at downfield region in the ^{13}C NMR spectra of **VK1–VK3** further supports the structural confirmation of **VK1–VK3**. Moreover, the signals at δ 194.7, δ 167.9 and δ 45.7 ppm corresponding to $-\text{C}=\text{S}$, $-\text{COOH}$ and $-\text{N}-\text{CH}_2$ carbons, respectively, in the ^{13}C NMR spectrum of **VK3** clearly illustrate the structure of **VK3**. The mass spectrum of **VK1** and **VK2** shows a molecular ion peaks at m/z 417.10 and m/z 411.10 corresponding to $[\text{M}+\text{H}]$ of **VK1** and **VK2**, respectively, confirm the structure. In addition to the spectral characterizations, the elemental analysis further evidences the structures of all the

intermediates and final compounds. The ^1H NMR, ^{13}C NMR and mass spectra of intermediates and final compounds are presented in the following **Figures 3.1–3.17**.

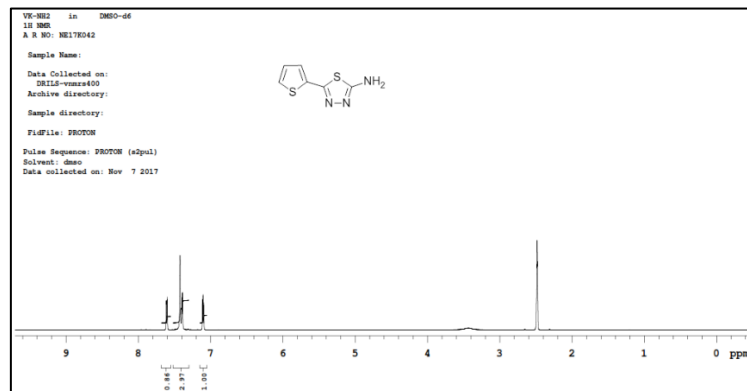


Figure 3.1 ^1H NMR spectrum of **3**

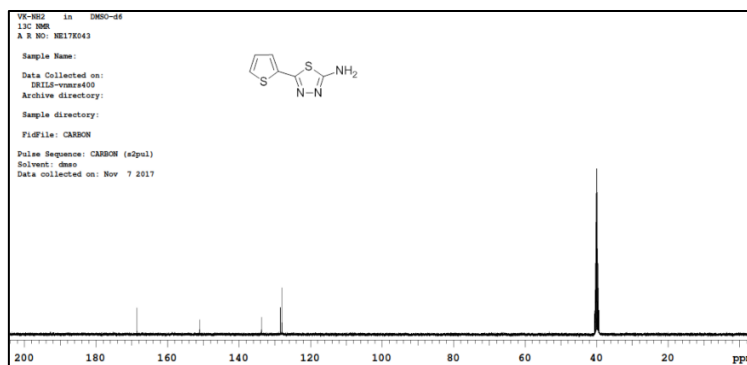


Figure 3.2 ^{13}C NMR spectrum of **3**

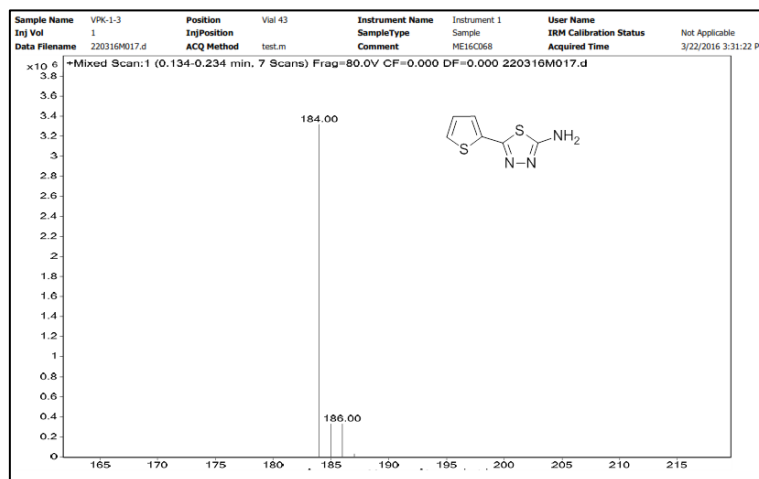


Figure 3.3 Mass spectrum of **3**

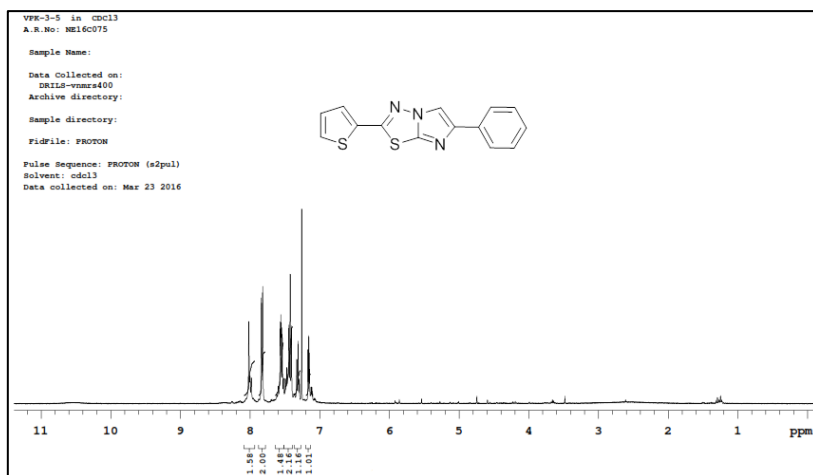


Figure 3.4 ^1H NMR spectrum of **4**

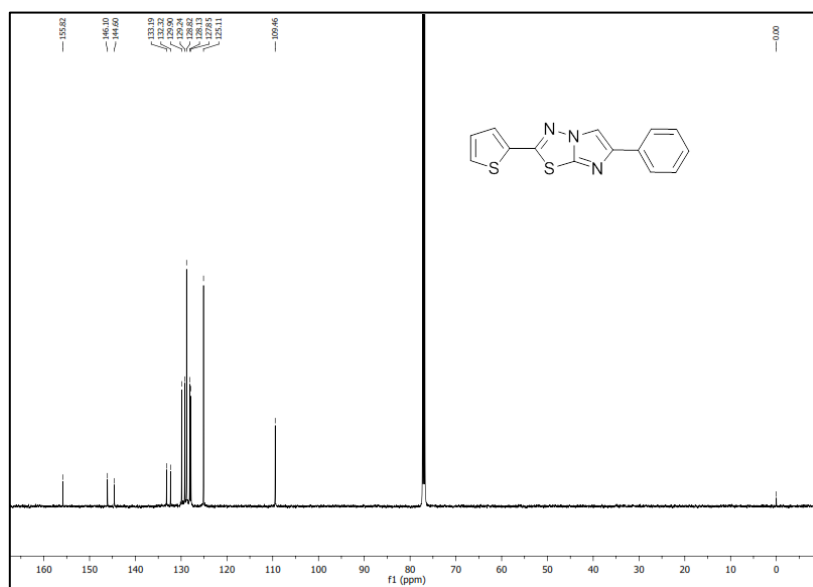


Figure 3.5 ^{13}C NMR spectrum of **4**

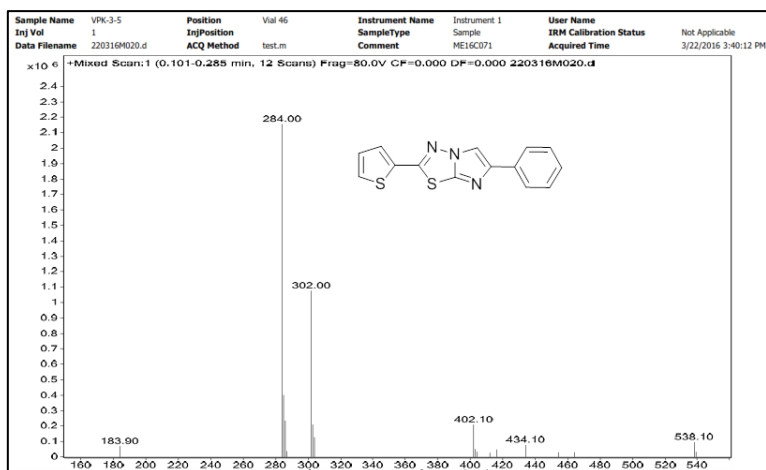


Figure 3.6 Mass spectrum of **4**

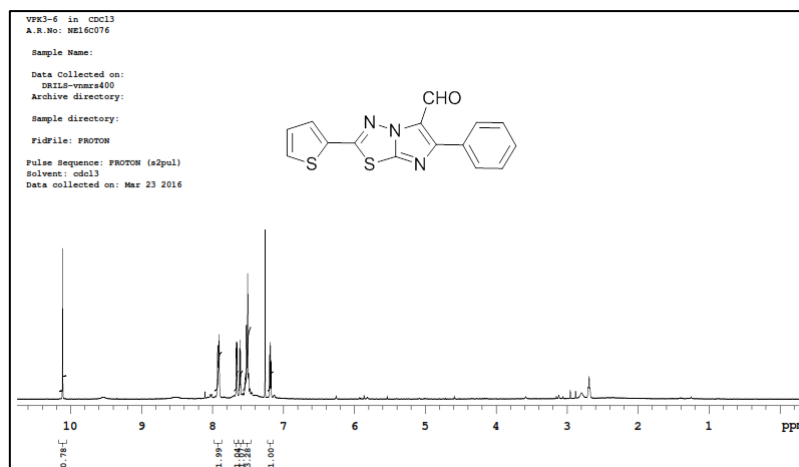


Figure 3.7 ¹H NMR spectrum of 5

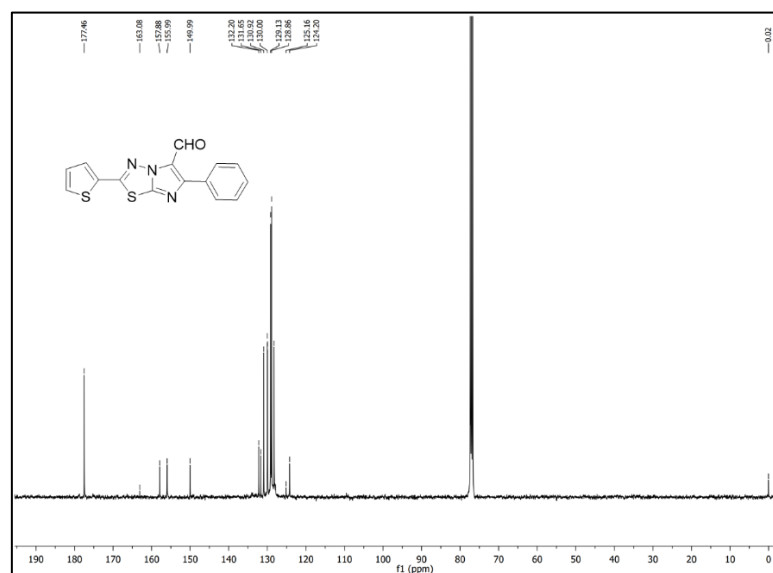


Figure 3.8 ¹³C NMR spectrum of 5

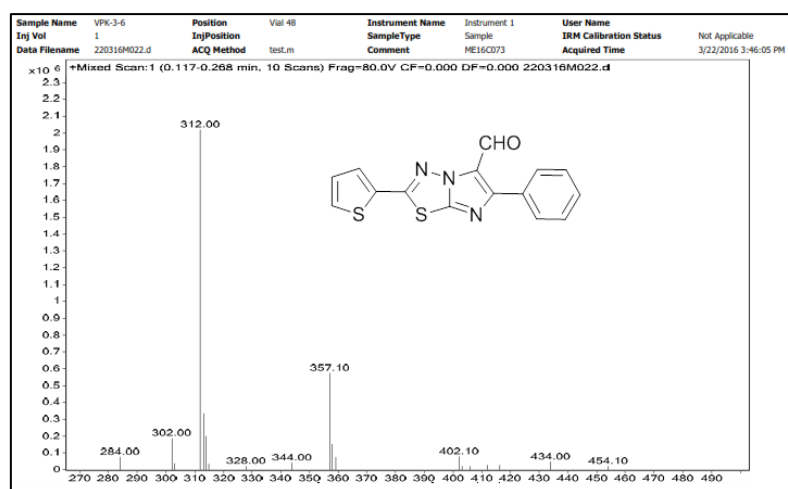


Figure 3.9 Mass spectrum of 5

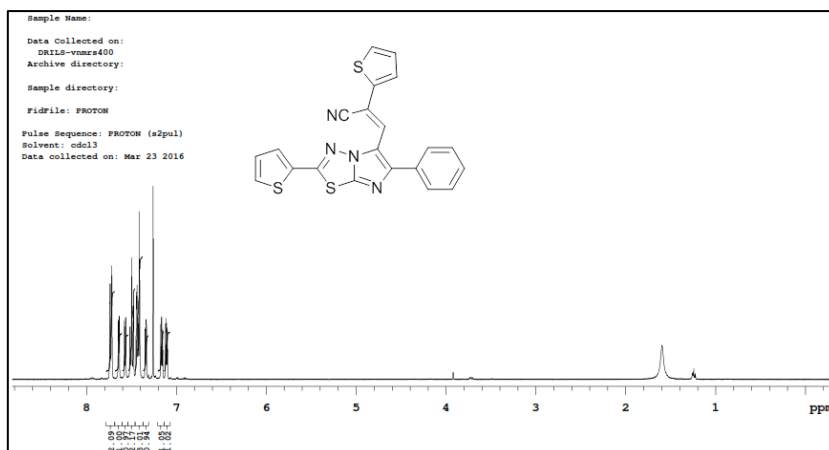


Figure 3.10 ^1H NMR spectrum of VK1

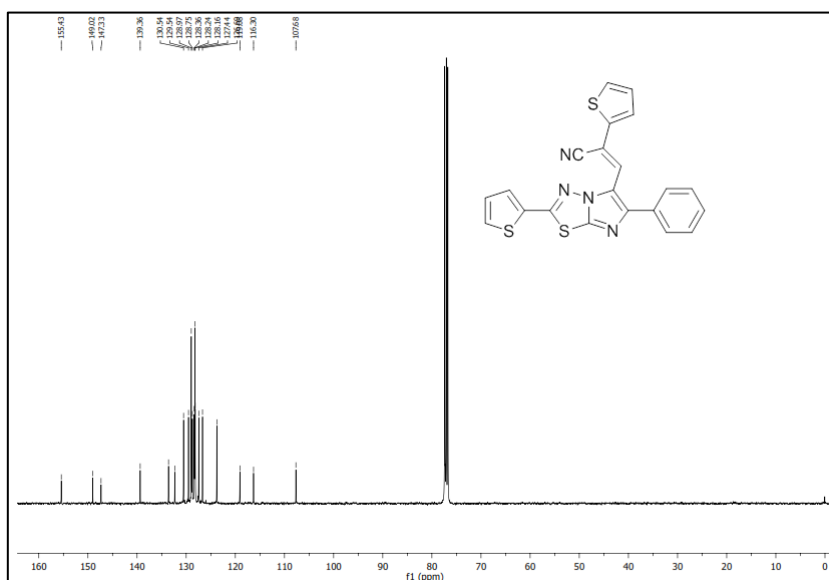


Figure 3.11 ^{13}C NMR spectrum of VK1

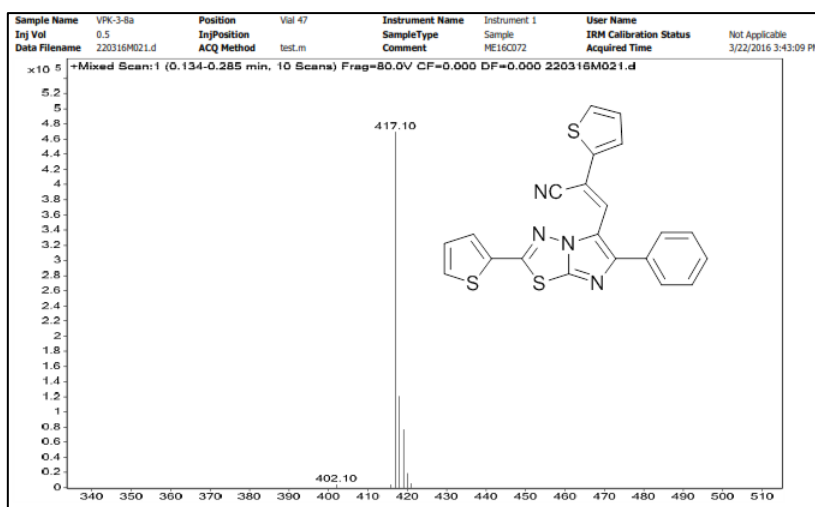


Figure 3.12 Mass spectrum of VK1

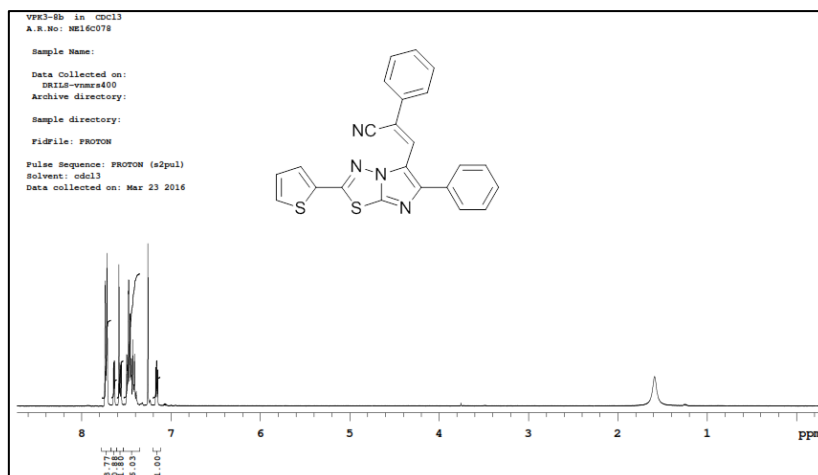


Figure 3.13 ^1H NMR spectrum of VK2

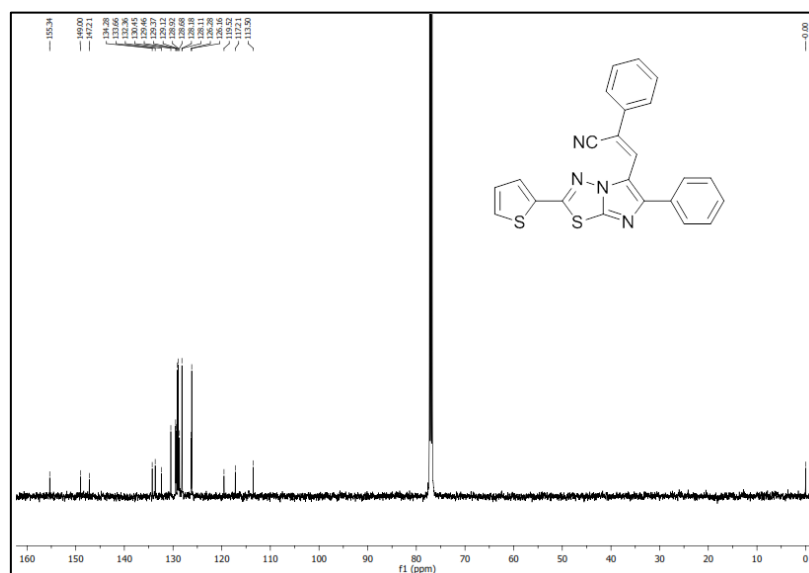


Figure 3.14 ^{13}C NMR spectrum of VK2

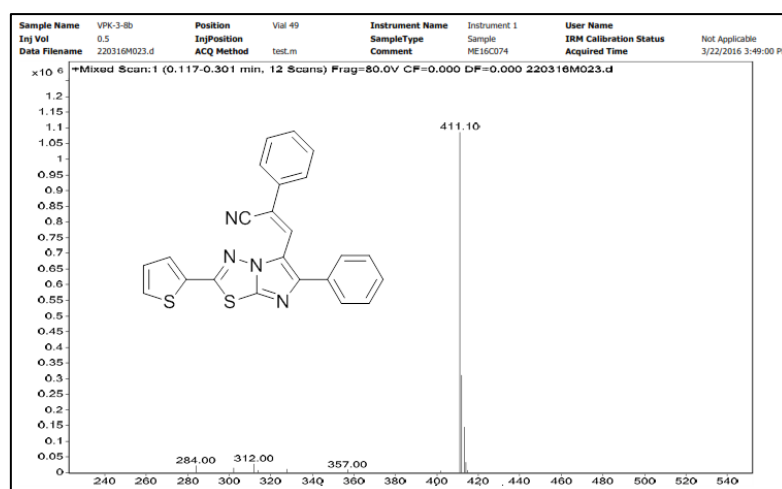


Figure 3.15 Mass spectrum of VK2

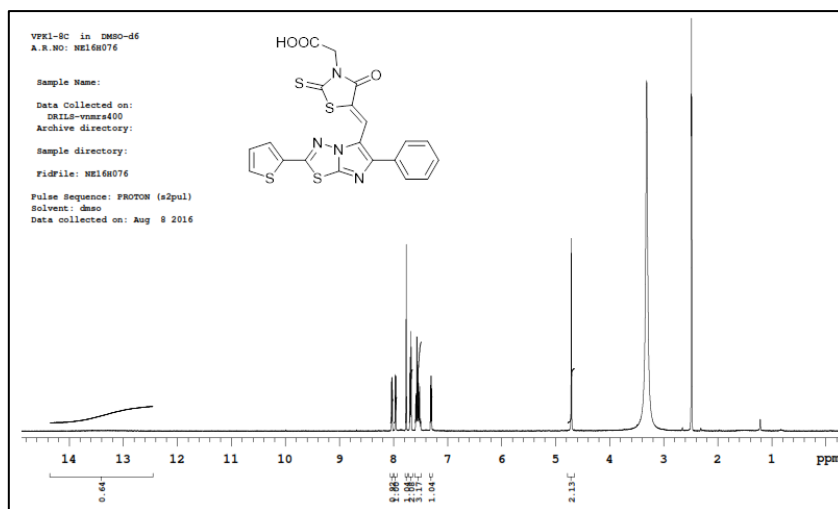


Figure 3.16 ^1H NMR spectrum of VK3

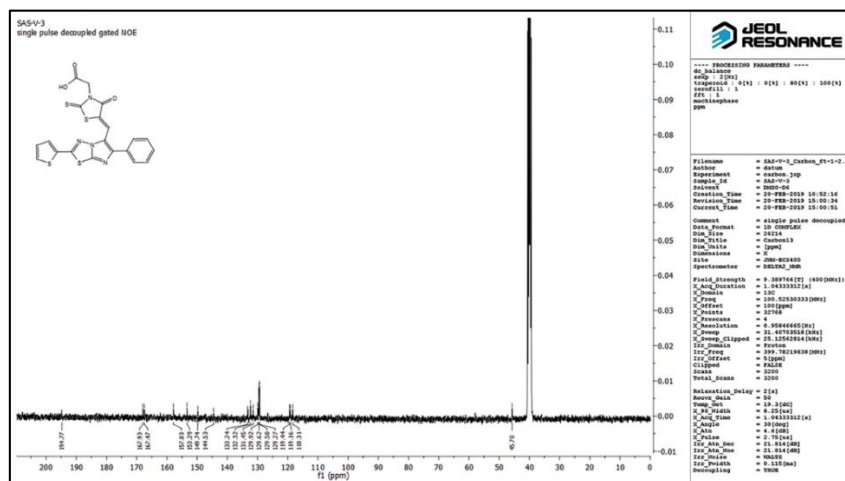


Figure 3.17 ^{13}C NMR spectrum of VK3

3.1.2 Photophysical studies

Figure 3.18 shows the normalized UV–Vis absorption and PL emission spectra of VK1–VK3 and the corresponding spectral data are listed in **Table 3.1**. The absorption spectra exhibit two separate bands: one at around 250–270 nm, which is ascribed to the π – π^* electronic excitations and the other, in the range of 300–440 nm, is attributed to ICT from the donor (thiophene, phenyl) to the acceptor (ITD) unit (Roquet et al. 2006). The large bathochromic shift in **VK3** as compared to that in **VK1** and **VK2** is due to the strong electron-withdrawing nature of rhodanine–3–acetic acid, which further leads to the extension of conjugation (Park et al. 2009; Tian et al. 2008). The E_g determined from the intersection point of absorption and emission spectra are 2.83, 2.95 and 2.72 eV for **VK1**, **VK2** and **VK3**, respectively. The emission spectra

exhibit maximum emission for **VK1**, **VK2** and **VK3** at 483, 480 and 509 nm, respectively, under excitation at their corresponding λ_{max} ; this establishes their luminescence properties.

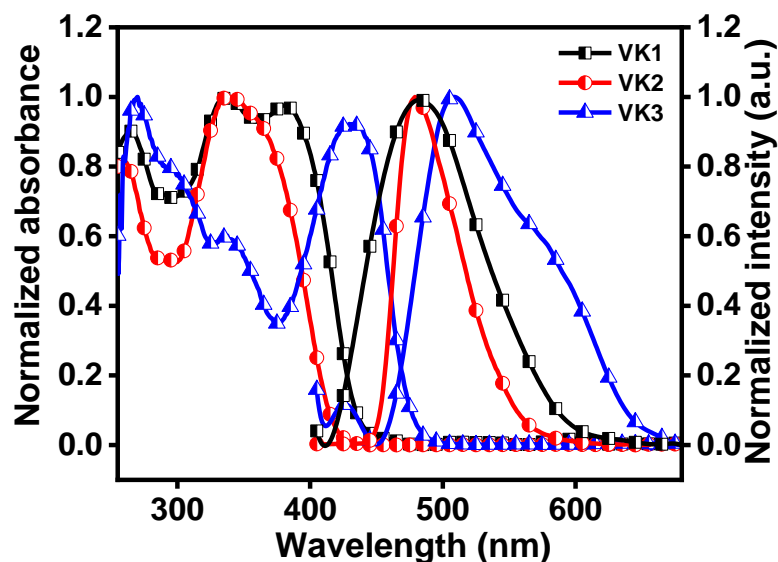


Figure 3.18 Normalized UV-vis absorption and PL spectra of **VK1**–**VK3** in CHCl_3 (1×10^{-5} M).

3.1.3 Electrochemical studies

Figures 3.19a–c show the cyclic voltammograms of **VK1**, **VK2** and **VK3**, respectively. Considering the onset oxidation potential, E_{HOMO} was calculated using the **Equation 2.1**. Furthermore, the LUMO levels were obtained from the electrochemically measured HOMO energy and spectroscopically determined band gap, using the **Equation 2.2**. The HOMO energy levels are -5.66 , -5.77 and -5.83 eV vs SCE, whereas the LUMO energy levels are -2.83 , -2.82 and -3.11 eV vs SCE for **VK1**, **VK2** and **VK3**, respectively. The significant reduction in the LUMO level is mainly attributed to the presence of strong electron withdrawing rhodanine-3-acetic acid group in **VK3**, reducing the band gap as compared to the cyano groups present in **VK1** and **VK2**. The experimentally obtained HOMO and LUMO values from CV are in agreement with the theoretically determined HOMO and LUMO values (**Table 3.1**).

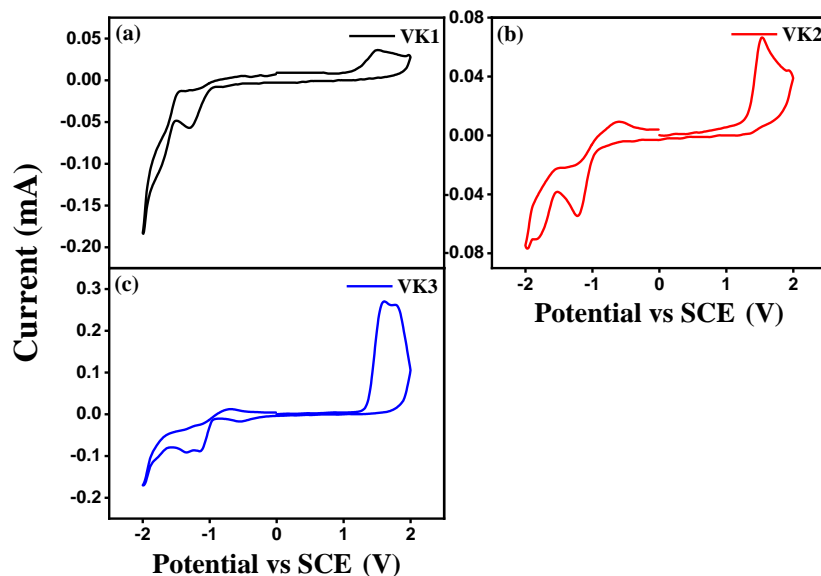


Figure 3.19 Cyclic voltammograms of (a) **VK1**, (b) **VK2** and (c) **VK3**.

Table 3.1 Summary of optical, electrochemical and theoretical data of **VK1–VK3**.

Molecules	$\lambda_{\max}^{\text{abs}}$ (nm)	$\lambda_{\max}^{\text{pl}}$ (nm)	E_g^{opt} (eV)	$E^{\text{ox}}_{\text{onset}}$ (V vs SCE)	HOMO (eV)	LUMO (eV)
VK1	385	483	2.89	1.18	-5.66 ^a	-2.83 ^b
					-5.96 ^c	-2.61 ^c
VK2	338	480	2.95	1.29	-5.77 ^a	-2.82 ^b
					-6.03 ^c	-2.54 ^c
VK3	434	509	2.64	1.35	-5.83 ^a	-3.11 ^b
					-6.21 ^c	-3.19 ^c

E_g^{opt} Optical band gap calculated from the intersection of normalized absorption and emission spectra.

$E^{\text{ox}}_{\text{onset}}$ Experimental onset oxidation potential vs SCE.

^a Experimental values from CV using Equation 2.1 with Fc/Fc⁺ as internal standard.

^b Experimental values using Equation 2.2.

^c Theoretical results.

3.1.4 Theoretical studies

Figure 3.20 depicts the optimized geometry and frontier orbital distribution of the molecules **VK1–VK3**. The effect of thiophene functioning as an electron donor

appended with ITD and the cyano/rhodanine-3-acetic acid group as an acceptor species governs the effective HOMO orbital distribution. This distribution is commonly observed in the three molecules **VK1–VK3**. The nature of the electronic distribution in the molecules **VK1** and **VK2** pertaining to the LUMO portrays a π – π^* -type transition, whereas in **VK3**, the electron density is mostly localized on ITD and rhodanine units. This type of distribution observed in the system effectively facilitates the charge transfer transition between the acceptor group and the entire molecular network. The effect of the rhodanine-3-acetic acid moiety, which imparts a stronger electron withdrawing nature in the orbital distribution of the LUMO level of **VK3**, is not observed in the case of **VK1** and **VK2**, possessing a cyano group as the electron acceptor.

Furthermore, the optimized structures of the compounds shown in **Figure 3.20** reveal that after the introduction of double bonds, the dihedral angle between ITD and thiophene-2-acetonitrile plane is 36.51° , and that between ITD and benzene plane is 29.31° in **VK1**; on the other hand, the dihedral angle between ITD and the phenyl acetonitrile plane is 39.51° , and that between ITD and the benzene plane is 30.21° in **VK2**; moreover, the dihedral angle between ITD and rhodanine-3-acetic acid plane is 23.01° , and that between ITD and benzene plane is 42.41° in **VK3**. The steric hindrance caused by the rhodanine moiety due to the lesser dihedral angle of 23.01° between ITD and the rhodanine-3-acetic acid plane increases the dihedral angle between ITD and the benzene plane in **VK3** to maintain the most stable conformation. The dihedral angles between the ITD plane and the substituted groups and the ITD plane and the phenyl group are listed in **Table 3.2**, and the structures are represented in **Figure 3.21**.

TD-DFT calculations of **VK1–VK3** were carried out to estimate the electronic excited state transitions and corroborate the experimental absorption transitions. The simulated absorption spectra of **VK1–VK3** are shown in **Figure 3.22**. The spectra exhibit two bands, wherein the higher energy band corresponds to the π – π^* transition and the lower energy band corresponds to the charge transfer transition. The results obtained by theoretical simulations are in agreement with the experimental results. Overall, the trend remains the same for both the theoretical and experimental calculations; however, small inconsistencies observed in energy transition are due to

theoretical overestimation (Mohan et al. 2018). The estimated HOMO and LUMO energy levels are listed in **Table 3.1** along with the experimental results.

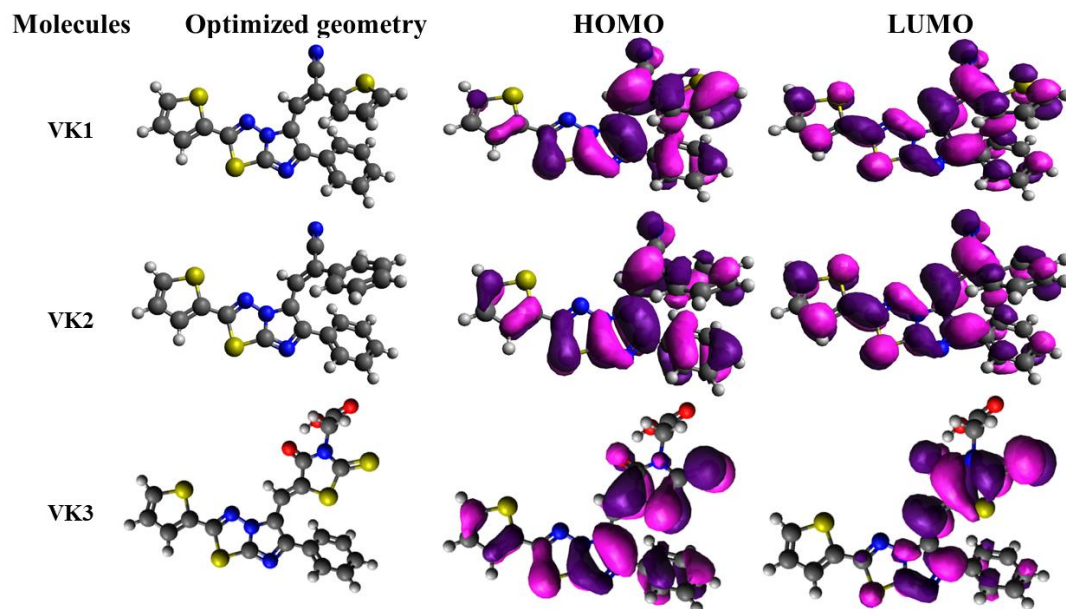


Figure 3.20 Ground-state optimized geometry and molecular orbitals (HOMO and LUMO) of **VK1–VK3**.

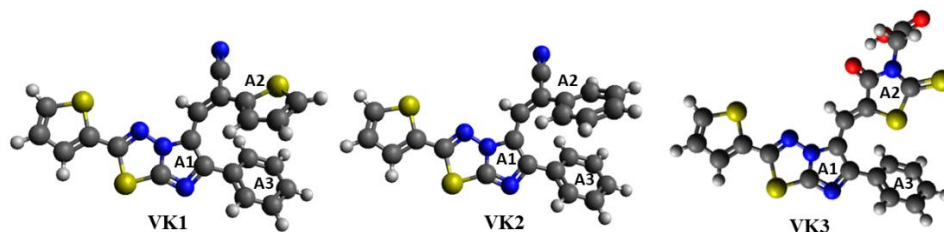


Figure 3.21 Optimized geometries of **VK1–VK3**.

Table 3.2 Selected dihedral angles of **VK1–VK3**.

Dihedral angles	VK1	VK2	VK3
A1-A2	36.5°	39.5°	23.0°
A1-A3	29.3°	30.2°	42.4°

A1- ITD plane, A2- thiophene -2-acetonitrile plane of **VK1**, phenyl acetonitrile plane of **VK2** and rhodanine–3–acetic acid plane of **VK3**, A3- benzene plane.

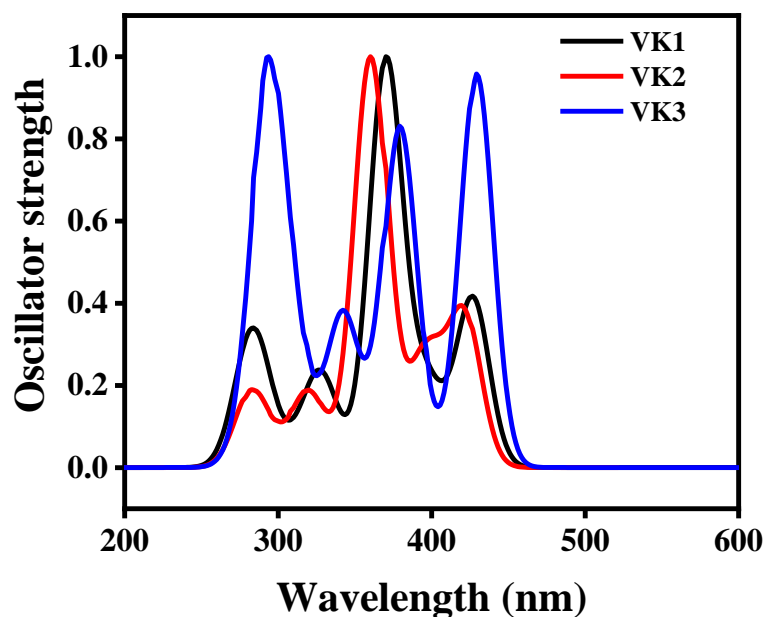


Figure 3.22 Simulated absorption spectra of **VK1–VK3**.

3.1.5 Thermal properties

As shown in **Figure 3.23**, **VK1–VK3** show satisfactory thermal stability. The decomposition temperatures (T_d) for **VK1**, **VK2** and **VK3** are 330, 357 and 346°C, respectively. The lower T_d of the molecules **VK1** and **VK3** than that of **VK2** is due to the presence of heterocyclic rings attached to the Th–ITD core moiety in **VK1** and **VK3**. The results show that the molecules could be relevant materials for electronic / photonic applications.

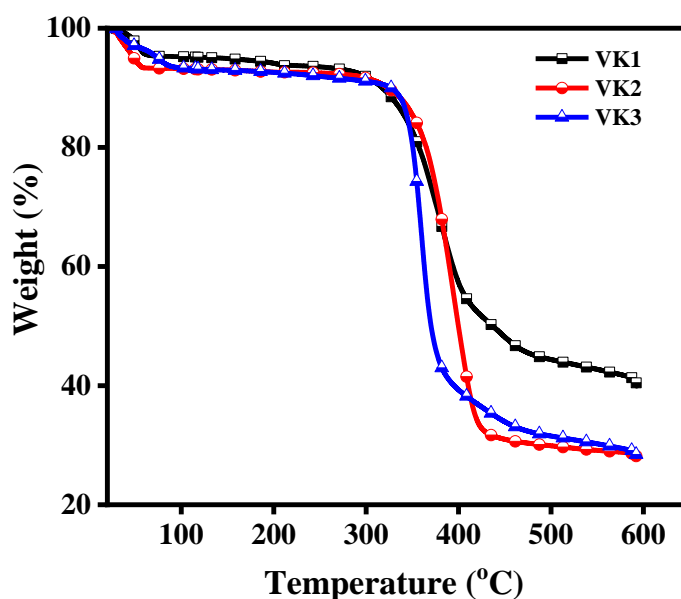


Figure 3.23 TGA plots of **VK1–VK3**.

3.1.6 Third-order NLO properties

3.1.6.1 Nonlinear absorption studies

Figures 3.24a–c show the OA Z-scan curves of the molecules **VK1–VK3**, respectively, in DMF solutions with the transmittance maintained at 75%. The molecules **VK1–VK3** were excited using the intensity of 1.386 GWcm^{-2} ($50 \mu\text{J}$). From the plots it is observed that the transmittance is minimum at the focus ($z=0$) and all the transmission curves are symmetric about the focus. Thus, the absorption is dependent on the excitation intensity. The molecules **VK1–VK3** show TPA along with RSA; thus, the net effect becomes the “effective TPA” process (Vishnumurthy et al. 2011). In all the cases, the data are found to match well with the theoretical model for the ESA. Thus, the effective nonlinear absorption coefficient ($\alpha(I)$), the nonlinear propagation equation (dI/dz), the normalized transmittance ($T(z)$) and finally, the imaginary part of third order nonlinear susceptibility ($\text{im } \chi^{(3)}$) for OA configuration were determined using the **Equations 2.3–2.6**, respectively. The NLA parameters were obtained by fitting the experimental data to the theoretical model using **Equation 2.3** and **2.5**.

As shown in **Figure 3.24a–c**, the experimental data are in a good agreement with the theoretical simulation and thus, the estimated β_{eff} values are 0.49×10^{-10} , 1.05×10^{-10} and $1.55 \times 10^{-10} \text{ m W}^{-1}$ for the molecules **VK1**, **VK2** and **VK3**, respectively. Under similar excitation conditions many NLO materials have shown effective NLA coefficient in the order of $10^{-10} \text{ m W}^{-1}$. The β_{eff} values obtained in the present study are comparable and better than that of many other organic NLO materials reported in the literature (**Table 3.3**). Therefore, these materials could act as better optical limiters for high energy devices.

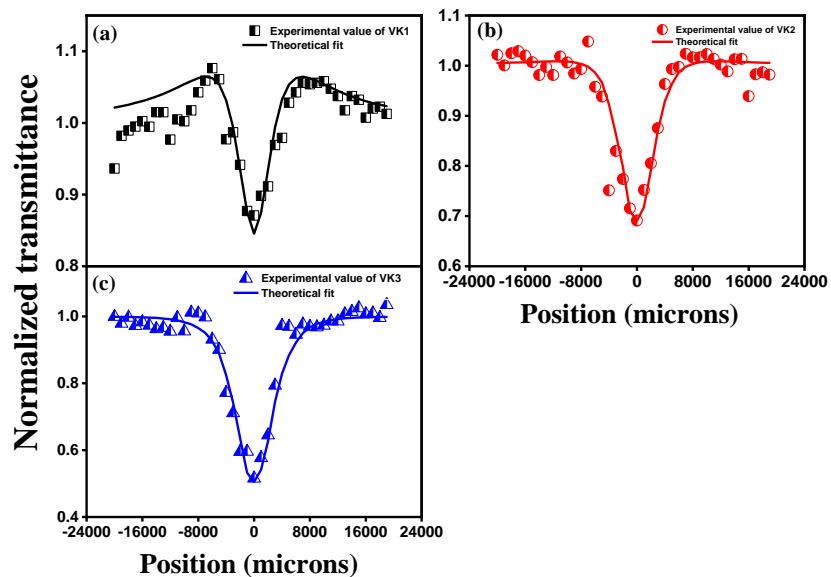


Figure 3.24 OA Z-scan curves of (a) VK1, (b) VK2 and (c) VK3 at 50 μJ .

3.1.6.2 Optical limiting studies

The graphs of the transmittance *versus* input fluence are shown in **Figure 3.25a–c** which reveal the results of optical limiting studies of the molecules VK1–VK3. The onset values are at 1.60, 0.78 and 0.66 J cm^{-2} for VK1, VK2 and VK3, respectively. Thus, the molecules can act as protective layers in devices with intense laser beam.

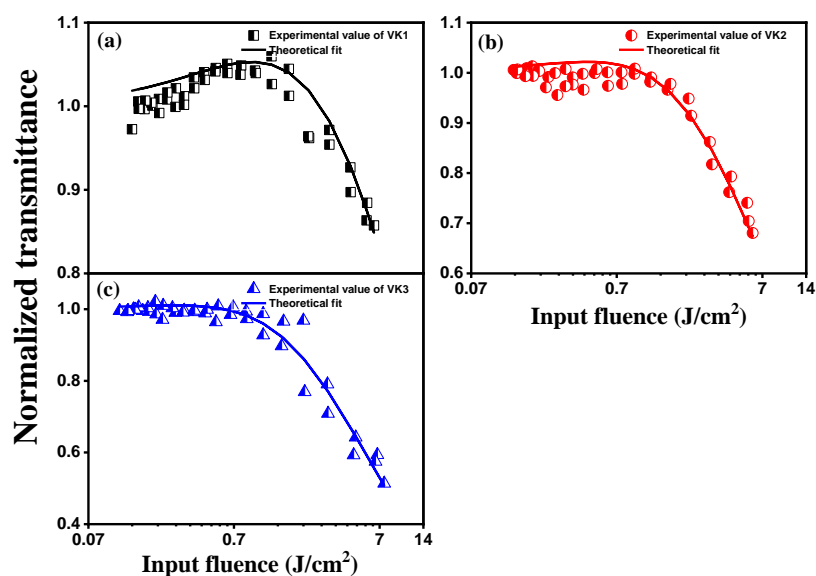


Figure 3.25 Optical limiting studies of (a) VK1, (b) VK2 and (c) VK3 at 50 μJ .

3.1.6.3 Nonlinear refraction studies

The **Figures 3.26a–c** represent normalized closed by open Z–scan curves of the molecules **VK1–VK3**. The graphs show a change in the transmission with a characteristic peak, followed by a null and a valley as the sample is moved from the input lens towards the output lens through the focus. This is the signature of negative nonlinearity. Due to this effect the molecules **VK1–VK3** behave like diverging lenses when in contact with the incoming beam; this results in the defocusing of the beam.

The normalized transmittance (T) at CA condition, the nonlinear refractive index (n_2) and the real part of third order nonlinear susceptibility (real $\chi^{(3)}$) were fitted using **Equations 2.7–2.9**, respectively. A comparison of the obtained NLO parameters for **VK1–VK3** with those reported in a few similar studies is presented in **Table 3.3**.

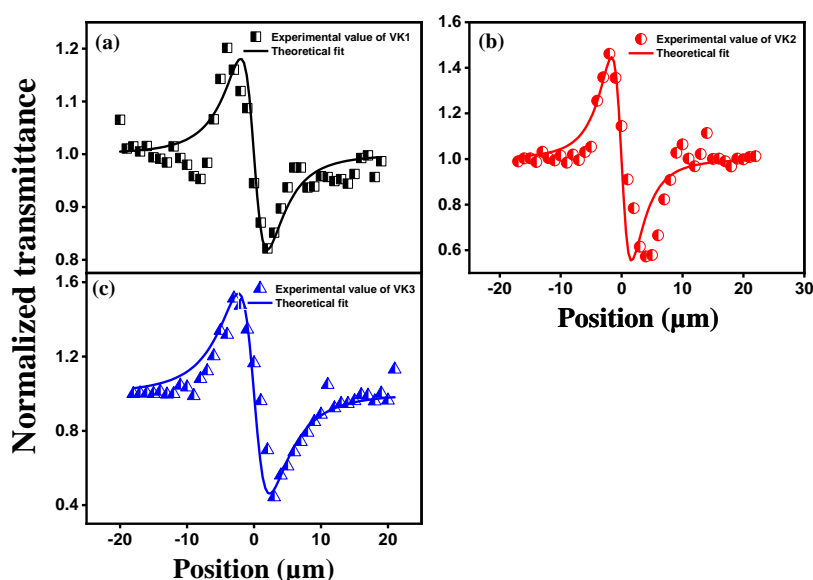


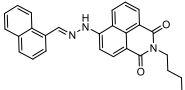
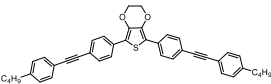
Figure 3.26 CA Z–scan curves of (a) **VK1**, (b) **VK2** and (c) **VK3** at 50 μJ .

In the present study, the introduction of ITD as an acceptor unit in between the high electron-donating thiophene and the phenyl moieties improves the rigidity and planarity of the molecules; thus, the strength of the D–A–D backbone is increased; this in turn enhances the extent of delocalization in the entire molecule. Thus, the synthesized molecules **VK1–VK3** exhibit substantially improved optical nonlinearity when subject to the Z–scan analysis; this is due to the presence of D–A arrangement and π –delocalization in them (Roncali 1999; Vishnumurthy et al. 2013).

Furthermore, the stronger electron accepting nature and polarity of rhodanine–3–acetic acid moiety in **VK3** than those of the cyano groups in **VK1** and **VK2** increases

the rigidity, hyperpolarizability and conjugation length in **VK3**; this results in larger NLO properties and improved β_{eff} and χ^3 values of **VK3** as compared to those of **VK1** and **VK2**. The studied molecules would be potential candidates for application in optical limiters in photonic devices.

Table 3.3 NLO parameters of **VK1–VK3** and few comparisons

Sample	β_{eff} 10^{-10} (mW ⁻¹)	η_2 10^{-11} (esu)	$\chi^{(3)}$ 10^{-12} (esu)	References
VK1	0.49	2.09	1.63	This work
VK2	1.05	5.40	3.29	This work
VK3	1.55	6.57	4.90	This work
Phenothiazine–Gold (Au) nanocomposite	1.74	8.0	-	(Edappadikkunnummal et al. 2017)
 1.41	1.41	-	4.65	(Gu et al. 2014)
phthalocyanine– 0.5% Au nanoparticles matrix	1.60	-	-	(Gowda et al. 2016)
 0.56	0.56	-	-	(Gowda et al. 2018)

3.1.7 The important findings from the experimental data

The high absorption maxima and low LUMO level of **VK3** as compared to those of **VK1** and **VK2** are due to the strong electron withdrawing ability of rhodanine–3–acetic acid present in **VK3**. The third–order NLO studies confirm the effective TPA of the molecules, exhibiting large third–order nonlinearity with a high β_{eff} in the order of 10^{-10} m W⁻¹ and optical limiting property. The higher β_{eff} value of **VK3** as compared to that of **VK1** and **VK2** is due to the strong electron accepting nature of rhodanine–3–acetic acid moiety, which also results in rigidity and enhanced π –delocalization in **VK3**. The results unveil that the molecule **VK3** could be a good choice for an optical limiter in laser photonics and also advance the development of other optoelectronic / photovoltaic devices.

3.2 AN INVESTIGATION ON PHOTOPHYSICAL AND THIRD-ORDER NONLINEAR OPTICAL PROPERTIES OF NOVEL THERMALLY-STABLE THIOPHENE-IMIDAZO [2,1-*b*][1,3,4] THIADIAZOLE BASED AZOMETHINES (VK4-VK6)

Among a wide variety of π -linkers used, the use of azomethine (also known as Schiff bases or imines, $-\text{N}=\text{CH}-$) as conjugated π -linkage in organic optoelectronic molecules is at its prime level of exploration as it provides more economic and less complicated path towards photovoltaic, optoelectronic and NLO materials (Iwan and Sek 2008; Mulholland et al. 2014; Petrus et al. 2015; Sicard et al. 2013; Yang and Jenekhe 1991). The facile one-step synthesis of azomethines via Schiff base condensation between an amine and an aldehyde gives a desired product with relatively good yield and producing water as the by-product of the reaction (Petrus et al. 2014; Schiff 1864). Besides that, the reaction can be performed in mild conditions without the usage of catalyst and the product obtained needs minimal purification (Isik et al. 2012). The materials possessing imine bond in them are emerging as fascinating materials due to their chemical stability (Barik et al. 2011; Bolduc et al. 2010; Dufresne et al. 2010), interesting photo physical properties and electrochemical properties (Barik et al. 2011; Bourgeaux and Skene 2007; Dufresne et al. 2009).

In this context, anticipating promising results from small molecular NLO materials, three new class of azomethines with thiophene and ITD as the invariable donor and acceptor moieties were designed and synthesized in which three different π -conjugated systems viz., pyrene (**VK4**), anthracene (**VK5**) and triphenylamine (**VK6**) were bonded to the Th-ITD core unit via azomethine linkage as π -spacer. The pyrene, anthracene and triphenylamine units were selected to study the influence of fused, rigid and conjugated π -extenders on optoelectronic properties, which is discussed herein.

3.2.1 Structural elucidation of the intermediates and final compounds

The molecular ion peak at m/z 329 corresponding to $[\text{M}+\text{H}]$ of intermediate **6** confirms the structure. The reduction of **6** to form intermediate **7** is clearly specified by the ^1H NMR spectrum wherein, the two $-\text{NH}_2$ protons at δ 3.76 ppm along with eight aromatic protons at δ 7.87–6.74 ppm prove the formation of **7**. The peaks resonating at δ 154.7–107.9 ppm, corresponding to the aromatic carbon atoms in ^{13}C NMR spectrum of **7** further confirm the structure. Also, a molecular ion peak at m/z 299 in mass

spectrum, corresponding to [M+H] of intermediate **7** further confirms the structure. The confirmation of structures of final compounds **VK4–VK6** is done by ^1H NMR, ^{13}C NMR, mass and elemental analyses. The NMR spectral characterizations of one of the representative molecules **VK4** is discussed herewith. The ^1H NMR spectrum of **VK4** shows a prominent singlet signal at δ 9.55 ppm, corresponding to imine ($-\text{CH}=\text{N}-$) protons, seventeen multiplets at δ 9.06–7.16 ppm, corresponding to the aromatic protons of thiophene, ITD, phenyl ring and pyrene units and the absence of $-\text{NH}_2$ protons at δ 3.76 ppm clarify the structure. The structure is further confirmed by ^{13}C NMR spectrum wherein, the aromatic carbons resonate at δ 157.38–108.28 ppm. Similar patterns of signals were observed in the ^1H and ^{13}C NMR spectrum of **VK5** and **VK6** as well. Furthermore, molecular ion peaks at m/z 511.50, 487.10 and 554.20 in the mass spectrum, corresponding to [M+H] of **VK4**, **VK5** and **VK6**, respectively, confirm the structure of **VK4–VK6**. In addition to the spectral characterizations, the elemental analysis further evidences the structures of all the intermediates and final compounds. The ^1H NMR, ^{13}C NMR and mass spectra of intermediates and final compounds **VK4–VK6** are presented in the following **Figures 3.27–3.39**.

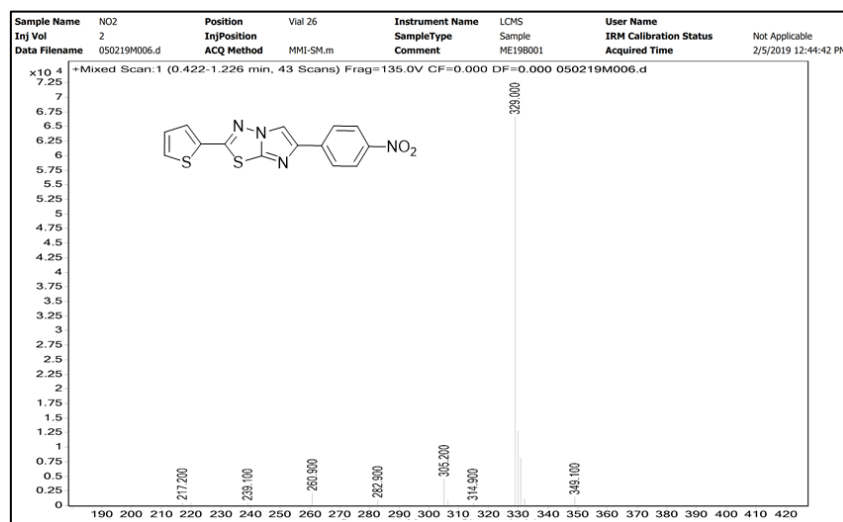


Figure 3.27 Mass spectrum of **6**

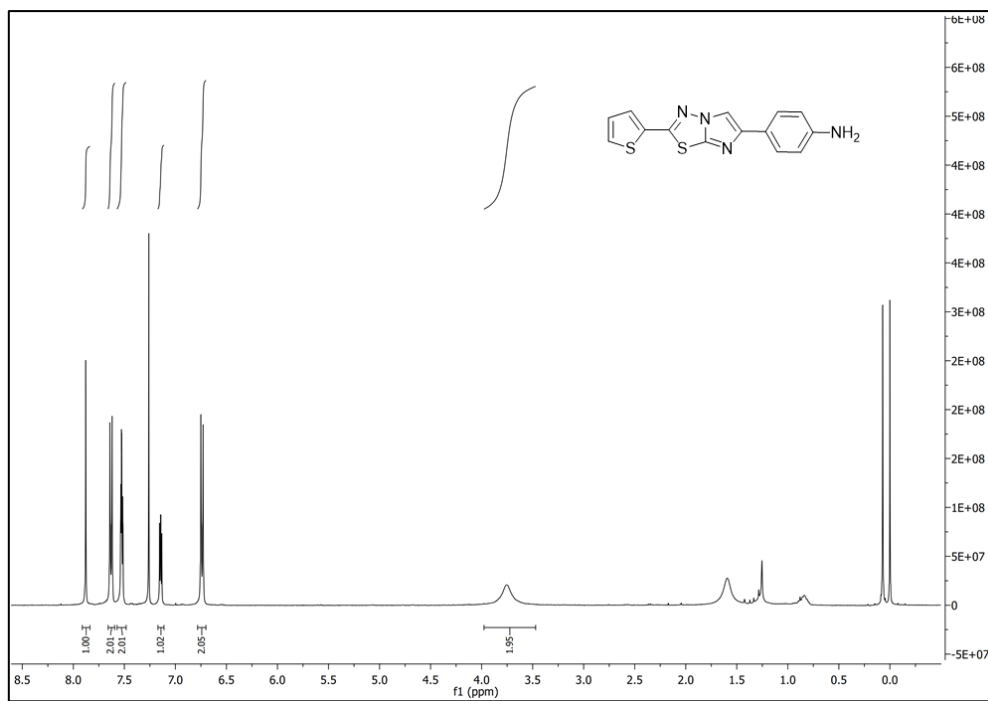


Figure 3.28 ^1H NMR spectrum of **7**

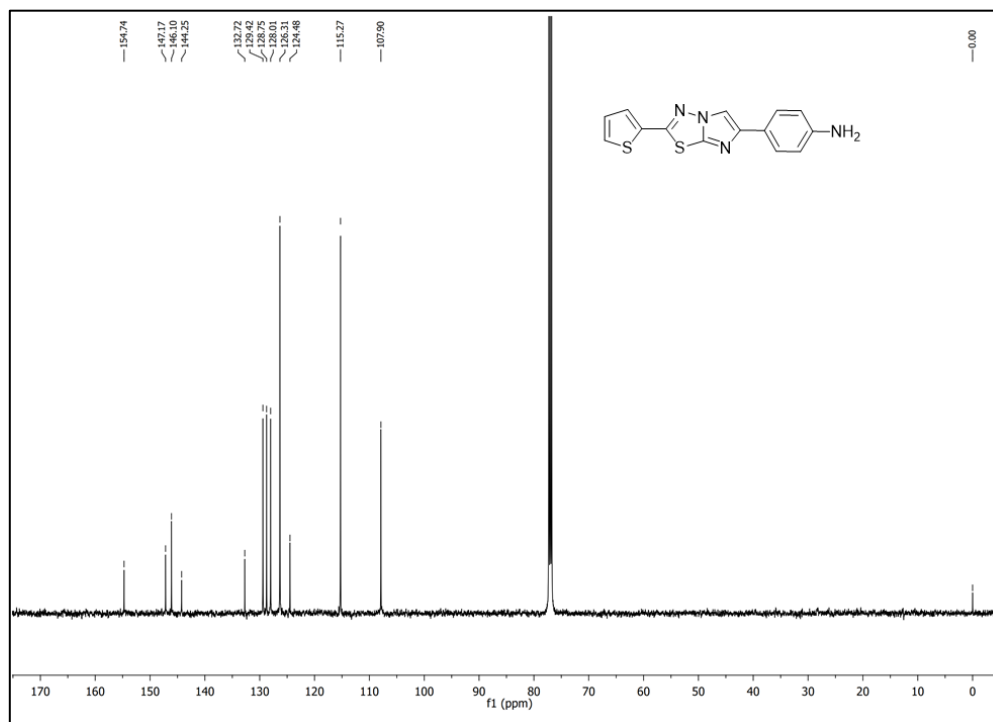
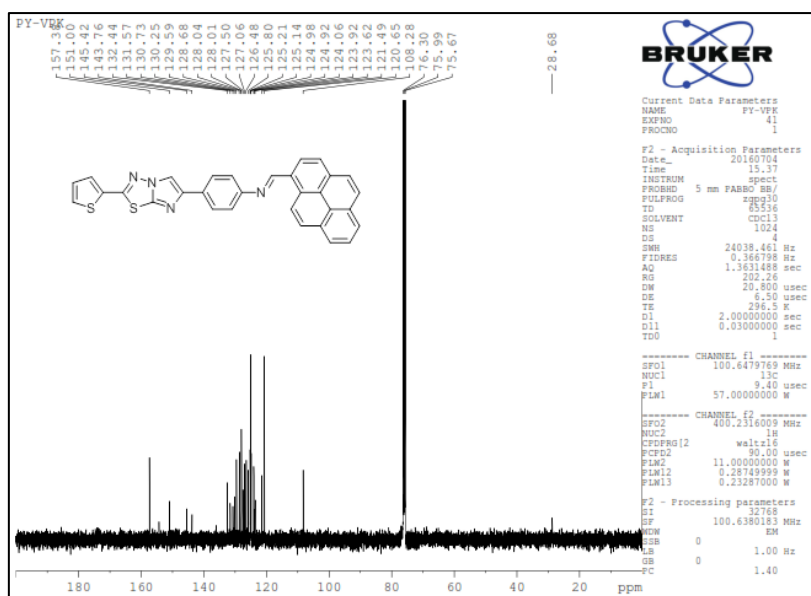
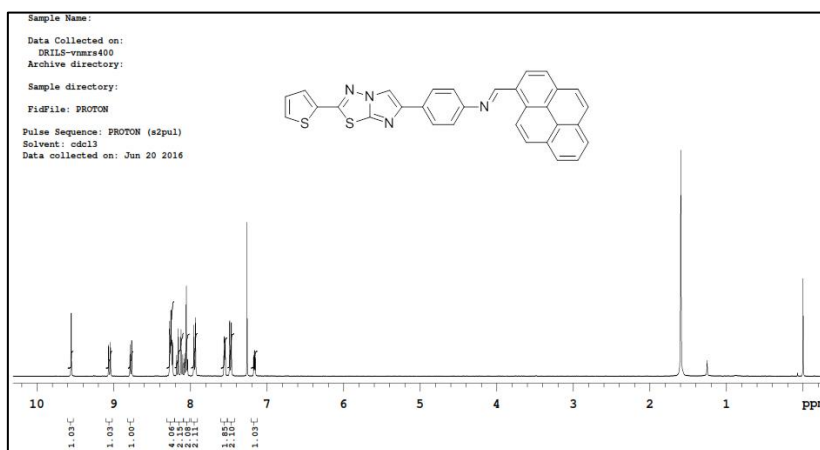
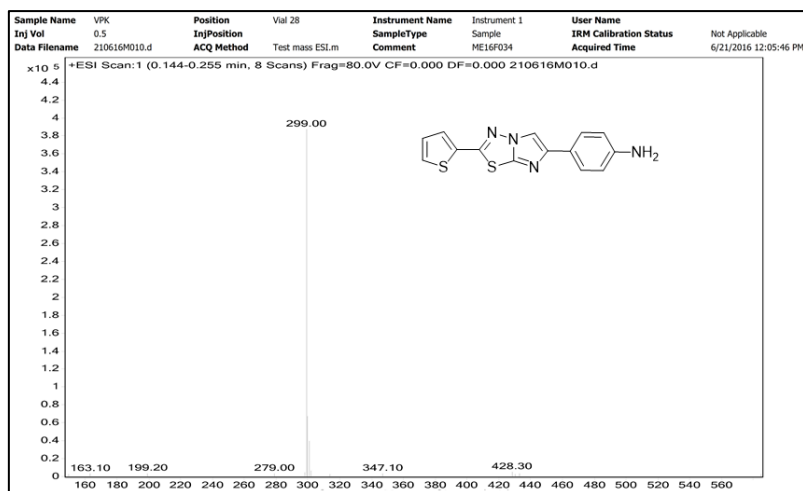


Figure 3.29 ^{13}C NMR spectrum of **7**



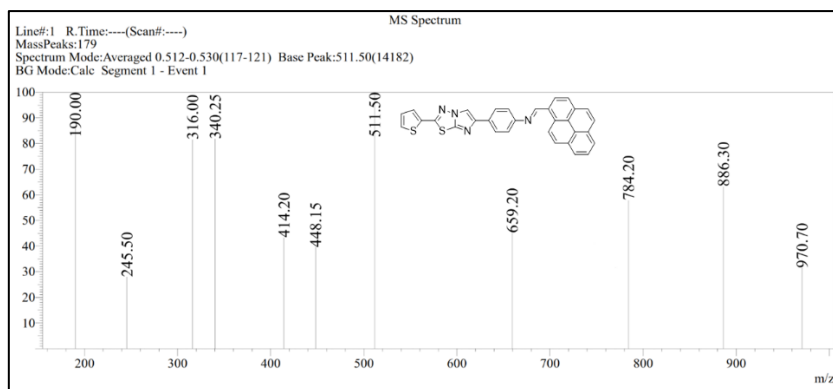


Figure 3.33 Mass spectrum of VK4

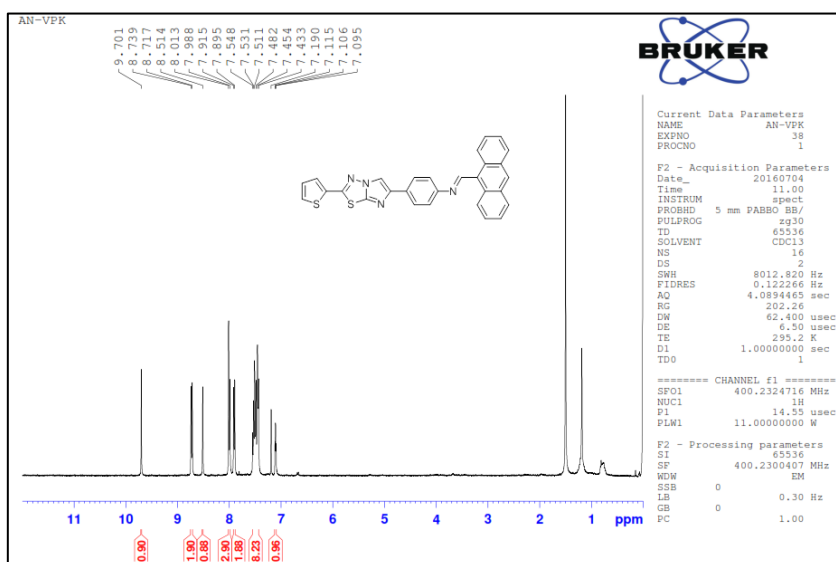


Figure 3.34 ¹H NMR spectrum of VK5

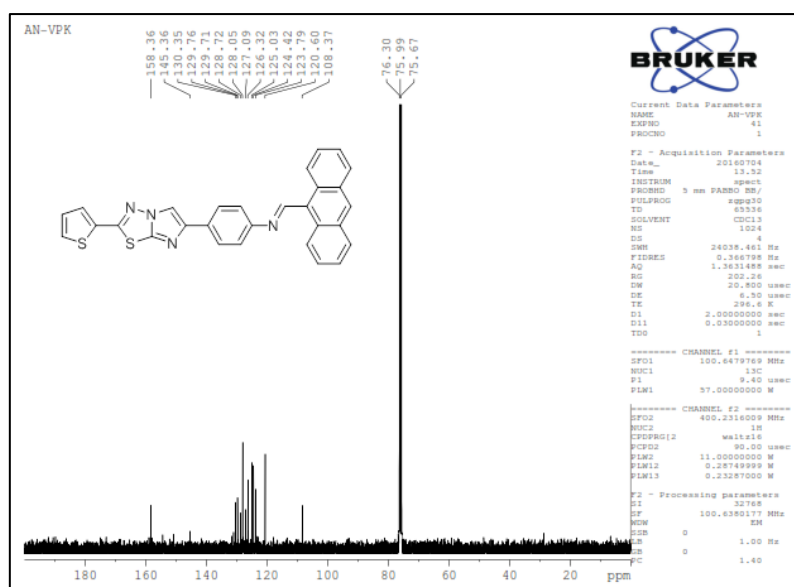


Figure 3.35 ¹³C NMR spectrum of VK5

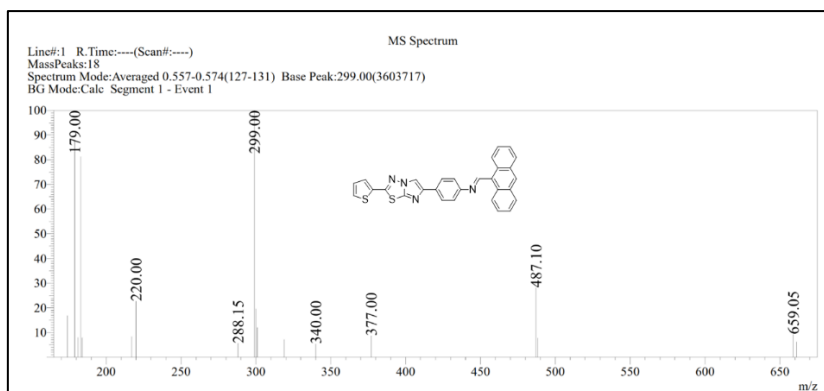


Figure 3.36 Mass spectrum of VK5

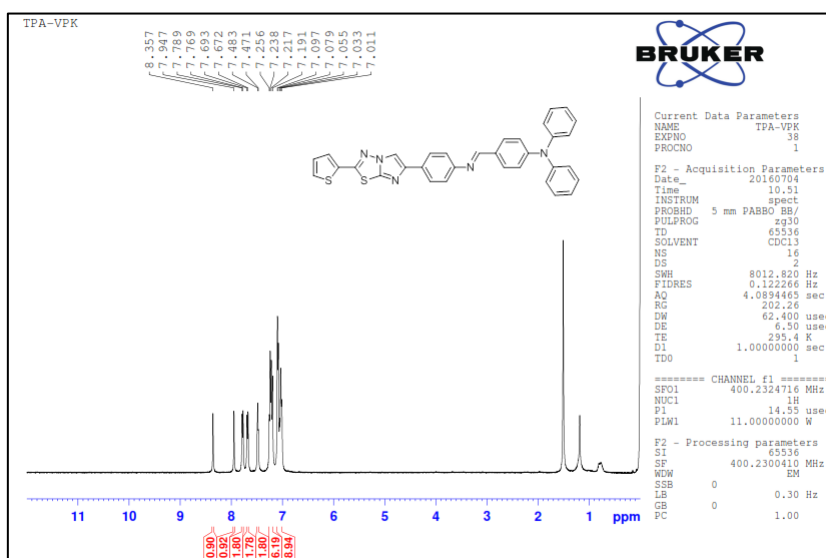


Figure 3.37 ¹H NMR spectrum of VK6

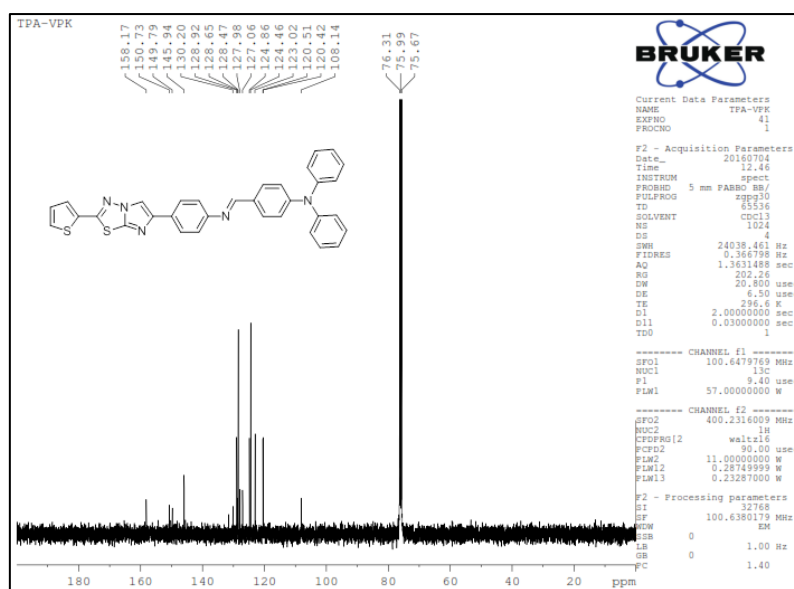


Figure 3.38 ¹³C NMR spectrum of VK6

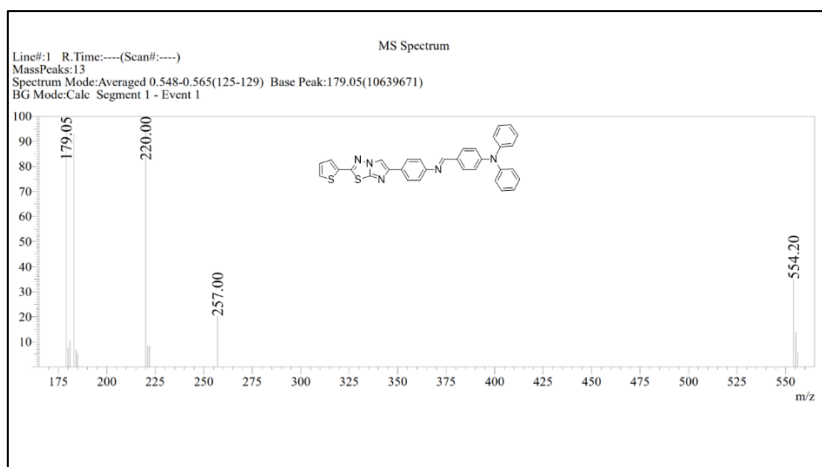


Figure 3.39 Mass spectrum of **VK6**

3.2.2 Photophysical studies

The UV–Vis absorption and fluorescence emission spectra of **VK4–VK6** are shown in **Figure 3.40**. As shown in **Figure 3.40**, the λ_{max} of **VK4**, **VK5** and **VK6** is located at 403, 380 and 390 nm, respectively. The molecules **VK4** and **VK6** exhibited three distinct absorption peaks in the range of 250–310, 315–470 and 480–560 nm region, wherein two higher energy peaks observed at 294 and 403 nm for **VK4**, 297 and 390 nm for **VK6** correspond to the π – π^* electronic transitions in the molecules, while a weak and broad band at lower energy region (480–560 nm) corresponds to the ICT from electron donor to the acceptor unit which is due to the additional pyrene and triphenylamine groups in **VK4** and **VK6**, respectively, leading to the extension of π –conjugation. In the case of molecule **VK5** the observed peaks at 264 and 320–360 nm region is attributed to π – π^* electronic excitations and the absence of ICT band in **VK5** compared to that of **VK4** and **VK6** is due to the steric hindrance by anthracene group which distorts the π –conjugation in **VK5**. The absorption bands of the molecules are in the order of **VK4**>**VK6**>**VK5**, since the conjugation of substituents are in the order pyrene> triphenylamine> anthracene. The normalized fluorescence spectra showed single emission peak at 572, 526 and 552 nm for **VK4**, **VK5** and **VK6**, respectively. The E_g calculated from the intersection of normalized absorption and emission spectra are 2.23, 2.68 and 2.28 eV for **VK4**, **VK5** and **VK6**, respectively. The decrease in the band gap for **VK4** and **VK6** is due to the higher extent of conjugation in **VK4** and **VK6** compared to that of **VK5**. The results of the optical studies are given in **Table 3.4**.

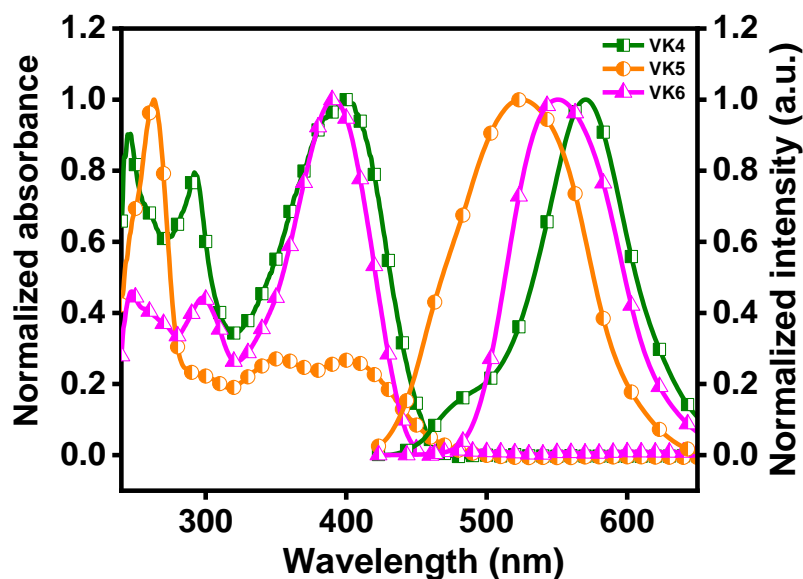


Figure 3.40 Normalized UV–Vis absorption and PL spectra of **VK4–VK6** recorded in CHCl_3 (10^{-5} M).

3.2.3 Electrochemical studies

The cyclic voltammograms of the molecules **VK4**, **VK5** and **VK6** are shown in **Figure 3.41a–c**, respectively. The molecules exhibit one oxidation peak in the anodic region and the onset of oxidation is at 0.73, 1.01 and 0.88 V vs SCE for **VK4**, **VK5** and **VK6**, respectively. The HOMO energy levels of **VK4–VK6** determined using onset potentials of oxidation process, calculated using the **Equation 2.1**, are -5.26 , -5.54 and -5.41 eV, respectively. Similarly, the LUMO energy levels determined using the **Equation 2.2**, are -3.03 , -2.86 and -3.13 eV for **VK4–VK6**, respectively.

The observed higher HOMO of **VK4** than that of **VK5** and **VK6** is due to the increased π -conjugation of pyrene group present in **VK4** (Zhou et al. 2010). The experimental data are listed in **Table 3.4**.

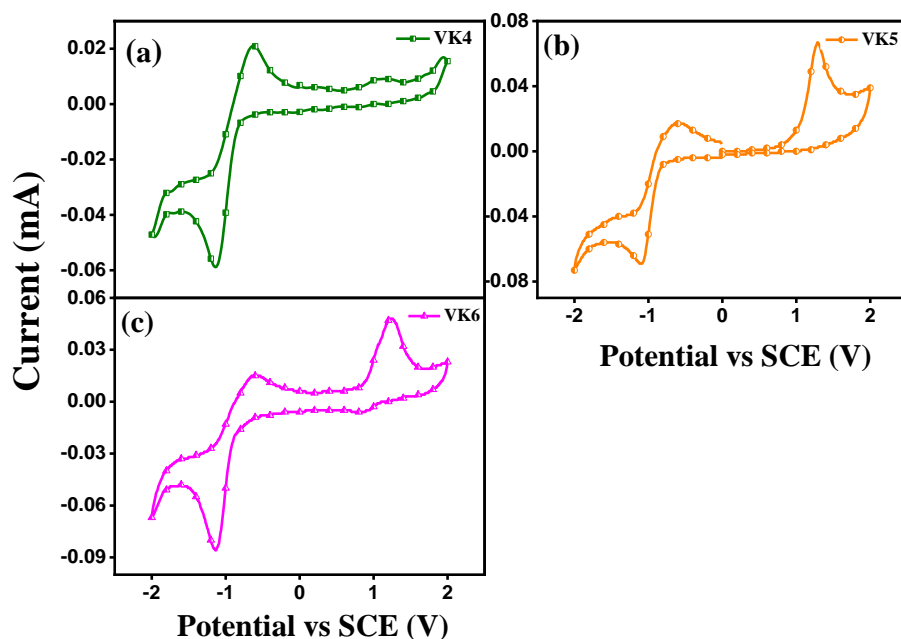


Figure 3.41 Cyclic voltammograms of (a) VK4, (b) VK5 and (c) VK6.

Table 3.4 Summary of optical, electrochemical and theoretical data of VK4–VK6.

Molecules	$\lambda_{\max}^{\text{abs}}$ (nm)	$\lambda_{\max}^{\text{pl}}$ (nm)	E_g^{opt} (eV)	$E^{\text{ox}}_{\text{onset}}$ (V vs SCE)	HOMO (eV)	LUMO (eV)
VK4	403	572	2.70	0.73	-5.26 ^a	-3.03 ^b
					-5.57 ^c	-2.51 ^c
VK5	380	526	2.81	1.01	-5.54 ^a	-2.86 ^b
					-5.54 ^c	-2.56 ^c
VK6	390	552	2.75	0.88	-5.41 ^a	-3.13 ^b
					-5.37 ^c	-2.28 ^c

E_g^{opt} Optical band gap calculated from the intersection of normalized absorption and emission spectra.

$E^{\text{ox}}_{\text{onset}}$ Experimental onset oxidation potential vs SCE.

^a Experimental values from CV using Equation 2.1 with Fc/Fc⁺ as internal standard.

^b Experimental values using Equation 2.2.

^c Theoretical results.

3.2.4 Theoretical studies

The optimized ground spatial arrangement, the HOMO and the LUMO energy levels of the molecules **VK4–VK6** are shown in **Figure 3.42**. The uniform distribution of electrons in the HOMO of **VK4** is due to the structural planarity of the molecule, whereas in **VK5** the anthracene moiety is twisted by 90° to the plane of Th–ITD core, as a result of which the electrons are localized mostly on anthracene, resulting in the non-uniform electronic distribution in the HOMO. Further, in molecule **VK6**, the electrons in the HOMO are majorly localized on high electron donating triphenylamine and phenyl moiety. There is a similar kind of distribution of electrons in LUMO as that of HOMO in **VK4** and **VK5**, which indicates $\pi-\pi^*$ type transition, whereas in **VK6** LUMO electron density is mainly localized on thiophene unit, indicating the charge transfer between the donor and acceptor groups within the molecule.

The excited state electronic transitions were analyzed using TD-DFT calculations. The simulated absorption spectra of **VK4–VK6** are depicted in **Figure 3.43**. There are distinct bands located at lower and higher wavelength regions. Except for **VK5**, the band at lower wavelength corresponds to $\pi-\pi^*$ transition whereas the band at higher wavelength region corresponds to charge transfer transition in **VK4** and **VK6**. As anthracene moiety is twisted by 90° to the plane of Th–ITD core, the band at higher wavelength region in **VK5** may correspond to the extended $\pi-\pi^*$ transition. The theoretical results are in consistence with the experimental results (**Table 3.4**).

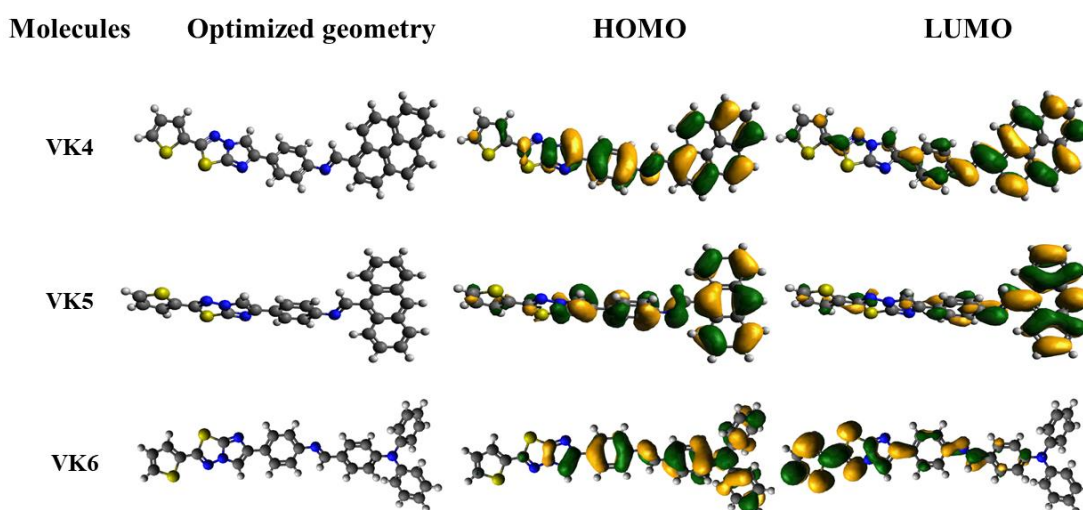


Figure 3.42 Ground state optimized geometry and representations of HOMO and LUMO of **VK4–VK6**.

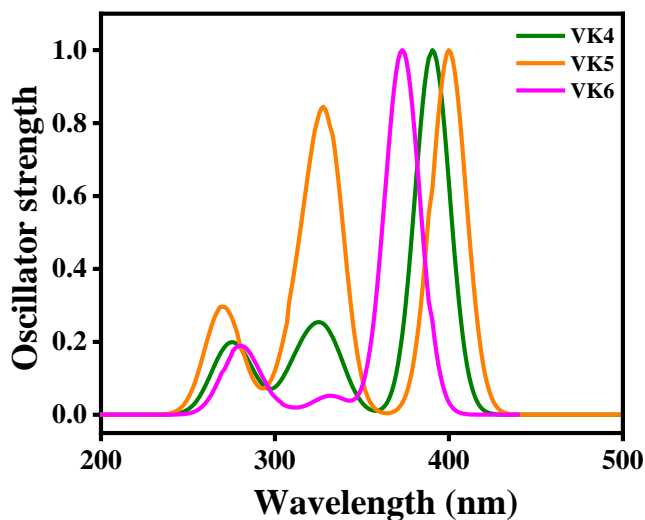


Figure 3.43 Simulated absorption spectra of **VK4–VK6**.

3.2.5 Thermal properties

The TGA plots of **VK4–VK6** are shown in **Figure 3.44**. The measurements disclose good thermal stability of molecules with the T_d of 380, 373 and 331°C for **VK4**, **VK5** and **VK6**, respectively. The presence of fused pyrene unit in **VK4** makes the molecule more rigid and stable compared to anthracene and triphenylamine unit in **VK5** and **VK6**, which results in higher T_d of **VK4** compared to that of **VK5** and **VK6**. From the analysis it is observed that the molecules **VK4–VK6** show sufficient stability towards photonic applications.

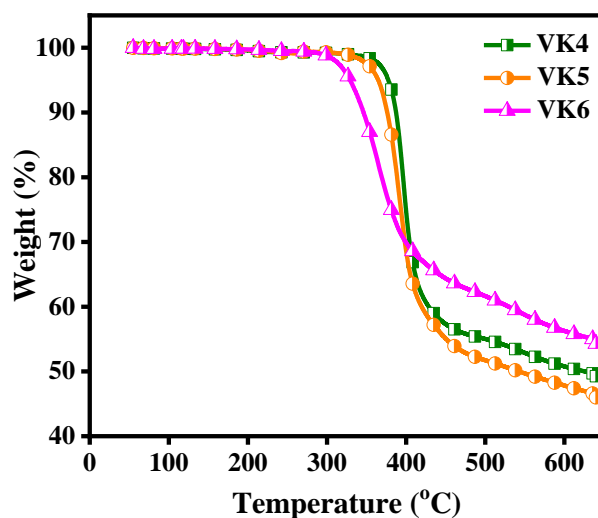


Figure 3.44 TGA plots of **VK4–VK6**.

3.2.6 Third-order NLO properties

3.2.6.1 Nonlinear absorption studies

The NLO properties of the molecules **VK4** and **VK5** were examined using 50 μJ laser pulse, corresponding to the peak on-axis intensity of 1.386 GWcm^{-2} . The experiment was carried out in DMF solution with the transmittance maintained at 71%. Unfortunately, the molecule **VK6** did not show any NLO property under nanosecond excitation rather, exhibited scattering due to the limited solubility in DMF. The **Figure 3.45a** and **b** represent the characteristic OA Z-scans obtained for **VK4** and **VK5**, respectively. It is observed that all the curves are symmetric about $z=0$, at the focus. The decrease in transmittance around the focal point is corresponding to RSA of the molecules. The RSA is mostly related with TPA process and also since solutions exhibit considerable absorption at laser excitation wavelength, ESA is also contributing to the RSA (Kulyk et al. 2016; Vishnumurthy et al. 2011). The intensity dependent $\alpha(I)$ for a system where the net NLA is due to both TPA and ESA (RSA) (associated with SA), the nonlinear propagation and the normalized transmittance were obtained using **Equations 2.3–2.5**. The experimental data were numerically fitted to the theoretical model using **Equation 2.3** and **2.5** to obtain the values of NLA parameters. The imaginary part of $\chi^{(3)}$ was determined using **Equation 2.6**. All the calculated NLA coefficients are listed in **Table 3.5**. The values of β_{eff} are $0.81 \times 10^{-10} \text{ m W}^{-1}$ and $0.55 \times 10^{-10} \text{ m W}^{-1}$ for **VK4** and **VK5**, respectively.

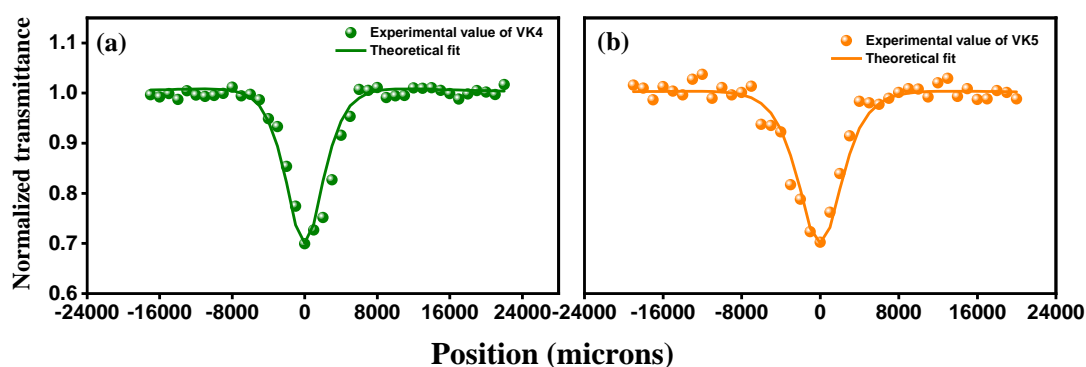


Figure 3.45 OA Z-Scan curves of (a) **VK4** and (b) **VK5** at 50 μJ .

3.2.6.2 Optical limiting studies

The optical limiting behavior of **VK4** and **VK5** was studied from the graphs of normalized transmittance versus input fluence (**Figure 3.46a** and **b**, respectively), that

show the decrease in transmittance with the increase in the input laser fluence. The optical limiting onset values are at 0.79 and 0.90 J cm⁻² for **VK4** and **VK5**, respectively, which are relatively low compared to other organic conjugated small molecular NLO materials. Thus, both the molecules exhibit considerably efficient optical power limiting. The obtained β_{eff} for **VK4** and **VK5** in the present study are comparable and reasonably higher than that of a few of the organic small molecular NLO materials reported (**Table 3.5**). For example, Zheng *et al.* (Zheng *et al.* 2019) reported TPA–quinazolinone derivatives with the excellent third–order NLO responses with β_{eff} of 0.36×10^{-10} m W⁻¹ while, Jia *et al.* (Jia *et al.* 2017, 2018) studied NLO properties of quinacridone and quinazolinone derivatives which showed remarkable NLO responses with β_{eff} of 0.76×10^{-10} and 0.47×10^{-11} m W⁻¹, respectively, whereas, Gowda *et al.* (Gowda *et al.* 2018) synthesized EDOT based bent-core and hockey stick like liquid crystals which exhibited large optical nonlinear properties with β_{eff} of 0.56×10^{-10} m W⁻¹.

The improved and remarkable NLO responses of **VK4** and **VK5** compared to the reported values (**Table 3.5**) indicate that these materials could have immense potential as optical limiters to be used in photonic devices.

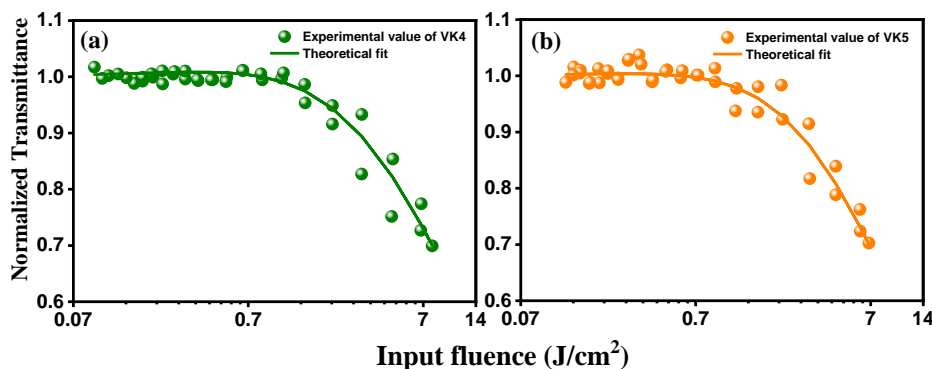


Figure 3.46 Optical limiting studies of (a) **VK4** and (b) **VK5** at 50 μJ.

3.2.6.3 Nonlinear refraction studies

The pure NLR curves were obtained by dividing CA transmittance data by the corresponding OA data. **Figure 3.47a** and **b** represent the closed by open aperture curves for **VK4** and **VK5**, respectively and it is seen that there is a peak–valley configuration in the obtained plot, which is a signature of negative nonlinearity of the materials. As a result of this, there is a gradient in refractive index with the lowest value at the beam axis and gradual increase towards the periphery which is produced by the

Gaussian laser beam. Thus, the materials behave like diverging lens when the laser beam falls on the detector and hence, diverge (defocus) the beam (Edappadikkunnummal et al. 2017). The normalized transmittance (T) at CA condition, the η_2 and real $\chi^{(3)}$ were fitted using **Equations 2.7–2.9**, respectively. The NLR parameters of **VK4** and **VK5** are tabulated in **Table 3.5**.

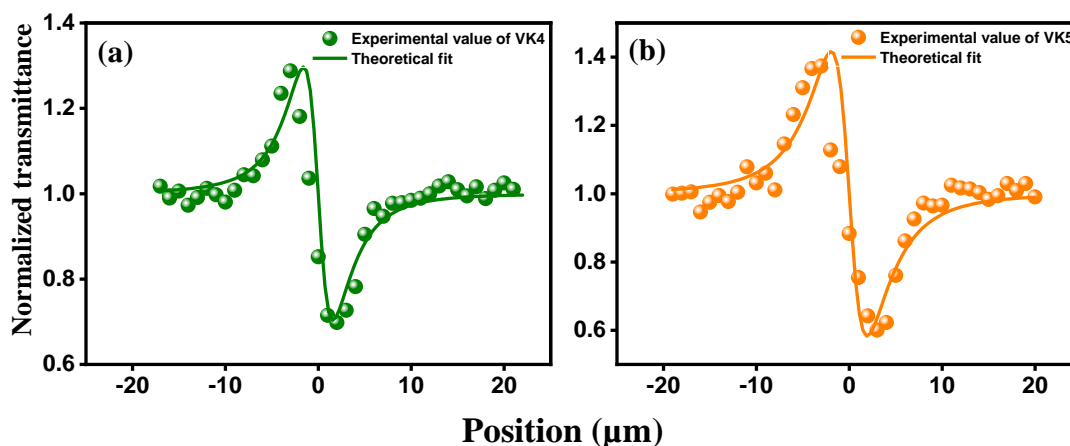
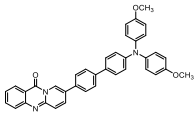
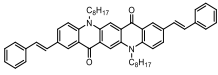
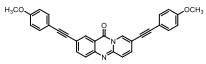
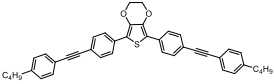


Figure 3.47 CA Z–Scan curves of (a) **VK4** and (b) **VK5** at 50 μJ .

The superposition of p_z atomic orbitals of carbon in conjugated system facilitate the movement of π –electrons in large molecular orbitals. The planarity and rigidity of conjugated backbone optimizes the overlapping of π –orbitals which results in enhanced electron delocalization, leading to the enhancement in optical nonlinearity which increases with the extension of conjugation (Rustagi and Ducuing 1974; Vishnumurthy et al. 2013; Yu and Dalton 1989). In the present work, both the molecules **VK4** and **VK5** possess thiophene as strong electron donor and ITD as an electron acceptor moiety, which provide a D–A type arrangement. Thus, both the molecules exhibit considerably enhanced third–order NLO properties. Amongst the studied molecules, molecule **VK4** has a highly conjugated pyrene group whose four fused benzene rings provide planarity and rigidity to the system, exhibiting extensive electron delocalization than that of anthracene present in **VK5**. As a result of which the molecule **VK4** shows improved NLO behavior compared to that of **VK5**. In summary, the presence of pyrene and anthracene groups in **VK4** and **VK5** as π –extending systems, respectively, provides a better nonlinearity to the molecules. The results indicate the suitability of **VK4** and **VK5** for their use in power limiting and optical switching applications.

Table 3.5 Comparison of third order NLO parameters of **VK4–VK6** with similar work reported.

Sample	β_{eff} (mW ⁻¹)	η^2 (esu)	χ^3 (esu) (10 ⁻¹²)	References
VK4	0.81×10⁻¹⁰	4.7874×10⁻¹¹	2.45	This work
VK5	0.55×10⁻¹⁰	3.2542×10⁻¹¹	1.82	This work
	0.36×10 ⁻¹⁰	1.651×10 ⁻¹⁸	0.9295	(Zheng et al. 2019)
	0.76×10 ⁻¹⁰	6.27×10 ⁻¹⁹	4.423	(Jia et al. 2017)
	0.47×10 ⁻¹¹	0.220×10 ⁻¹⁸	0.1184	(Jia et al. 2018)
	0.56×10 ⁻¹⁰	-	-	(Gowda et al. 2018)

3.2.7 The important findings from the experimental data

The introduction of different π -extenders to Th-ITD backbone plays significant role in tuning the extent of π -conjugation and bettermenting the photoelectronic properties of **VK4–VK6**. With the pyrene as highly conjugated π -system, **VK4** exhibits broader absorption band, high HOMO energy level and high thermal stability compared to that of **VK5** and **VK6**. The presence of azomethine bond further extends the conjugation length and hyperpolarizability in molecules **VK4–VK6**. The Z-scan analysis reveals that the extent of π -conjugation in these systems influences their NLO performance and optical limiting action. The molecule **VK4** with highly conjugated pyrene group exhibits enhanced NLO response with higher β_{eff} compared to that of **VK5**. The results of the present study prove that the molecule **VK4** could be a potential candidate to be utilized as optical limiter in laser photonics and in integrated NLO devices.

3.3 IMPACT OF DONOR–ACCEPTOR ALTERNATION ON OPTICAL POWER LIMITING BEHAVIOR OF H–SHAPED THIOPHENE–IMIDAZO[2,1-*b*][1,3,4]THIADIAZOLE FLANKED CONJUGATED OLIGOMERS (VK7–VK10)

Functionalization of conjugated materials via the D–A approach is one of the most successful methods to tailor the optoelectronic properties. The extended π –conjugation and small local changes in the molecular backbone lead to the copious changes in the entire molecule. Thus, a detailed discussion on the structure-property relationship of a new series of four D–A–D configured conjugated oligomers with H–type structure, possessing two Th–ITD branches and thiophene (VK7), thiophene–1,3,4-oxadiazole–thiophene (VK8), tztz (VK9), phenyl–tztz–phenyl (VK10) units as central core moieties is presented herein. These core moieties were specifically selected to increase the planarity, rigidity, stability, extend the π –conjugation and to understand the influence of central core on the optoelectronic properties.

3.3.1 Structural elucidation of the intermediates and final compounds

The presence of nine aromatic protons in the region of δ 7.91–6.78 ppm along with the broad –OH signal at δ 9.5 ppm in the ^1H NMR spectrum of **8** confirm the cyclization of intermediate **3** to **8** which is further confirmed by the ^{13}C NMR spectrum wherein, the aromatic carbons resonate at δ 157.5–109.4 ppm. The disappearance of –OH signal and appearance of a triplet at δ 3.98 ppm, multiplet at δ 1.81–1.27 ppm and a triplet δ 0.87 ppm corresponding to –OCH₂, –CH₂ and –CH₃ alkyl protons, respectively, in the ^1H NMR spectrum of **9** confirm the alkylation of **8** to form intermediate **9**. Similarly, the signals at δ 68.0, 31.8–22.6 and 14.1 ppm corresponding to –OCH₂, –CH₂ and –CH₃ alkyl carbons, respectively, in the ^{13}C NMR spectrum further confirm the structure. The formylation of **9** is clearly confirmed by the sharp singlet signal of –CHO at δ 10.09 ppm and 177.3 ppm in the ^1H NMR and ^{13}C NMR spectrum, respectively, of **10**. Also, a molecular ion peak at m/z 300.00, 440.10 and 468.10 in the mass spectrum, corresponding to [M+H] of intermediate **8**, **9** and **10**, respectively, further confirms the structure. The presence of thirty aromatic protons at δ 7.76–7.59 ppm corresponding to phenyl aromatic protons, singlet at δ 6.70 ppm corresponding to thiophene protons, along with a doublet at δ 5.53 ppm corresponding to –CH₂– signals in the ^1H spectrum of intermediate **13** confirm its structure. And

aromatic carbon signals at δ 135.3–116.7 ppm, $-\text{CH}_2-$ carbon signals at δ 27.1 and 26.6 ppm in the ^{13}C NMR spectrum also confirm the structure of **13**. A clear singlet at δ 10.34 ppm of $-\text{NHC}=\text{O}$ in the ^1H NMR spectrum of **16** confirms the structure. Similarly, missing of $-\text{NHC}=\text{O}$ protons and formation of new aromatic protons in the ^1H NMR spectrum of **17** confirms the structure of **17**. The bromination of methyl groups is confirmed by the signal at δ 5.13 ppm and δ 27.4 ppm in the ^1H and ^{13}C NMR spectrum, respectively, which is corresponding to $-\text{CH}_2\text{Br}$ of **18**. Further, thirty aromatic protons at δ 7.93–7.71 ppm corresponding to phenyl aromatic protons, singlet at δ 6.90 ppm corresponding to thiophene protons, along with a doublet at δ 5.68 ppm corresponding to $-\text{CH}_2-\text{P}$ signals observed in the ^1H NMR spectrum of **19**, confirm its structure, which are evidenced by the aromatic carbons and $-\text{CH}_2-\text{P}$ signals at δ 162.7–117.3 ppm, and δ 36.2 and 31.2 ppm, respectively in its ^{13}C NMR spectrum. The ^1H NMR spectrum of intermediate **22** display doublets at δ 7.91 ppm and 7.36 ppm corresponding to eight aromatic protons and singlet at δ 2.37 ppm corresponding to six methyl protons, which evidence the structural confirmation. Similar signals as those of intermediates **18** and **19** were found in the ^1H and ^{13}C NMR spectrum of intermediate **23** and **24**, which confirm the structure. The NMR spectral characterizations of one of the representative molecules, **VK8** is discussed herewith. The ^1H NMR spectrum shows twenty-two aromatic protons in the region of δ 7.89–6.72 ppm corresponding to thiophene and phenyl protons. The disappearance of sharp signal of aldehydic proton at δ 10 ppm and thirty aromatic protons due to phenyl group of triphenylphosphine and appearance of peak due to $-\text{CH}=\text{CH}-$ in the aromatic region (δ 7.89–6.72 ppm) along with a triplet at δ 3.95 ppm, multiplet at δ 1.86–1.27 ppm and a triplet δ 0.88 ppm corresponding to $-\text{OCH}_2$, $-\text{CH}_2$ and $-\text{CH}_3$ of alkoxy protons, respectively, clearly confirm the formation of **VK8** which is supported by the ^{13}C NMR spectrum wherein, the aromatic carbons resonate at δ 160.0–114.5 ppm and alkyl carbons resonate at δ 68.1, 68.0, 31.8 – 226.6 and 14.1 ppm, validating the structure. Similar type of signal pattern was observed in the ^1H and ^{13}C NMR spectrum of **VK7**, **VK9** and **VK10**, which confirm the structure of final compounds. A molecular ion peak at m/z 1012.346 ($\text{M}+\text{H}$), 1159.100 (M^+), 1016.989 ($\text{M}+\text{H}$) and 1222.723 ($\text{M}+\text{H}$) in MALDI–TOF–MS spectrum of oligomers **VK7**, **VK8**, **VK9** and **VK10**, respectively, further confirms the structure. In addition to the spectral characterizations, the elemental analysis further

evidences the structures of all the intermediates and final compounds. The ^1H NMR, ^{13}C NMR and mass spectra of some important intermediates and final compounds VK7–VK10 are presented in **Figure 3.48–3.74**.

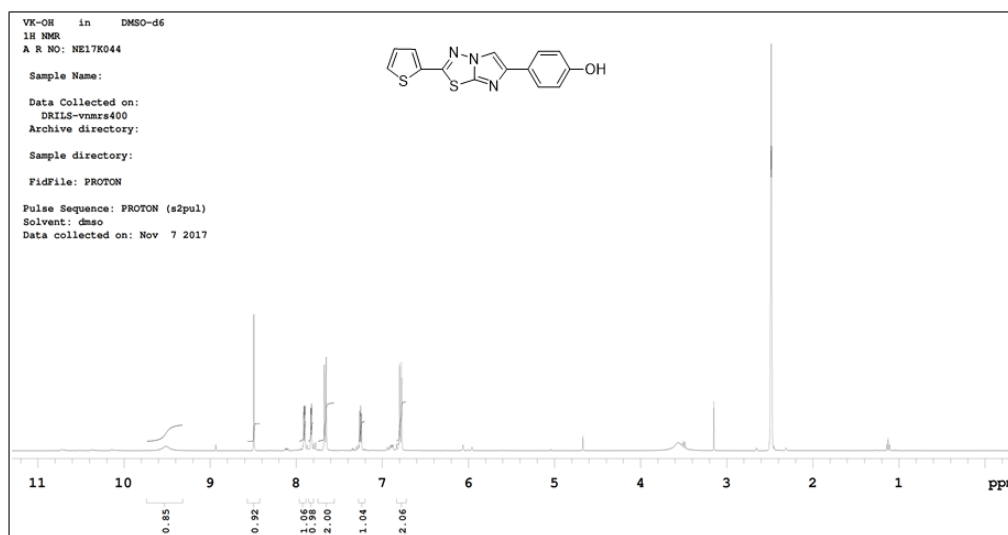


Figure 3.48 ^1H NMR spectrum of **8**

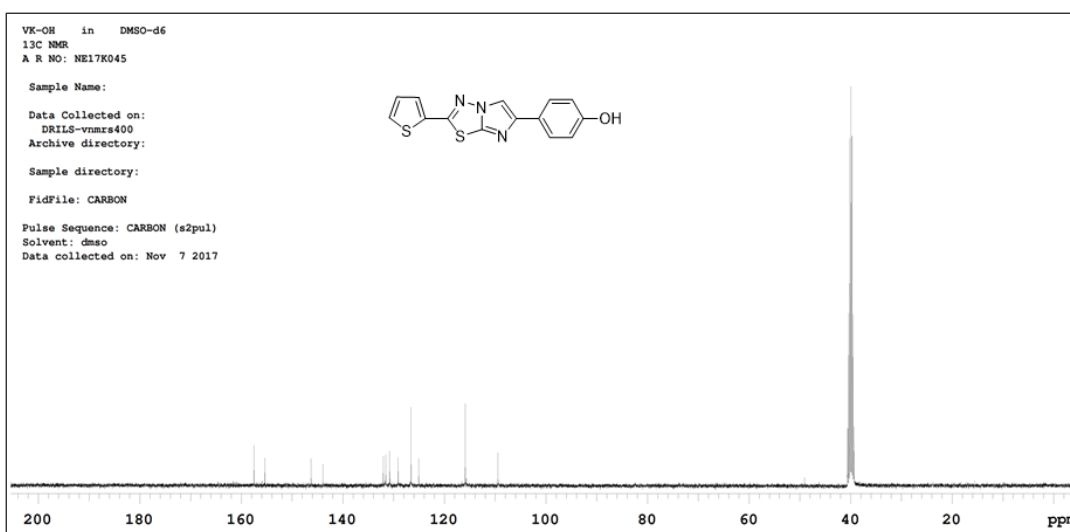


Figure 3.49 ^{13}C NMR spectrum of **8**

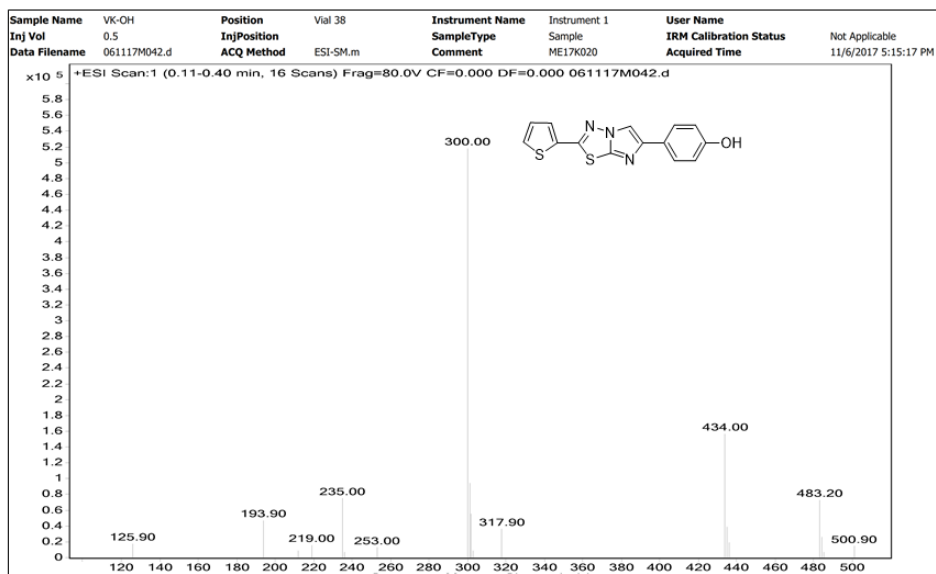


Figure 3.50 Mass spectrum of 8

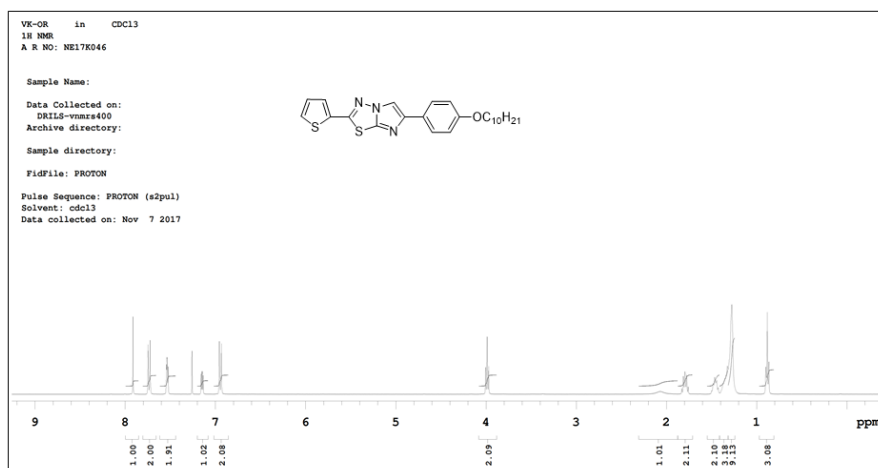


Figure 3.51 ¹H NMR spectrum of 9

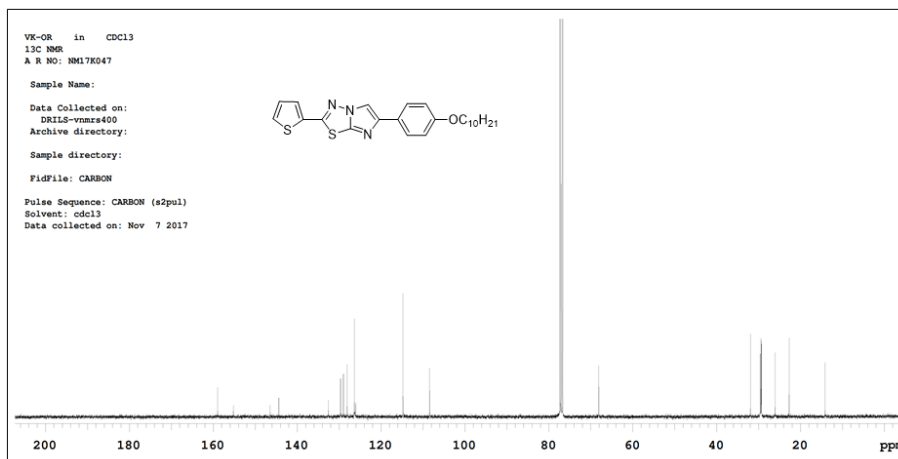


Figure 3.52 ¹³C NMR spectrum of 9

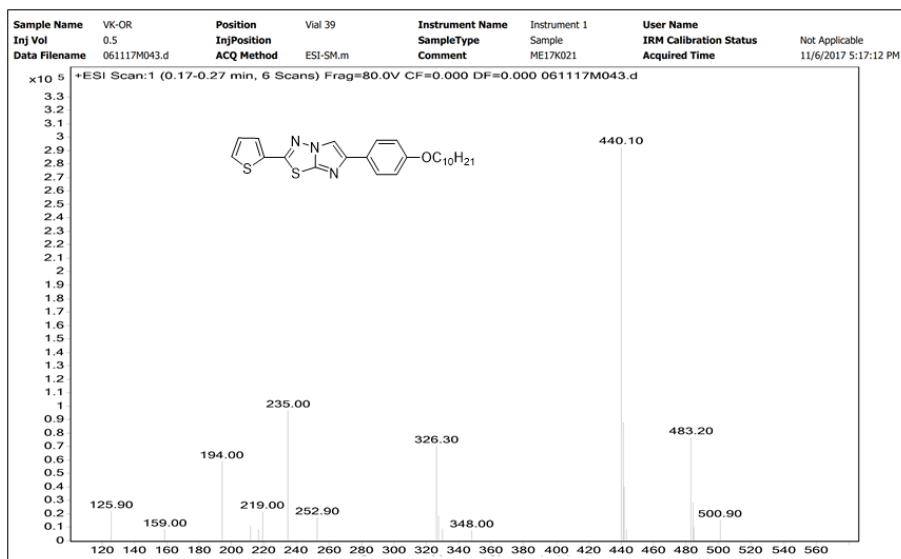


Figure 3.53 Mass spectrum of 9

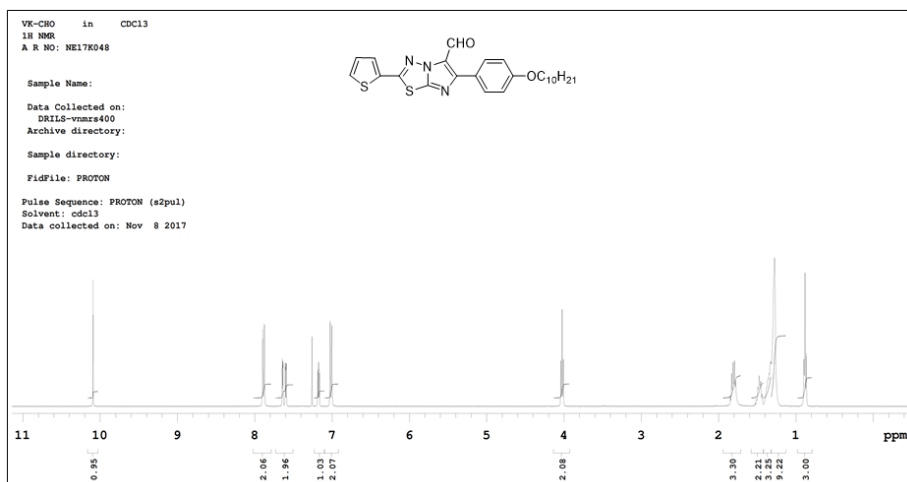


Figure 3.54 ¹H NMR spectrum of 10

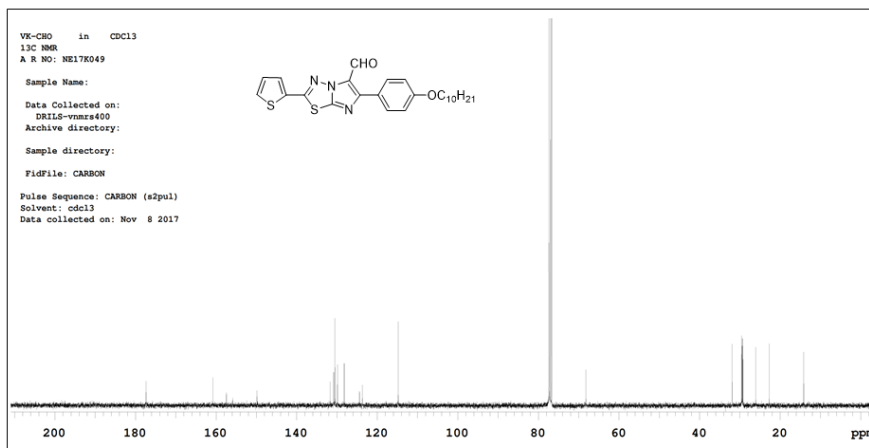


Figure 3.55 ¹³C NMR spectrum of 10

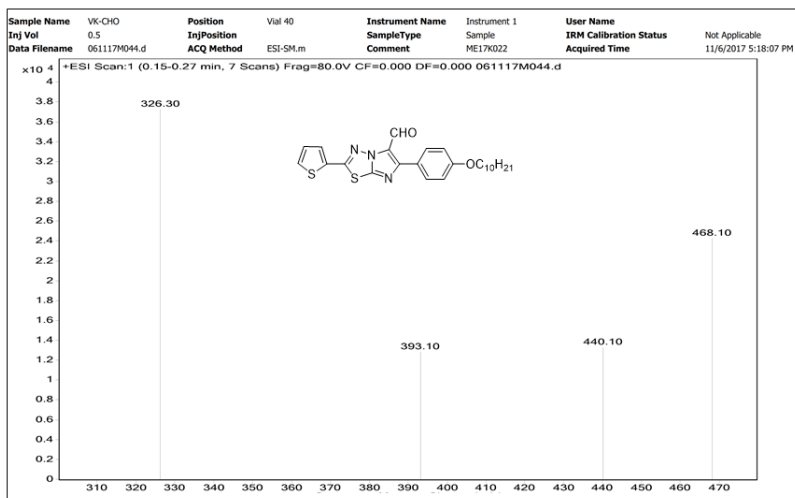


Figure 3.56 Mass spectrum of 10

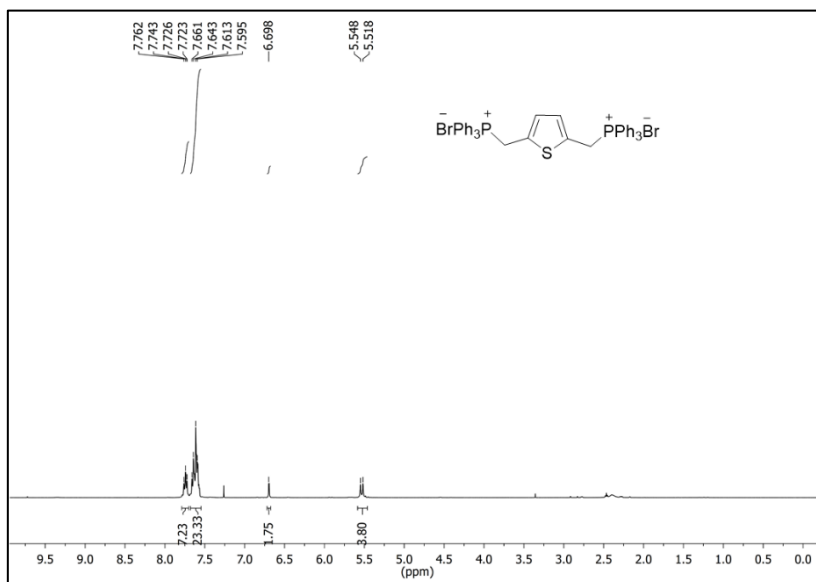


Figure 3.57 ¹H NMR spectrum of 13

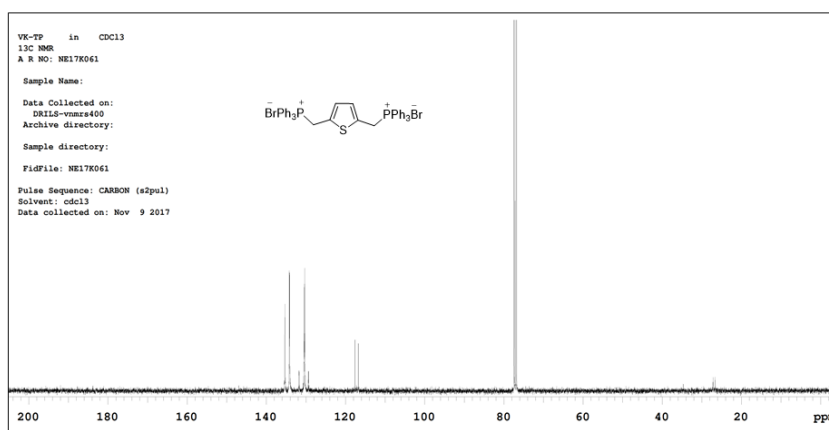


Figure 3.58 ¹³C NMR spectrum of 13

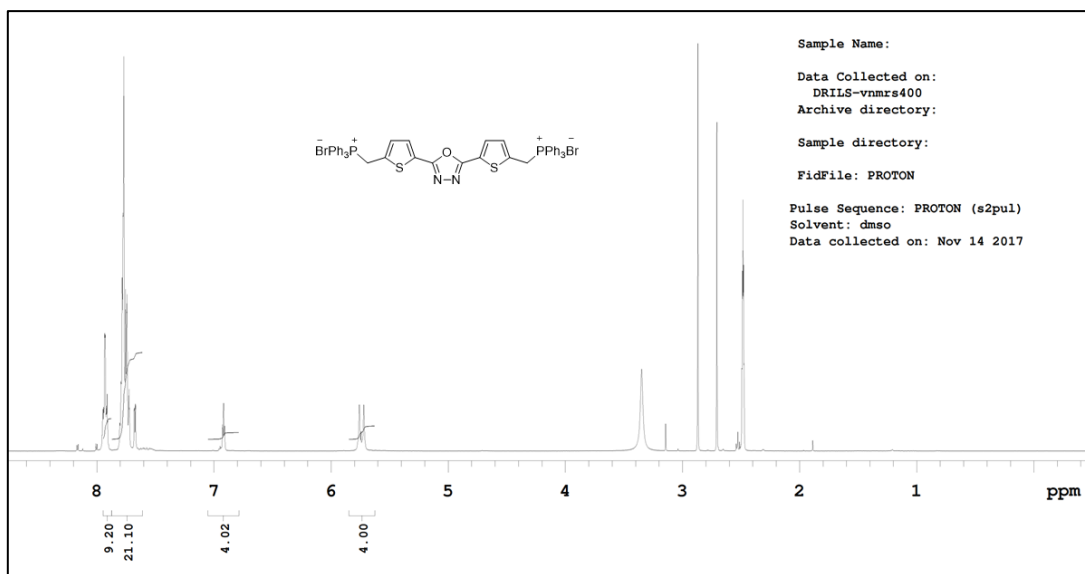


Figure 3.59 ^1H NMR spectrum of **19**

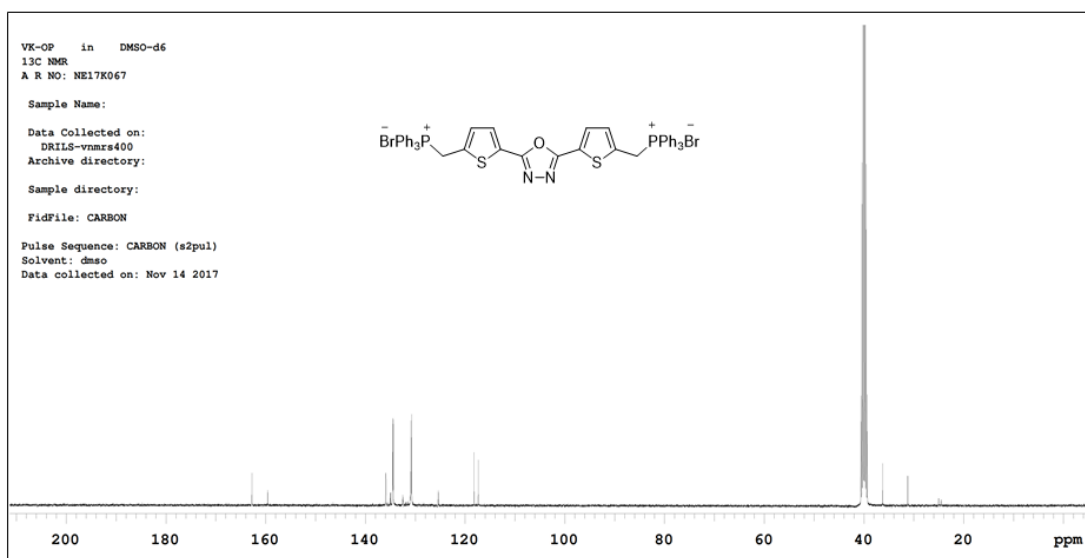
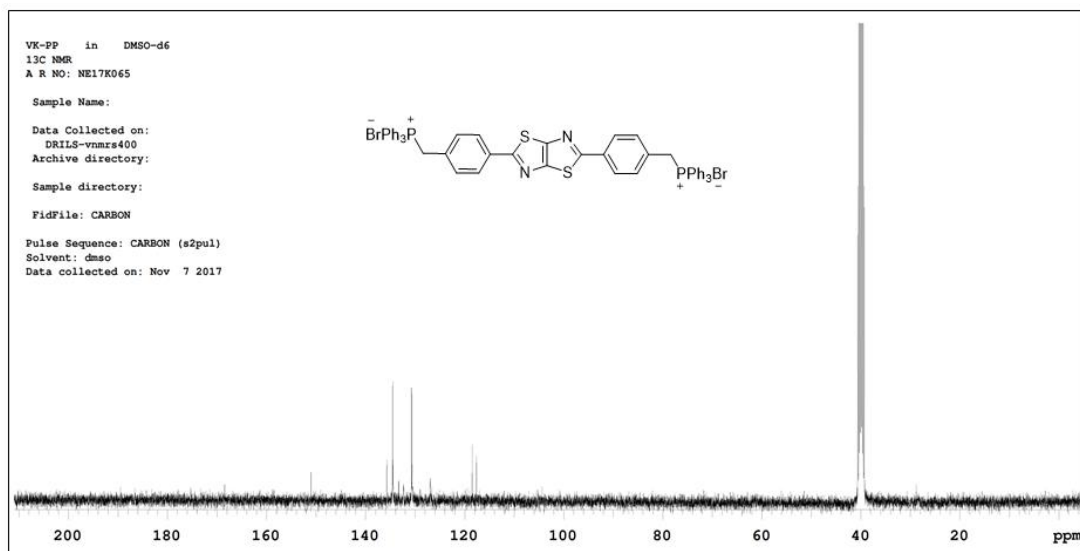
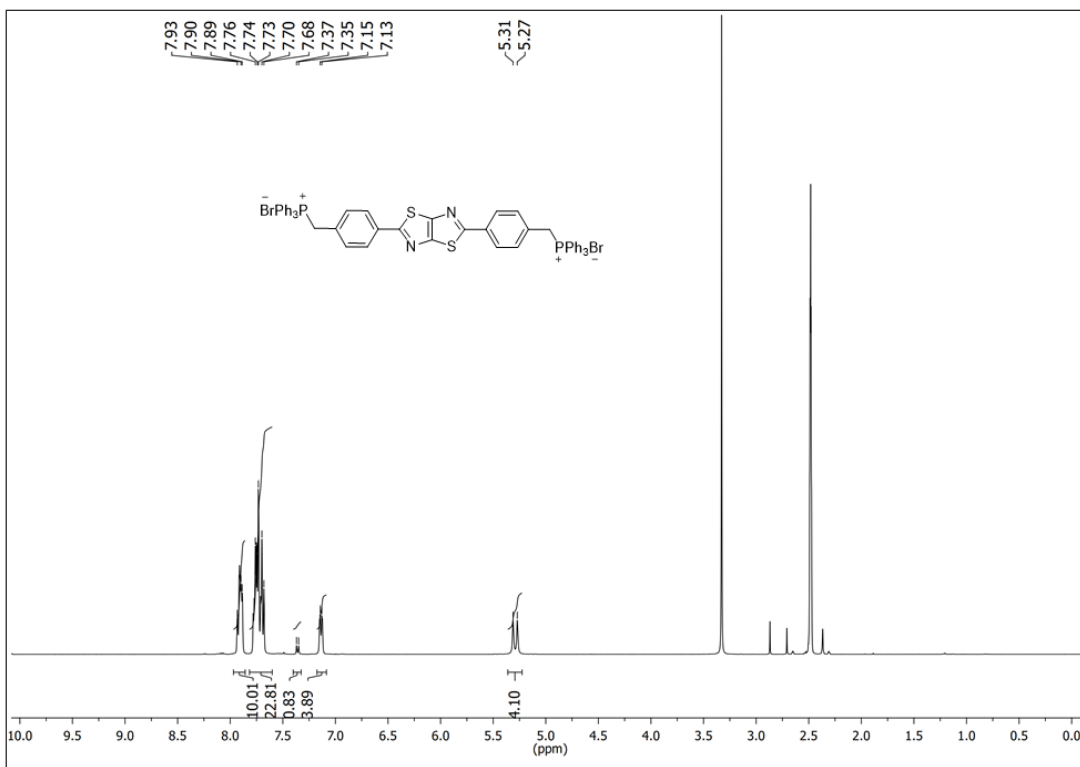


Figure 3.60 ^{13}C NMR spectrum of **19**



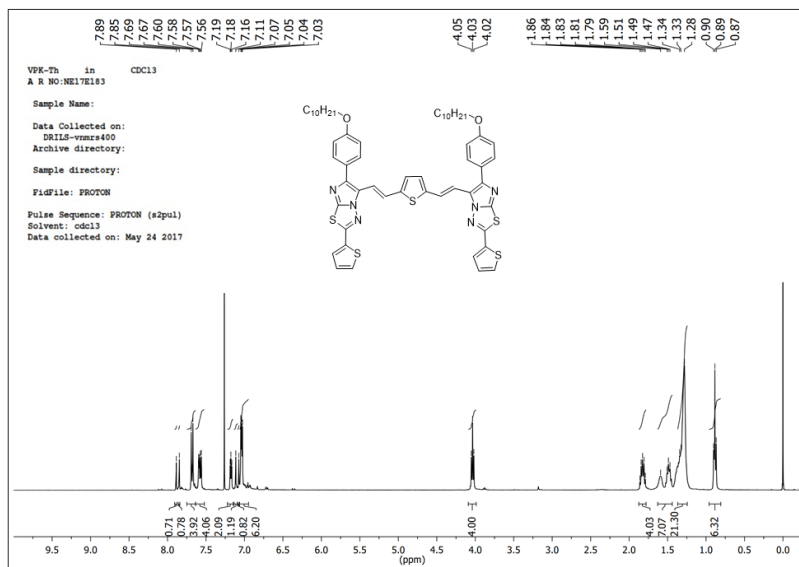


Figure 3.63 ¹H NMR spectrum of VK7

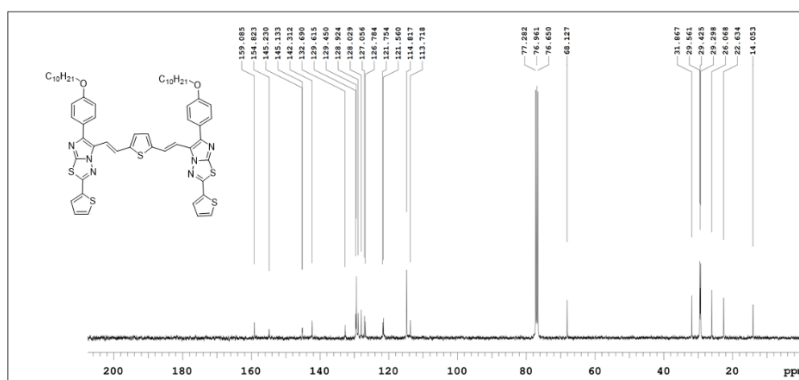


Figure 3.64 ¹³C NMR spectrum of VK7

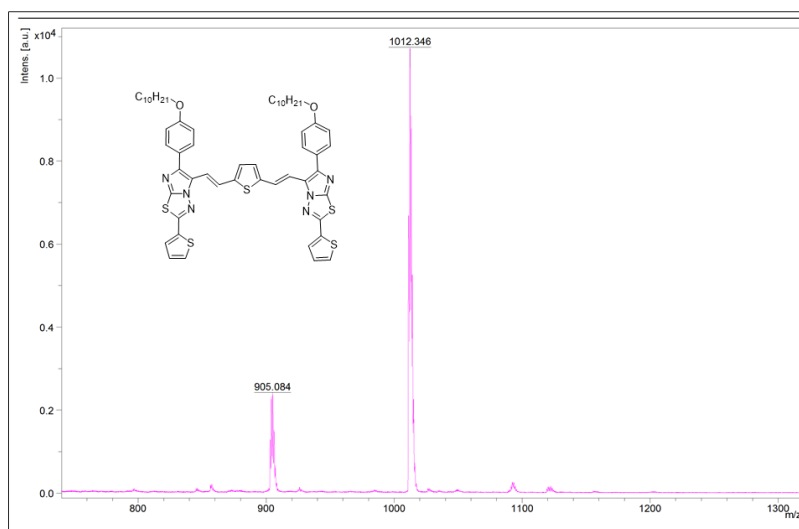


Figure 3.65 MALDI-TOF Mass spectrum of VK7

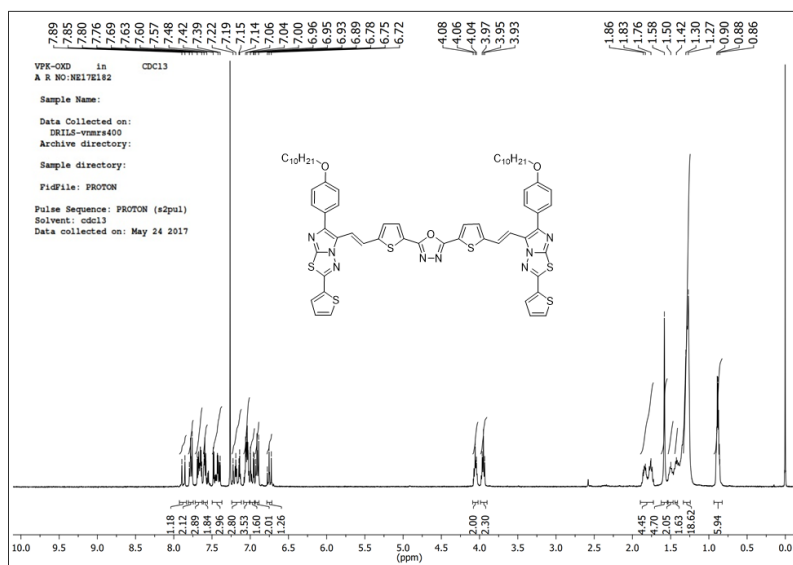


Figure 3.66 ¹H NMR spectrum of VK8

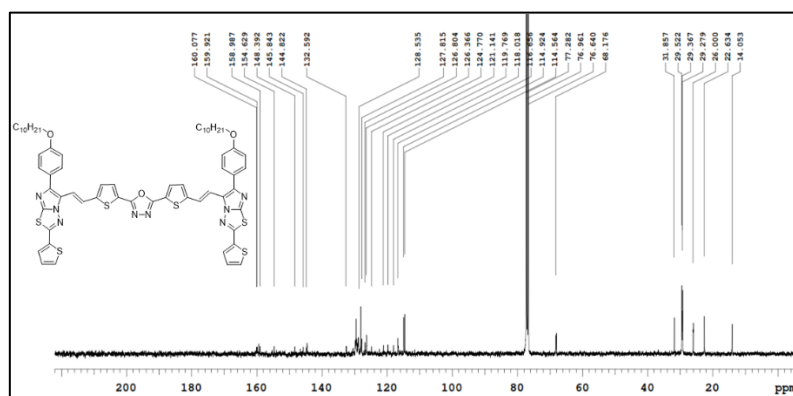


Figure 3.67 ¹³C NMR spectrum of VK8

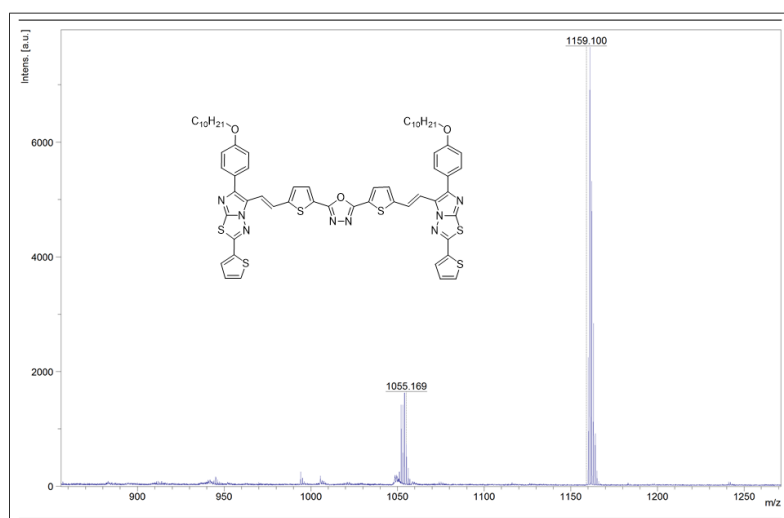


Figure 3.68 MALDI-TOF Mass spectrum of VK8

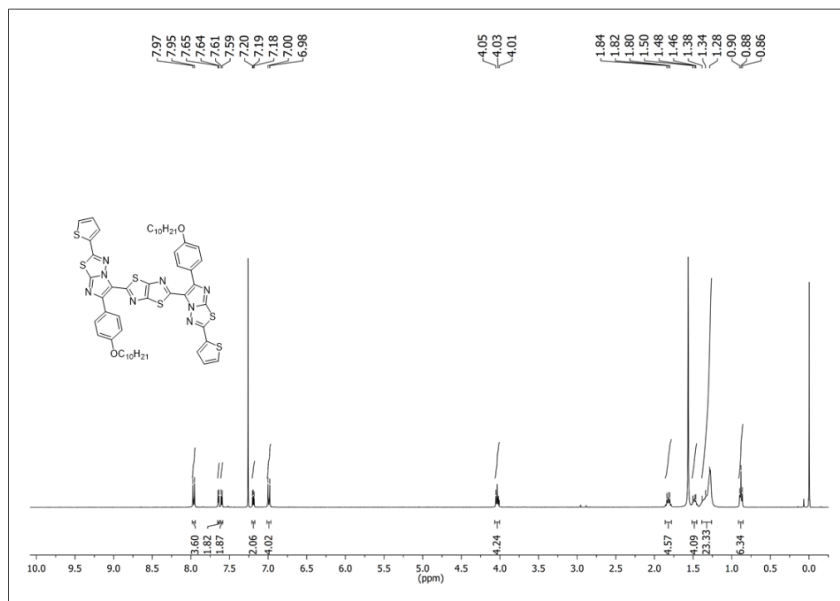


Figure 3.69 ^1H NMR spectrum of VK9

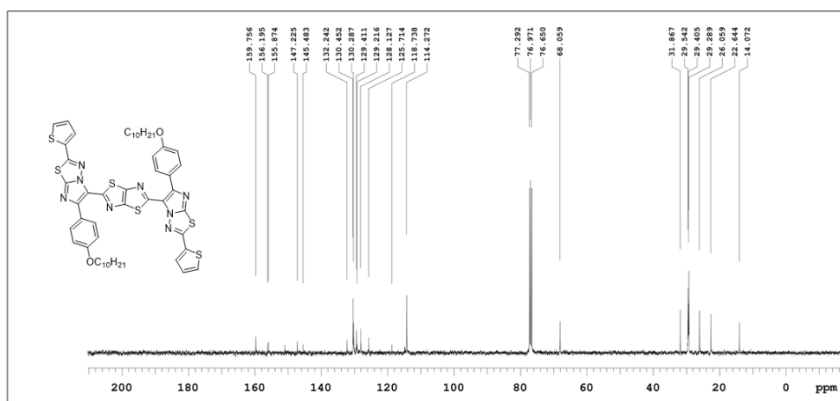


Figure 3.70 ^{13}C NMR spectrum of VK9

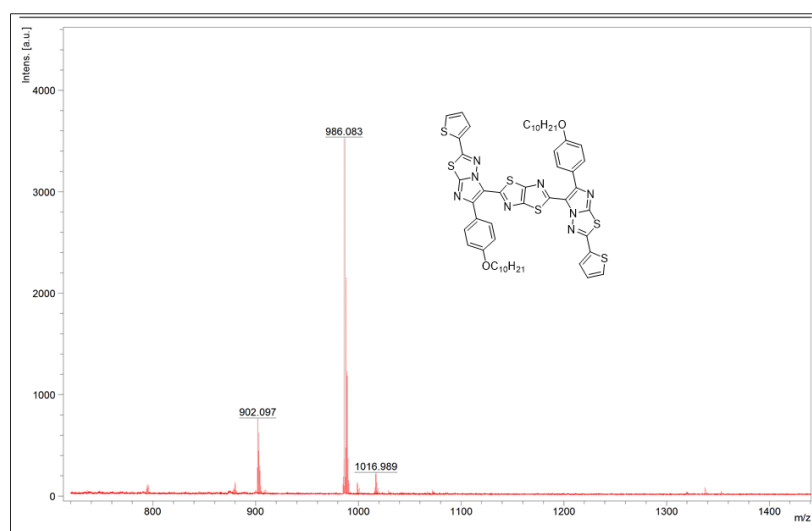


Figure 3.71 MALDI-TOF Mass spectrum of VK9

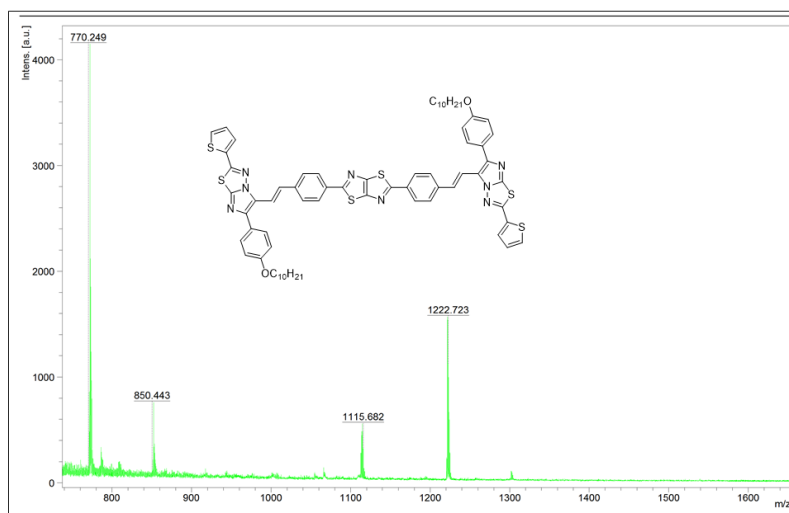
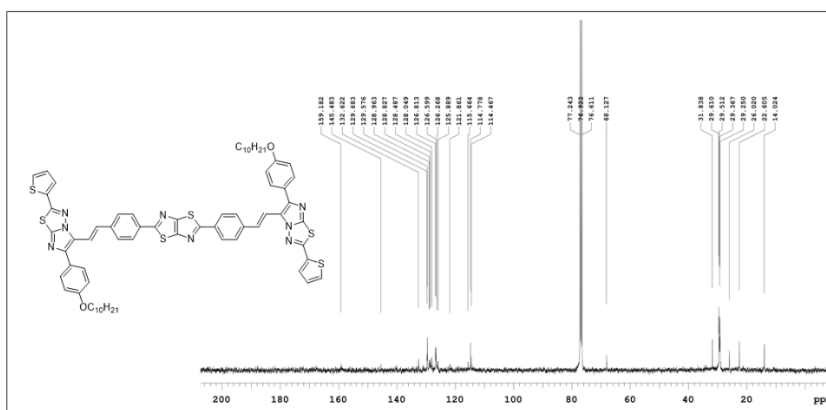
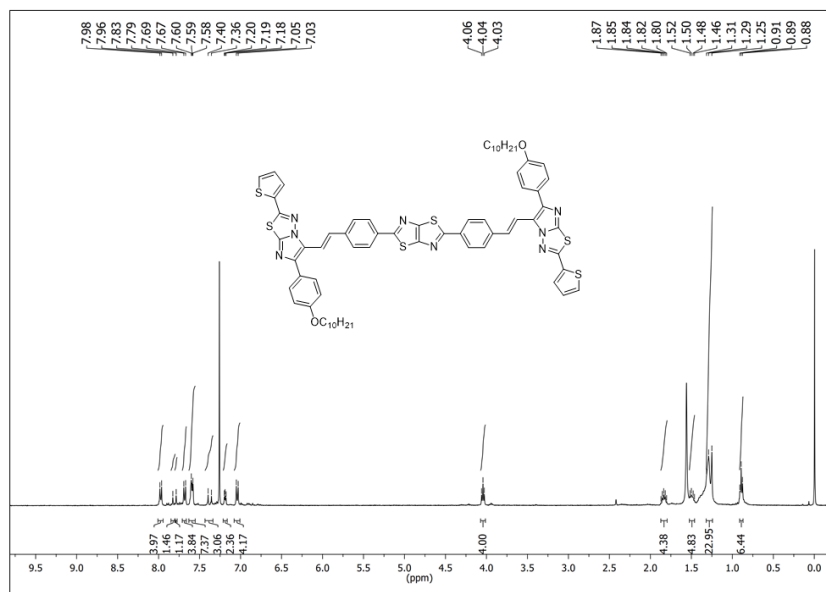


Figure 3.74 MALDI-TOF Mass spectrum of VK10

3.3.2 Photophysical studies

The normalized UV–Vis and PL spectra of **VK7–VK10** are shown in **Figure 3.75** and the corresponding spectral data are listed in **Table 3.6**. As it is seen in **Figure 3.75**, there are three absorption bands situated between 260–500 nm region for each of the four oligomers. The absorption bands observed at higher energy regions (260–340 nm) attribute to the π – π^* transitions of the aromatic conjugated skeleton, whereas, those at lower energy (400–460 nm) region ascribe to the ICT from the electron donor to the acceptor moieties. The λ_{max} of **VK7**, **VK8**, **VK9** and **VK10** are 429, 451, 408 and 438 nm, respectively. Moreover, the introduction of 1,3,4-oxadiazole, a strong electron acceptor moiety, to the central core is considerably shifting the λ_{max} of **VK8** to higher wavelength region due to stronger D–A interaction (Roncali 2007) when compared to that of **VK7**, where, only thiophene moiety is present in the central core. Similarly, there is a considerable red shift in the λ_{max} of **VK10** compared to that of **VK9** due to the introduction of phenyl group (π –linker) to the central part, which increases the D–A interaction in **VK10**, causing the extension of conjugation. Further, the fluorescence emission spectra were recorded by exciting the oligomers at their excitation wavelengths. All the four oligomers exhibit single emission peak in the 500–540 nm region, with the green light emission in solution state. The E_g calculated from the intersection of normalized absorption and emission spectra are 2.63, 2.46, 2.66 and 2.55 eV for **VK7**, **VK8**, **VK9** and **VK10**, respectively. The extended π –conjugation in **VK8** and **VK10** considerably reduce the E_g of **VK8** and **VK10** compared to that of **VK7** and **VK9**.

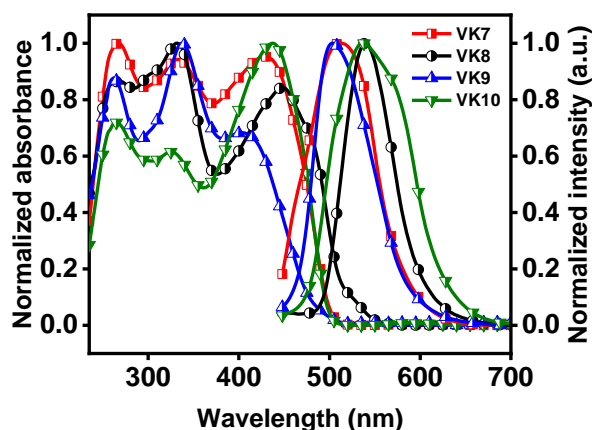


Figure 3.75 Normalized UV–Vis absorption and PL spectra of **VK7–VK10** recorded in CHCl_3 (10^{-5} M).

3.3.3 Electrochemical studies

Figures 3.76a–d represent the cyclic voltammograms of **VK7–VK10**, respectively. The onset oxidation potentials of the oligomers are at 0.54, 0.66, 0.60 and 0.55 V vs SCE for **VK7**, **VK8**, **VK9** and **VK10**, respectively. The HOMO energy levels determined using the **Equation 2.1** are -5.08 , -5.20 , -5.14 and -5.09 eV for **VK7**, **VK8**, **VK9** and **VK10**, respectively. Similarly, the LUMO energy levels of the oligomers calculated using the **Equation 2.2** are -2.45 , -2.74 , -2.48 and -2.54 eV for **VK7**, **VK8**, **VK9** and **VK10**, respectively.

There is a slight increase in the HOMO energy levels of **VK7** and **VK10** when compared to that of **VK8** and **VK9**. This increment is attributed to the presence of thiophene in **VK7** and phenyl group in **VK10** in the central core as electron donor and π -linker, respectively (Zhou et al. 2010), while, the decrease in the LUMO level of **VK8** compared to that of **VK7**, **VK9** and **VK10** is due to the presence of strong electron withdrawing 1,3,4-oxadiazole moiety in **VK8** (Randell et al. 2018). The results of CV studies and the values of energy levels are summarized in **Table 3.6**.

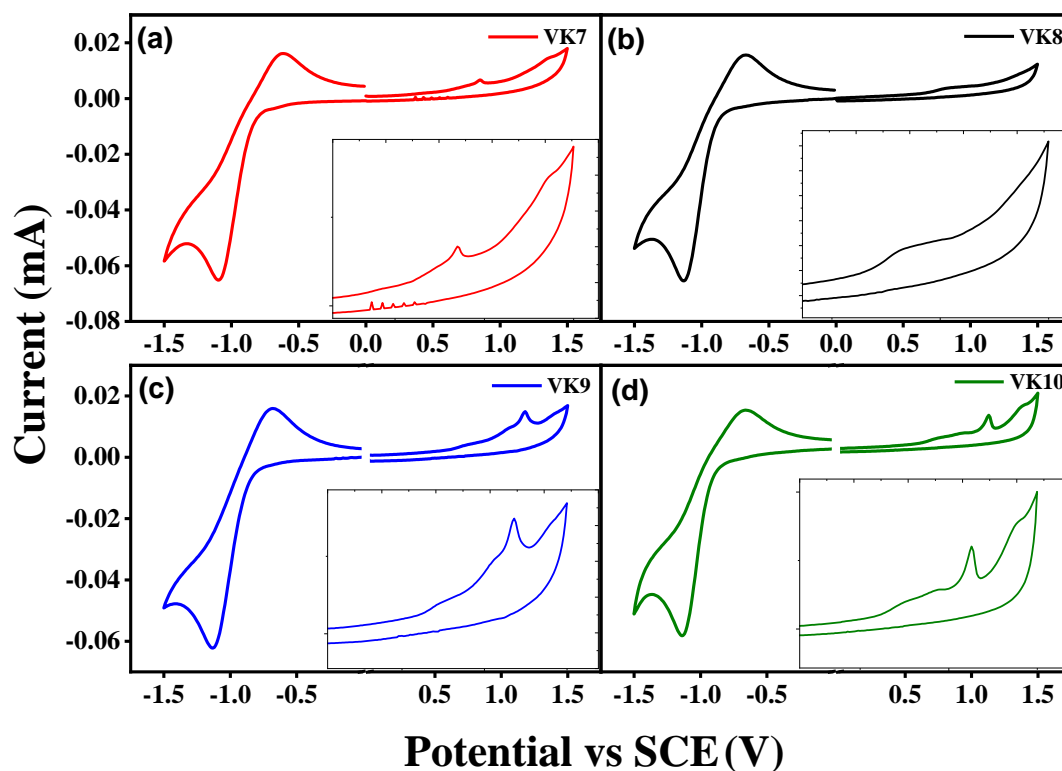


Figure 3.76 Cyclic voltammograms of (a) **VK7**, (b) **VK8**, (c) **VK9** and (d) **VK10**. Insets show the enlarged image of oxidation peaks in the anodic region.

Table 3.6 Summary of optical, electrochemical and theoretical data of **VK7–VK10**.

Molecules	$\lambda_{\max}^{\text{abs}}$ (nm)	$\lambda_{\max}^{\text{pl}}$ (nm)	$E_{\text{g}}^{\text{opt}}$ (eV)	$E_{\text{onset}}^{\text{ox}}$ (V vs SCE)	HOMO (eV)	LUMO (eV)
VK7	429	512	2.63	0.54	-5.08 ^a	-2.45 ^b
					-4.52 ^c	-2.06 ^c
VK8	451	540	2.46	0.66	-5.20 ^a	-2.74 ^b
					-4.84 ^c	-2.20 ^c
VK9	408	503	2.66	0.60	-5.14 ^a	-2.48 ^b
					-5.08 ^a	-2.02 ^b
VK10	438	537	2.55	0.55	-5.09 ^a	-2.54 ^b
					-4.83 ^c	-2.19 ^c

$E_{\text{g}}^{\text{opt}}$ Optical band gap calculated from the intersection of normalized absorption and emission spectra.

$E_{\text{onset}}^{\text{ox}}$ Experimental onset oxidation potential vs SCE.

^a Experimental values from CV using Equation 2.1 with Fc/Fc⁺ as internal standard.

^b Experimental values using Equation 2.2.

^c Theoretical results.

3.3.4 Theoretical studies

The long alkoxy chain was considered as methoxy group in order to reduce the calculation time. As shown in **Figure 3.77**, both the HOMO and LUMO electrons are mainly populated on vinylic linkage and central part of the system in **VK7**, **VK8**, **VK9** and **VK10**. The HOMO distribution is further extended on the imidazole and decyloxy substituted phenyl ring of the terminal groups, whereas, the LUMO is mostly distributed on thiophene and ITD ring of the peripheral group and also, distribution in the central core of all the four oligomers is seen. This type of separated spatial distribution suggests the balanced charge transfer process within the system (Kothavale and Sekar 2017). The theoretical HOMO/LUMO values are given in **Table 3.6**.

The presence of long decyloxy chain causes the twisting of the decyloxy substituted phenyl group by an angle of $\sim 32^\circ$ from thiophene–imidazo[2,1-*b*][1,3,4]thiadiazole plane of peripheral Th–ITD moiety in all the four oligomers. In the

case of **VK9** the two peripheral Th–ITD moieties are present orthogonal to each other (**Figure 3.78**). This is due to the steric hindrance between ITD and tztz moieties, resulting from the direct bond present between them. In all the four oligomers, the Th–ITD plane is present 90° to the plane of central unit, giving a H-shaped structure. As it is seen from the optimized geometry of **VK8** and **VK10**, the higher degree of conjugation in central core decreases the twisting due to steric effects between the side groups and the central unit, providing a perfect H-shaped structure. The dihedral angles and the optimized geometries are shown in **Figure 3.79**.

Further, the simulated absorption spectra of **VK7–VK10** are shown in **Figure 3.80**. There exist two absorption bands, the one at lower energy region corresponds to charge transfer transition and the other at higher energy region is due to π – π^* transition. In general, the tiny discrepancy is attributed to the theoretical overestimation. Nevertheless, the trend remains the same and the theoretical results are in good agreement with the experimental results.

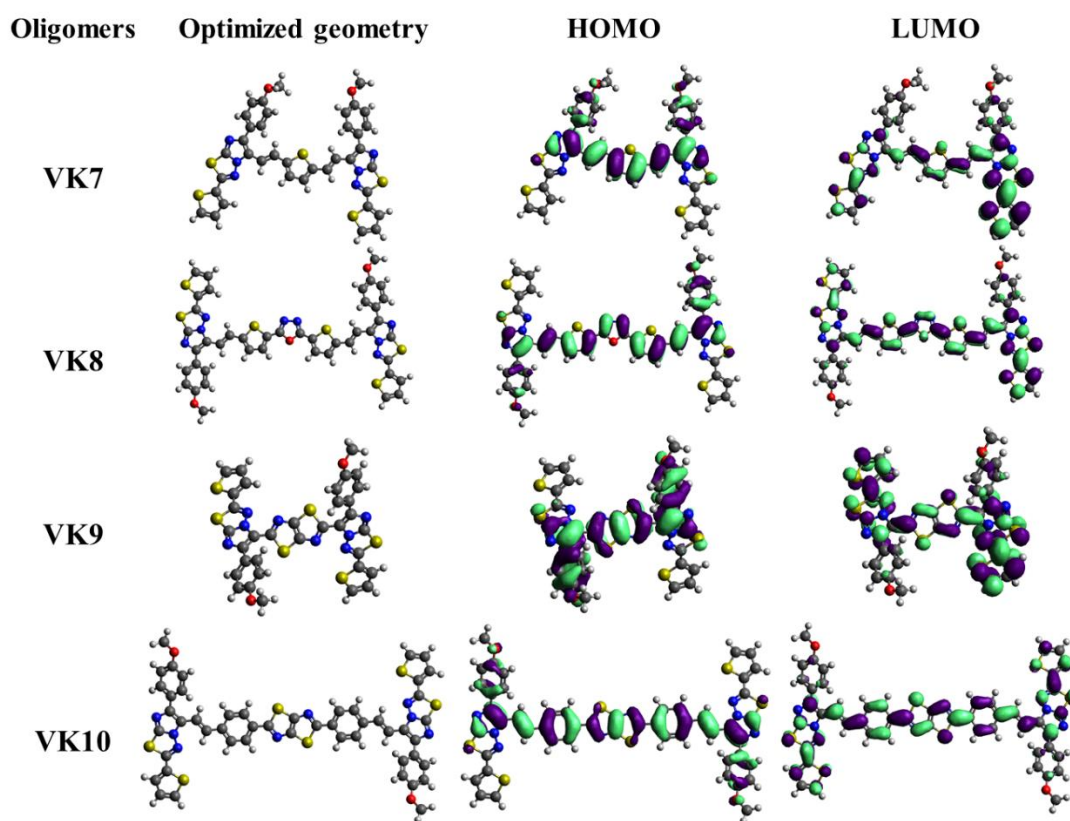


Figure 3.77 Optimized geometry and HOMO/LUMO electronic distributions of **VK7–VK10**.

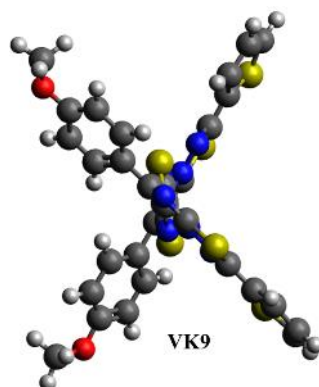


Figure 3.78 The side view of **VK9** wherein the side groups are arranged orthogonal to each other.

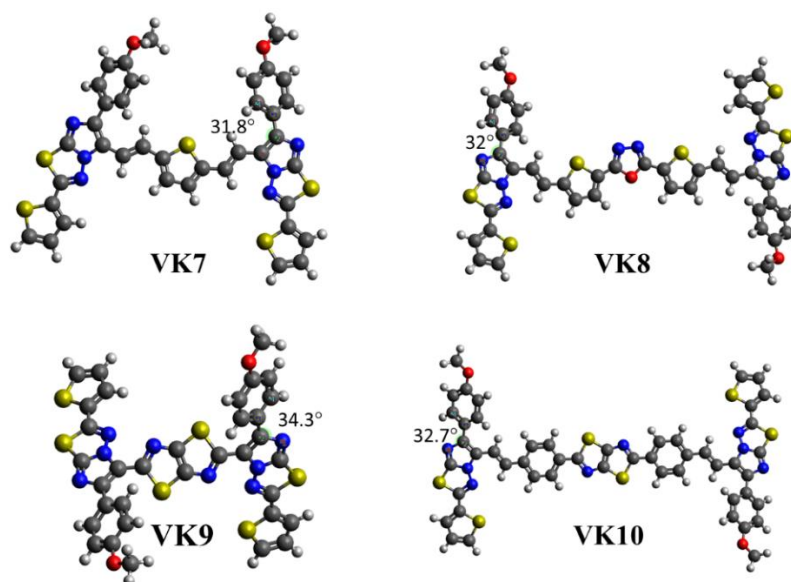


Figure 3.79 Dihedral angles between decyloxy substituted phenyl ring and Th-ITD plane.

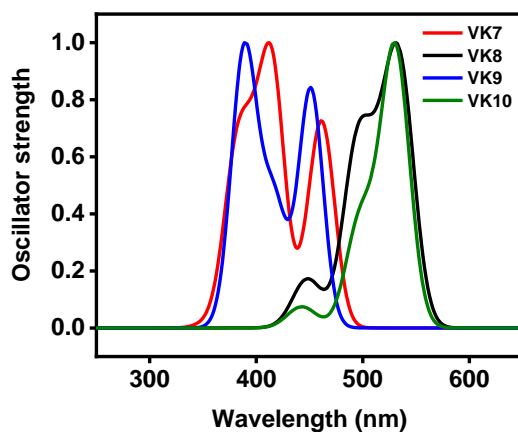


Figure 3.80 Simulated absorption spectra of **VK7–VK10**.

3.3.5 Thermal properties

Figure 3.81 represents the graph of weight loss as a function of temperature of **VK7–VK10**. As it is seen from the plot, the onset of T_d corresponding to a 5% weight loss for **VK7** and **VK8** are 370 and 384°C, respectively and that corresponding to a 20% weight loss for **VK9** and **VK10** are 378 and 348°C, respectively. Further, there is a minor decomposition at 183 and 115°C observed for **VK9** and **VK10**, which is attributed to the decomposition of central units of **VK9** and **VK10**, respectively. Between **VK7** and **VK8**, **VK8** exhibits higher T_d , which is ascribed to the extended D–A–D structure with the presence of thermally stable 2,5–disubstituted–1,3,4–oxadiazole in the central unit. However, the higher T_d of **VK9** compared to that of **VK10** is due to the direct attachment of central tztz unit to the partially rigid ITD moiety of the terminal group in **VK9**, making the oligomer structurally more rigid compared to **VK10**. All the four oligomers exhibited good thermal stability, which reveal the suitability of these materials for practical application in optoelectronics.

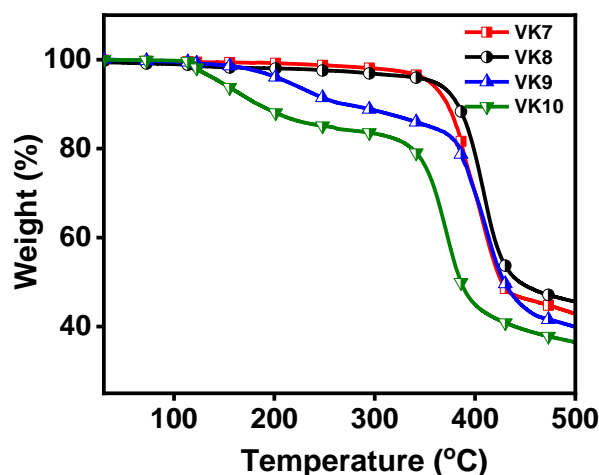


Figure 3.81 TGA plots of **VK7–VK10**.

3.3.6 Third–order NLO properties

3.3.6.1 Nonlinear absorption studies

The oligomers were excited at an energy of 50 μJ (on–axis intensity of 1.386 GW cm^{-2}) with a linear transmittance maintained at 70–72%. The OA Z–scan traces of **VK7–VK10** are shown in **Figure 3.82a–d**, respectively. As shown in the **Figure 3.82a–d**, there is a decrease in the transmittance as the samples are moved near to the focus and reaches a minimum value at the focus, displaying a deep transmittance trough near the focal plane which is the signature of RSA. Further, on the nanosecond time

scale this RSA is combined with TPA and ESA, collectively called as “effective TPA” process (Poornesh et al. 2009; Vishnumurthy et al. 2011). The experimental results are matching well with the theoretical model for effective TPA process in all the samples. Thus, the effective nonlinear absorption coefficient ($\alpha(I)$), the nonlinear propagation equation (dI/dz), the normalized transmittance ($T(z)$) and finally, the $\text{im } \chi^{(3)}$ for OA configuration were determined using the **Equations 2.3–2.6**, respectively. The NLA parameters were obtained by fitting the experimental data to the theoretical model using **Equation 2.3** and **2.5**. All the calculated NLA coefficients are listed in **Table 3.7**.

The numerically estimated β_{eff} values are 0.52×10^{-10} , 1.62×10^{-10} , 1.55×10^{-10} and $2.71 \times 10^{-10} \text{ m W}^{-1}$ for **VK7**, **VK8**, **VK9** and **VK10**, respectively. These obtained β_{eff} values are very much closer and predominantly higher than that reported in the literature (**Table 3.7**). For example, the NLO properties of quinacridone derivatives were studied by Jia *et al.* (Jia et al. 2017), which showed notable NLO responses with β_{eff} of $0.76 \times 10^{-10} \text{ m W}^{-1}$. Gowda *et al.* (Gowda et al. 2018, 2016) synthesized EDOT based bent-core and hockey stick like liquid crystals and studied the effect of metal nanoparticles (gold/silver), dispersed in phthalocyanine discotic liquid crystal matrix, which exhibited large optical nonlinear properties with β_{eff} of 0.56 and $2.5 \times 10^{-10} \text{ m W}^{-1}$, respectively. Edappadikkunnummal *et al.* (Edappadikkunnummal et al. 2017) synthesized phenothiazine–gold nanoparticles by laser ablation method and studied the third–order NLO properties, which exhibited significant enhancement in NLA with β_{eff} of $1.7 \times 10^{-10} \text{ m W}^{-1}$. Gopi *et al.* (Gopi et al. 2020) synthesized new quinoxaline based push–pull molecules with 1,3-indandione as acceptor and investigated the NLO properties of the molecule, which showed an effective TPA with very high β_{eff} of $2.0 \times 10^{-10} \text{ m W}^{-1}$. Zhang *et al.* (Zhang et al. 2011) studied the NLO and optical limiting properties of graphene oxide– Fe_3O_4 hybrid material, which showed an enhanced β_{eff} of $2.6 \times 10^{-10} \text{ m W}^{-1}$. Therefore, all the aforementioned studies involve uses of one or the other dopant for the enhancement of nonlinear response but the observed phenomenal increment in the nonlinear responses in the present study without any dopants, of the synthesized oligomers suggests that these oligomers would serve as effective optical limiters for sensors and eye protection.

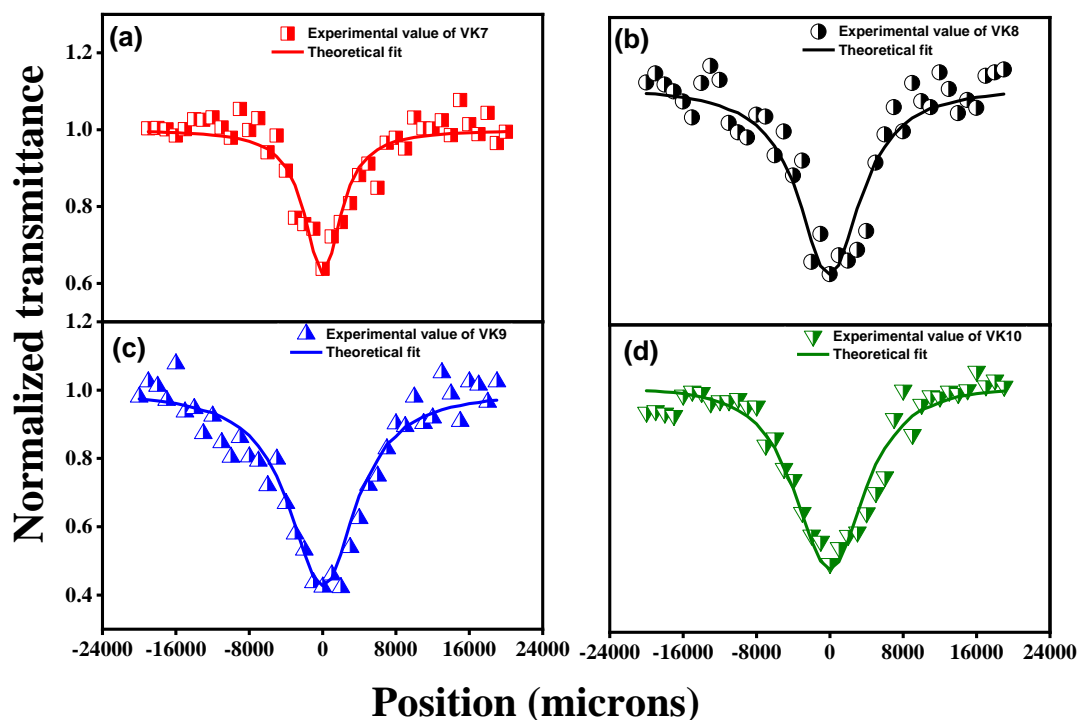


Figure 3.82 OA Z-scan curves of (a) **VK7**, (b) **VK8**, (c) **VK9** and (d) **VK10** at 50 μJ .

3.3.6.2 Optical limiting studies

In order to explain the optical limiting properties of the present oligomers, graphs of input fluence versus the normalized transmission of pulse intensity of **VK7**–**VK10** were plotted and are shown **Figure 3.83a–d**, respectively. The onset values of limiting action are 0.349, 0.231, 0.270 and 0.151 J cm^{-2} for **VK7**, **VK8**, **VK9** and **VK10**, respectively and the LT values are 6.02, 4.51 and 3.14 J cm^{-2} for **VK8**, **VK9** and **VK10**, respectively. Such a low onset and LT values of the synthesized oligomers infer that these materials would be powerful candidates in optical power limiting devices. The oligomer **VK7** did not show LT, as the output transmittance did not reach 50 % of its initial value at the input fluence used.

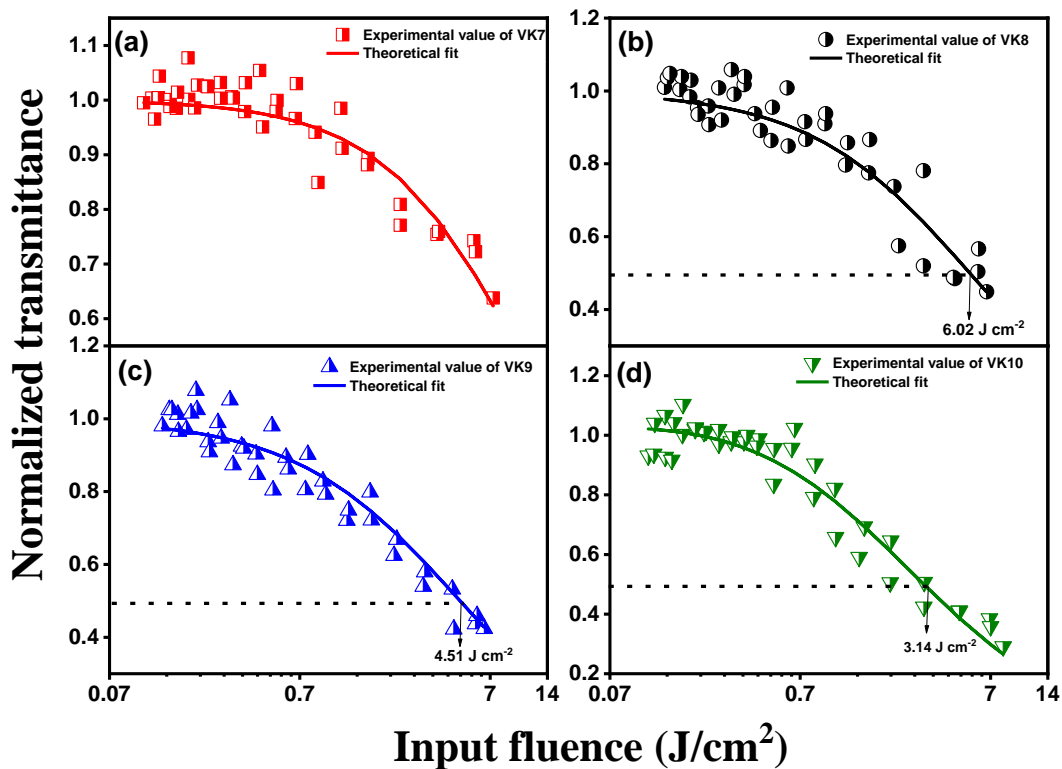


Figure 3.83 Optical power limiting studies of (a) VK7, (b) VK8, (c) VK9 and (d) VK10 at 50 μJ .

3.3.6.3 Nonlinear refraction studies

The CA Z-scan was performed to determine both the magnitude and sign of the NLR. The pure NLR trace was obtained by dividing CA data by OA data to avoid the contribution of NLA and the corresponding plots of VK7–VK10 are shown in **Figure 3.84a–d**, respectively. All the four oligomers show negative nonlinearity and exhibit peak-valley pattern which are associated with self-defocusing nature of the oligomers. The normalized transmittance (T) at CA condition, the real $\chi^{(3)}$ and the η_2 were fitted using **Equations 2.7–2.9**, respectively. The data of NLR coefficients are summarized in **Table 3.7**.

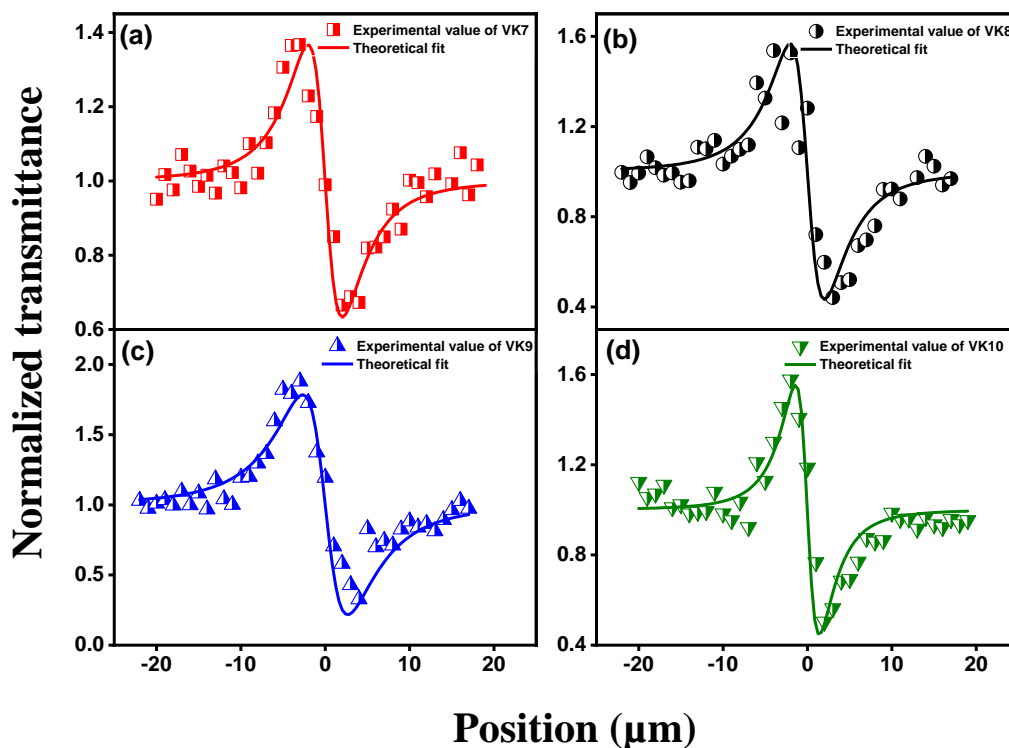
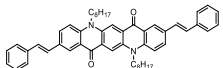
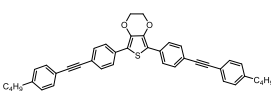
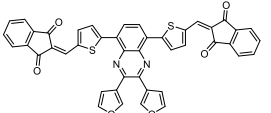


Figure 3.84 CA Z-scan curves of (a) **VK7**, (b) **VK8**, (c) **VK9** and (d) **VK10** at 50 μJ .

In the present study, introduction of strong electron acceptor groups such as 1,3,4-oxadiazole (**VK8**) and tztz (**VK10**), between the electron rich groups (thiophene in **VK8** and phenyl in **VK10**) at the central position of conjugated backbone ameliorate the planarity of the oligomers which extends the π -electron delocalization over the entire conjugated system and improves the effective charge transfer between the donor and acceptor groups which in turn increases the polarizability of the oligomers. And the cyclic groups (ITD) present at the peripheral position of the oligomers improve the rigidity and strengthen the molecular backbone (Yu and Dalton 1989). As a result, the oligomers **VK8** and **VK10** exhibit predominant increment in the NLO properties (enhanced β_{eff} of the order 10^{-10} , considerably low onset of limiting action and LT) compared to that of **VK7** and **VK9**. The enhanced conjugation facilitated by D-A-D framework of all the four oligomers substantially improve their NLO characteristics, as confirmed by Z-scan analysis.

Table 3.7 Comparison of NLA and NLR parameters of **VK7, VK8, VK9** and **VK10** with similar work reported.

Sample	β_{eff} ($\times 10^{-10}$ m W^{-1})	LT (J cm^{-2})	η^2 (esu)	χ^3 (esu) (10^{-12})	References
VK7	0.52	-	4.1637×10^{-11}	1.69375	This work
VK8	1.62	6.02	6.4593×10^{-11}	5.16077	This work
VK9	1.55	4.51	5.8669×10^{-11}	4.95886	This work
VK10	2.71	3.14	8.4294×10^{-11}	8.55506	This work
	0.76		6.27×10^{-19}	4.423	(Jia et al. 2017)
	0.56		-	-	(Gowda et al. 2018)
Phenothiazine– Gold (Au) nanocomposite	1.74		8.0	-	(Edappadikk unnummal et al. 2017)
phthalocyanine– 0.5% gold nanoparticles matrix	2.5		-	-	(Gowda et al. 2016)
	2.0		-	-	(Gopi et al. 2020)
Graphene oxide– Fe_3O_4	2.6		-	-	(Zhang et al. 2011)

3.3.7 The important findings from the experimental data

Extensive tuning of the optoelectronic properties and the energy levels of the molecules is observed by the incorporation of different D–A groups in the central unit. The presence of 1,3,4-oxadiazole and tztz units in **VK8** and **VK10** results in the red shift of the absorption and emission maxima of **VK8** and **VK10**, respectively. Similarly, the electron rich thiophene and phenyl groups (π -spacer) present in the central position of the **VK7** and **VK10** increase the HOMO level of **VK7** and **VK10**, respectively. The high thermal stability of $>350^{\circ}\text{C}$ is due to the extended conjugation and the rigidity of the oligomers. The improved ICT and high polarization of **VK8** and **VK10** give rise to high β_{eff} of 1.62 and $2.71 \times 10^{-10} \text{ m W}^{-1}$, very low onset of limiting of 0.231 and 0.151 J cm^{-2} and limiting thresholds of 6.02 and 3.14 J cm^{-2} , respectively. The attractive NLO responses of the **VK8** and **VK10** prove that these oligomers could be excellent candidates for all-optical limiting and opto-electronic device applications.

3.4 EXPLORATION OF EXCITED STATE ASSISTED TWO-PHOTON ABSORPTION PROPERTY OF D–A–D TYPE THIOPHENE–PYRIDINE DERIVATIVES (VK11–VK14)

The increase in the conjugation enhances the ICT and polarizability of the conjugated system. Keeping this in mind, trigonal-shaped molecules (**VK11** and **VK12**) and polymers (**VK13** and **VK14**) with D–A–D structural arrangement possessing thiophene acetonitrile (**VK11**), phenyl acetonitrile groups (**VK12**, **VK14**) and thiophene units (**VK13**) as side groups in order to expand the π -conjugation were synthesized to study the effect of conjugation on the fundamental photophysical, electrochemical and third-order NLO properties. The polymers **VK13** and **VK14** were synthesized with the expectation that this would bring a drastic improvement in the optical nonlinearity compared to small molecules (**VK11** and **VK12**).

3.4.1 Structural elucidation of the intermediates and final compounds

In the ^1H NMR spectrum of intermediate **27**, hydroxy proton resonates as broad singlet at δ 5.31 ppm, aromatic protons of pyridine ring resonate as singlet at δ 7.72 ppm and all the new aromatic protons corresponding to thiophene and phenyl units resonate at δ 7.65–6.97 ppm, confirming its structure. The aromatic carbons resonating in the downfield region in ^{13}C NMR spectrum further supports the structure of **27**. The disappearance of hydroxy proton and formation of new triplet at δ 4.03 ppm, multiplet at δ 1.88–1.29 ppm and triplet at δ 0.92 ppm corresponding to $-\text{OCH}_2$, $-\text{CH}_2$ and $-\text{CH}_3$ protons, respectively, of decyloxy group in the ^1H NMR spectrum and signals at δ 68.18, 31.91–22.70 and 14.15 ppm corresponding to $-\text{OCH}_2$, $-\text{CH}_2$ and $-\text{CH}_3$ carbons, respectively, of decyloxy group in the ^{13}C NMR spectrum of intermediate **28** clearly confirm its structure. The ^1H NMR spectrum of intermediate **29** clearly displays a sharp singlet at δ 9.88 ppm which is a characteristic peak of aldehyde proton, confirming the structure. Similarly, in the ^{13}C NMR spectrum the aldehyde peak resonates at δ 183 ppm, which further validates the structure. The mass spectrum shows molecular ion ($\text{M}+1$) peak at m/z 336.21, 476.34 and 532.43 for intermediates **27**, **28** and **29**, respectively, which corresponds to their molecular formula, confirms the structure. The structural elucidation of one of the final compounds **VK11** is discussed herewith. The successful formation of **VK11** is evident by the disappearance of aldehydic proton and appearance of new additional eight aromatic protons at δ 7.77–7.04 ppm corresponding

to thiophene and vinyl protons in its ^1H NMR spectrum, whereas in its ^{13}C NMR spectrum, missing of aldehydic carbon signal and appearance of new aromatic carbons δ 160.4–103.3 ppm further confirm the structure. Also, MALDI-TOF mass spectrum showing a molecular ion peak at 742.194 corresponding to its (M+1) peak further validates the structure. Similar type of NMR patterns is observed for **VK12**, **VK13** and **VK14**, which confirms their structure. A molecular ion peak at 730.221 corresponding to (M+1) peak of **VK12** also confirms its structure. The molecular weight distribution of Mw= 4,241 and 10,426 obtained from GPC of **VK13** and **VK14**, respectively, prove the formation of polymers. In addition to the spectral characterizations, the elemental analysis further evidences the structures of all the intermediates and final compounds. The ^1H NMR, ^{13}C NMR and mass spectra of the intermediates and final compounds **VK11–VK14** are presented in **Figure 3.85–3.105**.

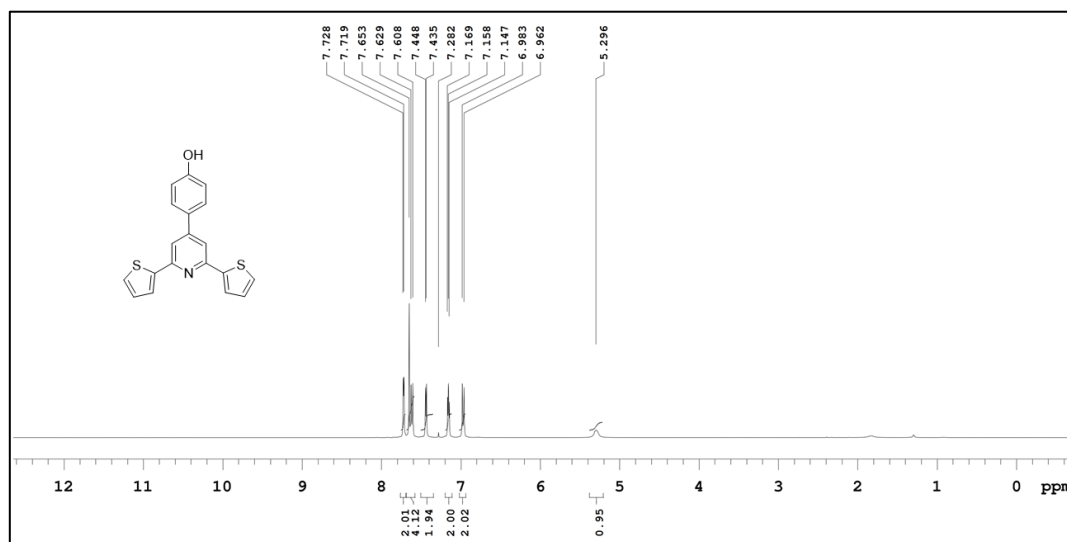


Figure 3.85 ^1H NMR spectrum of **27**

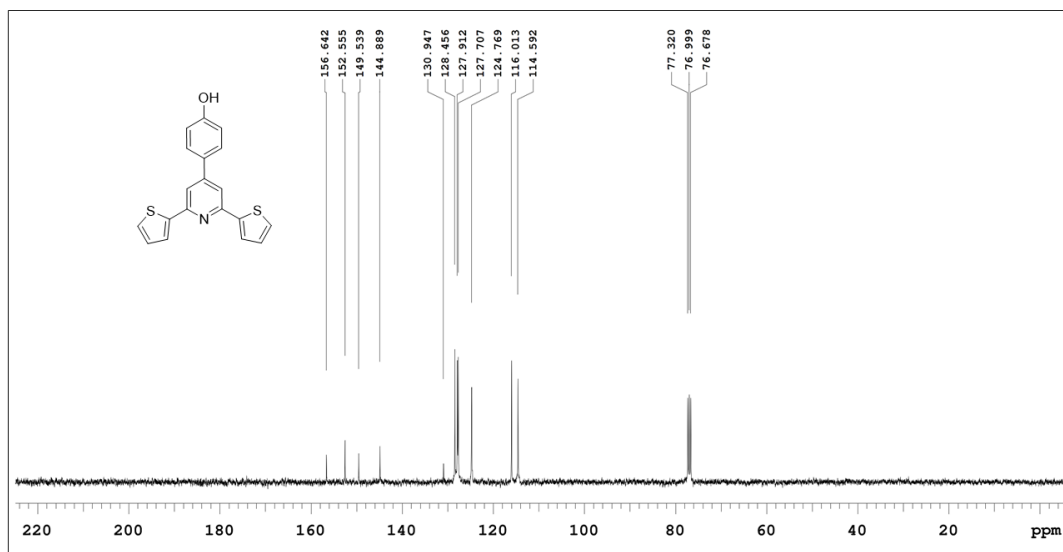


Figure 3.86 ^{13}C NMR spectrum of **27**

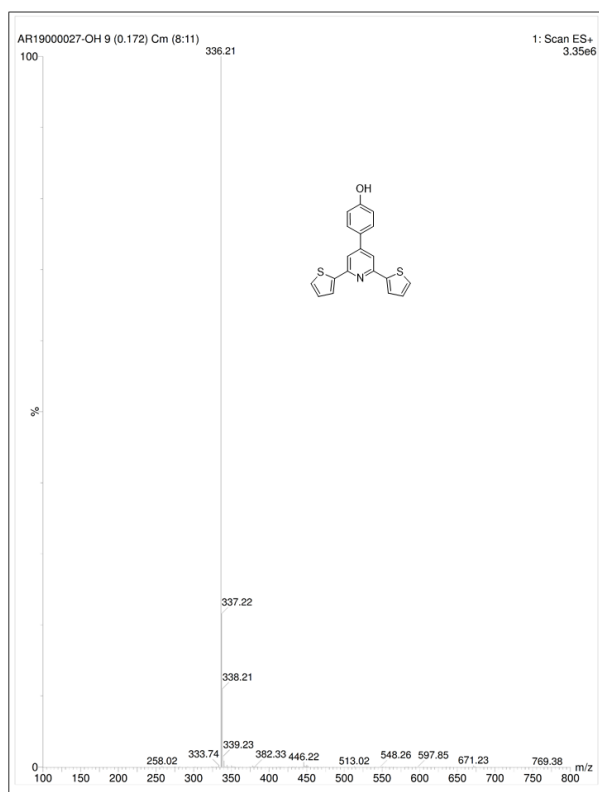


Figure 3.87 Mass spectrum of **27**

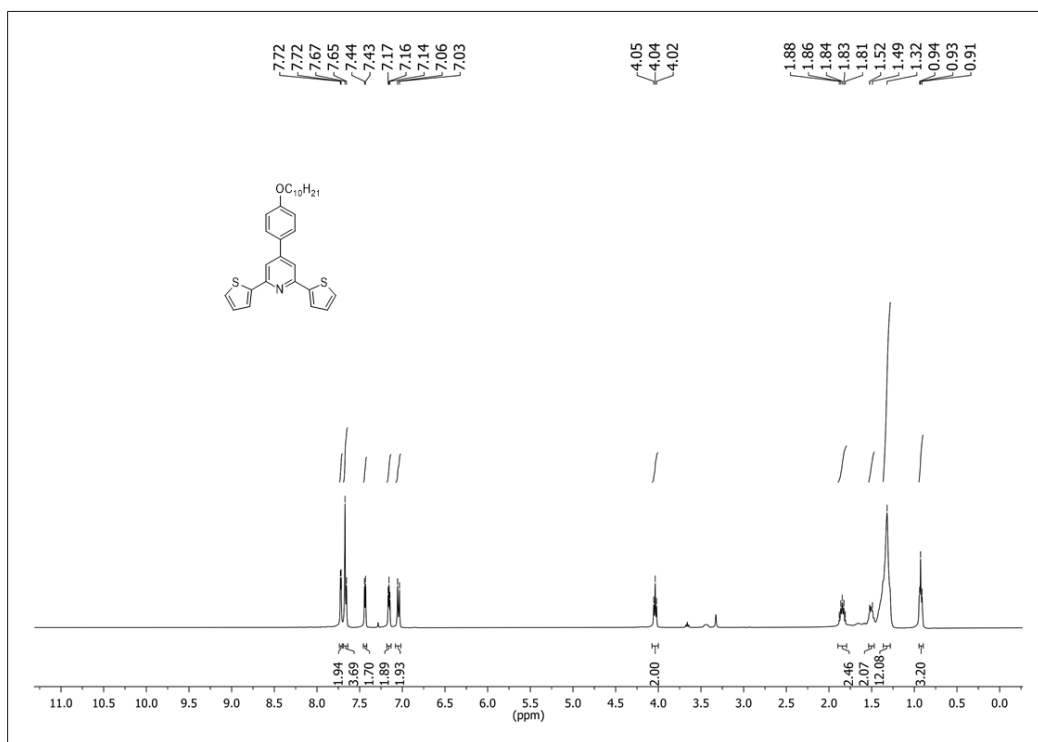


Figure 3.88 ^1H NMR spectrum of **28**

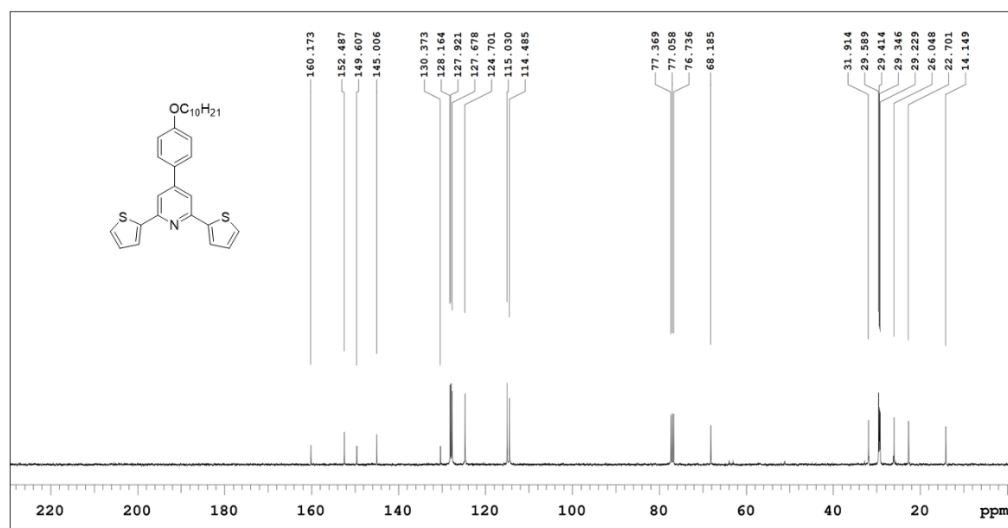


Figure 3.89 ^{13}C NMR spectrum of **28**

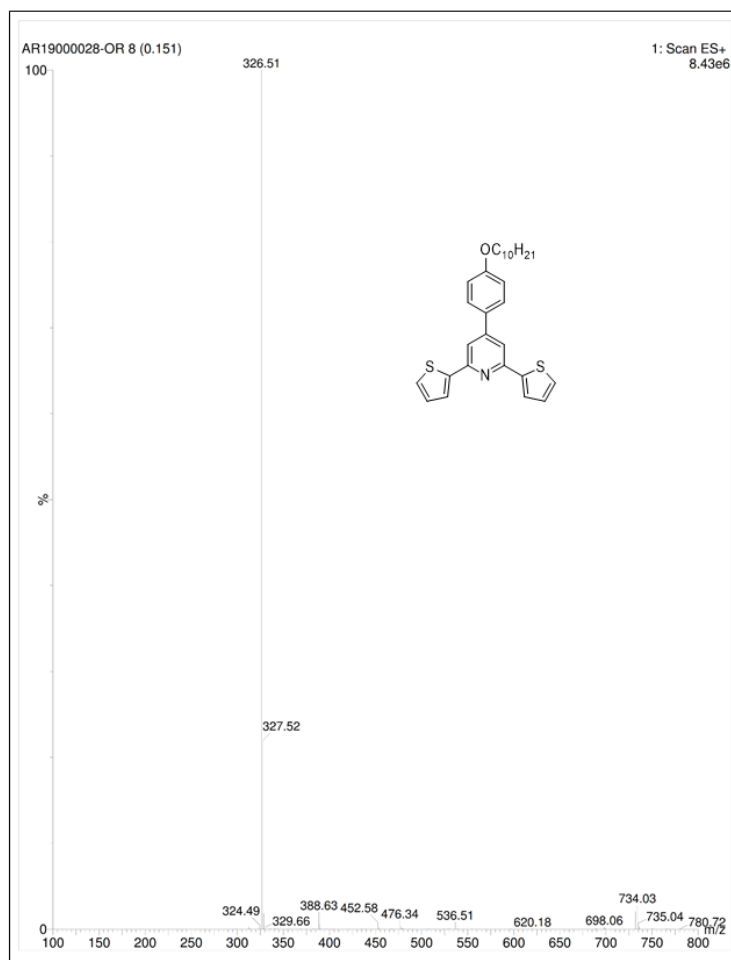


Figure 3.90 Mass spectrum of 28

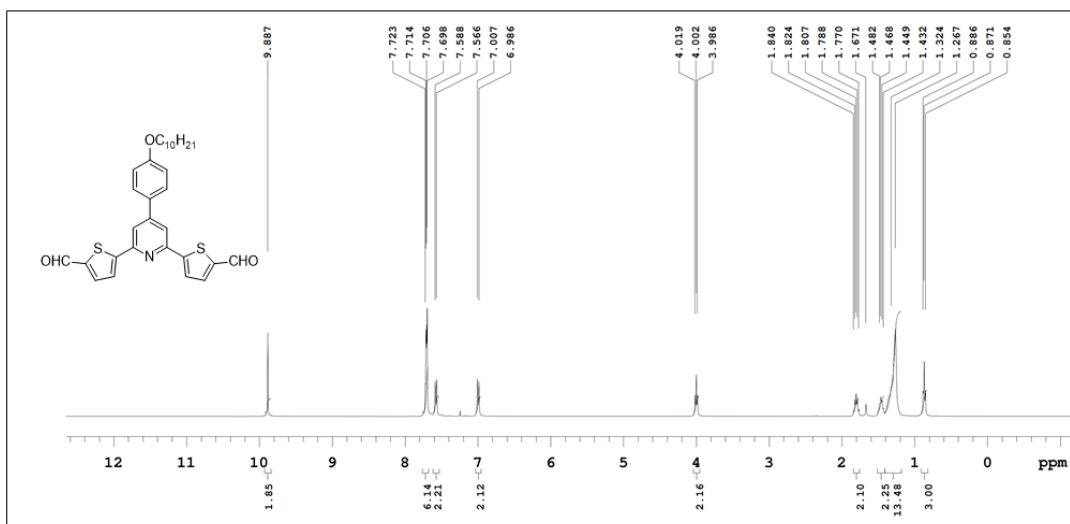


Figure 3.91 ¹H NMR spectrum of 29

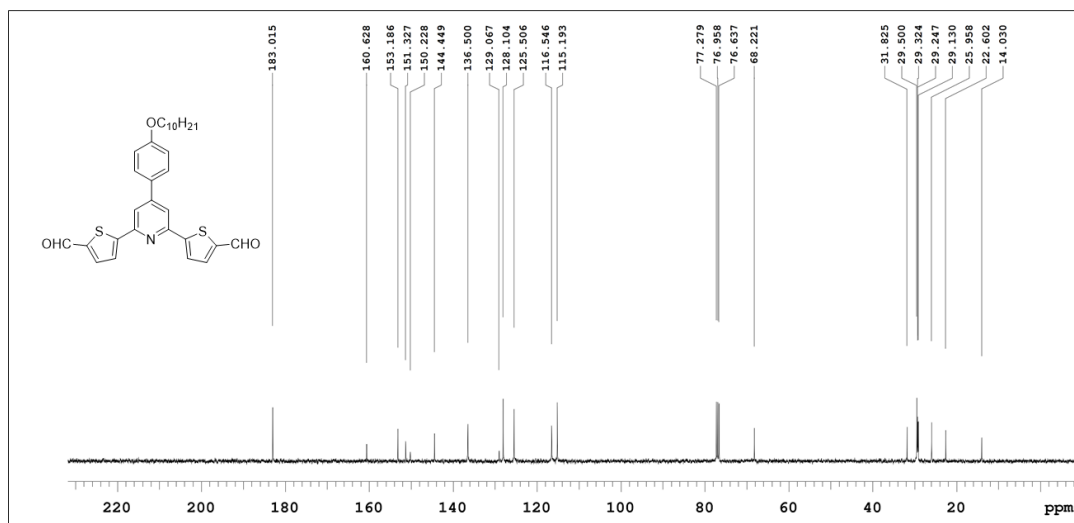


Figure 3.92 ¹³C NMR spectrum of **29**

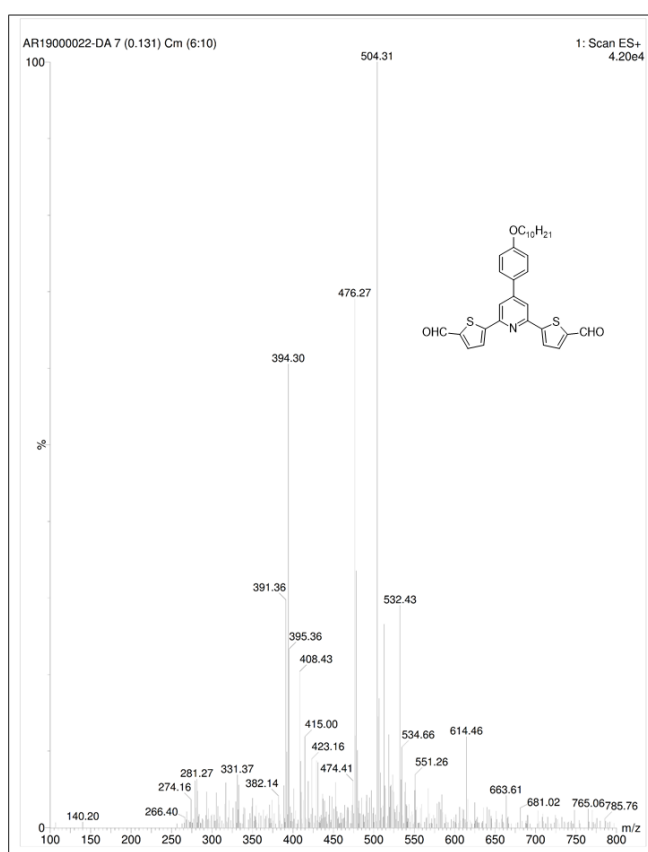


Figure 3.93 Mass spectrum of **29**

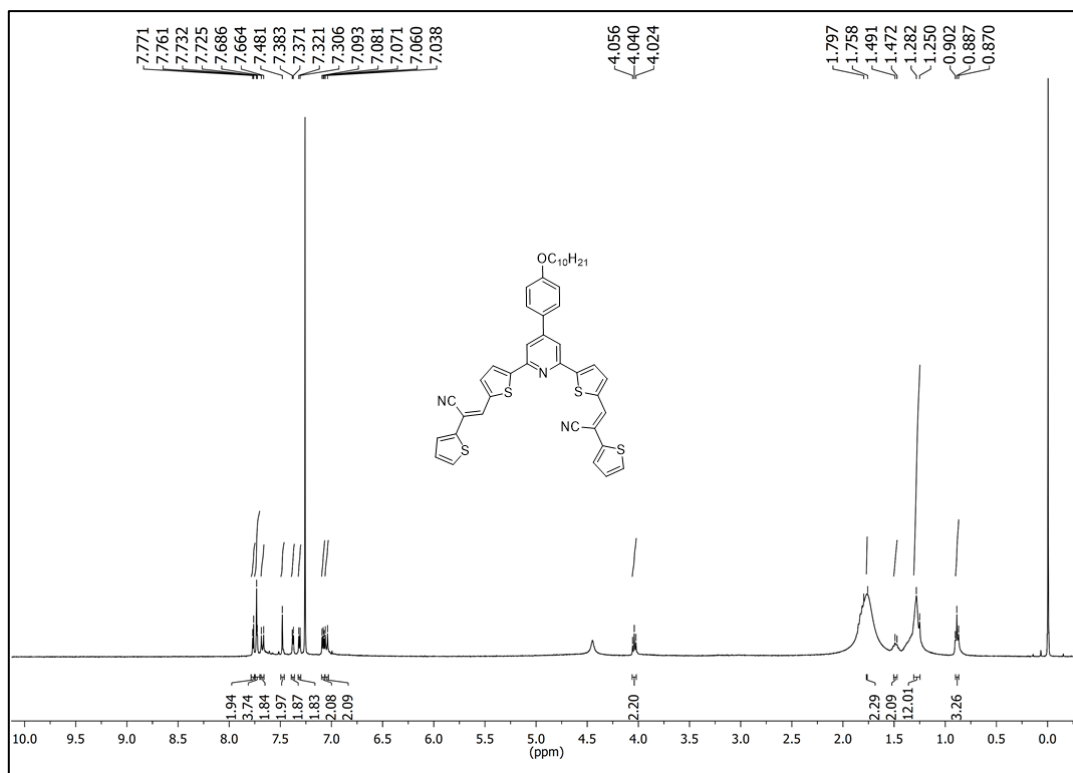


Figure 3.94 ^1H NMR spectrum of VK11

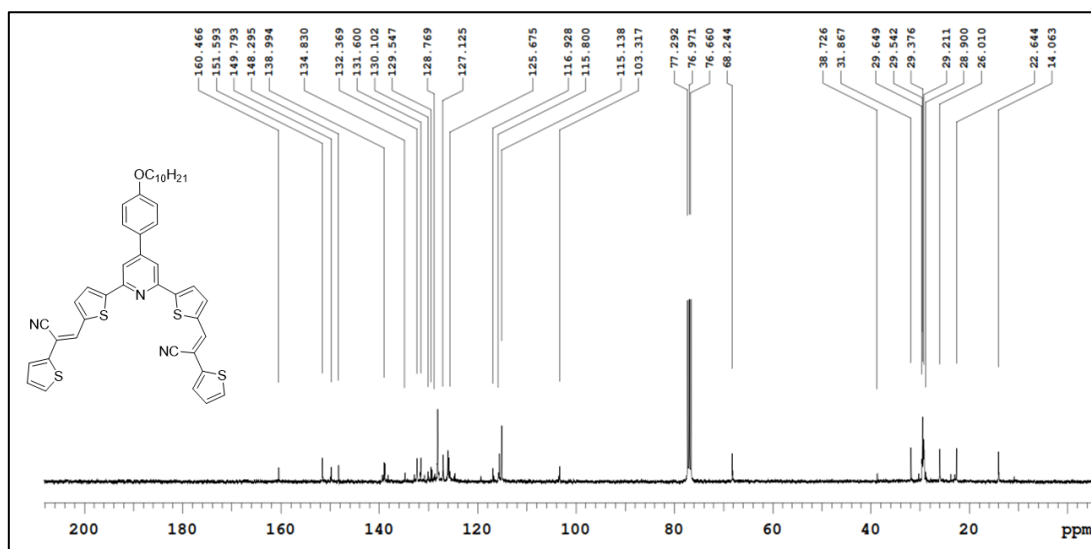


Figure 3.95 ^{13}C NMR spectrum of VK11

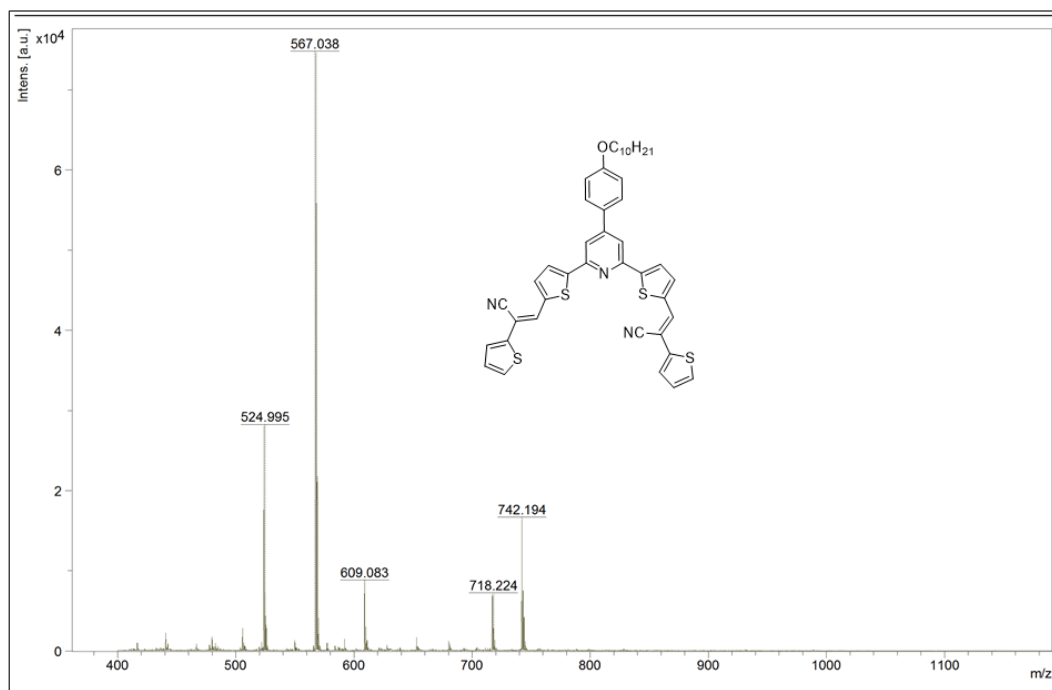


Figure 3.96 MALDI-TOF Mass spectrum of VK11

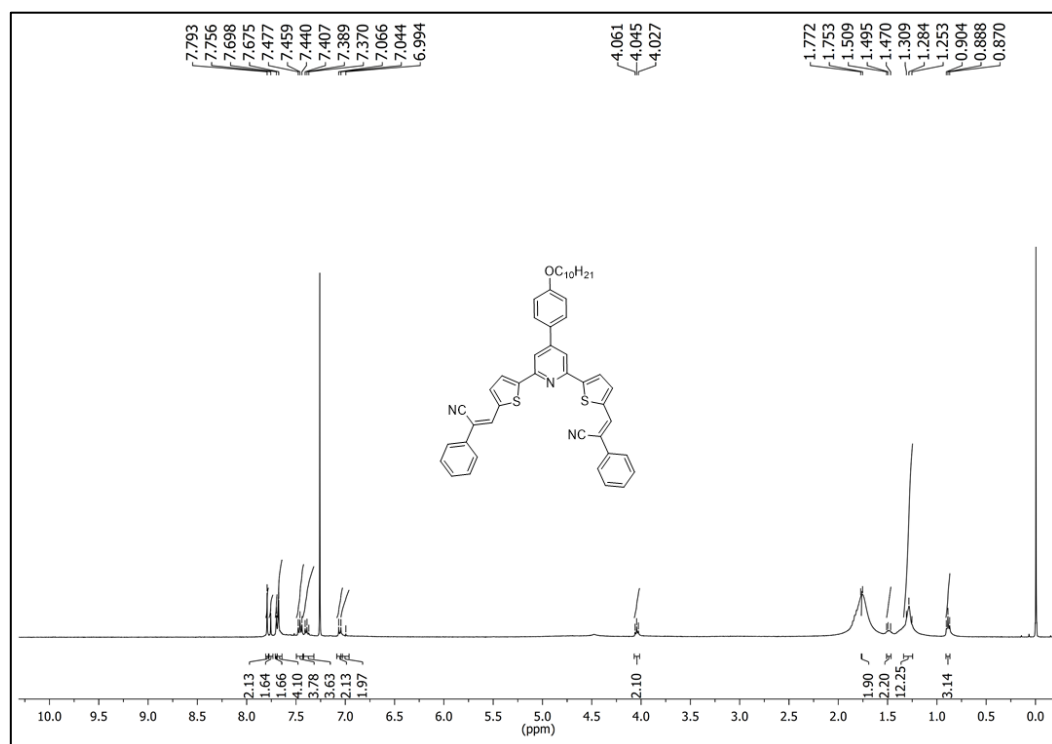


Figure 3.97 ¹H NMR spectrum of VK12

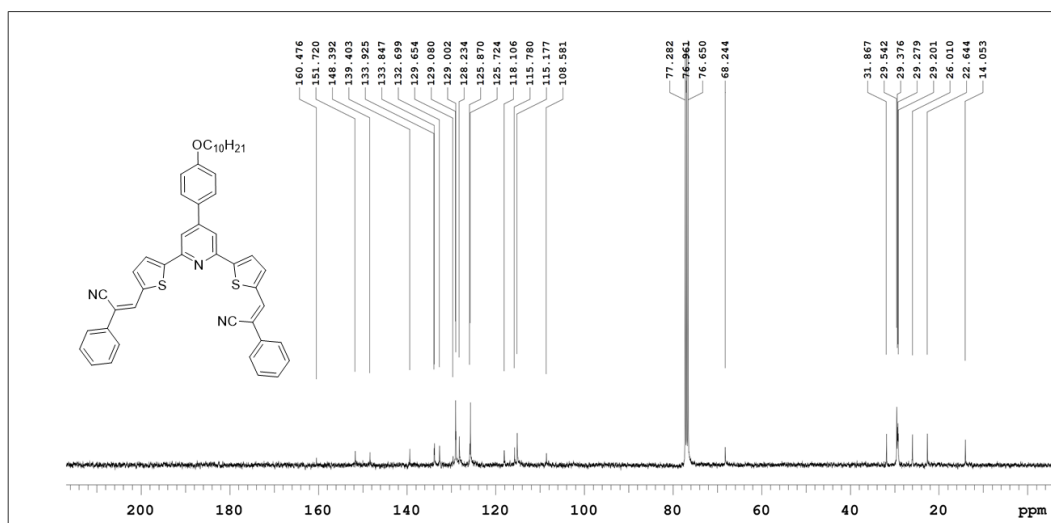


Figure 3.98 ^{13}C NMR spectrum of VK12

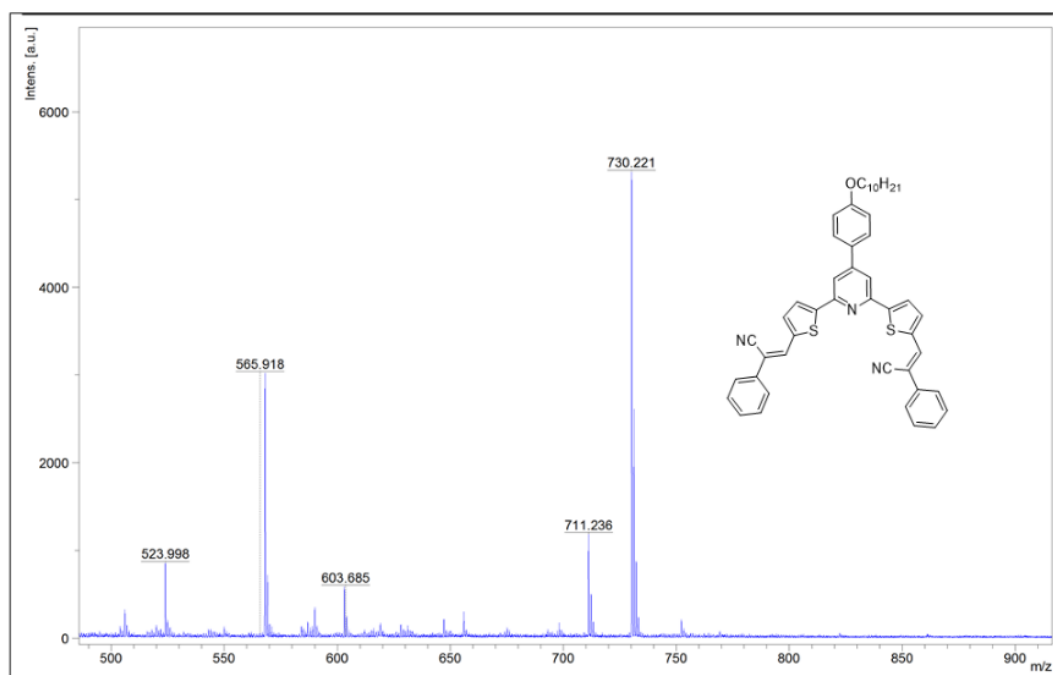


Figure 3.99 MALDI-TOF Mass spectrum of VK12

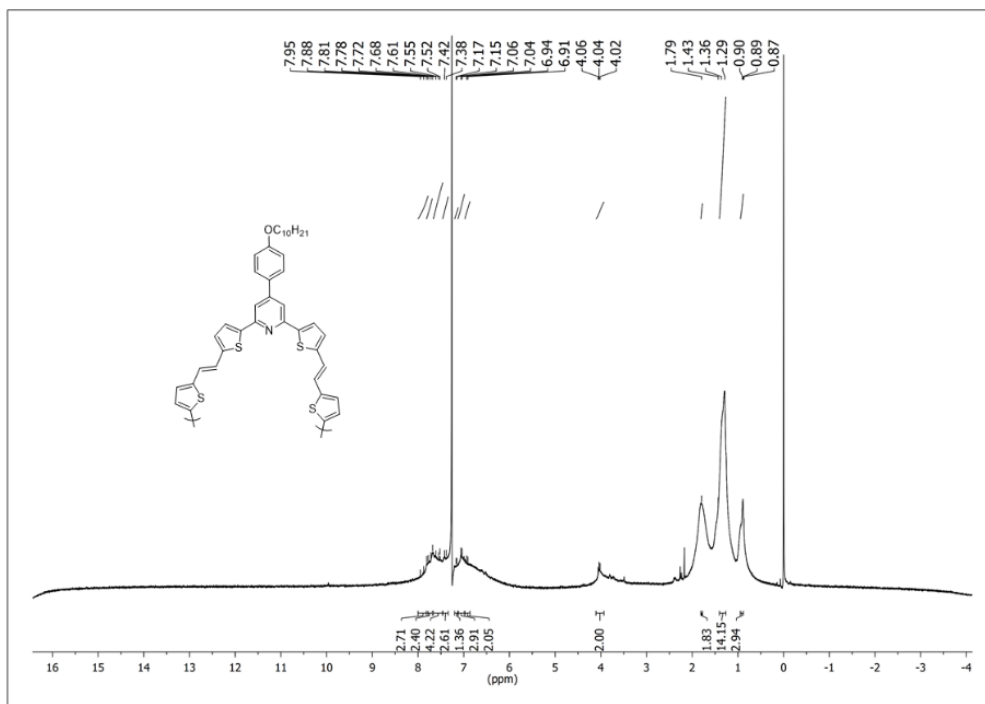


Figure 3.100 ^1H NMR spectrum of VK13

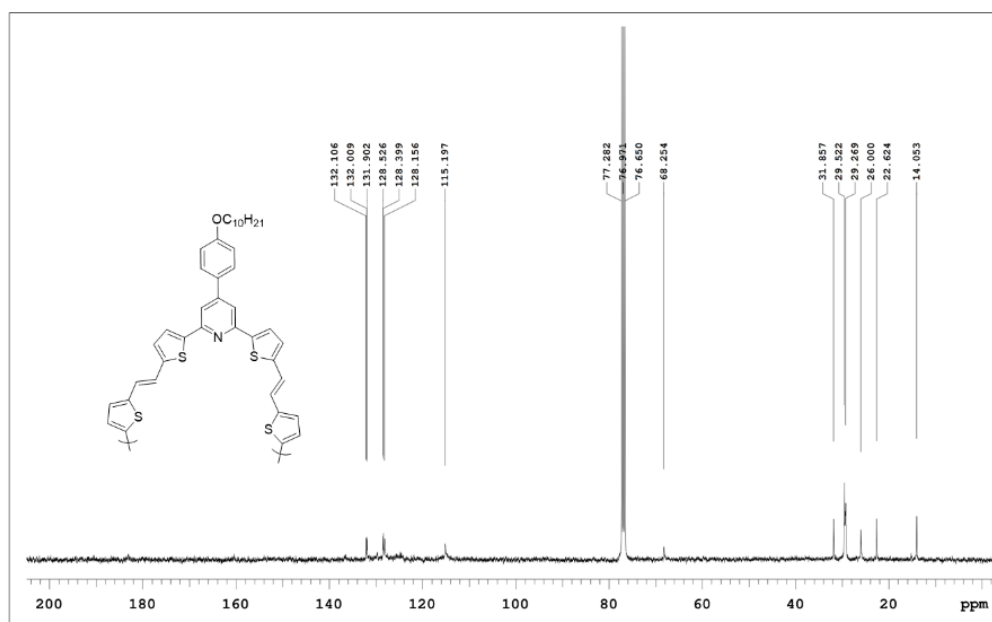


Figure 3.101 ^{13}C NMR spectrum of VK13

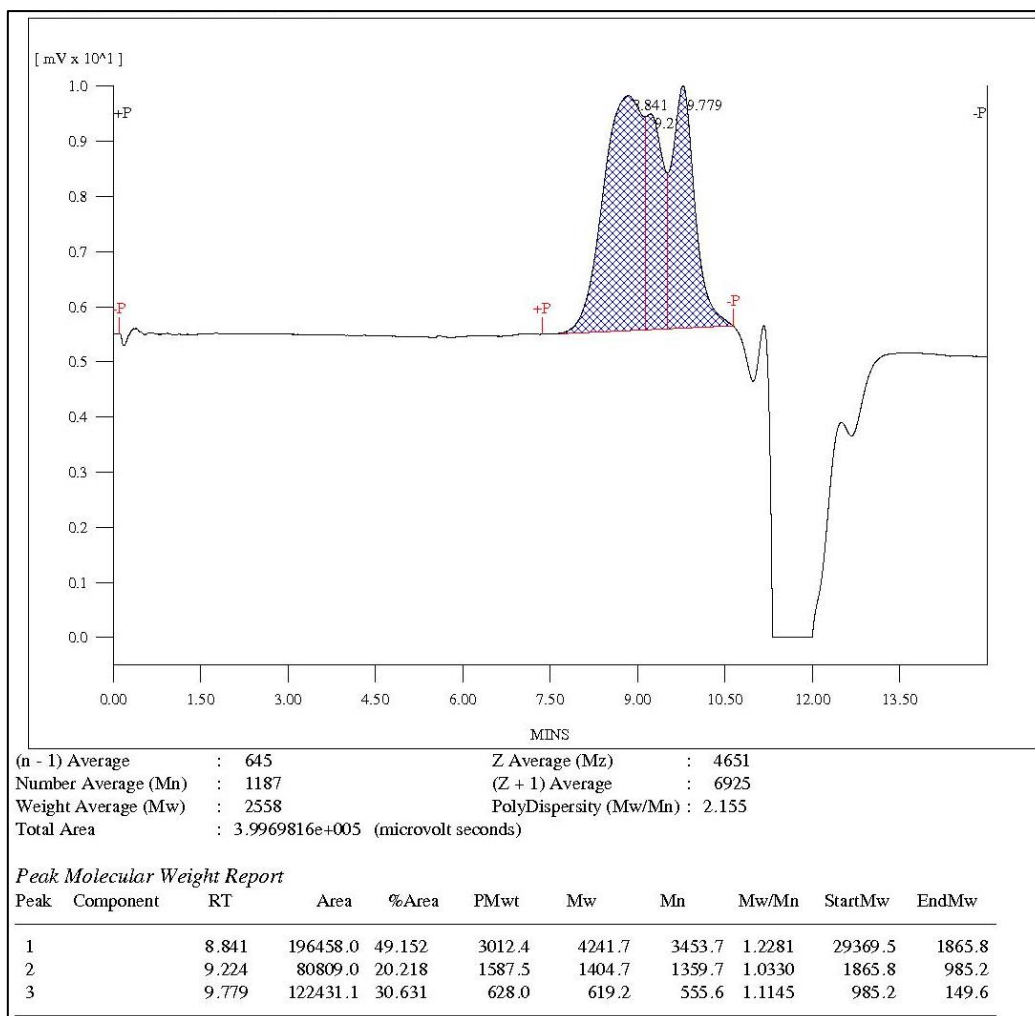


Figure 3.102 Gel permeation chromatogram of VK13

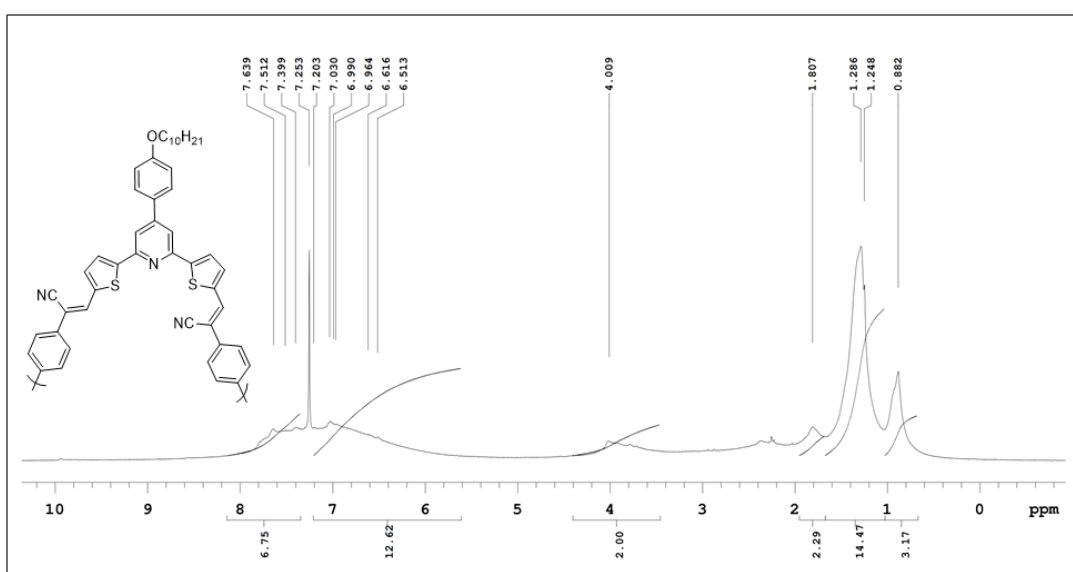


Figure 3.103 ¹H NMR spectrum of VK14

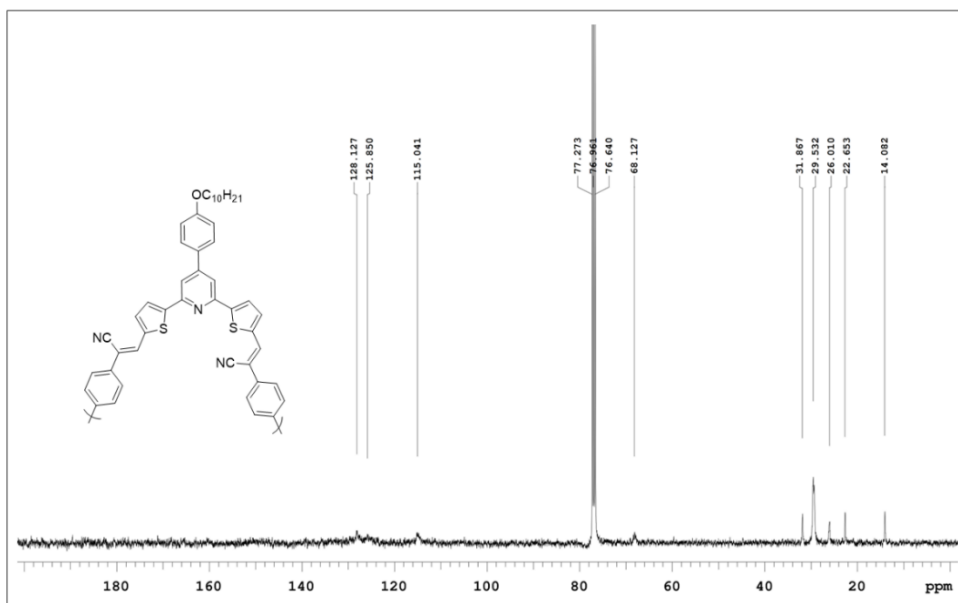


Figure 3.104 ^1H NMR spectrum of VK14

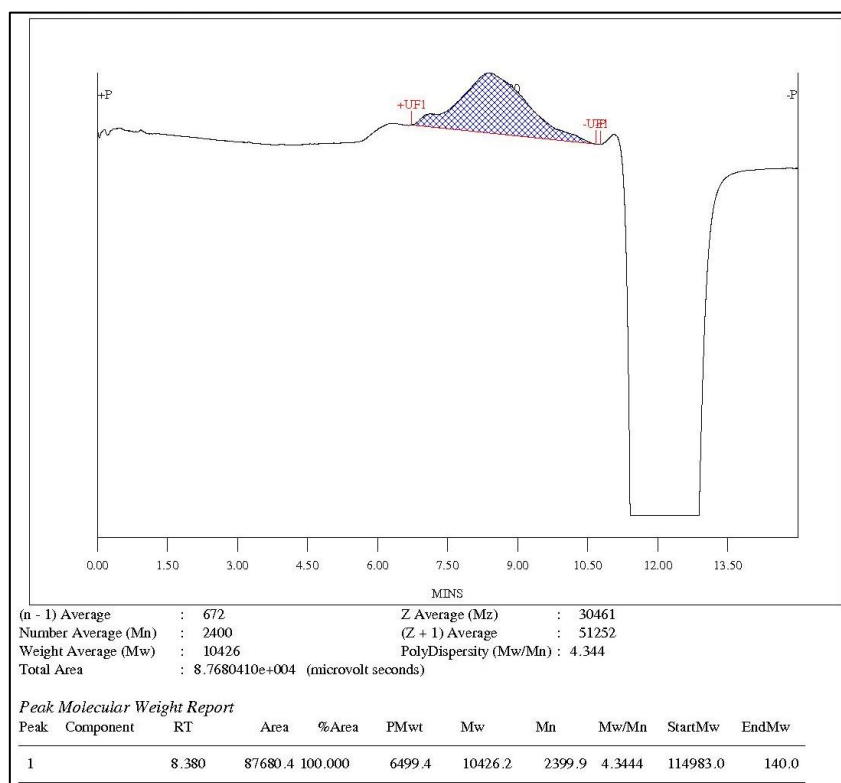


Figure 3.105 Gel permeation chromatogram of VK14

3.4.2 Photophysical studies

Figure 3.106 depicts the combined normalized UV–Vis absorption and PL emission spectra of compounds VK11–VK14. The corresponding numeral data are summarized in **Table 3.8**. As shown in **Figure 3.106**, there exist strong peaks of

maximum absorption at wavelengths 395, 377, 312 and 419 nm for **VK11**, **VK12**, **VK13** and **VK14**, respectively. These observed λ_{max} are the results of $\pi-\pi^*$ transition within the conjugated backbone. The molecules **VK11** and **VK12** exhibit similar absorption profiles from 300 to near 500 nm region. The effective D–A interaction between the thiophene and the cyanovinylene groups in **VK11** compared to that between phenyl and cyanovinylene groups in **VK12** shift the absorption of **VK11** to higher wavelength region compared to that of **VK12**. Similarly, the λ_{max} of **VK14** is bathochromically shifted compared to that of **VK13** due to the presence of cyanovinylene group in **VK14**. On the other hand, the absence of strong electron withdrawing, cyano group weakens the effective intramolecular interaction between the D and A units, resulting a large hypsochromic shift in the λ_{max} of **VK13** compared to that of **VK14**. As the molecular weights of **VK13** and **VK14** are widely different, the blue shift in the absorption spectrum of **VK13** could also arise from the short chains of the polymer compared to that of **VK14**. Further, by exciting all the four compounds at their respective λ_{max} , the emission profiles were recorded, which exhibit similar trend as those of absorption profiles with the emission wavelengths at 537, 500, 494 and 562 nm for **VK11**, **VK12**, **VK13** and **VK14**, respectively. The E_g calculated from the intersection point of absorption and emission spectra are 2.66, 2.74, 2.78 and 2.55 eV for **VK11**, **VK12**, **VK13** and **VK14**, respectively. The presence of strong electron accepting cyanovinylene group results in a considerable reduction of E_g in **VK11**, **VK12** and **VK14** when compared to that of **VK13**.

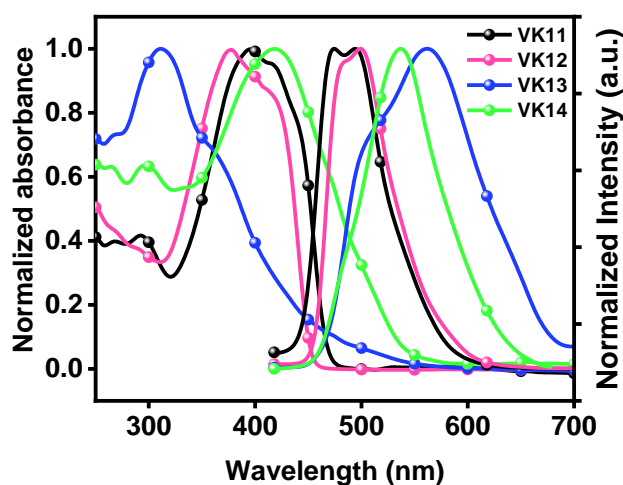


Figure 3.106 Normalized UV–Vis absorption and PL spectra of **VK11–VK14** recorded in CHCl_3 (10^{-5} M).

3.4.3 Electrochemical studies

The cyclic voltammograms of **VK11–VK14** are shown in **Figure 3.107a–d**, respectively. The HOMO energies were determined using **Equation 2.1** from first oxidation potential whereas LUMO energies were calculated using **Equation 2.2**.

The onsets of oxidation potentials are at 0.82, 0.99, 0.55 and 0.91 V for **VK11**, **VK12**, **VK13** and **VK14**, respectively. And the HOMO levels are determined to be -5.35 , -5.52 , -5.08 and -5.44 eV for **VK11**, **VK12**, **VK13** and **VK14**, respectively. Similarly, the LUMO levels are at -2.69 , -2.78 , -2.30 and -2.89 eV for **VK11**, **VK12**, **VK13** and **VK14**, respectively. Due to the higher electron donating ability of thiophene than phenyl moiety, the molecule **VK11** possesses higher HOMO level compared to that of **VK12**. Similarly, due to the higher electron donating ability of thiophene and absence of cyano group, the polymer **VK13** possesses comparatively higher HOMO energy level than that of **VK14**. The electrochemical data are listed in **Table 3.8**.

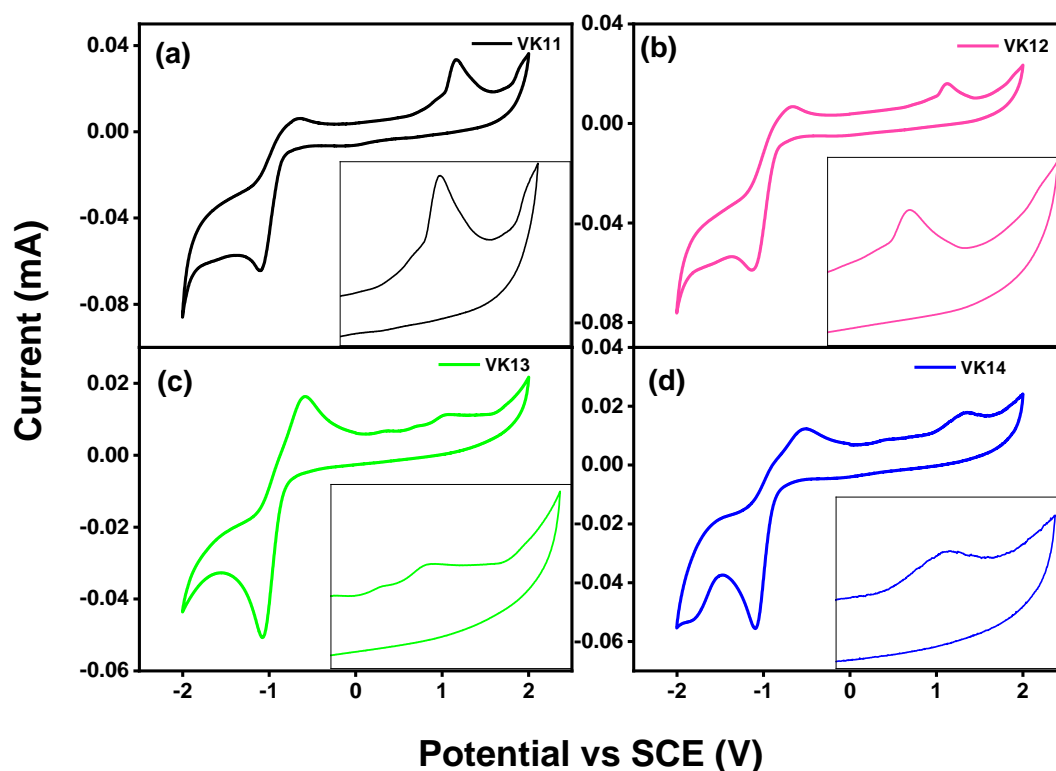


Figure 3.107 Cyclic voltammograms of (a) **VK11**, (b) **VK12**, (c) **VK13** and (d) **VK14**. Insets show the enlarged image of oxidation peaks in the anodic region.

Table 3.8 Summary of optical, electrochemical and theoretical data of **VK11–VK14**.

Molecules	$\lambda_{\max}^{\text{abs}}$ (nm)	$\lambda_{\max}^{\text{pl}}$ (nm)	$E_{\text{g}}^{\text{opt}}$ (eV)	$E_{\text{onset}}^{\text{ox}}$ (V vs SCE)	HOMO (eV)	LUMO (eV)
VK11	399	537	2.66	0.82	-5.35 ^a	-2.69 ^b
VK12	377	500	2.74	0.99	-5.52 ^a	-2.78 ^b
VK13	312	494	2.78	0.55	-5.08 ^a	-2.30 ^b
VK14	419	562	2.55	0.91	-5.44 ^a	-2.89 ^b

$E_{\text{g}}^{\text{opt}}$ Optical band gap calculated from the intersection of normalized absorption and emission spectra.

$E_{\text{onset}}^{\text{ox}}$ Experimental onset oxidation potential vs SCE.

^a Experimental values from CV using Equation 2.1 with Fc/Fc⁺ as internal standard.

^b Experimental values using Equation 2.2.

3.4.4 Theoretical studies

DFT calculations were performed to acquire better understanding of the electronic structure and distribution of electrons in the synthesized compounds. The electronic structure of **VK11**, **VK12** and two dimers simulating the structure of the polymers **VK13** and **VK14** were determined using tools of DFT as implemented in Gaussian 09 package. The optimization of the ground state geometry was carried out including solvent effects (chloroform) through the PCM using the B3LYP hybrid functional with 6-31G(d,p) basis set. Vibrational frequencies were computed at the same level of theory to confirm that these structures were minima on the energy surfaces. For computing the vertical transition energies, the TD-DFT tools as implemented in G09 were used. The performance of several functionals (B3LYP, M06, CAM-B3LYP, X3LYP, LC-wPBE, wB97XD, HSEh1PBE, and BMK) was tested by comparison of the calculated spectra to the experimental ones. It was observed that the best results were obtained using the wB97XD hybrid functional. Therefore, TD-DFT calculations were carried out at the wB97XD/6-31G(d,p)/PCM (chloroform) level of theory to produce a number of 15 singlet-to-singlet transitions. The calculated absorption spectra were obtained from the

outputs of G09 using the Gausssum free software. The ground state optimized geometry, HOMO and LUMO energy levels of **VK11–VK14** are shown in **Figure 3.108**. The decyloxy unit was considered as methoxy group for the easy calculation. As shown in **Figure 3.108**, except the decyloxy substituted phenyl group, which is twisted by an angle of $\sim 30^\circ$ from the thiophene–pyridine plane, the HOMO and LUMO orbitals are uniformly distributed over central pyridine, spacer thiophene, cyanovinylene and on the peripheral groups as a result of structural planarity in the case of **VK11** and **VK12**. This type of spatial distribution on entire molecular backbone suggests the π – π^* type transition in **VK11** and **VK12**, whereas, in the case of **VK13** the HOMO is majorly distributed on thiophene and vinylene linkage present in the right wing. Also, a minor distribution of HOMO can be seen on thiophene and vinylene linkage present in the left wing as well. This may be attributed to the twisting of polymeric chain from the planarity. Further, the LUMO is majorly localized on central pyridine, thiophene and the vinylene linkage present in the right wing. Similarly, in **VK14** the HOMO is majorly distributed on thiophene and 1,4-phenyleneacrylonitrile group present in the right wing and partially distributed on central pyridine and thiophene present in the left wing. There is a twisting of 1,4-phenyleneacrylonitrile group in the left wing, as a result of which the HOMO distribution is restricted to thiophene unit. The LUMO in **VK14** is majorly localized on central pyridine, thiophene and 1,4-phenyleneacrylonitrile group present in the right wing. Further, to study the excited state electronic transitions, the TD-DFT calculations were carried out. Structural optimizations were performed on various conformational isomers (dimers) of **VK13** and one simple structure (monomer, **VK13f**). Of the five conformations **VK13a**, **VK13b**, **VK13c**, **VK13d**, and **VK13e**, **VK13e** is of lowest energy conformation (**Figure 3.110**). The simple structure (**VK13f**) cannot be compared in energy to the others as it has a smaller number of total atoms. Similarly, structural optimizations were performed on **VK14** (dimer) and one simple structure (monomer, **VK14f**). Simulated absorption spectra were taken for all the conformers along with **VK11** and **VK12**. Out of all the five conformers of **VK13**, **VK13e** exhibits a closer agreement with experimental results. However, the experimental absorption spectrum of **VK13** can be described better with the electronic structure of the monomer **VK13f**. This latter fact suggests that for a more accurate simulation of the absorption spectrum of **VK13** it is necessary that the inclusion of a

larger number of units including several conformations. Similarly, simulated spectra of **VK14** and **VK14f** showed good results in terms of comparison with experimental data and it seems that extending the number of units shifts the spectrum to longer wavelength region. **Figure 3.109** shows the predicted spectra for **VK11**, **VK12** and for the most stable conformations (dimer) and monomer of **VK13** and **VK14** compared to the experimental solution spectrum.

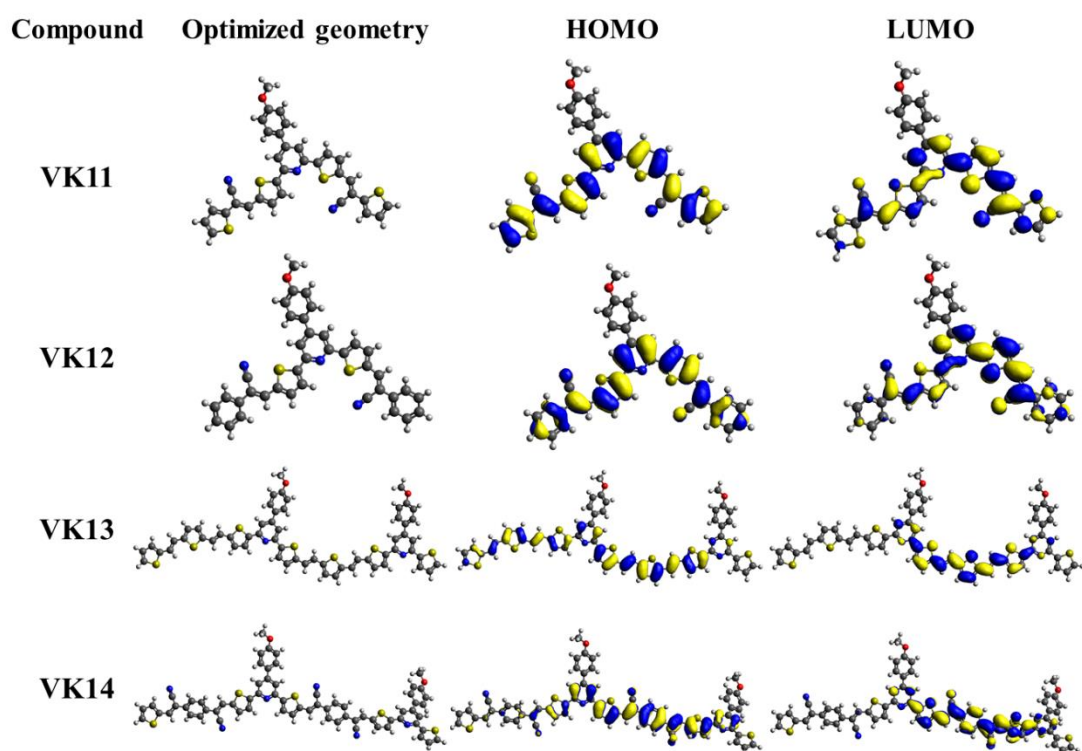


Figure 3.108 Optimized ground state geometry and HOMO/LUMO distribution of **VK11–VK14**.

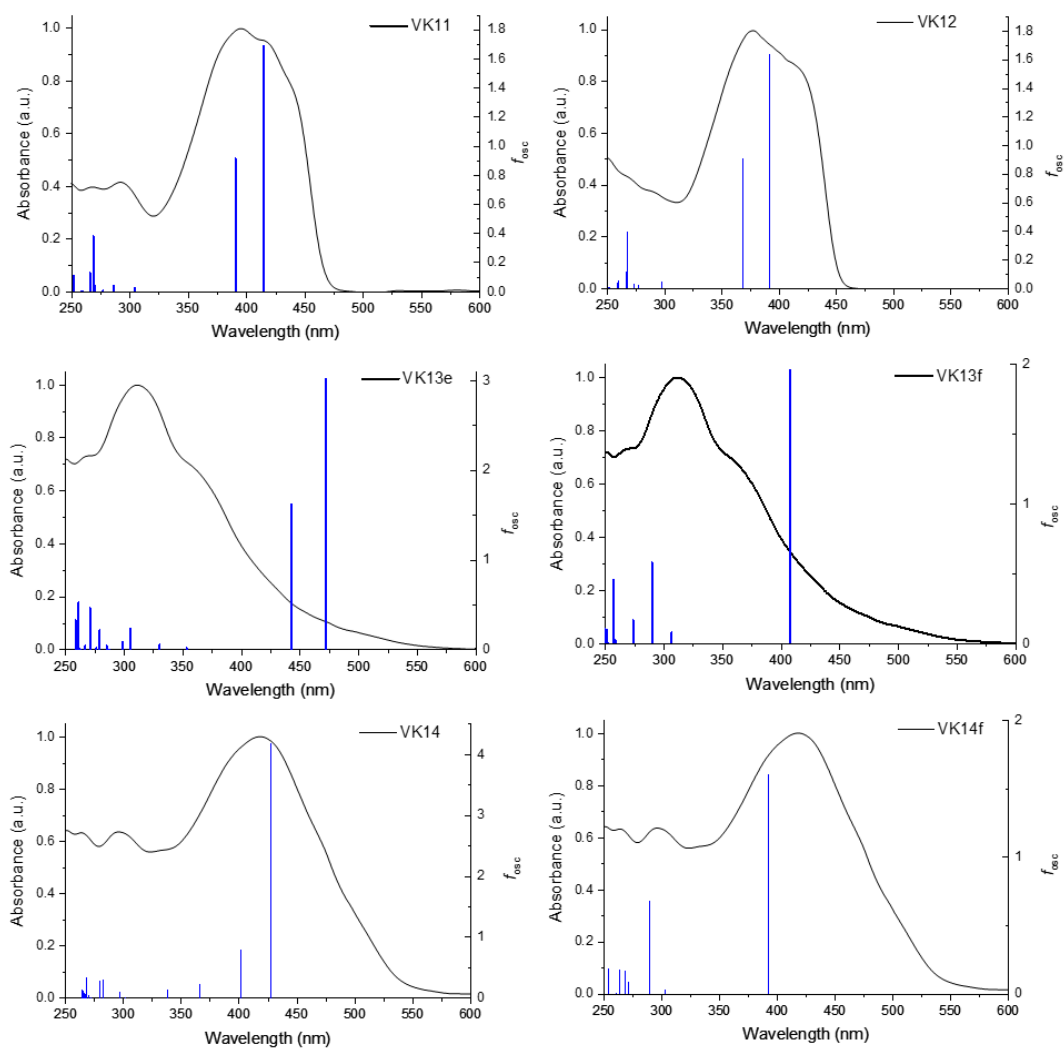


Figure 3.109 Predicted spectra (lines) for **VK11**, **VK12** and, most stable conformations (dimers) and monomers of **VK13** and **VK14** compared to the experimental solution spectrum.

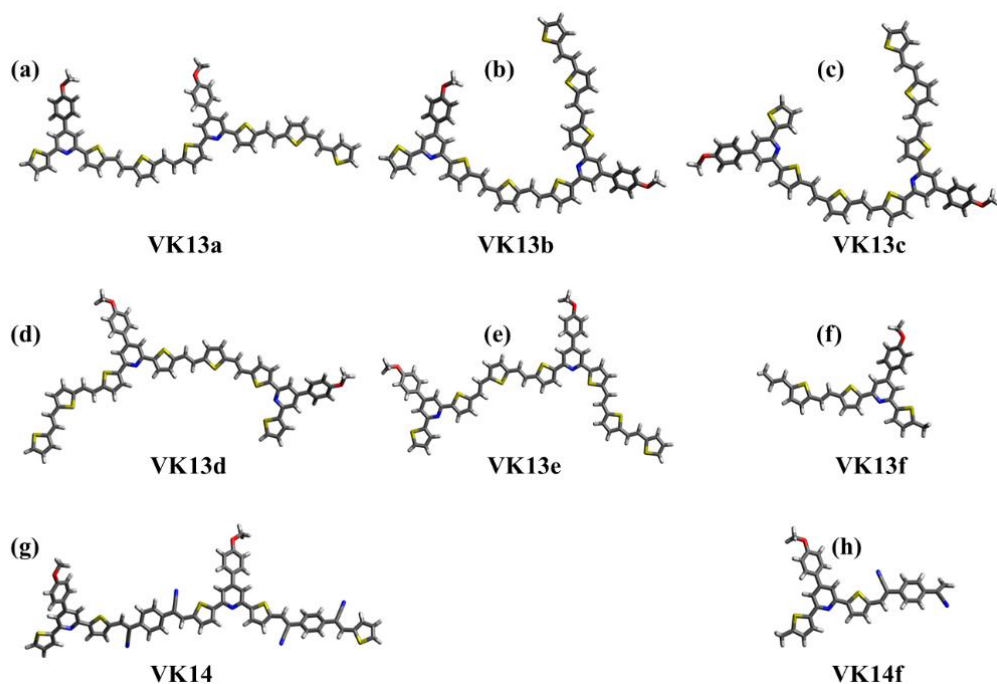


Figure 3.110 (a)–(e) The optimized geometry of **VK13** dimer in conformations a to e (f) optimized geometry of **VK13** monomer (g) optimized geometry of **VK14** dimer (h) optimized geometry of **VK14** monomer.

3.4.5 Thermal properties

As shown in the TGA plots of **VK11–VK14** (**Figure 3.111**), no significant weight loss is observed up to a temperature of $\sim 350^\circ\text{C}$ for **VK11** and **VK12**, after which, an abrupt weight loss is observed for both the molecules, indicating the complete decomposition of the molecules. The onset of T_d corresponding to **VK11** and **VK12** are 347 and 369°C , respectively. The higher T_d of **VK12** is due to the presence of 2-phenylacrylonitrile unit in **VK12** which is more stable than 2-thiopheneacrylonitrile present in **VK11**. However, the onset of T_d for the polymer **VK13** is observed at 260°C . The weight loss at 76°C corresponds to the moisture and that at 260°C is due to the degradation of polymer backbone, whereas the polymer **VK14** exhibits the thermal stability up to 384°C and a sharp weight loss above 384°C , indicating the complete decomposition of polymer backbone. Since 1,4-phenylacrylonitrile is more stable than thiophene, the presence of 1,4-phenylacrylonitrile in **VK14** is fetching the higher stability to **VK14** compared to that of **VK13**, as in the case of **VK12**. It is seen from the TGA plots of **VK11**, **VK12** and **VK14** that they exhibit T_d higher than that of **VK13**. This is attributed to the presence of cyanovinylene moiety in **VK11**, **VK12** and **VK14**

which makes them thermally stable (Park et al. 2016). From the TGA results it can be concluded that the stability of the materials is good enough to be used in photovoltaics/optoelectronics.

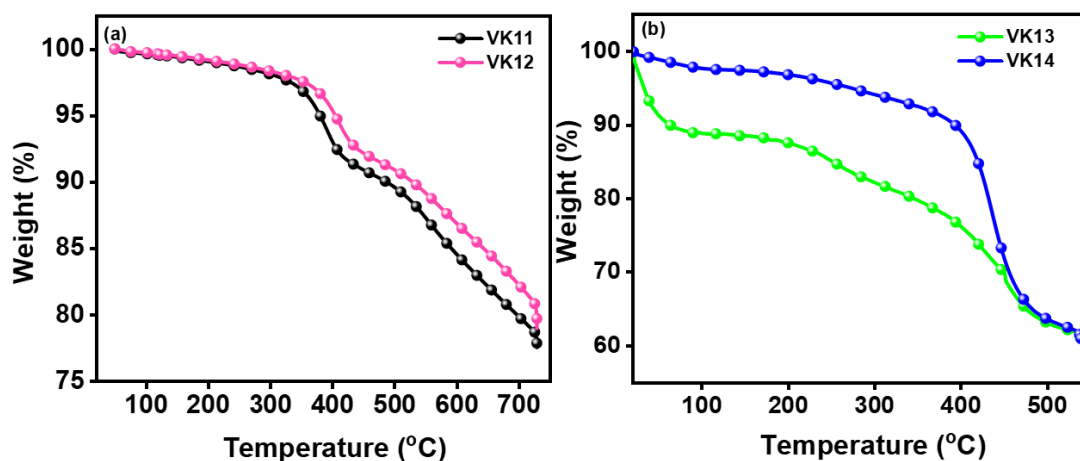


Figure 3.111 TGA plots of (a) VK11 and VK12, (b) VK13 and VK14.

3.4.6 Third order NLO properties

3.4.6.1 Nonlinear absorption studies

The OA Z-scan measurements were carried out to study the NLA behavior of VK11–VK14. A 50 μJ laser beam with a pulse width of 7 ns, corresponding to the peak on-axis intensity of 1.386 GW cm^{-2} was used to examine the NLA behavior of the compounds. The linear transmittance was set at 60–65%. The OA Z-scan curves obtained from VK11–VK14, by dissolving them in CHCl_3 , are shown in **Figure 3.112a–d**, respectively. On analysing the figures, it is observed that at the focus ($z=0$), the curves are symmetric and there is a decrease in the transmittance which becomes minimum at the focus, revealing the RSA of the compounds. At high laser energies, the RSA is associated with TPA, which is assisted with ESA. Therefore, the net effect is termed as “effective TPA” process (Vishnumurthy et al. 2011). In order to determine the β_{eff} of VK11–VK14, the experimental data were theoretically fitted to an ESA assisted TPA using **Equation 2.3**. Further, on solving the nonlinear propagation (dI/dz) using **Equation 2.4**, (fourth-order Runge–Kutta method), the output laser intensity was numerically calculated for a given input intensity. The obtained experimental results were fitted with less error with the normalized transmittance ($T(z)$) (**Equation 2.5**), which was derived from **Equations 2.3** and **2.4**. The $\text{im } \chi^{(3)}$ for OA configuration was determined using the **Equation 2.6**. The calculated β_{eff} and $\text{im } \chi^{(3)}$ are given in **Table**

3.9. The calculated β_{eff} values for **VK11**, **VK12**, **VK13** and **VK14** are 1.48×10^{-10} , 2.08×10^{-10} , 6.12×10^{-10} and $7.02 \times 10^{-10} \text{ m W}^{-1}$, respectively. The obtained β_{eff} values of **VK11–VK14** are comparable with β_{eff} values of some of the well-known materials (**Table 3.9**).

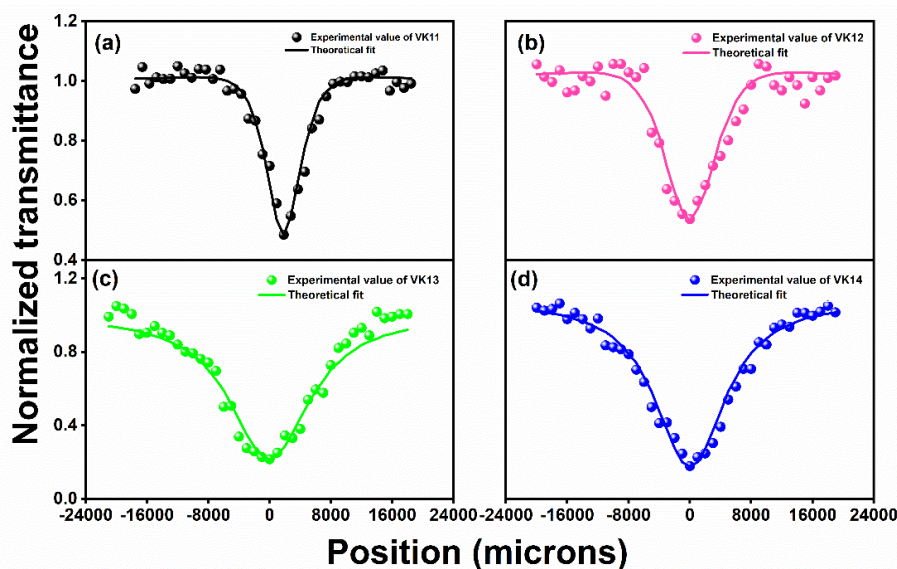


Figure 3.112 Z-scan curves of (a) **VK11**, (b) **VK12**, (c) **VK13** and (d) **VK14** under OA configuration.

3.4.6.2 Optical limiting studies

The optical limiting data of **VK11–VK14** are obtained by plotting a graph of normalized transmittance versus input intensity (**Figure 3.113a–d**), obtained from the OA Z-scan analysis. From the graph, it is seen that the onset of optical limiting values of the compounds **VK11**, **VK12**, **VK13** and **VK14** are at 1.11, 0.83, 0.22 and 0.16 J cm^{-2} , respectively and the LT values are 8.34, 4.16, 1.69 and 1.42 J cm^{-2} for **VK11**, **VK12**, **VK13** and **VK14**, respectively. The polymers **VK13** and **VK14** possess significantly low onset and LT values compared to that of molecules **VK11** and **VK12** and moreover, the obtained relatively low optical limiting data are comparable and are even better than the similar materials reported (**Table 3.9**).

For an instance, Gopi *et al.* (Gopi *et al.* 2020) synthesized a new solution processable quinoxaline based push-pull molecule with 3-ethyl rhodanine as acceptor unit and investigated the NLO properties of the molecule, which showed an effective TPA with β_{eff} value as high as $10.0 \times 10^{-10} \text{ m W}^{-1}$ with the LT of 2.46 J cm^{-2} . Vintu *et al.* (Vintu *et al.* 2019) synthesized a novel anthracene supported 5,11-dihydroindolo

[3,2-*b*] carbazole- based polymer for nonlinear optical application, which showed a very high β_{eff} of $11.6 \times 10^{-10} \text{ m W}^{-1}$ with the LT of 1.03 J cm^{-2} . Zawadzka *et al.* (Zawadzka *et al.* 2013) synthesized two 5,10-A₂B₂ porphyrin series with different metals in the core and investigated the NLO properties, and with tin (IV) complex, SnCl₂_CCTMS, porphyrin showed RSA with the β_{eff} of $6.4 \times 10^{-10} \text{ m W}^{-1}$. Praseetha *et al.* (Praseetha *et al.* 2019) observed the enhancement in the NLO property of 4'-Heptyl-4-biphenylcarbonitrile (7CB) nematic liquid crystal upon doping it with CdSe quantum dot (QD) in different concentrations. The pure 7CB nematic liquid crystal showed β_{eff} of $2.0 \times 10^{-10} \text{ m W}^{-1}$ while after doping with 0.75 and 1% of CdSe QD, the β_{eff} raised to $5.5 \times 10^{-10} \text{ m W}^{-1}$ with the LT of 3.02 J cm^{-2} and $7.8 \times 10^{-10} \text{ m W}^{-1}$ with the LT of 2.1 J cm^{-2} , respectively. The available reports indicate that in most of the cases the optical nonlinearity is increased by doping with some inorganic materials, whereas, few of the pure organic materials have also shown increase in the β_{eff} as a result of conjugation. However, the synthesized compounds **VK11**, **VK12**, **VK13** and **VK14** exhibit higher NLA, improved β_{eff} and significantly low onset and LT values, establishing their efficient optical power limiting behavior in their pristine state compared to some of the reported molecules. The results reveal that these synthesized compounds could serve the potentials as optical limiters for human eye and other sensitive sensors in laser photonics. Unfortunately, **VK11–VK14** did not show NLR properties as the NLA was much stronger than refraction of the compounds.

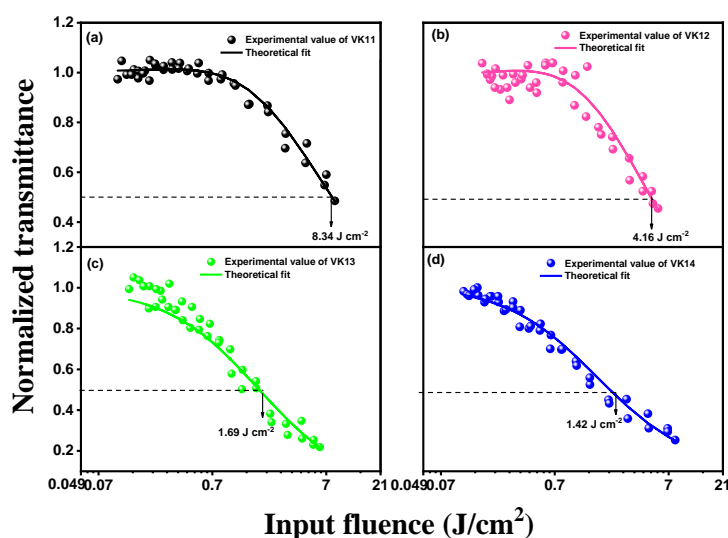
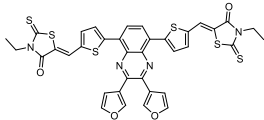
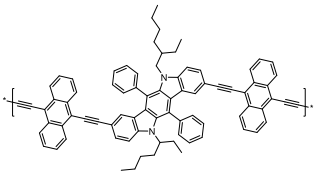


Figure 3.113 Optical limiting curves of (a) **VK11**, (b) **VK12**, (c) **VK13** and (d) **VK14** at an input intensity of 1.386 GW cm^{-2} .

Table 3.9 NLO parameters of **VK11–VK14** and few comparisons with work reported under similar experimental conditions.

Sample	β_{eff} ($\times 10^{-10} \text{ mW}^{-1}$)	Limiting threshold (Jcm^{-2})	Im $\chi^{(3)}$ (esu) (10^{-12})	References
VK11	1.48	8.34	4.67596	This work
VK12	2.08	4.16	6.56524	This work
VK13	6.12	1.69	19.2738	This work
VK14	7.02	1.42	22.1203	This work
	10	2.46	-	(Gopi et al. 2020)
	11.6	1.03	32.331	(Vintu et al. 2019)
5,10-A ₂ B ₂ porphyrin– SnCl ₂ _CCTMS complex	6.4	-	-	(Zawadzka et al. 2013)
7CB	2.0	-	7.42	(Praseetha et al. 2019)
7CB + 0.75% CdSe QD	5.5	3.02	20.4	(Praseetha et al. 2019)
7CB + 1.0% CdSe QD	7.8	2.1	28.9	(Praseetha et al. 2019)

As the optical nonlinearity of organic materials is solely resulting from the conjugation, the extended conjugation in **VK11–VK14** enhances the NLO properties

of the materials. Moreover, the predominant increment in the β_{eff} and substantial reduction in optical limiting values of polymers **VK13** and **VK14** compared to that of molecules **VK11** and **VK12** is due to the higher extension of conjugation, improved interaction between the electron donor and acceptor units, increased ICT and the polarizability in **VK13** and **VK14**. Between the **VK11** and **VK12**, the **VK12** shows higher NLO property due to the presence of phenyl acrylonitrile moiety which extends the conjugation in **VK12** compared to that of thiophene acrylonitrile in **VK11**. Similarly, between the **VK13** and **VK14**, the **VK14** shows higher NLO property due to the presence of phenyl acrylonitrile moiety which extend the conjugation in **VK14** compared to that of thiophene alone in **VK13**.

3.4.7 The important findings from the experimental data

The substituted acrylonitrile group present in **VK11**, **VK12** and **VK14** results in the red shift of the absorption and emission maxima; and improves the thermal stability compared to that of **VK13**. The presence of phenylacrylonitrile unit results in the enhanced NLA in **VK12** and **VK14** compared to that of **VK11** and **VK13**. The higher degree of conjugation in **VK13** and **VK14** improves the interaction between the electron donor and acceptor units, the ICT and the polarizability of the polymers, resulting in the predominant increment in the β_{eff} (6.12×10^{-10} and 7.02×10^{-10} m W⁻¹ for **VK13** and **VK14**, respectively) and substantial reduction in optical limiting values (1.69 and 1.42 J cm⁻² for **VK13** and **VK14**, respectively) compared to that of **VK11** and **VK12**. The results obtained here for **VK13** and **VK14** are better than some of the NLO materials reported. Therefore, the materials synthesized here could be of promising candidates for all-optical limiting devices in laser photonics.

3.5 BUTTERFLY-SHAPED THIOPHENE-PYRIDINE HYBRIDS (VK15–VK18): GREEN ELECTROLUMINESCENCE AND LARGE THIRD-ORDER OPTICAL NONLINEARITIES

Designing and developing new families of organic molecules with the specific features is at the heart of optoelectronics. Though, a number of organic molecules have drawn immense attention due to their prime applications in the fields like NLO, OLED, OSCs and OFETs, in particular, ample interest has been developed towards OLEDs owing to their advantages such as light weight, low cost, thinness, flexibility, high brightness, wide viewing angles and in addition, they are also considered as one of the most anticipated device architectures for solid state lighting sources as well as a key technology for flat-panel displays (Baldo et al. 1999; Ding et al. 2010; Tang and VanSlyke 1987; White et al. 2009). Although it is difficult to develop high color purity emitters and achieve excellent devices, from the point of chemical approach, one way of improving the major factors such as low thermal stability, chemical purity and poor efficiency that restrict the device performance is designing of rigid either star/butterfly shaped or dendrite shaped molecules (Jiang et al. 2010; Ren et al. 2010; Thelakkat 2002). Moreover, due to the advantages like good thermal stability, high purity, good thin film formation and good solution processability of star/butterfly shaped molecules over the linear molecules, they have gained enormous attention in recent past (Huang et al. 2013).

Though, there are well documented literatures on phenyl-pyridine based star/butterfly-shaped molecules, thiophene–pyridine core structured butterfly-shaped molecules remained unexplored. Given that, in the present study it is planned to explore simple thiophene–pyridine derivatives possessing D– π –A– π –D structural configuration (**VK15** and **VK16**) and D–A– π –D– π –A–D configuration (**VK17** and **VK18**) to the optoelectronic industry (OLED and NLO).

3.5.1 Structural elucidation of the intermediates and final compounds

Similar type of pattern was observed in the ^1H NMR and ^{13}C NMR spectrum of intermediate **30** as that of **29**, which confirms the structure. The reduction of intermediate **29** was confirmed by the ^1H NMR spectrum of intermediate **32**, wherein the disappearance of aldehydic proton and appearance of a singlet at δ 4.83 ppm and δ 2.50 ppm corresponding to the alcoholic proton and secondary protons of $-\text{CH}_2\text{OH}$

group, respectively, confirm the structure. The structure was further confirmed by its ^{13}C NMR spectrum. Similar type of pattern was observed in the ^1H NMR and ^{13}C NMR spectrum of **31** as that of **32**, which confirms the structure. The mass spectrum shows molecular ion (M+1) peak at m/z 504.37 and 536.44 for intermediates **30** and **32**, respectively, which corresponds to their molecular formula, confirming the structure. A doublet resonating at δ 5.94 ppm as a result of secondary protons of $-\text{CH}_2-\text{P}$ group and formation of additional aromatic protons at δ 7.87–6.88 ppm in the ^1H NMR spectrum of intermediate **34** confirms the formation of Wittig salt. Further, in the ^{13}C NMR spectrum of intermediate **34**, the peak resonating at δ 59.3 ppm corresponding to $-\text{CH}_2-\text{P}$ carbon and all the aromatic carbons resonating in the downfield region clearly confirm the structure. Similar type of pattern was observed in the ^1H NMR and ^{13}C NMR spectrum of **33** as that of **34**, which confirms the structure. The structural elucidation of one of the final compounds, **VK15** is discussed herewith. The successful formation of **VK15** is evident by the disappearance of $-\text{CH}_2-\text{P}$ protons at δ 5.94 ppm and formation of new aromatic protons at δ 7.65–7.02 ppm corresponding to triphenylamine and vinyl protons in its ^1H NMR spectrum, and also, missing of $-\text{CH}_2-\text{P}$ carbon signal at δ 59.3 ppm and additional signals of new aromatic carbons in the downfield region in its ^{13}C NMR spectrum further confirm the structure. Similar type of patterns was observed in the ^1H NMR and ^{13}C NMR spectrum of **VK16**, **VK17** and **VK18**, which confirm the structure. Also, MALDI-TOF mass spectrum shows a molecular ion peak at 1013.849, 913.652, 1243.866 and 1193.815 corresponding to (M+1) peak of **VK15**, **VK16**, **VK17** and **VK18**, respectively, which further validates the structure. In addition to the spectral characterizations, the elemental analysis further evidences the structures of all the intermediates and final compounds. The ^1H NMR, ^{13}C NMR and mass spectra of the intermediates and final compounds **VK15–VK18** are presented in **Figure 3.114–3.129**.

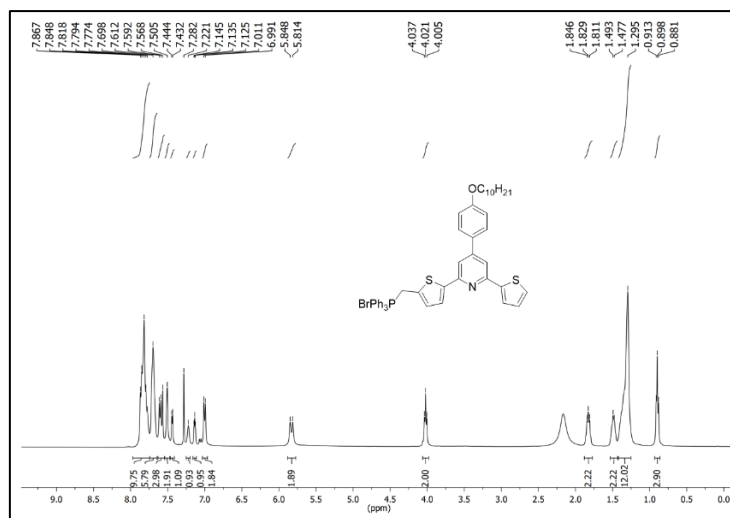


Figure 3.114 ¹H NMR spectrum of 33

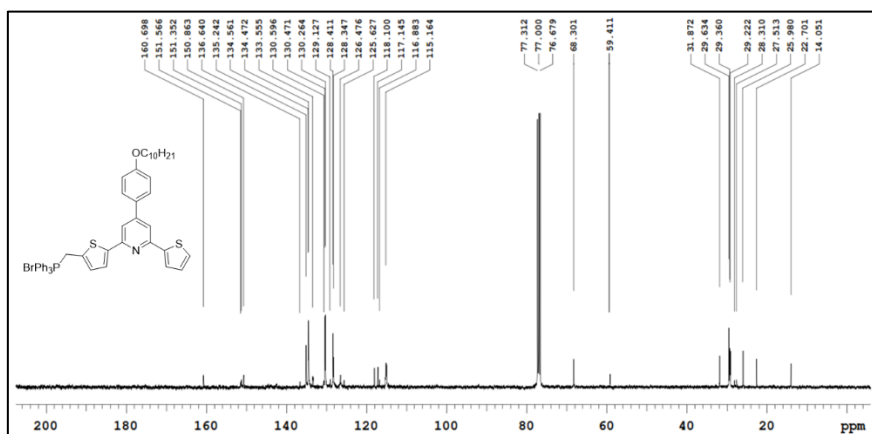


Figure 3.115 ¹³C NMR spectrum of 33

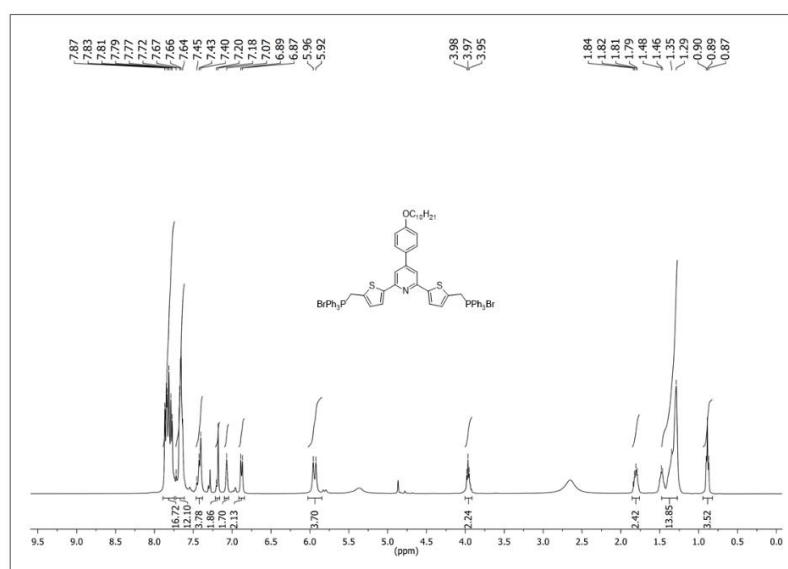


Figure 3.116 ¹H NMR spectrum of 34

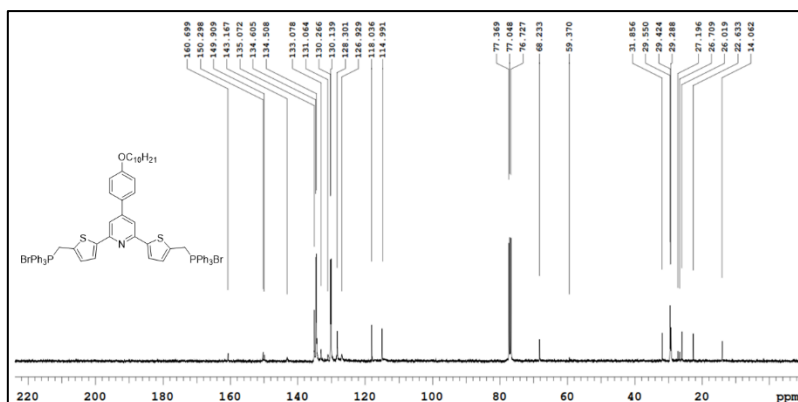


Figure 3.117 ¹³C NMR spectrum of 34

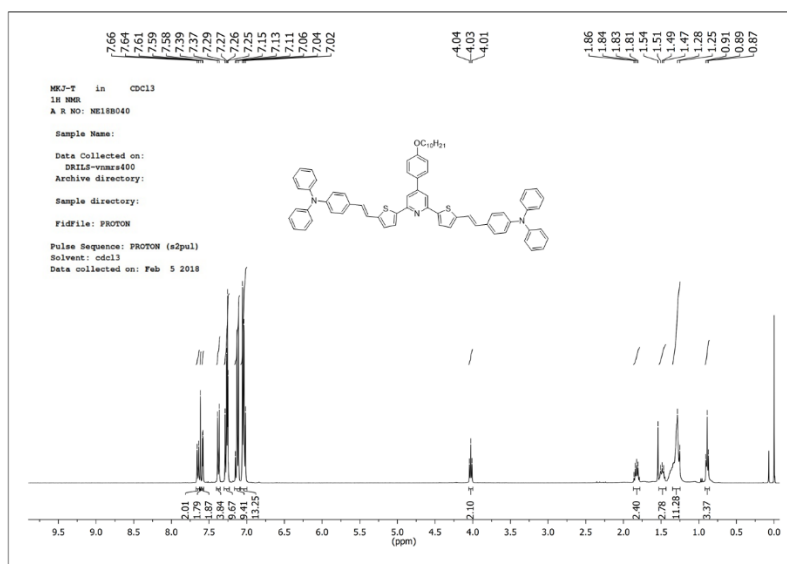


Figure 3.118 ¹H NMR spectrum of VK15

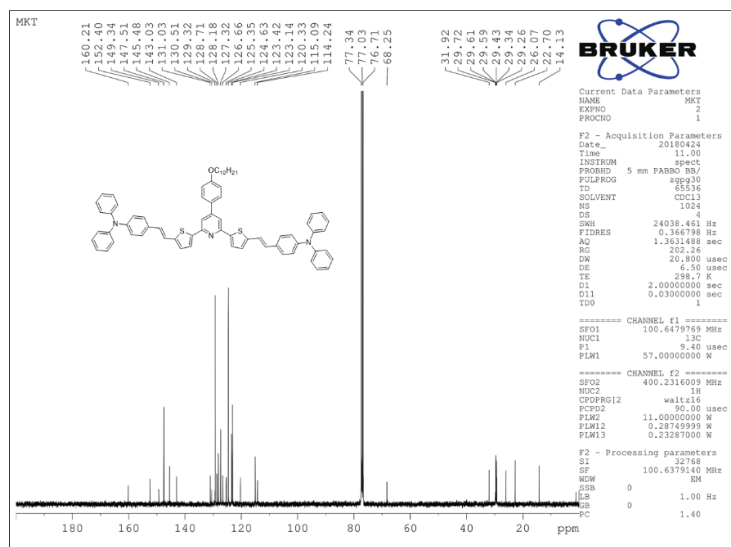


Figure 3.119 ¹³C NMR spectrum of VK15

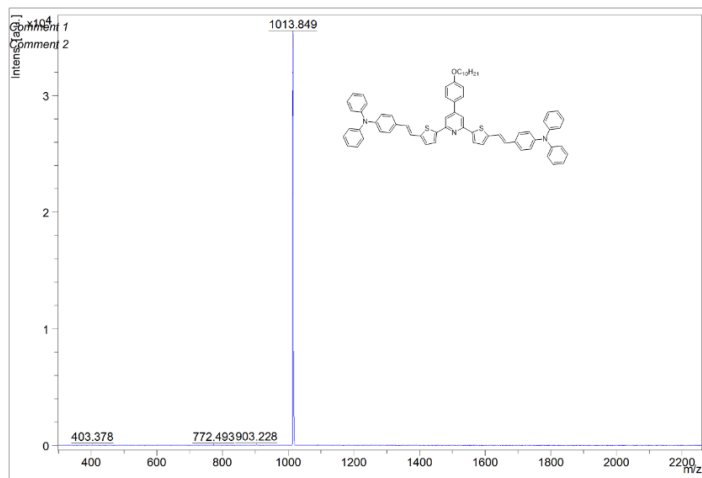


Figure 3.120 MALDI-TOF Mass spectrum of VK15

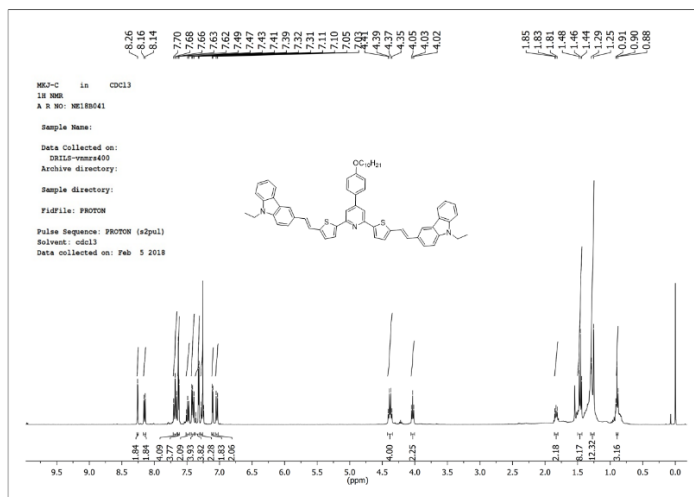


Figure 3.121 ¹H NMR spectrum of VK16

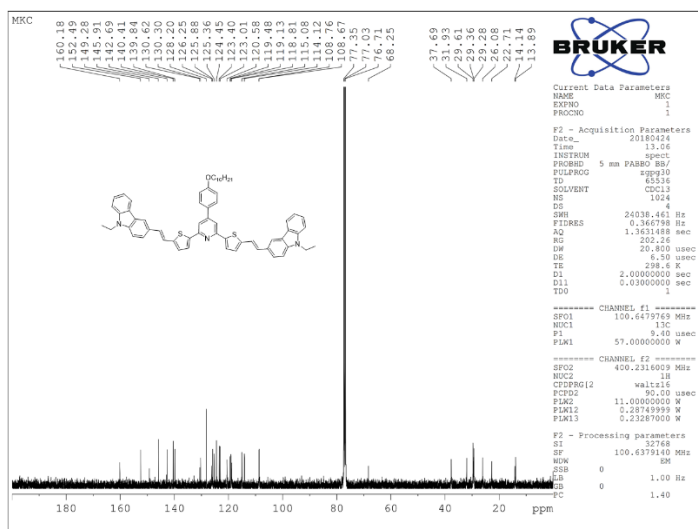


Figure 3.122 ¹³C NMR spectrum of VK16

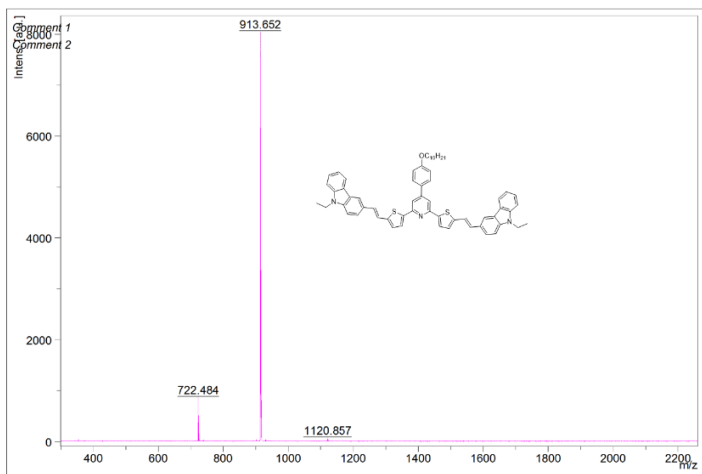


Figure 3.123 MALDI-TOF Mass spectrum of VK16

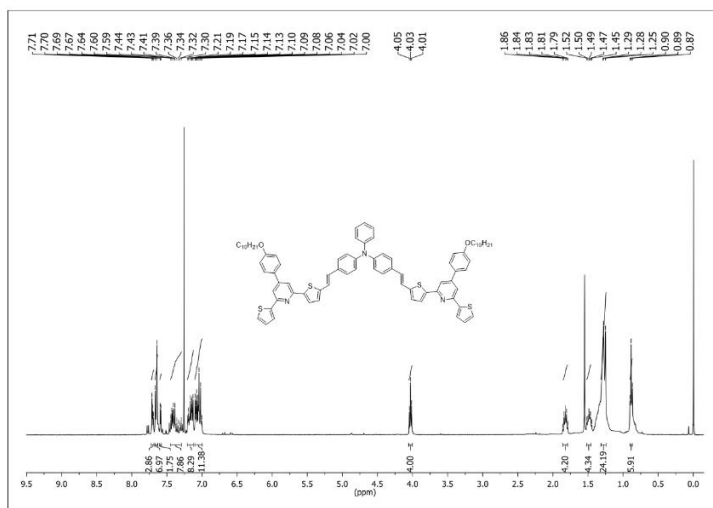


Figure 3.124 ¹H NMR spectrum of VK17

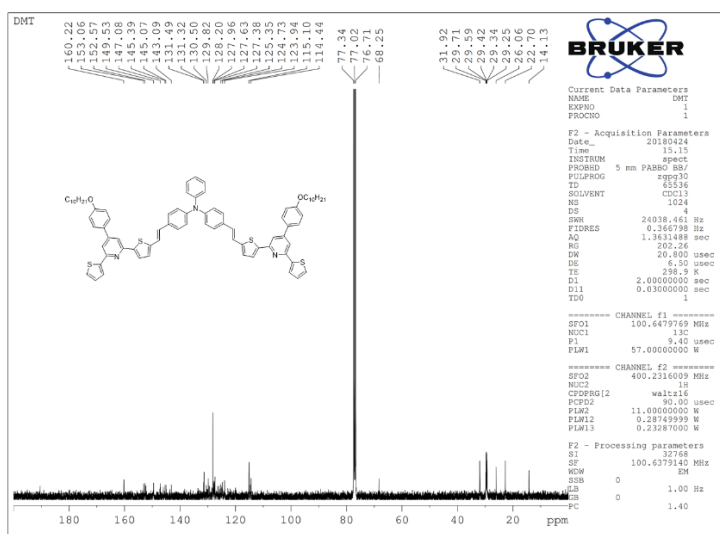


Figure 3.125 ¹³C NMR spectrum of VK17

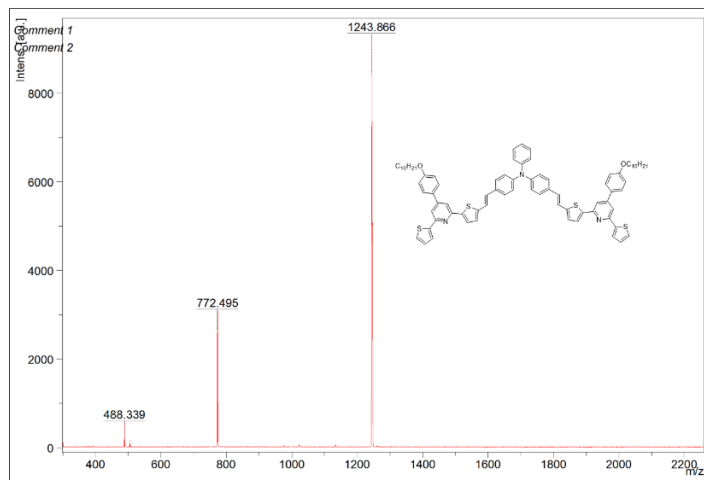


Figure 3.126 MALDI-TOF Mass spectrum of VK17

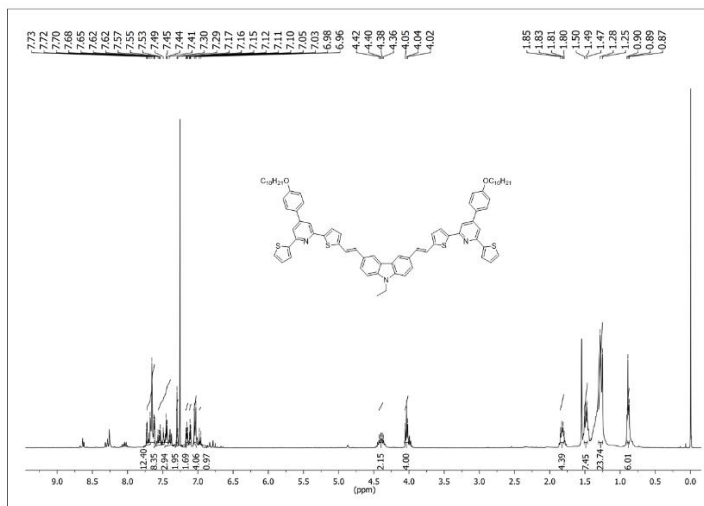


Figure 3.127 ¹H NMR spectrum of VK18

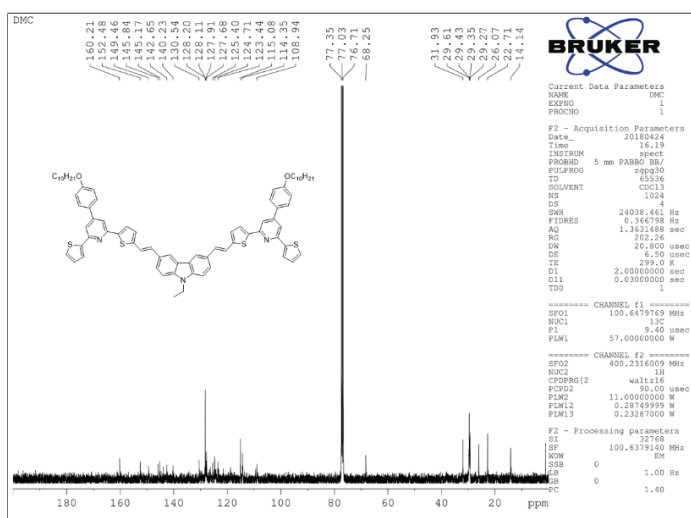


Figure 3.128 ¹³C NMR spectrum of VK18

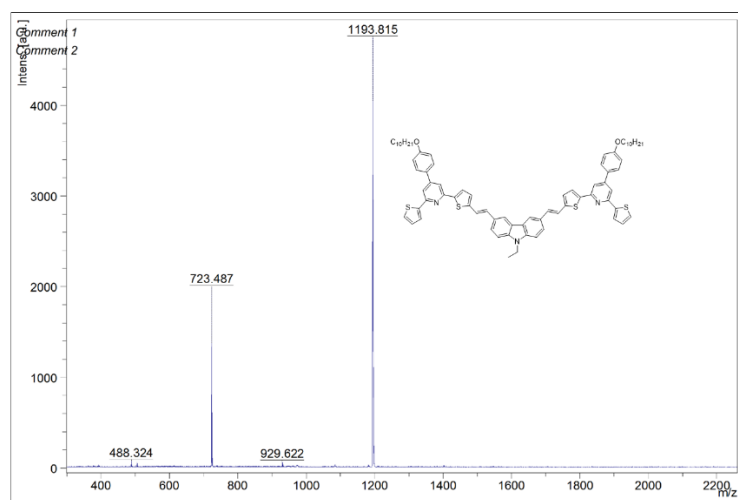


Figure 3.129 MALDI-TOF Mass spectrum of **VK18**

3.5.2 Photophysical studies

The UV–vis absorption spectra of **VK15**, **VK16**, **VK17** and **VK18** exhibit two absorption bands (**Figure 3.130a–d**). One absorption band is located at higher energy UV region (280–330 nm) and the other is located at lower energy visible region (350–460 nm). The band at higher energy region is attributed to π - π^* transition and that at lower energy region ascribes to ICT transition from the electron donating triphenylamine/carbazole moiety to the electron accepting pyridine group. The absorption maxima (λ_{max}) of **VK15**, **VK16**, **VK17** and **VK18** are observed at 409, 394, 419 and 404 nm, respectively. The absorption spectra clearly display the effect of variation of peripheral groups on the conjugation and hence, the absorption of the molecules. As it is seen in **Figure 3.130a–d**, there is a considerable red shift in the absorption of **VK15** and **VK17** compared to that of **VK16** and **VK18**. This bathochromic shift is attributed to the higher electron donating ability of triphenylamine group in **VK15** and **VK17** compared to that of carbazole in **VK16** and **VK18**. Moreover, the higher λ_{max} of **VK17** is resulted from the higher degree of conjugation in **VK17** compared to that of **VK15**, **VK16** and **VK18**. The optical band gap (E_g) determined from the point of intersection of absorption and emission spectra is 2.64, 2.71, 2.62 and 2.76 eV for **VK15**, **VK16**, **VK17** and **VK18**, respectively.

The fluorescence spectra at RT show an emission peak at 503, 450, 488 and 461 nm for **VK15**, **VK16**, **VK17** and **VK18**, respectively (**Figure 3.130a–d**), by exciting at their corresponding λ_{max} . In addition, there is a considerable red shift in the absorption

(**Figure 3.130e**) and emission spectra (**Figure 3.130f**) of all the four molecules in the solid state compared to that of solution state. This is due to the increased intermolecular interactions in the solid state. For an ideal fluorophore, fluorescence quantum yield (Φ_F) is one of the deciding factors. In view of this, their absolute solid-state fluorescence quantum yields were obtained, and they are 0.153, 0.021, 0.041 and 0.038 for **VK15**, **VK16**, **VK17** and **VK18**, respectively. The emission profiles of the four molecules were also measured at 77 K in degassed toluene to ensure the emission from the triplet state. It is observed that the low temperature emission profiles are overlapping with the RT emission profiles (**Figure 3.130a–d**), which suggests the nonexistence of phosphorescence and validates the pure fluorescence emission (with the enhanced vibronic bands). Further, the time-resolved photoluminescence decay dynamics were studied at RT to measure the lifetime of the molecules. The time-resolved photoluminescence decay profiles for the molecules in the degassed toluene are given in **Figure 3.131a–d**. The molecules **VK15**, **VK16**, **VK17** and **VK18** possess a short lifetime (τ_F) of 2.93, 2.42, 1.17 and 1.18 ns, respectively, which is attributing to the relaxation from S_1 to S_0 . And there is no any delayed component observed, indicating the pure fluorescence emission. The data of absorption and emission studies are summarized in **Table 3.10**.

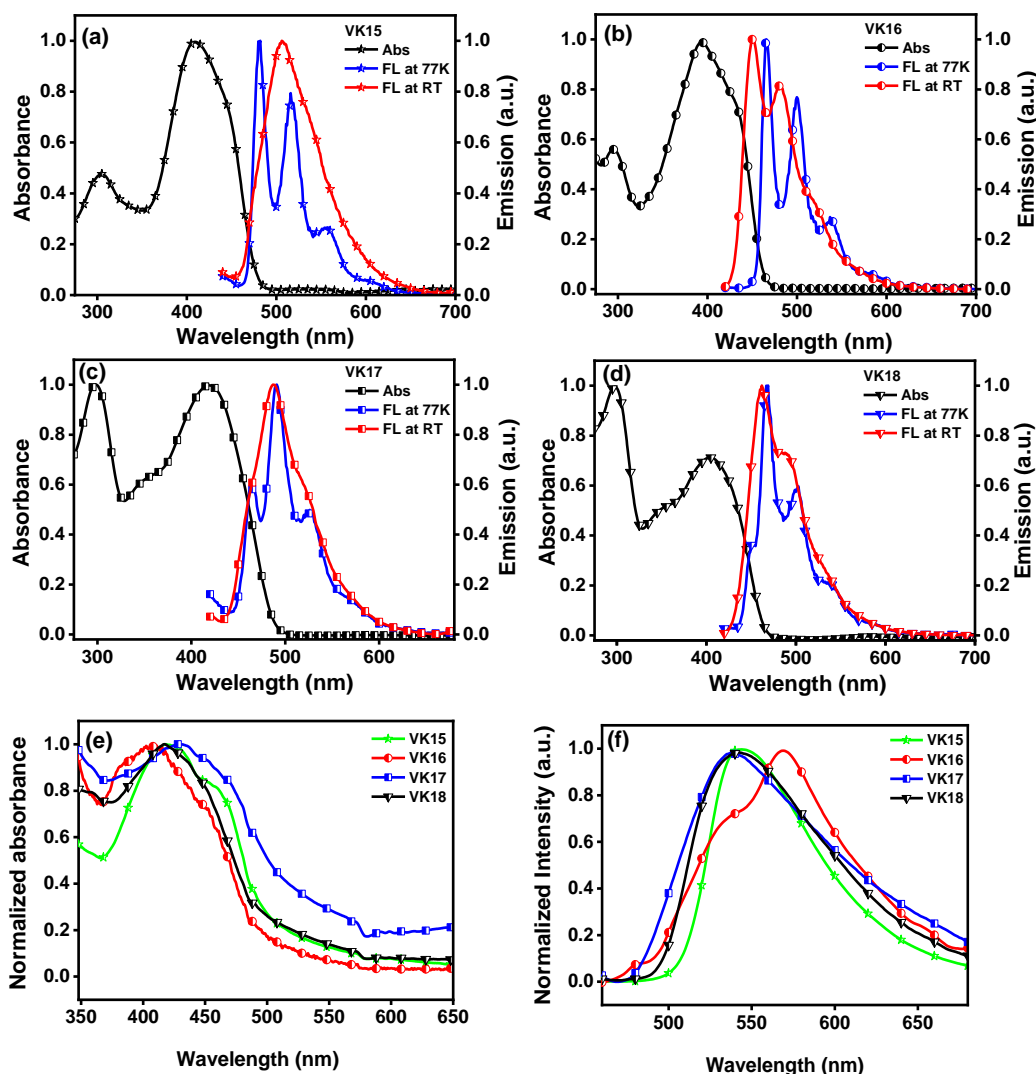
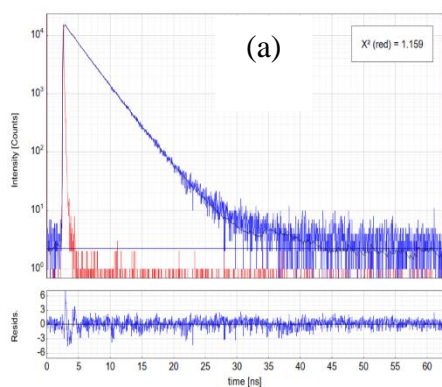


Figure 3.130 UV-Vis absorption spectra at RT (measured in CHCl_3 , 10^{-5} M) and fluorescence emission spectra at RT and 77K (measured in toluene, 10^{-5} M) of (a) **VK15**, (b) **VK16**, (c) **VK17** (d) **VK18**, (e) absorption in thin film and (f) emission profiles in the solid state of **VK15–VK18**.

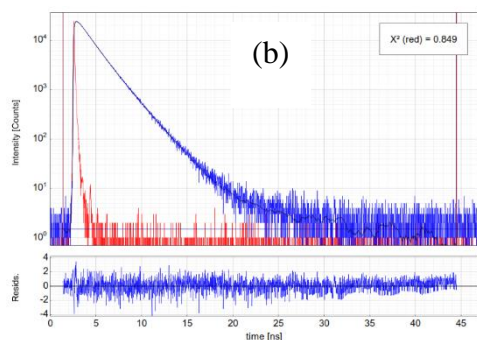


Parameter	Value	Conf. Lower	Conf. Upper	Conf. Estimation
A_1 [Cnts]	4866	-132	+132	Fitting
τ_1 [ns]	2.1848	-0.0528	+0.0528	Fitting
A_2 [Cnts]	11881.2	-92.3	+92.3	Fitting
τ_2 [ns]	3.2344	-0.0169	+0.0169	Fitting
Bkgr. Dec [Cnts]	2.252	-0.433	+0.433	Fitting
Bkgr. IRF [Cnts]	0.1022	-0.0223	+0.0223	Fitting
Shift IRF [ns]	0.56400	-0.00245	+0.00245	Fitting
A_{Scat} [Cnts]	6650	-1810	+1810	Fitting

Average Lifetime:

$$\tau_{\text{Av},1} = 3.0070 \text{ ns (intensity weighted)}$$

$$\tau_{\text{Av},2} = 2.9294 \text{ ns (amplitude weighted)}$$

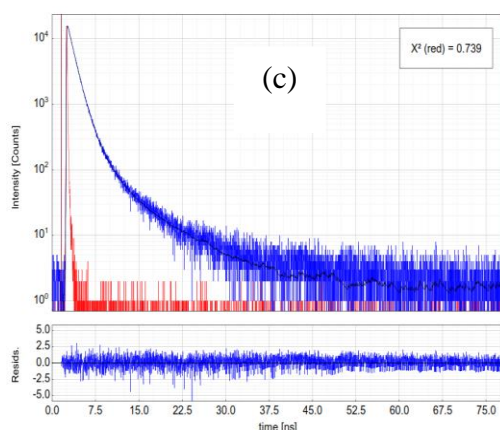


Parameter	Value	Conf. Lower	Conf. Upper	Conf. Estimation
A ₁ [Cnts]	14503	-103	+103	Fitting
τ ₁ [ns]	2.13833	-0.00951	+0.00951	Fitting
A ₂ [Cnts]	-11594	-429	+429	Fitting
τ ₂ [ns]	0.2507	-0.0128	+0.0128	Fitting
A ₃ [Cnts]	19444	-159	+159	Fitting
τ ₃ [ns]	1.33644	-0.00991	+0.00991	Fitting
Bkgr. Dec [Cnts]	1.483	-0.335	+0.335	Fitting
Bkgr. IRF [Cnts]	0.2500	-0.0229	+0.0229	Fitting
Shift IRF [ns]	0.02858	-0.00143	+0.00143	Fitting
A Scat [Cnts]	-16100	-2190	+2190	Fitting

Average Lifetime:

$$\tau_{Av,1} = 1.85452 \text{ ns (intensity weighted)}$$

$$\tau_{Av,2} = 2.41988 \text{ ns (amplitude weighted)}$$

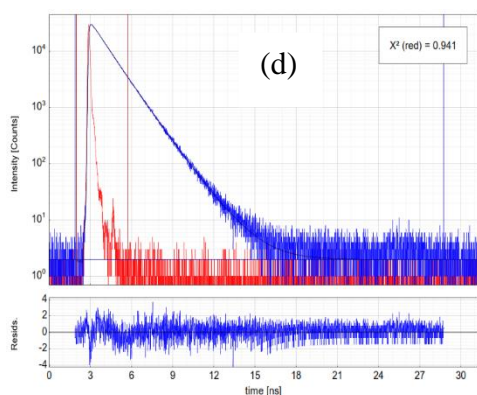


Parameter	Value	Conf. Lower	Conf. Upper	Conf. Estimation
A ₁ [Cnts]	1705.2	-69.4	+69.4	Fitting
τ ₁ [ns]	2.2314	-0.0507	+0.0507	Fitting
A ₂ [Cnts]	17218	-171	+171	Fitting
τ ₂ [ns]	1.02193	-0.00832	+0.00832	Fitting
A ₃ [Cnts]	139.33	-9.96	+9.96	Fitting
τ ₃ [ns]	7.202	-0.277	+0.277	Fitting
Bkgr. Dec [Cnts]	0.635	-0.301	+0.301	Fitting
Bkgr. IRF [Cnts]	-0.0341	-0.0314	+0.0314	Fitting
Shift IRF [ns]	0.26804	-0.00197	+0.00197	Fitting
A Scat [Cnts]	11160	-2990	+2990	Fitting

Average Lifetime:

$$\tau_{Av,1} = 1.5041 \text{ ns (intensity weighted)}$$

$$\tau_{Av,2} = 1.1753 \text{ ns (amplitude weighted)}$$



Parameter	Value	Conf. Lower	Conf. Upper	Conf. Estimation
A ₁ [Cnts]	4417.4	-98.2	+98.2	Fitting
τ ₁ [ns]	1.6236	-0.0194	+0.0194	Fitting
A ₂ [Cnts]	33002	-148	+148	Fitting
τ ₂ [ns]	1.12974	-0.00384	+0.00384	Fitting
Bkgr. Dec [Cnts]	1.974	-0.383	+0.383	Fitting
Bkgr. IRF [Cnts]	0.441	-0.779	+0.779	Fitting
Shift IRF [ns]	0.06958	-0.00104	+0.00104	Fitting
A Scat [Cnts]	-25680	-4680	+4680	Fitting

Average Lifetime:

$$\tau_{Av,1} = 1.2094 \text{ ns (intensity weighted)}$$

$$\tau_{Av,2} = 1.1880 \text{ ns (amplitude weighted)}$$

Figure 3.131 Time-resolved photoluminescence decay of (a) **VK15**, (b) **VK16**, (c) **VK17** and (d) **VK18** in toluene at RT. Right: Fitting parameters including pre-exponential factors and confidence limits.

3.5.3 Electrochemical studies

Figure 3.132a–d depict the cyclic voltammograms of **VK15–VK18**, respectively. The observed onset oxidation peaks of first oxidation peak are 0.77, 0.80, 0.71 and 0.82 V vs SCE for **VK15**, **VK16**, **VK17** and **VK18**, respectively. As observed, the molecules undergo multistep oxidation process. The oxidation peaks other than the first oxidation peak could be due to the oxidation of different units present in the

molecule. The small oxidation peaks observed at ~ 1.67 – 1.7 V in all the four molecules could be associated with vinylene bond oxidation. The oxidation peak observed at ~ 1.2 V may be due to the oxidation of N-substituted carbazole in **VK16** and **VK18** whereas, the potential range between 0.8 – 1.5 V in **VK15** and **VK17** could be related to the oxidation of triphenylamine unit which depends on the substituents attached to the phenyl ring of triphenylamine unit. The energy of HOMO calculated from **Equation 2.1** is -5.31 , -5.34 , -5.25 and -5.36 eV for **VK15**, **VK16**, **VK17** and **VK18**, respectively. Similarly, the energy of LUMO determined from the **Equation 2.2** is -2.67 , -2.63 , -2.63 and -2.60 eV for **VK15**, **VK16**, **VK17** and **VK18**, respectively.

As a consequence of the presence of stronger electron donating triphenylamine group, **VK15** and **VK17** possess a lower oxidation potential compared to carbazole containing **VK16** and **VK18**. As the electron donating groups increase the HOMO level, **VK15** and **VK17** possess higher HOMO energy level compared to that of **VK16** and **VK18**. The electrochemical data are listed in **Table 3.10**.

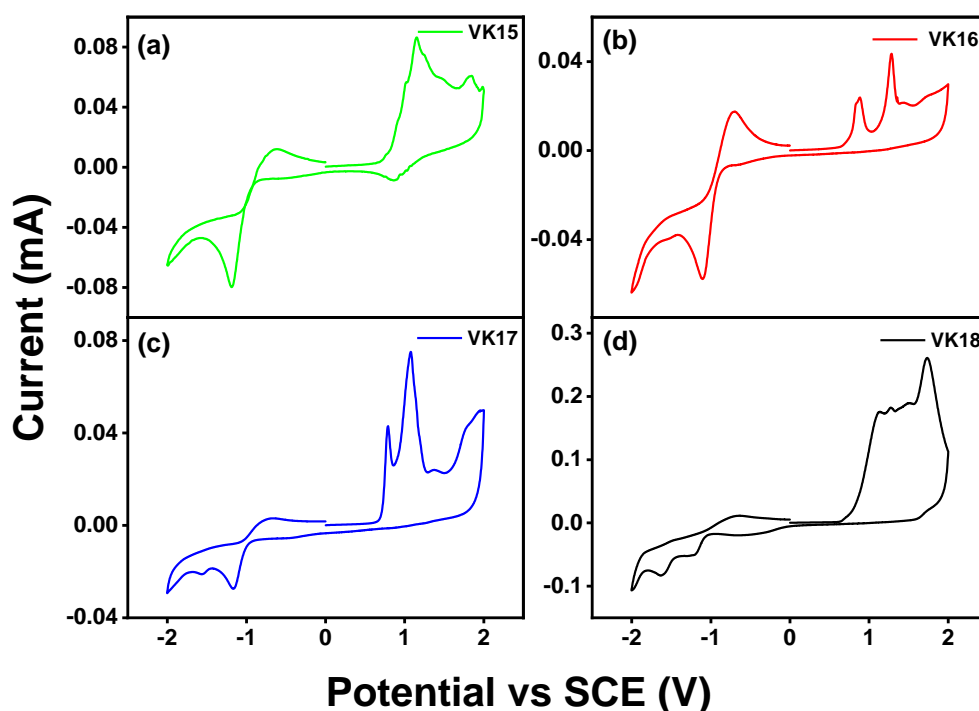


Figure 3.132 Cyclic voltammograms of (a) **VK15**, (b) **VK16**, (c) **VK17** and (d) **VK18**.

Table 3.10 Summary of optical, electrochemical and theoretical data of **VK15–VK18**.

Molecules	$\lambda_{\max}^{\text{abs}}$ (nm)	$\lambda_{\max}^{\text{pl}}$ (nm)	$E_{\text{g}}^{\text{opt}}$ (eV)	Φ_{F} (± 0.02)	τ_{F} (ns)	$E^{\text{ox}}_{\text{onset}}$ (V vs SCE)	HOMO (eV)	LUMO (eV)
VK15	409 ^a	503 ^a	2.64	0.153	2.93	0.77	-5.31 ^c	-2.67 ^d
	420 ^b	543 ^b			± 0.03		-4.73 ^e	-1.68 ^e
VK16	394 ^a	493 ^a	2.71	0.021	2.42	0.80	-5.34 ^c	-2.63 ^d
	408 ^b	569 ^b			± 0.01		-4.76 ^e	-1.50 ^e
VK17	419 ^a	498 ^a	2.62	0.041	1.17	0.71	-5.25 ^c	-2.63 ^d
	430 ^b	538 ^b			$\pm 0.05^{[*]}$		-4.70 ^e	-1.72 ^e
VK18	404 ^a	474 ^a	2.76	0.038	1.19	0.82	-5.36 ^c	-2.60 ^d
	417 ^b	542 ^b			± 0.005		-4.77 ^e	-1.58 ^e

$E_{\text{g}}^{\text{opt}}$ Optical band gap calculated from the intersection of normalized absorption and emission spectra.

Φ_{F} Absolute quantum yield determined using an integrated sphere.

^a Determined in CHCl_3 (10^{-5} M).

^b Determined in solid state.

$E^{\text{ox}}_{\text{onset}}$ Experimental onset oxidation potential vs SCE.

^c Experimental values from CV using Equation 2.1 with Fc/Fc^+ as internal standard.

^d Experimental values using Equation 2.2.

^e Theoretical results.

τ_{F} Amplitude weighted average lifetime, biexponential, [*] triexponential.

3.5.4 Theoretical studies

Figure 3.133 represents the ground state optimized geometry and the HOMO/LUMO distribution of **VK15–VK18**. The long decyloxy chain was replaced by methoxy group to reduce the calculation time. As seen in **Figure 3.133**, in the case of **VK15** and **VK16**, except the decyloxy substituted phenyl group which is twisted by an angle of $\sim 41^\circ$ from the thiophene-pyridine plane, the HOMO is distributed majorly on spacer thiophene and vinylic linkage. The HOMO distribution is also extended on nitrogen atom and one of the phenyl group (which is attached to the vinylic bond) of peripheral triphenylamine in **VK15** and ethyl carbazole in **VK16**. Further, a partial distribution of HOMO over central pyridine is also seen. Since the free phenyl groups in the terminal triphenylamine unit are twisted by an angle of $\sim 42^\circ$ from the thiophene-

pyridine plane, HOMO is distributed to a less extent on triphenylamine group in **VK15**. Similarly, due to the small twisting from its co-planarity of unsubstituted phenyl group of terminal ethyl carbazole, HOMO is spread to a less extent on ethyl carbazole in **VK16**. On the other hand, the LUMO is mainly localized on central pyridine and spacer thiophene units; and partially distributed over vinylic linkage in **VK15** and **VK16**. In addition, there is a minor distribution of LUMO on substituted phenyl group of triphenylamine and ethyl carbazole in **VK15** and **VK16**, respectively. Correspondingly, in the case of **VK17** and **VK18**, the HOMO is majorly localized on spacer thiophene, vinylic linkage, central triphenylamine in **VK17** and on central carbazole in **VK18**, while the LUMO is localized primarily on electron acceptor pyridine ring, spacer thiophene and vinylic linkage. Also, there is a partial distribution of LUMO over substituted phenyl rings of triphenylamine and carbazole unit in **VK17** and **VK18**, respectively. It is observed that, the HOMO of all the four molecules is mainly situated on electron donors while LUMO is mainly localized on electron withdrawing pyridine unit, which indicates D-A type charge transfer character of the molecules. And, a significant overlap of orbitals is observed from the electron density distribution of HOMO and LUMO levels, suggesting the ambipolar property, which may support for the proper transport of holes/electrons and to maintain the active electronic communication between the acceptor and the donor (Li et al. 2018; Liu et al. 2018).

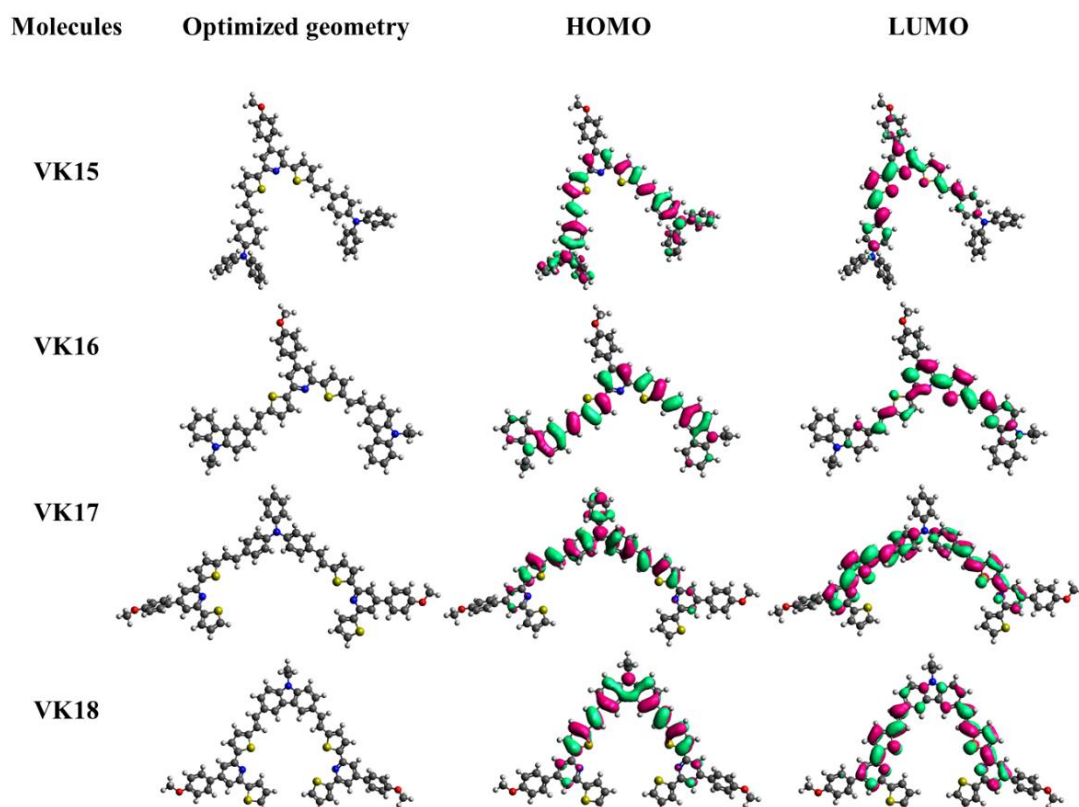


Figure 3.133 The optimized molecular structures and HOMO/LUMO distributions of **VK15–VK18**.

In order to examine the excited state transition, TD-DFT calculations were performed. **Figure 3.134** shows the simulated spectra of **VK15–VK18**. The appearance of distinct bands at lower and higher energy region indicates the existence of charge-transfer transition and π - π^* transition, respectively, within the molecules. The theoretical HOMO/LUMO values are summarized in **Table 3.10**. Overall, the theoretical estimation follows similar trend and are in support with the experimental results, however, the tiny discrepancy is due to the theoretical overestimation.

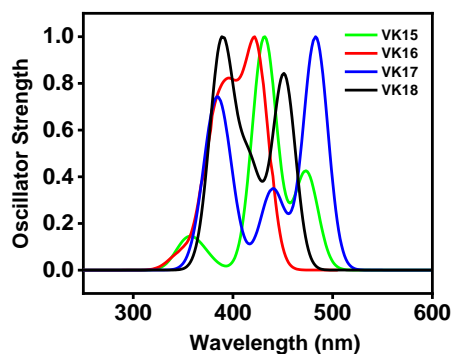


Figure 3.134 Simulated absorption spectra of **VK15–VK18**.

3.5.5 Thermal properties

Thermal properties of the molecules were analysed by differential scanning calorimetry (DSC) and TGA. The DSC and the TGA plots of **VK15–VK18** are depicted in **Figure 3.135** and **Figure 3.136**, respectively. The DSC analysis shows that the molecules are amorphous in nature, as there are no exothermic melting peaks observed during two heating cycles (**Figure 3.135**). And, all the four molecules exhibit a clear glass transition temperature (T_g) during the second heating cycle. In fact, molecules **VK17** and **VK18** show T_g of 27.63 and 36.33°C, respectively, whereas, molecules **VK15** and **VK16** exhibit comparatively better T_g of 72.32 and 66.12°C, respectively. The higher T_g of **VK15** and **VK16** compared to that of **VK17** and **VK18** is attributed to the presence of bulky side groups in **VK15** and **VK16**, which hinders the rotational flexibility, thereby increases the T_g (Yu et al. 2018).

The TGA results reveal that the molecules possess extremely good thermal stabilities with the high degradation temperatures. The T_d of **VK15** and **VK16** (corresponding to 5% weight loss) is observed at 426 and 432°C, respectively, whereas, the T_d of **VK17** and **VK18** is observed at 417 (corresponding to 20% weight loss) and 428°C (corresponding to 10% weight loss), respectively. In addition, a slight degradation is observed at 218 and 240°C (corresponding to 2% weight loss), in **VK17** and **VK18**, respectively, which is due to the decomposition of the peripheral, low molecular weight component (4-(4-(decyloxy)phenyl)-2,6-di(thiophen-2-yl)pyridine), present in them. The relatively higher T_d of **VK16** and **VK18** compared to that of triphenylamine containing **VK15** and **VK17** is due to the presence of carbazole (structurally more rigid compared to triphenylamine) unit in them, which improved the structural rigidity of **VK16** and **VK18**. Apparently, the excellent thermal stability with high T_d of all the four molecules is attributed to the bulky D- π -A- π -D/ D-A- π -D- π -A-D structural arrangement (Wang et al. 2019) with relatively large molecular weights, which can lead to a homogeneous and amorphous film and thus, improve the quality of the film at high temperatures, which is a criterion for their practical use in OLEDs.

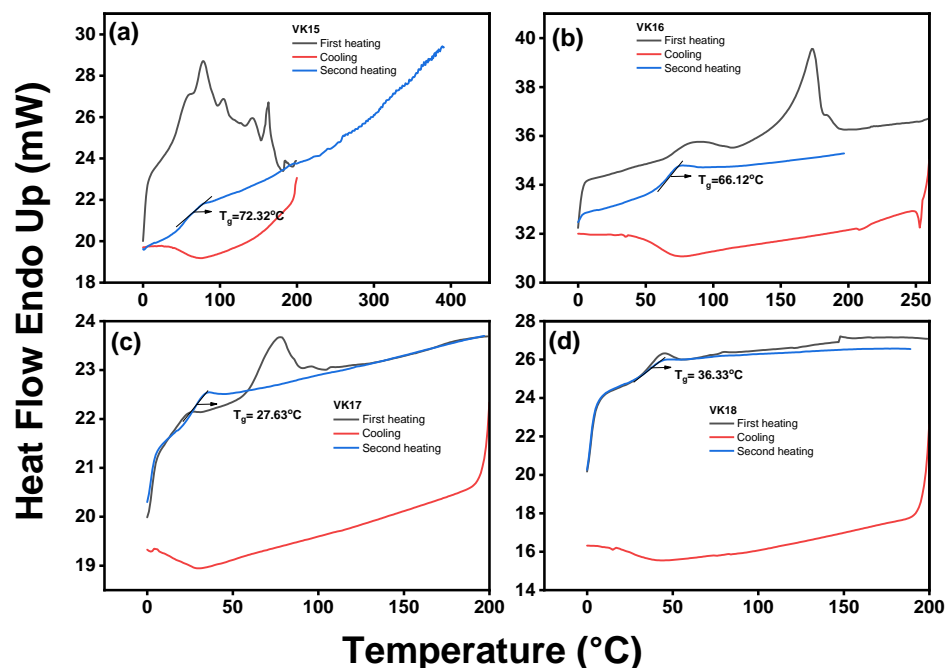


Figure 3.135 DSC plots of (a) VK15, (b) VK16, (c) VK17 and (d) VK18.

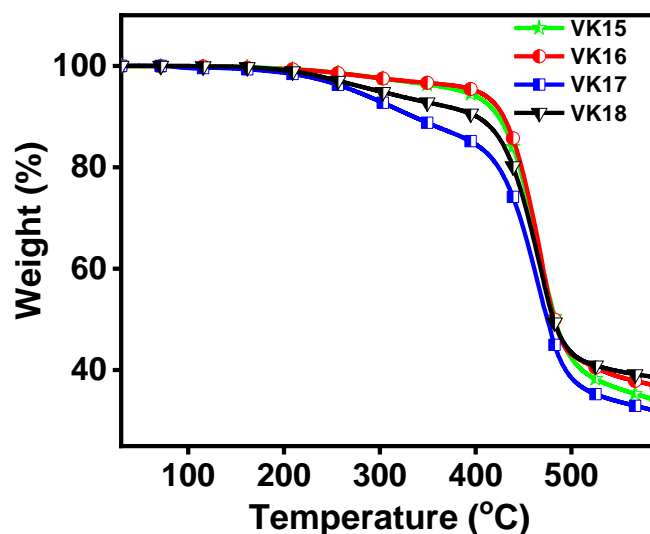


Figure 3.136 TGA plots of VK15–VK18.

3.5.6 Third-order NLO properties

3.5.6.1 Nonlinear absorption studies

Under ultra-short 50 μJ laser excitation (532 nm, 7 ns pulse width), corresponding to on-axis intensity of 1.386 GW cm^{-2} , OA Z-scan analysis was carried out, wherein the transmitted beam was measured without the aperture in front of the detector, to determine the NLA of the molecules. The linear transmittance was maintained at 70–72%. **Figure 3.137a–d** show the OA Z-scan signatures of **VK15–**

VK18 in CHCl_3 solution, respectively. The interaction of laser beam with the molecules produces a valley pattern i.e., the transmittance of the molecules decreases gradually towards the focal point and reaches a minimum with the deep transmittance trough at the focus where the curves are symmetric at $z=0$, which signifies the RSA behavior of the molecules with the positive NLA of the incident light. On the nanosecond time scale the RSA is combined with TPA and ESA, which are collectively called as “the effective TPA” process (Poornesh et al. 2009; Vishnumurthy et al. 2011). The experimental data are matching well with the theoretical model for ESA assisted TPA process in all the four molecules.

Following the intensity dependent absorption coefficient ($\alpha(I)$) for ESA assisted TPA (associated with SA), OA Z-scan recordings were theoretically fitted using **Equation 2.3–2.5** to determine β_{eff} . The $\chi^{(3)}$ was calculated by fitting to **Equation 2.6**. Using the **Equations 2.3** and **2.5**, the experimental data were fitted to the theoretical model to obtain NLA parameters (**Table 3.11**). The numerically fitted OA Z-scan results disclose enhanced NLO responses of the synthesized molecules. The β_{eff} values of **VK15**, **VK16**, **VK17** and **VK18** are 4.45, 3.65, 3.91 and $2.58 \times 10^{-10} \text{ m W}^{-1}$, respectively. The obtained β_{eff} values in the present study are very much closer and predominantly better than those reported in the literature (**Table 3.11**).

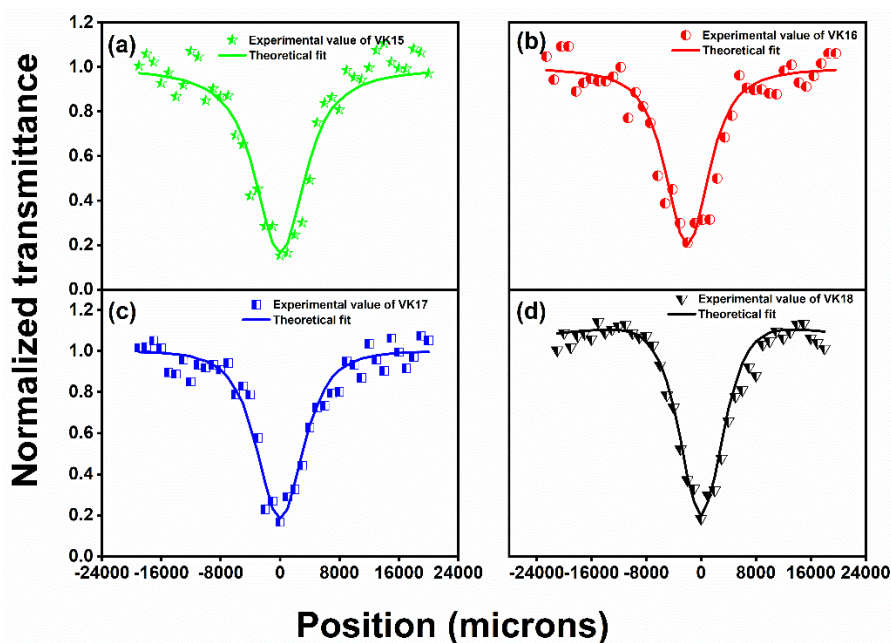


Figure 3.137 Z-scan curves of (a) **VK15**, (b) **VK16**, (c) **VK17** and (d) **VK18** under OA configuration.

3.5.6.2 Optical limiting studies

The OL data of **VK15–VK18** were extracted from the graphs of normalized transmittance obtained from OA Z-scan analysis against input fluence (**Figure 3.138 a–d**). From the graph, the onsets of limiting action are 0.18, 0.49, 0.38 and 0.65 J cm⁻² and the LT values are 1.73, 2.72, 2.68 and 4.68 J cm⁻² for **VK15**, **VK16**, **VK17** and **VK18**, respectively. From the results it is evidenced that the molecules in the present study exhibit exceptional OL action with very low onset and LT values. These significantly reduced values are analogous and better than those of many reported values. For an instance, under similar conditions, Praseetha *et al.* (Praseetha et al. 2019) observed the enhancement in the NLO property of 7CB nematic liquid crystal upon doping with CdSe QD in different concentrations. The pure 7CB nematic liquid crystal showed β_{eff} of 2.0×10^{-10} m W⁻¹ while after doping with 0.75 and 1% CdSe QD, the β_{eff} raised to 5.5×10^{-10} m W⁻¹ with the LT of 3.02 J cm⁻² and 7.8×10^{-10} m W⁻¹ with the LT of 2.1 J cm⁻², respectively. Shiju *et al.* (Shiju et al. 2019) investigated the NLO response of phenothiazine (PTZ)–silver (Ag) organometallic hybrid system, which showed β_{eff} of 3.60×10^{-10} m W⁻¹ and LT of 3.43 J cm⁻², which was two orders of magnitude higher than that of pristine PTZ. Zhang *et al.* (Zhang et al. 2011) studied the NLO and optical limiting properties of graphene oxide–Fe₃O₄ hybrid material, which showed an enhanced β_{eff} of 2.6×10^{-10} m W⁻¹ with the LT of 2.82 J cm⁻², whereas new quinoxaline based push–pull molecule with 1,3 indandione as acceptor was synthesized by Gopi *et al.* (Gopi et al. 2020) and its third-order NLO properties were studied, which showed an effective TPA with very high β_{eff} of 2.0×10^{-10} m W⁻¹ and low LT of 1.15 J cm⁻². Further, Mi *et al.* (Mi et al. 2016) synthesized Zn-complexed D– π –A type porphyrin derivative, Por–Zn–N, through [2+2] click reactions and studied the NLO response of the material, which showed RSA with β_{eff} of 4.8×10^{-10} m W⁻¹. Specifically, **VK15** and **VK16** of the present series having similar structural arrangement as that of molecules of series–4, wherein, the same core structure (i.e., thiophene-pyridine) was connected to small end groups such as thiophene/phenyl acrylonitriles, show enhanced NLO properties compared to the previous molecules. This is mainly attributed to the improved ICT, increased polarity and extended conjugation existed due to the presence of bulkier end groups (triphenylamine/carbazole) in the present molecules compared to thiophene/phenyl acrylonitriles. Moreover, the LT value of **VK15** (1.73 J cm⁻²) is

similar to that of polymer **VK14** (1.42 J cm^{-2}) which suggests that the proper selection of bulkier end group and structural modifications in small molecules could lead to comparable NLO properties as that of polymers and could replace the polymeric materials in optical limiting devices. From the literature reports it is noticed that the enhancement in the nonlinearity is mainly due to the doping of organic compounds with some inorganic materials with the exception of some of the pure organic materials which showed improved nonlinearity without any doping. However, the materials in the present study have shown remarkable nonlinear response with substantial increment in the β_{eff} which is of the order $10^{-10} \text{ m W}^{-1}$ and exceptionally well optical limiting behavior with very low LT in their pristine form, which is comparable and better than some of the well-known reported materials, making them capable materials for optical power limiting devices in photonics.

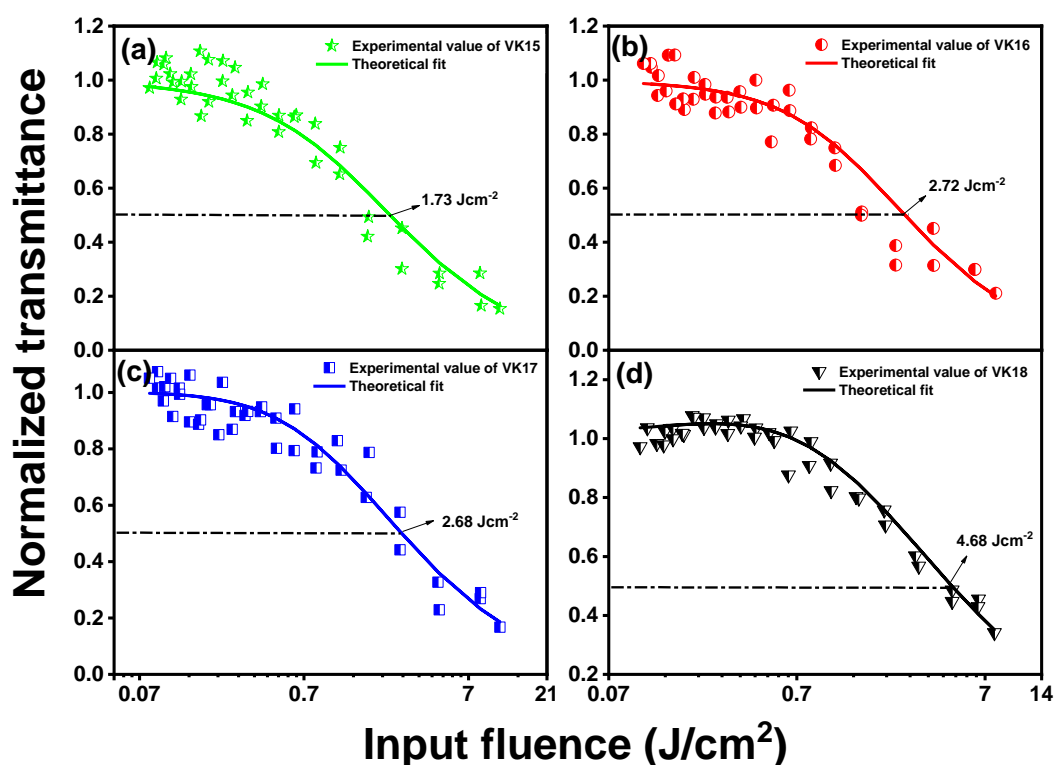


Figure 3.138 Optical limiting curves of (a) **VK15**, (b) **VK16**, (c) **VK17** and (d) **VK18** at an input intensity of 1.386 GW cm^{-2} .

3.5.6.3 Nonlinear refraction studies

The closed by open signatures of **VK15–VK18** are depicted in **Figure 3.139a–d**, respectively. As it is seen from the figure, there is a prefocal peak followed by null

and postfocal valley, which indicates the negative sign of refractive index, representing a self-defocusing nature and thus, negative nonlinearity of **VK15–VK18**. As a result, molecules act like diverging lens. By fitting experimental data to **Equation 2.7**, the normalized transmittance (T) at CA condition was determined. The η_2 and the real $\chi^{(3)}$ related to η_2 was calculated by **Equations 2.8** and **2.9**. The NLR parameters of **VK15–VK18** are listed in **Table 3.11**.

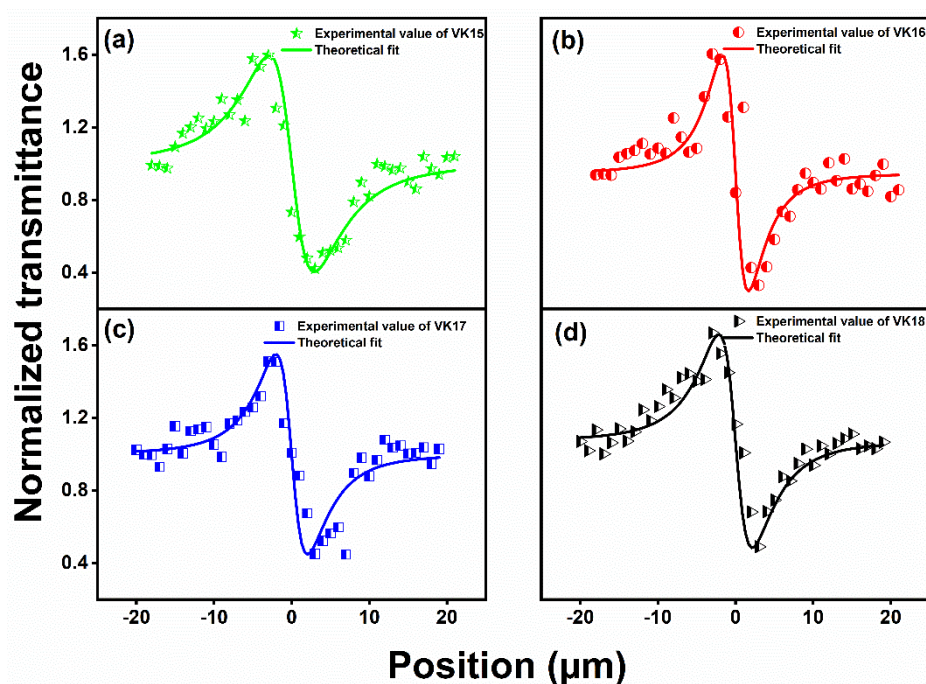
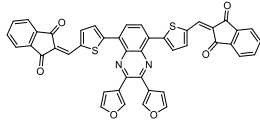


Figure 3.139 Z-scan curves of (a) **VK15**, (b) **VK16**, (c) **VK17** and (d) **VK18** under CA configuration.

The butterfly-shaped molecules in the present study possessed highly delocalized π -electronic cloud, resulting from the structural planarity, which provided a prolonged π -conjugation between the electron donor and acceptor groups via excellent ICT interactions, ultimately induced the polarization in the molecules, which led to a remarkably high β_{eff} value and extremely low LT values of pristine molecules. Further, the higher extent of electron donating ability of triphenylamine moiety than carbazole unit brought about notable increment in the β_{eff} value and exceptional reduction in the LT value in the case of **VK15** and **VK17** compared to that of **VK16** and **VK18**. Thus, it is worth to note that these materials would be efficient limiters which would provide safety for damages caused by high intensity sources.

Table 3.11. Comparison of NLA and NLR parameters of **VK15–VK18** with similar results reported.

Sample	β_{eff} ($\times 10^{-10}$ mW^{-1})	Limiting threshold (Jcm^{-2})	η^2 (esu)	$\chi^{(3)}$ (esu) (10^{-12})	References
VK15	4.45	1.73	7.06357×10^{-11}	14.0157	This work
VK16	3.65	2.72	6.21902×10^{-11}	11.5239	This work
VK17	3.91	2.68	7.63576×10^{-11}	12.3421	This work
VK18	2.58	4.68	4.78997×10^{-11}	8.1398	This work
7CB	2.0	-	-	-	(Praseetha et al. 2019)
7CB + 0.75% CdSe QD	5.5	3.02	-	-	(Praseetha et al. 2019)
7CB + 1.0% CdSe QD	7.8	2.1	-	-	(Praseetha et al. 2019)
Phenothiazine (PTZ)–silver (Ag) organometallic hybrid system	3.60	3.43	8.0	-	(Shiju et al. 2019)
Graphene oxide– Fe_3O_4	2.6	2.82	-	-	(Zhang et al. 2011)
	2.0	1.15	-	-	(Gopi et al. 2020)
Zn-complexed D– π –A type porphyrin derivative, (Por–Zn–N)	4.8	-	-	-	(Mi et al. 2016)

3.5.7 Electroluminescence properties

Out of four molecules synthesized, **VK15** exhibited comparatively higher Φ_F , better film forming property and high lying HOMO level. As a result, a multilayer non-doped OLED was fabricated employing **VK15** as the emissive material and the properties were investigated. The device configuration is as follows: ITO (150 nm)/PEDOT:PSS (30 nm)/NPB (20 nm)/VK15 (40 nm)/TPBi (35 nm)/LiF (1 nm)/Al (100 nm). In the device, patterned ITO-coated glass substrate was used as a transparent anode, PEDOT:PSS (Poly(3,4-ethylene dioxythiophene)-poly(styrenesulfonate)) as hole injecting material, NPB (N,N'-Di(1-naphthyl)-N,N'-diphenyl-(1,1'biphenyl)-4,4'-diamine) as HTL, VK15 as emissive material, TPBi (2,2',2''-(1,3,5-Benzinetriyl)-tris(1-phenyl-1-H-benzimidazole) as ETL and HBL, lithium fluoride (LiF) served as EIL and Al as cathode (**Figure 3.140a**) and their energy level diagram is given in **Figure 3.140b**. The current density-voltage-luminance (J - V - L) characteristic, current density-luminance, current density-current efficiency and electroluminescence (EL) spectra of the fabricated device are presented in **Figure 3.141a-d**, respectively. As shown in the figure, the device exhibits good diode characteristic with a turn-on voltage of 7.74 V (at 1 cd m⁻²), a maximum luminance of 207 cd m⁻², a η_{CE} of 1.51 cd A⁻¹, η_{Pmax} of 0.46 lm W⁻¹ and η_{EQE} of 0.48 % at 100 cd m⁻² (**Table 3.12**). The device emits bright green light having maximum emission (λ_{max}^{em}) at 512 nm with a narrow full width half maximum (FWHM) of 68 nm and commission internationale de leclairage (CIE) coordinates of (0.290, 0.606) at 12 V, which show the pure green emission from the device (**Figure 3.141e**). It is seen that the presence of triphenylamine unit as end groups with D- π -A- π -D configuration effectively reduced the aggregation and crystallinity, and thus, facilitated the formation of homogeneous film by solution processing. Also, there is no any change in the EL peak shape, that reveals the excellent spectral stability of the device. The fabricated device is unoptimized and there is a large scope for the optimization of various parameters which can further improve the device performance.

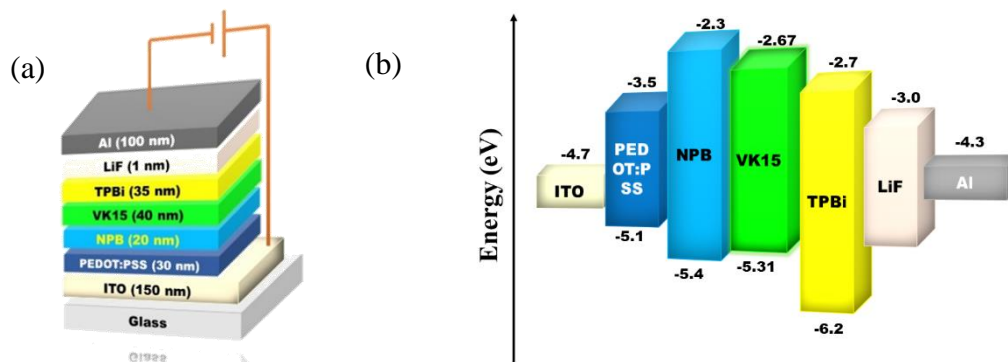


Figure 3.140 (a) Device configuration and (b) the energy level diagram showing the HOMO and LUMO energies of different component materials.

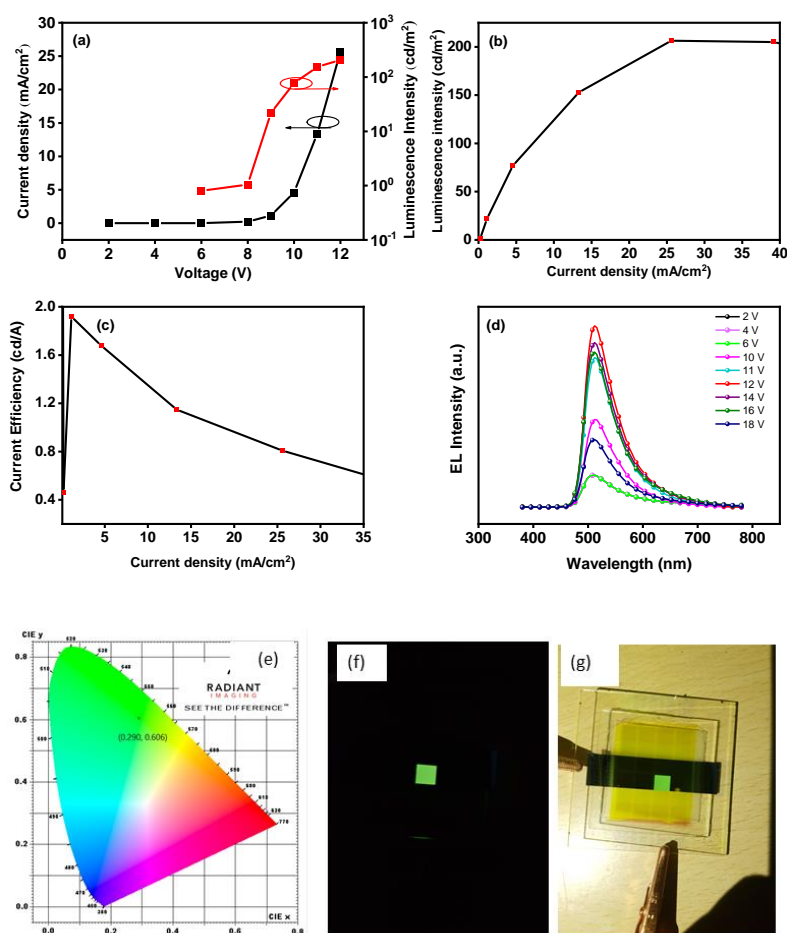


Figure 3.141 Device characteristics (a) J–V–L characteristic, (b) J–L curve, (c) J– η_{CE} curve, (d) EL spectrum of solution processed un-doped OLED fabricated using **VK15** as emissive material, (e) CIE 1931 chromaticity coordinates (x,y) of OLED based on **VK15**, (f) photograph of the device in dark and (g) photograph of the device in light.

Table 3.12 Electroluminescence data of **VK15** in OLED device.

Molecule	V_{onset} (V)	λ^{em}_{max} (nm)	L_{max} (cd m⁻²)	η_{CE} (cd A⁻¹)	η_{Pmax} (lm W⁻¹)	η_{EQE} (%)
VK15	7.74	512	207	1.51	0.46	0.48

3.5.8 The important findings from the experimental data

The triphenylamine present in **VK15** and **VK17** leads to a clear red shift in the absorption and emission maxima, and also shifts the HOMO to higher energy level. Localization of HOMO on electron donor and LUMO on acceptor renders D–A type charge transfer and the overlapping of orbitals provides ambipolar property for all the four molecules. The presence of bulky side groups increases the T_g in **VK15** and **VK16**, and the presence of carbazole in **VK16** and **VK18** imparts high thermal stability (> 420°C). The strong electron donating ability of triphenylamine and extended conjugation in **VK15** and **VK17** result in remarkably high β_{eff} of 4.45 and 3.91×10⁻¹⁰ m W⁻¹, and extremely low limiting threshold of 1.73 and 2.68 J cm⁻², respectively. The un-doped solution processed OLED using **VK15** as emitter exhibited bright green electroluminescence at 512 nm with narrow FWHM of 68 nm, a turn-on voltage of 7.74 V (at 1 cd m⁻²), a maximum luminance of 207 cd m⁻², a η_{CE} of 1.51 cd A⁻¹, η_{Pmax} of 0.46 lm W⁻¹ and η_{EQE} of 0.48 % at 100 cd m⁻². The striking results of **VK15** demonstrate its potential use as optical limiter in photonics and emissive material in OLEDs.

CHAPTER 4

SUMMARY AND CONCLUSIONS

4.1 SUMMARY

A total of five new D–A–D configured series, wherein **series–1** with three small molecules comprising of thiophene as the electron donor, ITD as the acceptor, and thiophene–2–acetonitrile (**VK1**), phenylacetonitrile (**VK2**) and rhodanine–3–acetic acid (**VK3**) as three different side groups; **series–2** with three small molecules comprising of thiophene and ITD as the invariable donor and acceptor moieties, and pyrene (**VK4**), anthracene (**VK5**) and triphenylamine (**VK6**) as three different π -conjugated systems; **series–3** with four H-shaped conjugated oligomers comprising of thiophene (**VK7**), thiophene–1,3,4–oxadiazole–thiophene (**VK8**), tztz (**VK9**) and phenyl–tztz–phenyl (**VK10**) units as central cores and the Th–ITD moiety at the periphery; **series–4** with two trigonal-shaped conjugated small molecules comprising of thiophene as the electron donor, 2,4,6-trisubstituted pyridine as the acceptor, and thiophene-2-acetonitrile (**VK11**) and phenyl acetonitrile groups (**VK12**) as side groups, and two polymers comprising of thiophene and 2,4,6-trisubstituted pyridine as the invariable donor and acceptor moieties, and thiophene (**VK13**) and 1,4-phenylenediacetonitrile (**VK14**) as π -extenders; and **series–5** with four butterfly-shaped conjugated molecules comprising of thiophene and 2,4,6-trisubstituted pyridine as the invariable donor and acceptor moieties, and triphenylamine (**VK15** and **VK17**) and carbazole (**VK16** and **VK18**) as secondary donor moieties were designed. The designed compounds were synthesized via appropriate multistep synthetic protocol using various well-known cost-effective named reactions such as Knoevenagel condensation, Schiff-base condensation, Wittig reactions and microwave assisted one pot green synthesis. All the reactions were optimized to acquire maximum yield. All the intermediates and final compounds were purified either by column chromatography or by recrystallization using appropriate solvent mixtures. The structures of the intermediates and final compounds were confirmed using ^1H NMR, ^{13}C NMR, mass spectral analysis, and elemental analysis. The molecular weights of polymers were determined by GPC technique. The photophysical properties of all the eighteen synthesized compounds were studied using UV-Vis absorption and fluorescence emission spectroscopy wherein, the optical band gaps were calculated. The electrochemical properties were studied by cyclic voltammetry using which the energies of HOMO and LUMO levels of the compounds were determined. The ground

state optimized geometry, HOMO/LUMO electronic distribution and excited state transitions were investigated by DFT and TD-DFT studies, which were used to further validate the experimental results. The thermal stabilities of these compounds were determined using TGA/DSC analysis. Finally, the third-order NLO properties of **VK1–VK18** were investigated using Z-scan technique which explored their optical limiting behaviour at high input intensity. The electroluminescent property of **VK15** was studied by fabricating OLED using **VK15** as the emissive material. Primarily, the influence of the structural modification on their property i.e., structure-property relationship of the synthesized compounds was studied in detail.

4.2 CONCLUSIONS

On the basis of the results obtained, the following conclusions are drawn:

1. The alternative donor and acceptor units provide a proper charge separation and delocalization of π -electrons via ICT in all the eighteen synthesized compounds (**VK1–VK18**).
2. The extension of conjugation and presence of strong electron donor and acceptor groups shift the absorption and emission maxima to higher wavelength region in **VK3, VK4, VK8, VK10, VK11, VK14, VK15** and **VK17**.
3. The presence of strong electron donor lowers the oxidation potential and increases the HOMO to the higher energy region in **VK4, VK7, VK10, VK13, VK15** and **VK17** while the presence of strong electron acceptor decreases the LUMO in **VK3, VK8, VK9, VK12** and **VK14**.
4. The alternative arrangement of strong electron donor and acceptor groups provides planarity to the system as confirmed by DFT.
5. All the compounds exhibit good thermal stability up to $\sim 350^\circ\text{C}$, which reveal the suitability of these materials for practical application in optoelectronics.
6. All the compounds exhibit excited state assisted TPA with high β_{eff} values of the order of $10^{-10} \text{ m W}^{-1}$ and a strong optical limiting behavior which is correlated to their unique chemical structures.
7. Except **series-4** compounds (**VK11–VK14**), all the other molecules possess negative nonlinearity, which show self-defocusing nature.

8. The polymers **VK13** and **VK14** exhibit highest β_{eff} values of 6.12 and $7.02 \times 10^{-10} \text{ m W}^{-1}$ and extremely low optical limiting thresholds of 1.69 and 1.42 J cm^{-2} , respectively.
9. Among the synthesized molecules, **VK3**, **VK8** and **VK10** of thiophene-ITD series, and **VK12**, **VK15** and **VK17** of thiophene-pyridine series exhibit enhanced optical nonlinearity than some of the well-known reported values.
10. The OLED based on **VK15** emits green light with good color stability under different bias voltages.

4.3 SCOPE FOR FURTHER WORK

1. In the present work, the thiophene-ITD and the thiophene-2,4,6-trisubstituted pyridine-based D-A-D configured conjugated materials are explored to the optoelectronic industry for the first time. As a result, there is a large scope for structural modification to improve the performance.
2. The preliminary third-order NLO studies revealed that the synthesized compounds exhibit TPA with excellent optical limiting behavior. Therefore, the practical applicability of these materials may be checked by fabricating all-optical limiting or integrated NLO devices.
3. The preliminary study of OLED device of **VK15** as a proof of concept revealed the suitability of this material as active emitting material and the device performance can be further improved by optimizing the device.
4. Excellent TADF materials may be achieved by proper modification of molecular structure of molecules of series-5.
5. The synthesized molecules may also be suitable as active materials for organic solar cells.

APPENDIX 1

Representative ^1H NMR, ^{13}C NMR and ESI-MS spectra of some intermediates.

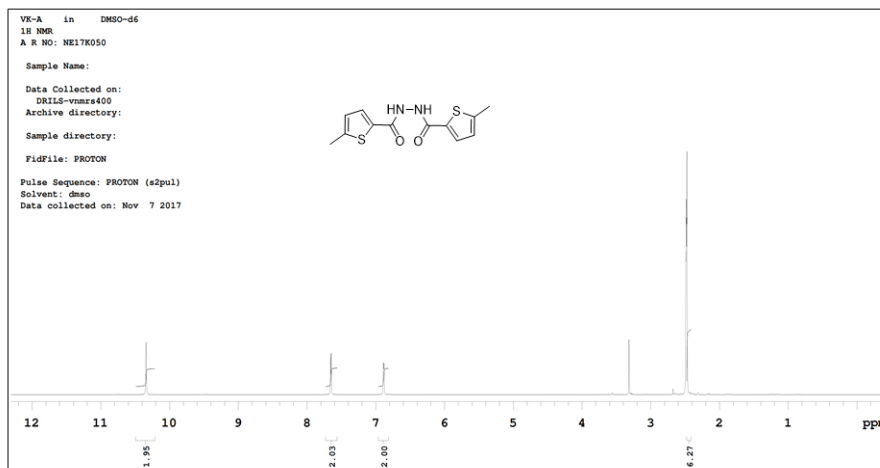


Figure A1 ^1H NMR spectrum of **16**

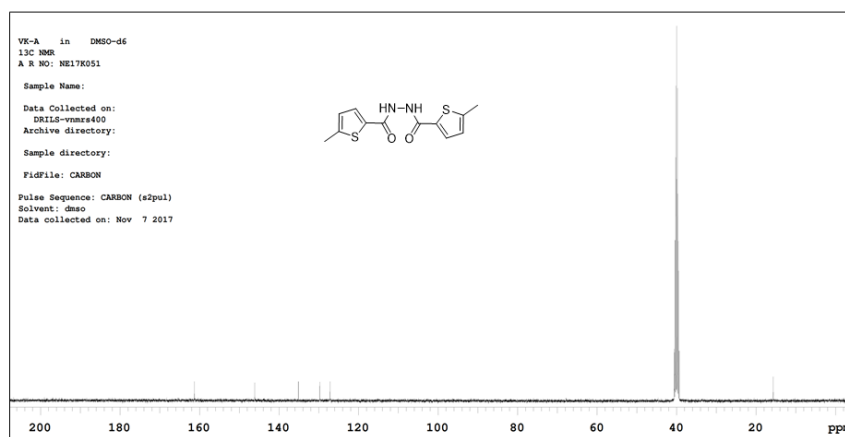


Figure A2 ^{13}C NMR spectrum of **16**

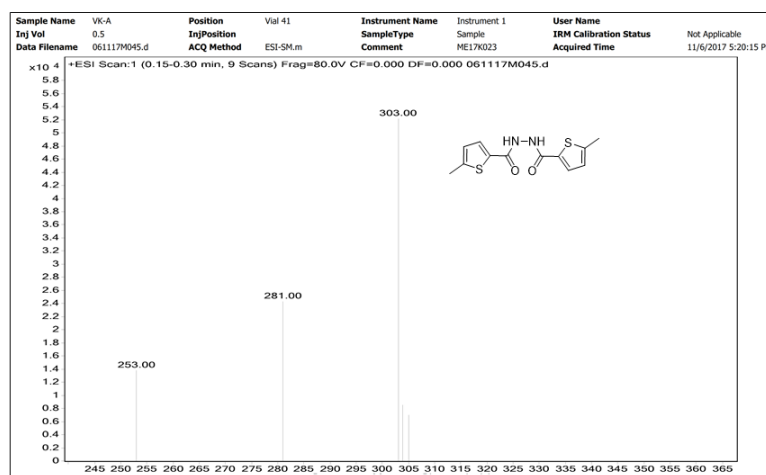


Figure A3 Mass spectrum of **16**

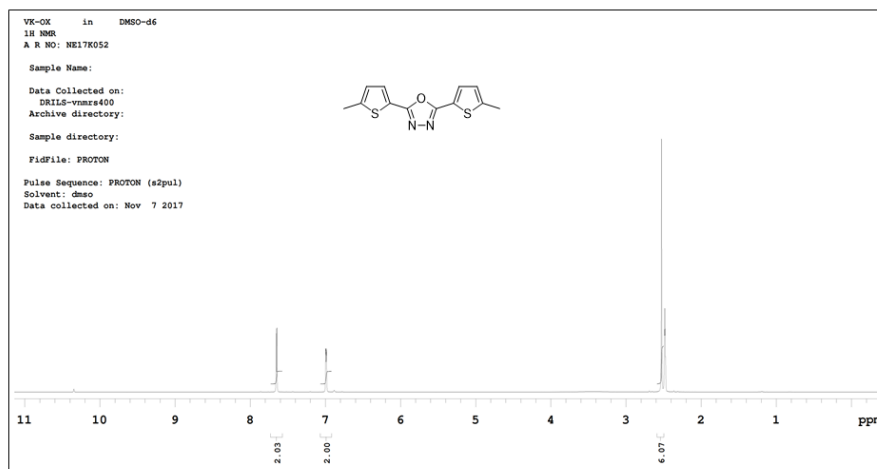


Figure A4 ^1H NMR spectrum of **17**

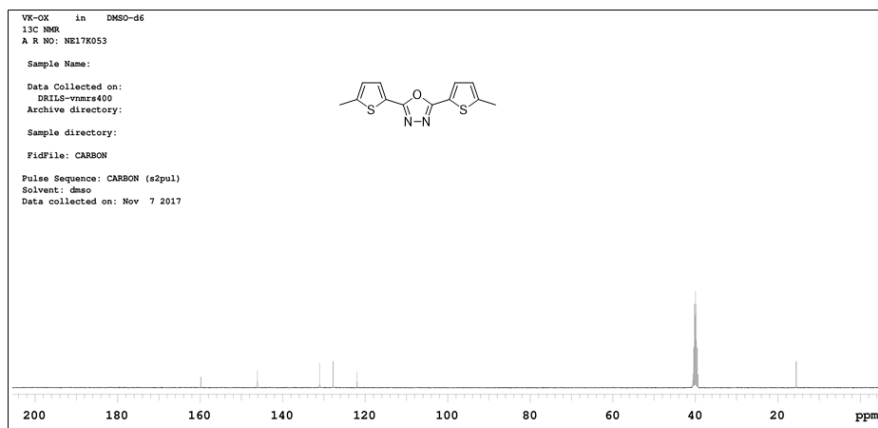


Figure A5 ^{13}C NMR spectrum of **17**

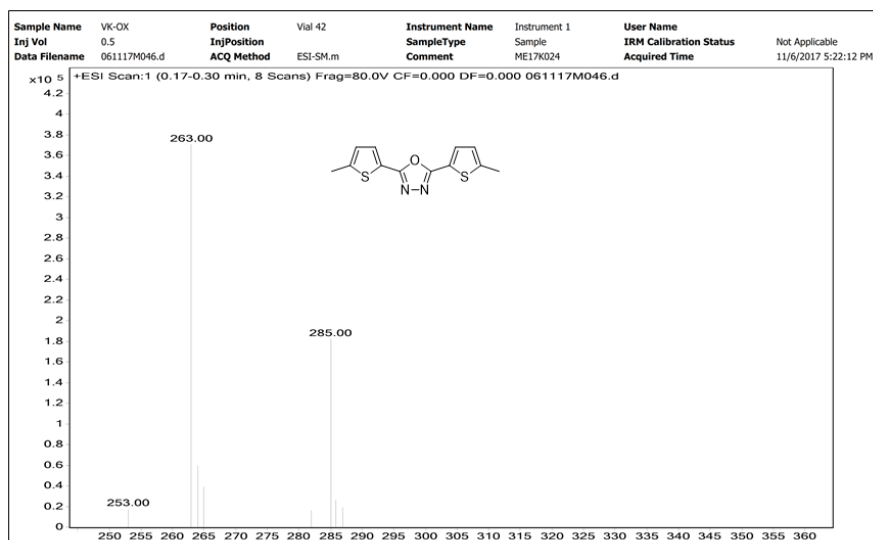


Figure A6 Mass spectrum of **17**

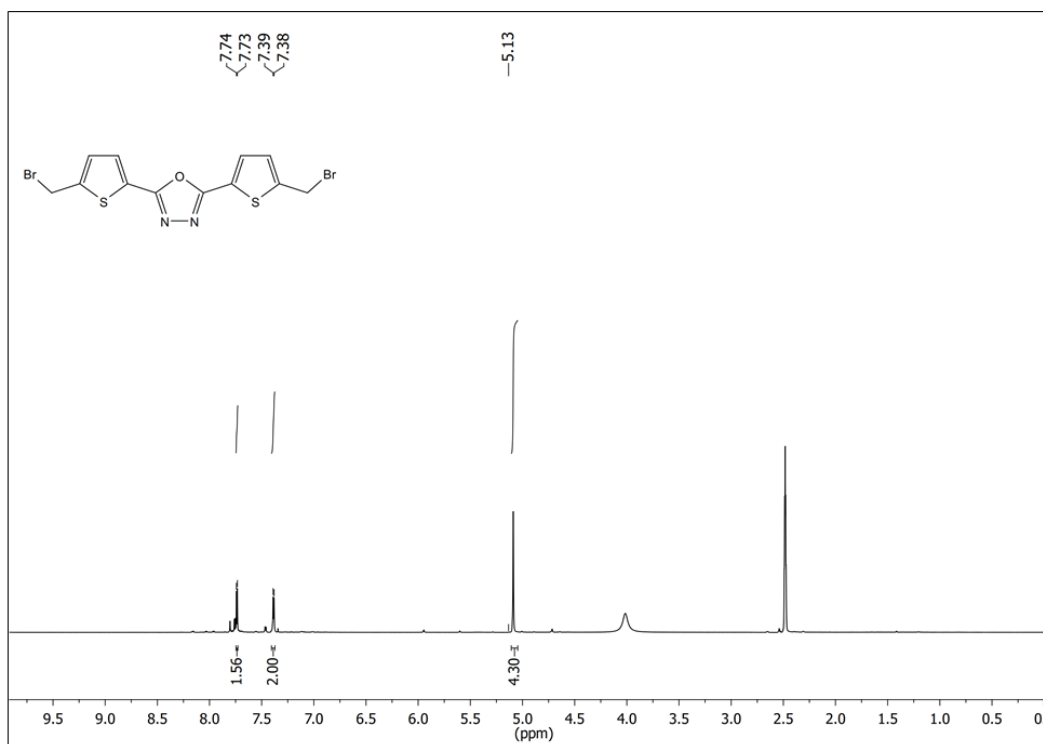


Figure A7 ^1H NMR spectrum of **18**

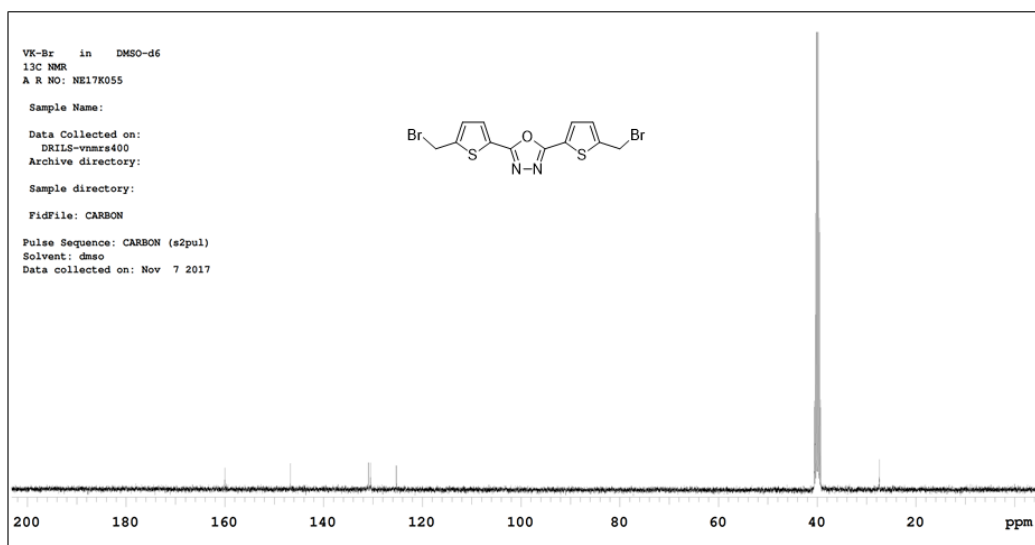


Figure A8 ^{13}C NMR spectrum of **18**

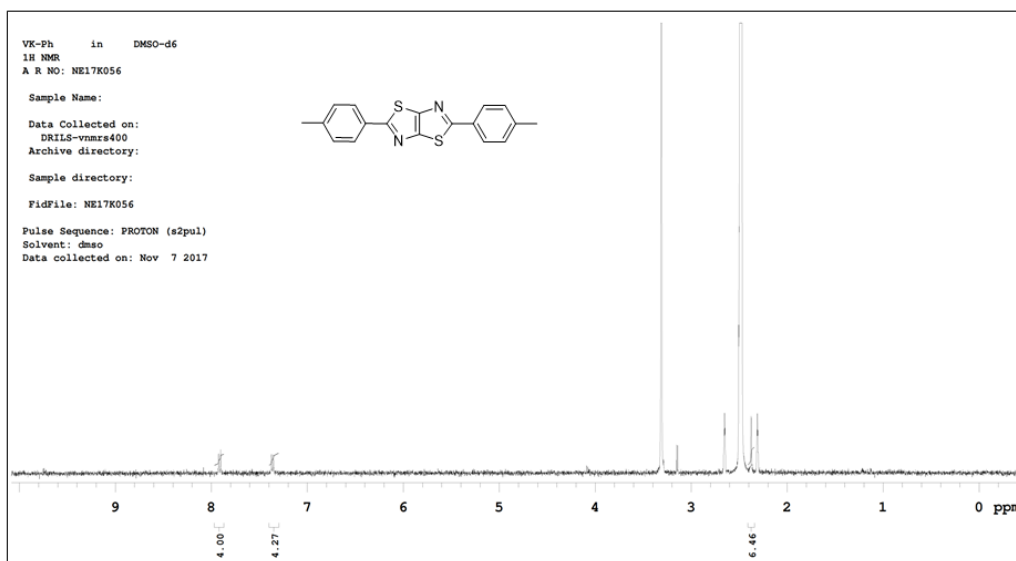


Figure A9 ¹H NMR spectrum of 22

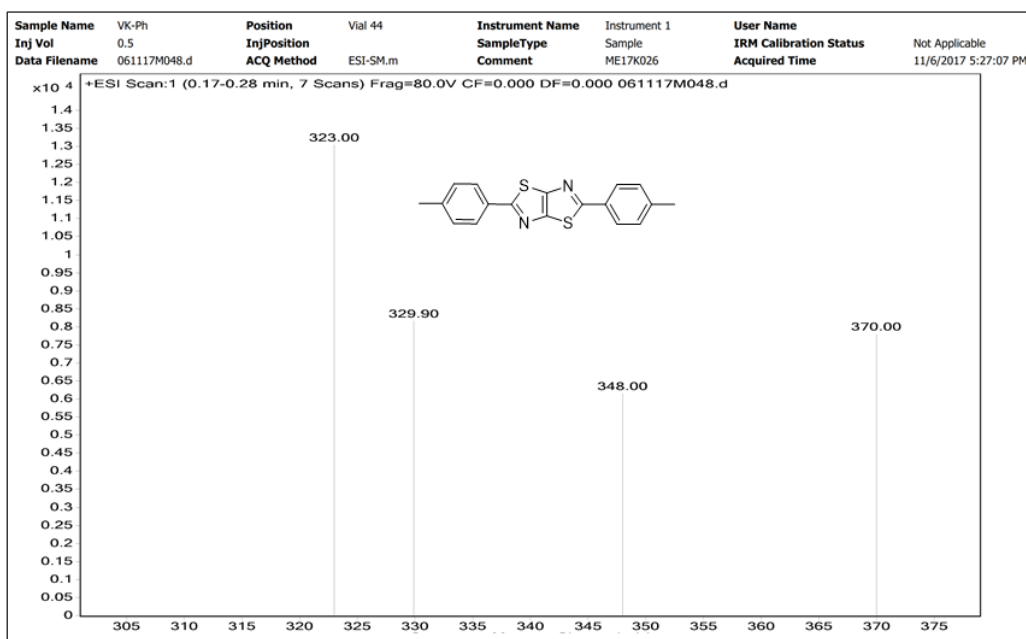


Figure A10 Mass spectrum of 22

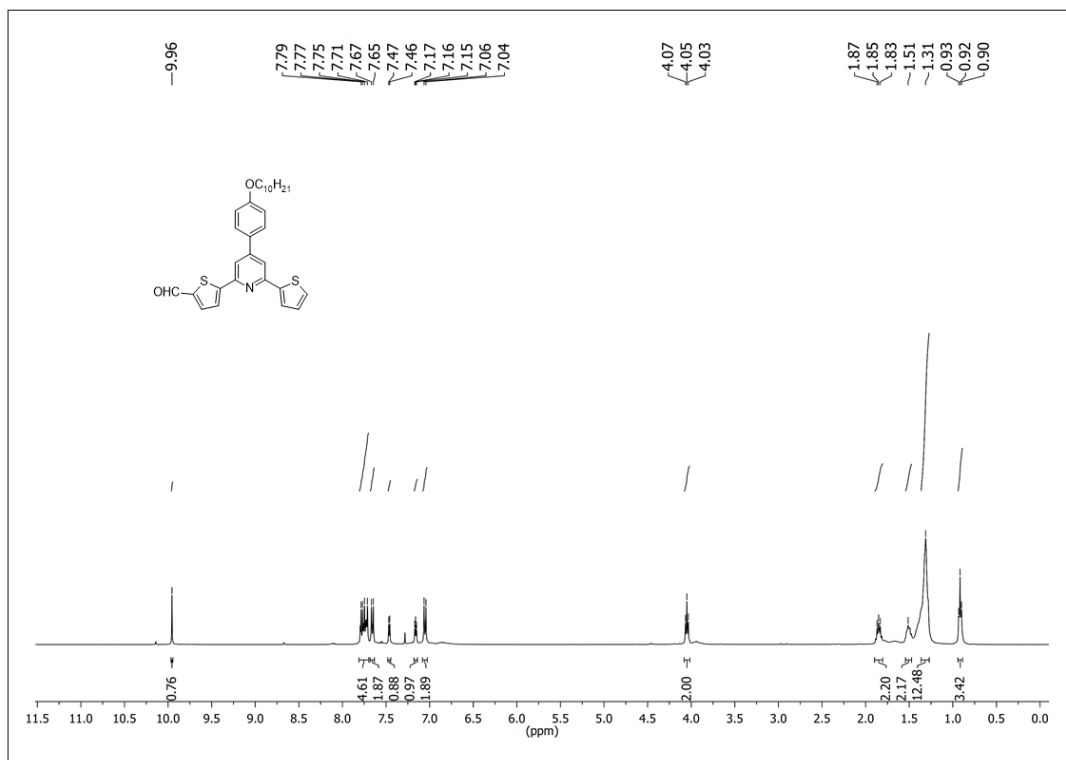


Figure A11 ^1H NMR spectrum of 30

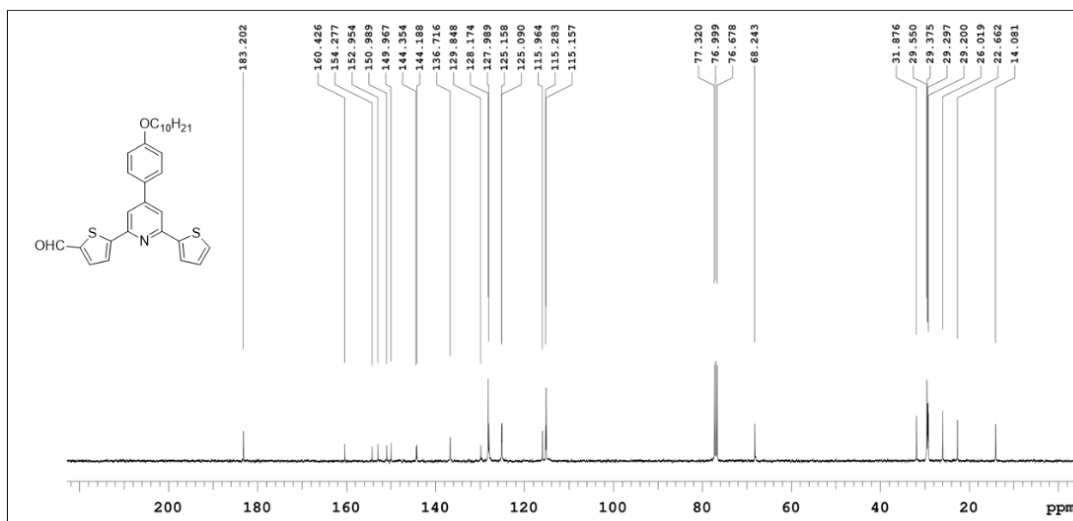


Figure A12 ^{13}C NMR spectrum of 30

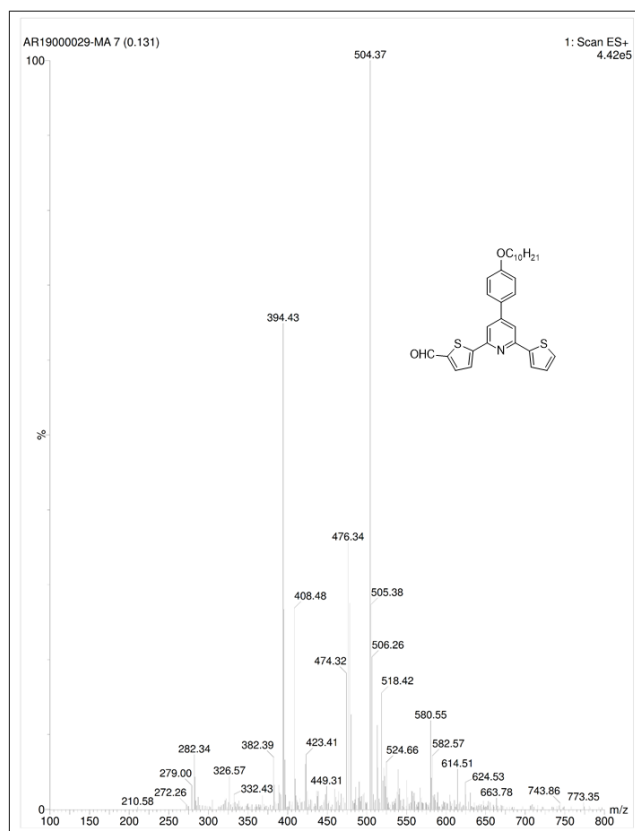


Figure A13 Mass spectrum of 30

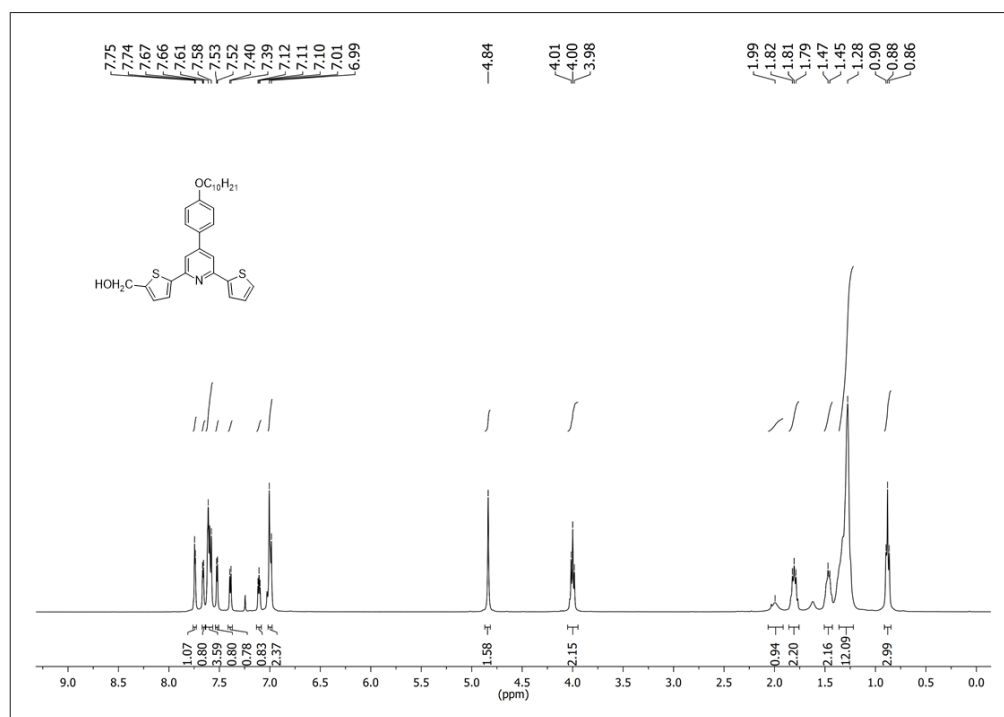
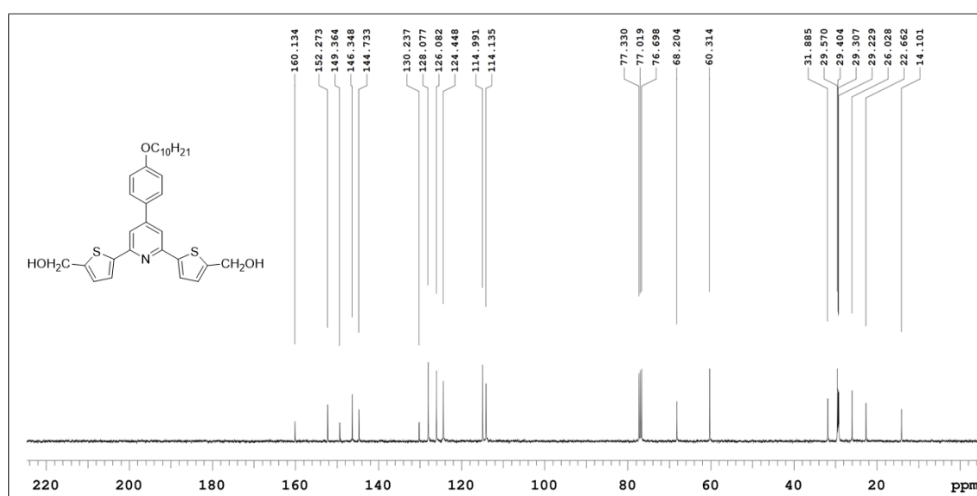
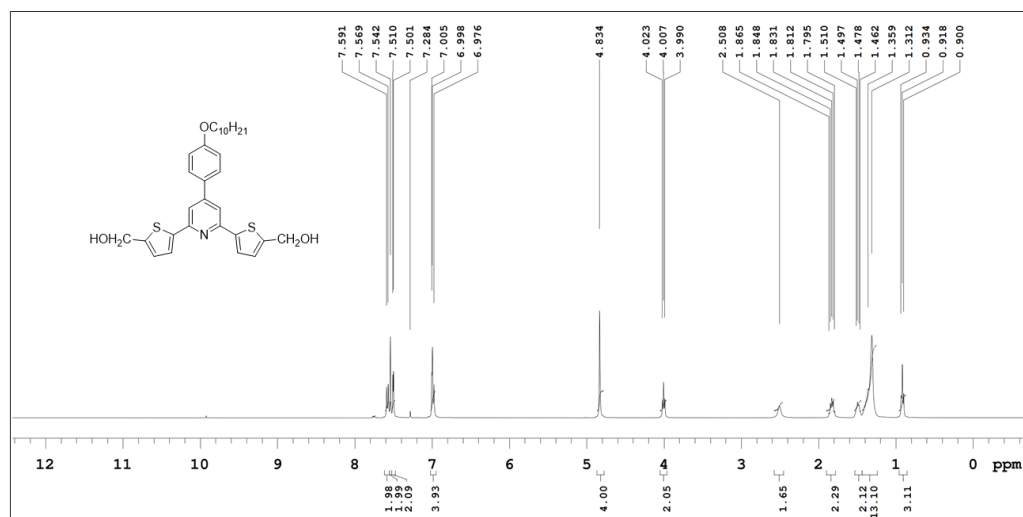
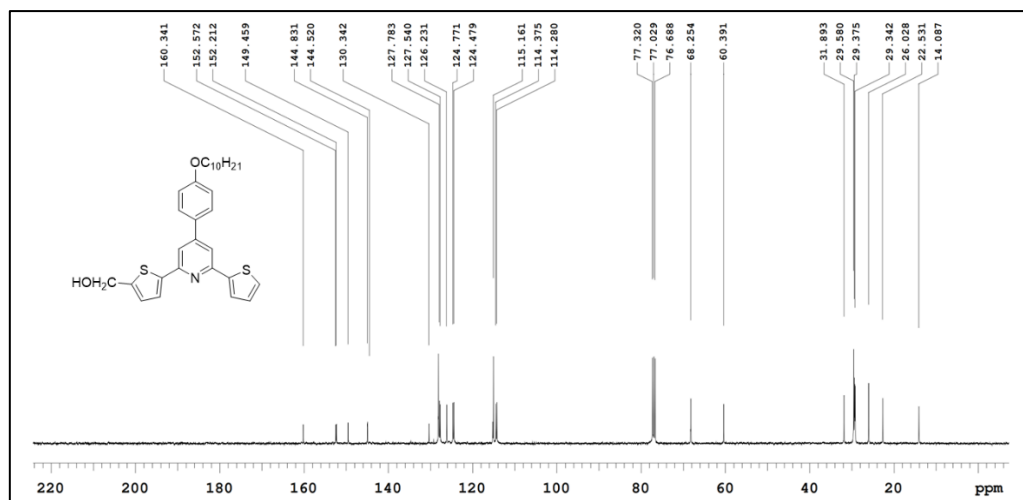


Figure A14 ^1H NMR spectrum of 31



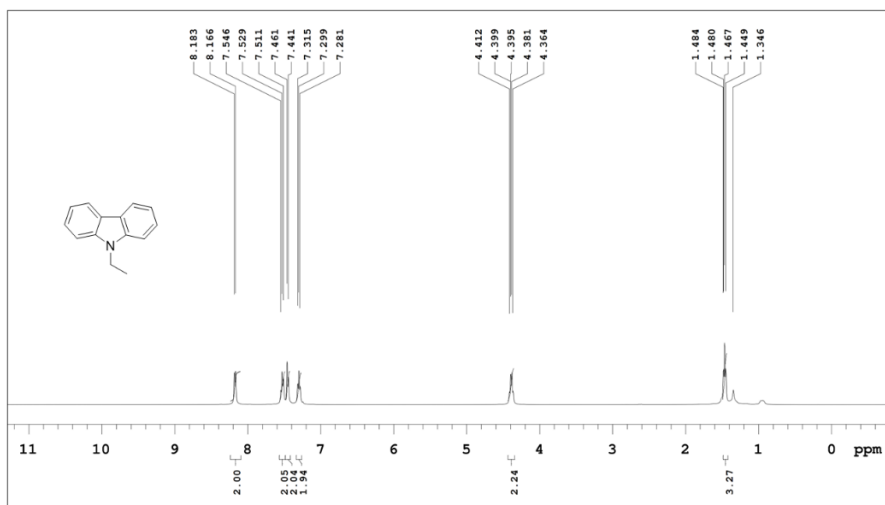


Figure A18 ^1H NMR spectrum of **36**

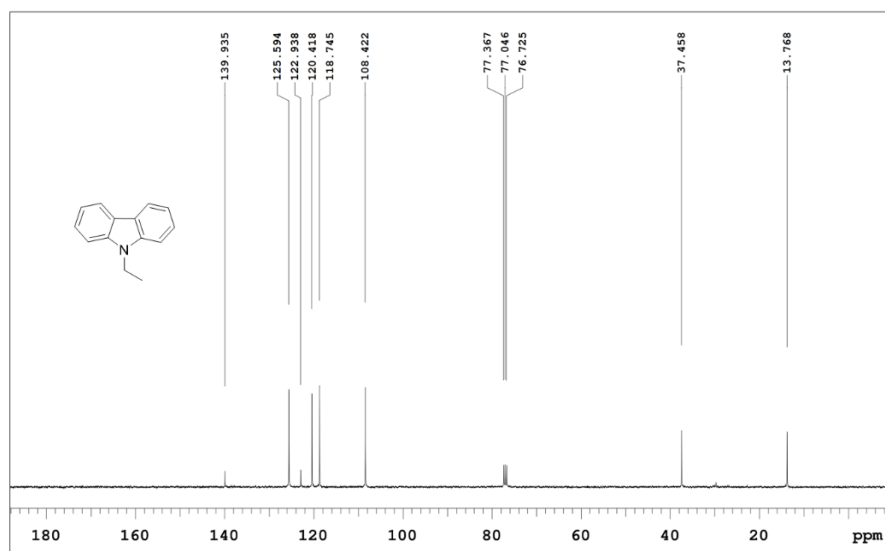


Figure A19 ^{13}C NMR spectrum of **36**

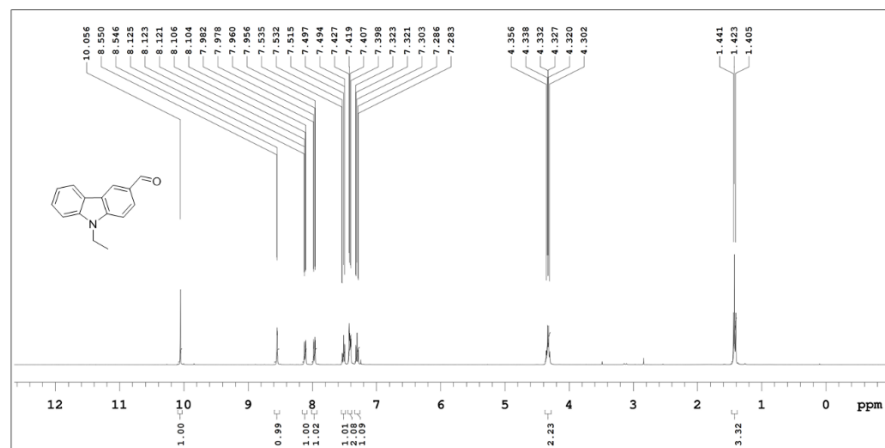


Figure A20 ^1H NMR spectrum of **37**

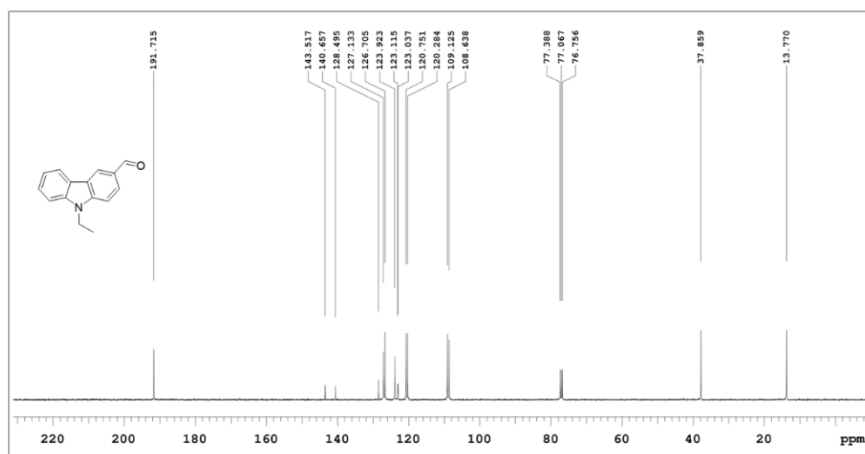


Figure A21 ^{13}C NMR spectrum of 37

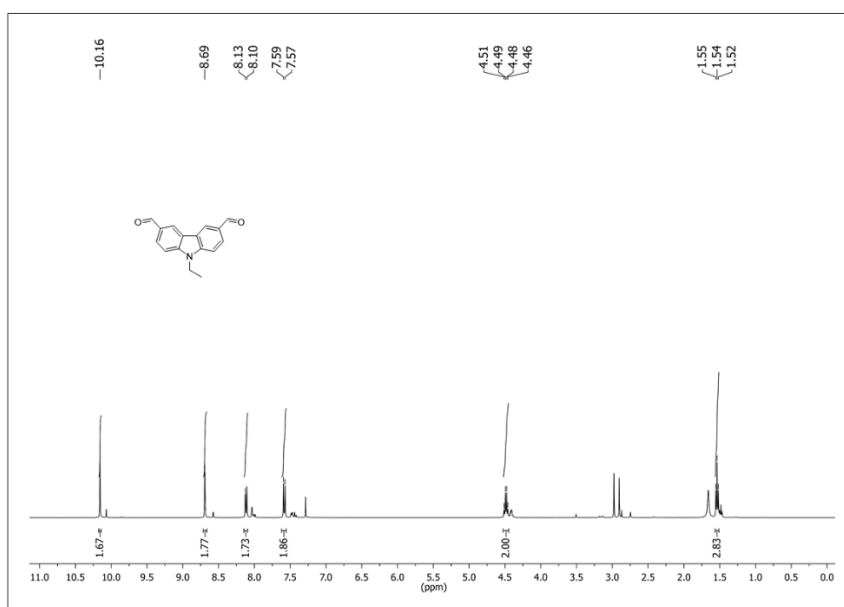


Figure A22 ^1H NMR spectrum of 38

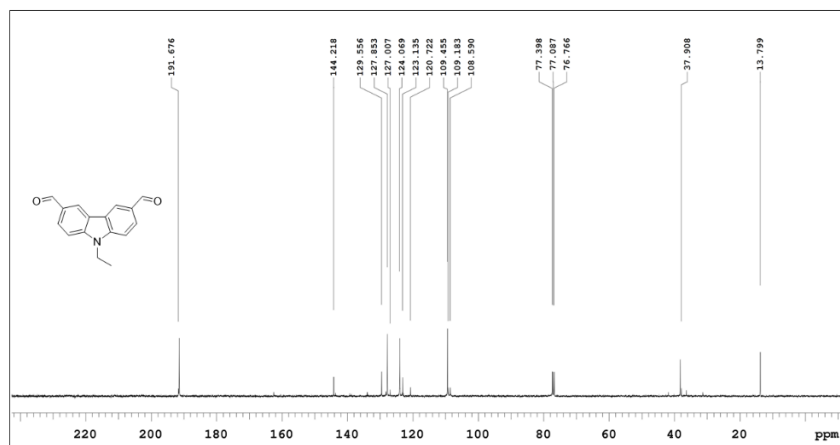


Figure A23 ^{13}C NMR spectrum of 38

REFERENCES

- Ajayaghosh, A. (2003). "Donor–acceptor type low band gap polymers: polysquaraines and related systems." *Chem. Soc. Rev.*, 32(4), 181–191.
- Albota, M., Beljonne, D., Bredas, J. L., Ehrlich, J. E., Fu, J. Y., Heikal, A. A., Hess, S. E., Kogej, T., Levin, M. D., Marder, S. R., McCord-Maughon, D., Perry, J. W., Rockel, H., Rumi, M., Subramaniam, G., Webb, W. W., Wu, X. L., and Xu, C. (1998). "Design of organic molecules with large two-photon absorption cross sections." *Science*, 281(5383), 1653–1656.
- Allard, S., Forster, M., Souharce, B., Thiem, H., and Scherf, U. (2008). "Organic semiconductors for solution-processable field-effect transistors (OFETs)." *Angew. Chem. Int. Ed.*, 47(22), 4070–4098.
- Anand, B., Ntim, S. A., Muthukumar, V. S., Sai, S. S. S., Philip, R., and Mitra, S. (2011). "Improved optical limiting in dispersible carbon nanotubes and their metal oxide hybrids." *Carbon*, 49(14), 4767–4773.
- Anandan, S., Manoharan, S., Narendran, N. K. S., Girisun, T. C. S., and Asiri, A. M. (2018). "Donor-acceptor substituted thiophene dyes for enhanced nonlinear optical limiting." *Opt. Mater.*, 85, 18–25.
- Audebert, P., Kamada, K., Matsunaga, K., and Ohta, K. (2003). "The third-order NLO properties of D- π -A molecules with changing a primary amino group into pyrrole." *Chem. Phys. Lett.*, 367(1–2), 62–71.
- Avhad, K. C., Patil, D. S., Chitrabalam, S., Sreenath, M. C., Joe, I. H., and Sekar, N. (2019). "Extensive study of rhodanine-arylamine-based chromophores: consolidated optical, DFT/TD-DFT and non-linear optical properties." *ChemistrySelect*, 4(1), 211–221.
- Balan, A., Gunbas, G., Durmus, A., and Toppare, L. (2008). "Donor–acceptor polymer with benzotriazole moiety: enhancing the electrochromic properties of the 'donor unit.'" *Chem. Mater.*, 20(24), 7510–7513.
- Baldo, M. A., Lamansky, S., Burrows, P. E., Thompson, M. E., and Forrest, S. R. (1999). "Very high-efficiency green organic light-emitting devices based on electrophosphorescence." *Appl. Phys. Lett.*, 75(1), 4.

- Barik, S., Bishop, S., and Skene, W. G. (2011). "Spectroelectrochemical and electrochemical investigation of a highly conjugated all-thiophene polyazomethine." *Mater. Chem. Phys.*, 129(1–2), 529–533.
- Becke, A. D. (1993). "Density-functional thermochemistry. III. The role of exact exchange." *J. Chem. Phys.*, 98(7), 5648–5652.
- Bloembergen, N. (1984). "Nonlinear optics - Past, present, and future." *IEEE J. Quantum Electron.*, 20(6), 556–558.
- Bolduc, A., Dufresne, S., Hanan, G. S., and Skene, W. G. (2010). "Synthesis, photophysics, and electrochemistry of thiophene–pyridine and thiophene–pyrimidine dyad comonomers." *Can. J. Chem.*, 88(3), 236–246.
- Bolduc, A., Dufresne, S., and Skene, W. G. (2010). "EDOT-containing azomethine: an easily prepared electrochromically active material with tuneable colours." *J. Mater. Chem.*, 20(23), 4820–4826.
- Bolduc, A., Lachapelle, V., and Skene, W. G. (2010). "Snap together bonds for amine capturing—new spectroscopic and amperometric sensors." *Macromol. Symp.*, Wiley Online Library, 87–93.
- Bourgeaux, M., and Skene, W. G. (2007). "A highly conjugated p-and n-type polythiophenoazomethine: synthesis, spectroscopic, and electrochemical investigation." *Macromolecules*, 40(6), 1792–1795.
- Boyd, R. W. (2003). *Nonlinear optics*. Elsevier.
- Brabec, C. J., Cravino, A., Meissner, D., Sariciftci, N. S., Fromherz, T., Rispiens, M. T., Sanchez, L., and Hummelen, J. C. (2001). "Origin of the open circuit voltage of plastic solar cells." *Adv. Funct. Mater.*, 11(5), 374–380.
- Brabec, C. J., Sariciftci, N. S., and Hummelen, J. C. (2001). "Plastic solar cells." *Adv. Funct. Mater.*, 11(1), 15–26.
- Bredas, J. L., Adant, C., Tackx, P., Persoons, A., and Pierce, B. M. (1994). "Third-order nonlinear optical response in organic materials: theoretical and experimental aspects." *Chem. Rev.*, 94(1), 243–278.
- Brocks, G., and Tol, A. (1996). "Small band gap semiconducting polymers made from dye molecules: polysquaraines." *J. Phys. Chem.*, 100(5), 1838–1846.
- Brutting, W., Berleb, S., and Muckl, A. G. (2001). "Device physics of organic light-emitting diodes based on molecular materials." *Org. Electron.*, 2(1), 1–36.

- Chen, J. J. (2001). "CDMA fiber-optic systems with optical hard limiters." *J. Light. Technol.*, 19(7), 950.
- Cheng, C., Yu, C., Guo, Y., Chen, H., Fang, Y., Yu, G., and Liu, Y. (2013). "A diketopyrrolopyrrole – thiazolothiazole copolymer for high performance organic field-effect transistors." *Chem. Commun.*, 49(20), 1998–2000.
- Cheng, L. T., Tam, W., Stevenson, S. H., Meredith, G. R., Rikken, G., and Marder, S. R. (1991). "Experimental investigations of organic molecular nonlinear optical polarizabilities. 1. Methods and results on benzene and stilbene derivatives." *J. Phys. Chem.*, 95(26), 10631–10643.
- Cheng, P., Shi, Q., Lin, Y., Li, Y., and Zhan, X. (2013). "Evolved structure of thiazolothiazole based small molecules towards enhanced efficiency in organic solar cells." *Org. Electron.*, 14(2), 599–606.
- Cheng, Y. J., Yang, S. H., and Hsu, C. S. (2009). "Synthesis of conjugated polymers for organic solar cell applications." *Chem. Rev.*, 109(11), 5868–5923.
- Chiang, C. K., Fincher, C. R., Park, Y. W., Heeger, A. J., Shirakawa, H., Louis, E. J., Gau, S. C., and MacDiarmid, A. G. (1977). "Electrical conductivity in doped polyacetylene." *Phys. Rev. Lett.*, 39(17), 1098–1101.
- Collins, S. D., Ran, N. A., Heiber, M. C., and Nguyen, T. Q. (2017). "Small is powerful: recent progress in solution-processed small molecule solar cells." *Adv. Energy Mater.*, 7(10), 1602242.
- Couris, S., Koudoumas, E., Ruth, A. A., and Leach, S. (1995). "Concentration and wavelength dependence of the effective third-order susceptibility and optical limiting of C60 in toluene solution." *J. Phys. B At. Mol. Opt. Phys.*, 28(20), 4537.
- Cristiano, R., Santos, D. M. P. de O., and author, H. G. C. (2005). "Synthesis and characterization of low molecular mass luminescent liquid crystalline materials with 1,3,4-oxadiazole units." *Liq. Cryst.*, 32(1), 7–14.
- Cunha, M. P. da, Do, T. T., Yambem, S. D., Pham, H. D., Chang, S., Manzhos, S., Katoh, R., and Sonar, P. (2018). "A triphenylamine substituted quinacridone derivative for solution processed organic light emitting diodes." *Mater. Chem. Phys.*, 206, 56–63.
- Dalton, L. R., Sullivan, P. A., and Bale, D. H. (2009). "Electric field poled organic electro-optic materials: state of the art and future prospects." *Chem. Rev.*, 110(1), 25–55.

De Leeuw, D. M., Simenon, M. M. J., Brown, A. R., and Einerhand, R. E. F. (1997). "Stability of n-type doped conducting polymers and consequences for polymeric microelectronic devices." *Synth. Met.*, 87(1), 53–59.

Demeter, D., Mohamed, S., Diac, A., Grosu, I., and Roncali, J. (2014). "Small molecular donors for organic solar cells obtained by simple and clean synthesis." *ChemSusChem*, 7(4), 1046–1050.

Ding, J., Wang, Q., Zhao, L., Ma, D., Wang, L., Jing, X., and Wang, F. (2010). "Design of star-shaped molecular architectures based on carbazole and phosphine oxide moieties: towards amorphous bipolar hosts with high triplet energy for efficient blue electrophosphorescent devices." *J. Mater. Chem.*, 20(37), 8126–8133.

Divyasree, M. C., Vasudevan, K., Basith, K. A., Jayakrishnan, P., Ramesan, M. T., and Chandrasekharan, K. (2018). "Third-Order nonlinear optical properties of phenothiazine-iodine charge transfer complexes in different proportions." *Opt. Laser Technol.*, 105, 94–101.

Dufresne, S., Bolduc, A., and Skene, W. G. (2010). "Towards materials with reversible oxidation and tuneable colours using heterocyclic conjugated azomethines." *J. Mater. Chem.*, 20(23), 4861–4866.

Dufresne, S., Guarin, S. A. P., Bolduc, A., Bourque, A. N., and Skene, W. G. (2009). "Conjugated fluorene-thiophenes prepared from azomethine connections part i. The effect of electronic and aryl groups on the spectroscopic and electrochemical properties." *Photochem. Photobiol. Sci.*, 8(6), 796–804.

Dutta, P., Park, H., Lee, W. H., Kang, I. N., and Lee, S. H. (2012). "A crystalline D- π -A organic small molecule with naphtho[1,2-*b*:5,6-*b'*]dithiophene-core for solution processed organic solar cells." *Org. Electron.*, 13(12), 3183–3194.

E, S., K, S. N. N., Rao D, N., and K, C. (2019). "A phenothiazine–silver hybrid system exhibiting switching and photo-induced enhancement in nonlinear optical absorption." *New J. Chem.*, 43(21), 7962–7971.

Edappadikkunnummal, S., Nherakkayil, S. N., Kuttippurath, V., Chalil, D. M., Desai, N. R., and Keloth, C. (2017). "Surface plasmon assisted enhancement in the nonlinear optical properties of phenothiazine by gold nanoparticle." *J. Phys. Chem. C*, 121(48), 26976–26986.

- Facchetti, A. (2011). “ π -conjugated polymers for organic electronics and photovoltaic cell applications.” *Chem. Mater.*, 23(3), 733–758.
- Farchioni, R., and Grosso, G. (2013). *Organic Electronic Materials: Conjugated Polymers and Low Molecular Weight Organic Solids*. Springer Science & Business Media.
- Fernandes, S. S. M., Herbivo, C., Aires-de-Sousa, J., Comel, A., Belsley, M., and Raposo, M. M. M. (2018). “Theoretical and experimental studies of aryl-bithiophene based push-pull π -conjugated heterocyclic systems bearing cyanoacetic or rhodanine-3-acetic acid acceptors for SHG nonlinear optical applications.” *Dyes Pigments*, 149, 566–573.
- Forrest, S. R. (2004). “The path to ubiquitous and low-cost organic electronic appliances on plastic.” *Nature*, 428(6986), 911–918.
- Garmire, E. (2013). “Nonlinear optics in daily life.” *Opt. Express*, 21(25), 30532–30544.
- Geusic, J. E., Singh, S., Tipping, D. W., and Rich, T. C. (1967). “Three-photon stepwise optical limiting in silicon.” *Phys. Rev. Lett.*, 19(19), 1126.
- Gibson, G. L., McCormick, T. M., and Seferos, D. S. (2012). “Atomistic band gap engineering in donor–acceptor polymers.” *J. Am. Chem. Soc.*, 134(1), 539–547.
- Gopi, V., Subbiahraj, S., Chemmanghattu, K., and Ramamurthy, P. C. (2020). “2,3-di(2-furyl) quinoxaline bearing 3-ethyl rhodanine and 1,3-indandione based heteroaromatic conjugated T-shaped push-pull chromophores: Design, synthesis, photophysical and non-linear optical investigations.” *Dyes Pigments*, 173, 107887.
- Gowda, A., Jacob, L., Joy, N., Philip, R., Pratibha, R., and Kumar, S. (2018). “Thermal and nonlinear optical studies of newly synthesized EDOT based bent-core and hockey-stick like liquid crystals.” *New J. Chem.*, 42(3), 2047–2057.
- Gowda, A. N., Kumar, M., Thomas, A. R., Philip, R., and Kumar, S. (2016). “Self-assembly of silver and gold nanoparticles in a metal-free phthalocyanine liquid crystalline matrix: structural, thermal, electrical and nonlinear optical characterization.” *ChemistrySelect*, 1(7), 1361–1370.
- Gu, P., Xu, X., Zhou, F., Zhao, T., Ye, G., Liu, G., Xu, Q., Ge, J., Xu, Q., and Lu, J. (2014). “Study of linear and nonlinear optical properties of four derivatives of substituted aryl hydrazones of 1,8-naphthalimide.” *Chin. J. Chem.*, 32(3), 205–211.

H. A.M. Mullekom, V. (2000). “The chemistry of high and low band gap π -conjugated polymers.”

Halls, J. J. M., Walsh, C. A., Greenham, N. C., Marseglia, E. A., Friend, R. H., Moratti, S. C., and Holmes, A. B. (1995). “Efficient photodiodes from interpenetrating polymer networks.” *Nature*, 376(6540), 498–500.

Hanwell, M. D., Curtis, D. E., Lonie, D. C., Vandermeersch, T., Zurek, E., and Hutchison, G. R. (2012). “Avogadro: an advanced semantic chemical editor, visualization, and analysis platform.” *J. Cheminformatics*, 4(1), 17.

Hariharan, P. C., and Pople, J. A. (1973). “The influence of polarization functions on molecular orbital hydrogenation energies.” *Theor. Chim. Acta*, 28(3), 213–222.

Havinga, E. E., Hoeve, W. ten, and Wynberg, H. (1993). “Alternate donor-acceptor small-band-gap semiconducting polymers; Polysquaraines and polycroconaines.” *Synth. Met.*, Proceedings of the International Conference on Science and Technology of Synthetic Metals, 55(1), 299–306.

Hehre, W. J., Ditchfield, R., and Pople, J. A. (2003). “Self—Consistent Molecular Orbital Methods. XII. Further Extensions of Gaussian—Type Basis Sets for Use in Molecular Orbital Studies of Organic Molecules.” *J. Chem. Phys.*, 56(5), 2257.

Hernandez, F. E., Yang, S., Stryland, E. W. V., and Hagan, D. J. (2000). “High-dynamic-range cascaded-focus optical limiter.” *Opt. Lett.*, 25(16), 1180–1182.

Hindson, J. C., Ulgut, B., Friend, R. H., Greenham, N. C., Norder, B., Kotlewski, A., and Dingemans, T. J. (2010). “All-aromatic liquid crystal triphenylamine-based poly (azomethine) s as hole transport materials for opto-electronic applications.” *J. Mater. Chem.*, 20(5), 937–944.

Huang, C., Sartin, M. M., Cozzuol, M., Siegel, N., Barlow, S., Perry, J. W., and Marder, S. R. (2012). “Photoinduced electron transfer and nonlinear absorption in poly(carbazole-alt-2,7-fluorene)s bearing perylene diimides as pendant acceptors.” *J. Phys. Chem. A*, 116(17), 4305–4317.

Huang, H. F., Xu, S. H., He, Y. B., Zhu, C. C., Fan, H. L., Zhou, X. H., Gao, X. C., and Dai, Y. F. (2013). “Synthesis and characterization of highly stable and efficient star-molecules.” *Dyes Pigments*, 96(3), 705–713.

- Hughes, G., and R. Bryce, M. (2005). "Electron-transporting materials for organic electroluminescent and electrophosphorescent devices." *J. Mater. Chem.*, 15(1), 94–107.
- Hwang, S. W., and Chen, Y. (2002). "Photoluminescent and electrochemical properties of novel poly (aryl ether)s with isolated hole-transporting carbazole and electron-transporting 1, 3, 4-oxadiazole fluorophores." *Macromolecules*, 35(14), 5438–5443.
- Invernale, M. A., Acik, M., and Sotzing, G. A. (2009). "Thiophene-based electrochromic materials." *Handb. Thiophene-Based Mater.*, John Wiley & Sons, Ltd, 757–782.
- Isik, D., Santato, C., Barik, S., and Skene, W. G. (2012). "Charge-carrier transport in thin films of π -conjugated thiopheno-azomethines." *Org. Electron.*, 13(12), 3022–3031.
- Iwan, A., Palewicz, M., Chuchmala, A., Gorecki, L., Sikora, A., Mazurek, B., and Pasciak, G. (2012). "Opto (electrical) properties of new aromatic polyazomethines with fluorene moieties in the main chain for polymeric photovoltaic devices." *Synth. Met.*, 162(1–2), 143–153.
- Iwan, A., and Sek, D. (2008). "Processible polyazomethines and polyketanils: from aerospace to light-emitting diodes and other advanced applications." *Prog. Polym. Sci.*, 33(3), 289–345.
- Jana, D., and Ghorai, B. K. (2012). "Triphenylpyridine-based star-shaped π -conjugated oligomers with triphenylamine core: synthesis and photophysical properties." *Tetrahedron Lett.*, 53(14), 1798–1801.
- Jebnoui, A., Chemli, M., Lévêque, P., Fall, S., Majdoub, M., and Leclerc, N. (2018). "Effects of vinylene and azomethine bridges on optical, theoretical electronic structure and electrical properties of new anthracene and carbazole based π -conjugated molecules." *Org. Electron.*, 56, 96–110.
- Jeong, S., Kim, M. K., Kim, S. H., and Hong, J. I. (2013). "Efficient deep-blue emitters based on triphenylamine-linked benzimidazole derivatives for nondoped fluorescent organic light-emitting diodes." *Org. Electron.*, 14(10), 2497–2504.
- Jia, J., Li, T., Cui, Y., Li, Y., Wang, W., Han, L., Li, Y., and Gao, J. (2019). "Study on the synthesis and third-order nonlinear optical properties of D-A poly-quinacridone optical materials." *Dyes Pigments*, 162, 26–35.

Jia, J., Li, Y., Wang, W., Luo, C., Han, L., Li, Y., and Gao, J. (2017). "New quinacridone derivatives: Structure-function relationship exploration to enhance third-order nonlinear optical responses." *Dyes Pigments*, 146, 251–262.

Jia, J., Wang, W., Cui, Y., Dong, H., Luo, C., Li, Y., Cao, K., and Gao, J. (2018). "New quinazolinone derivatives and its nonlinear optical properties." *Chem. Phys. Lett.*, 708, 201–209.

Jiang, W., Duan, L., Qiao, J., Zhang, D., Dong, G., Wang, L., and Qiu, Y. (2010). "Novel star-shaped host materials for highly efficient solution-processed phosphorescent organic light-emitting diodes." *J. Mater. Chem.*, 20(29), 6131–6137.

Jiang, Z., Chen, Y., Yang, C., Cao, Y., Tao, Y., Qin, J., and Ma, D. (2009). "A fully diarylmethylene-bridged triphenylamine derivative as novel host for highly efficient green phosphorescent OLEDs." *Org. Lett.*, 11(7), 1503–1506.

Jung Son, H., He, F., Carsten, B., and Yu, L. (2011). "Are we there yet? Design of better conjugated polymers for polymer solar cells." *J. Mater. Chem.*, 21(47), 18934–18945.

Junkers, T., Vandenbergh, J., Adriaensens, P., Lutsen, L., and Vanderzande, D. (2012). "Synthesis of poly(p -phenylene vinylene) materials via the precursor routes." *Polym. Chem.*, 3(2), 275–285.

Kanis, D. R., Ratner, M. A., and Marks, T. J. (1994). "Design and construction of molecular assemblies with large second-order optical nonlinearities. Quantum chemical aspects." *Chem. Rev.*, 94(1), 195–242.

Karthik, D., Thomas, K. R. J., Jou, J. H., and Chen, Y. L. (2016). "Synthesis, characterization and electroluminescence of carbazole-benzimidazole hybrids with thiophene/phenyl linker." *Dyes Pigments*, 133, 132–142.

Karuppanan, N., and Kalainathan, S. (2018). "A new nonlinear optical stilbazolium family crystal of (E)-1-ethyl-2-(4-nitrostyryl) pyridinium iodide: synthesis, crystal structure, and its third-order nonlinear optical properties." *J. Phys. Chem. C*, 122(8), 4572–4582.

Kelley, T. W., Baude, P. F., Gerlach, C., Ender, D. E., Muyres, D., Haase, M. A., Vogel, D. E., and Theiss, S. D. (2004). "Recent progress in organic electronics: materials, devices, and processes." *Chem. Mater.*, 16(23), 4413–4422.

- Khazi, I. A. M., Gadad, A. K., Lamani, R. S., and Bhongade, B. A. (2011). "Chemistry of imidazo [2, 1-*b*][1, 3, 4] thiadiazoles." *Tetrahedron*, 19(67), 3289–3316.
- Kothavale, S., and Sekar, N. (2017). "Novel pyrazino-phenanthroline based rigid donor- π -acceptor compounds: A detail study of optical properties, acidochromism, solvatochromism and structure-property relationship." *Dyes Pigments*, 136, 31–45.
- K.p., P., M.c., D., John V., N., K., C., and Varghese, S. (2019). "Enhanced optical nonlinearity in nematic liquid crystal on doping with CdSe quantum dot." *J. Mol. Liq.*, 273, 497–503.
- Kraft, A., Burn, P. L., Holmes, A. B., Bradley, D. D. C., Friend, R. H., and Martens, J. H. F. (1993). "Hole-transporting compounds for multi-layer polymer light-emitting diodes." *Synth. Met.*, Proceedings of the International Conference on Science and Technology of Synthetic Metals, 57(1), 4163–4167.
- Kraft, A., Grimsdale, A. C., and Holmes, A. B. (1998). "Electroluminescent conjugated polymers—seeing polymers in a new light." *Angew. Chem. Int. Ed.*, 37(4), 402–428.
- Kulyk, B., Guichaoua, D., Ayadi, A., El-Ghayoury, A., and Sahraoui, B. (2016). "Metal-induced efficient enhancement of nonlinear optical response in conjugated azo-based iminopyridine complexes." *Org. Electron.*, 36, 1–6.
- Kyu Lee, S., Min Cho, J., Goo, Y., Suk Shin, W., Lee, J. C., Lee, W. H., Kang, I. N., Shim, H. K., and Moon, S. J. (2011). "Synthesis and characterization of a thiazolo[5,4-*d*]thiazole-based copolymer for high performance polymer solar cells." *Chem. Commun.*, 47(6), 1791–1793.
- Lee, C., Yang, W., and Parr, R. G. (1988). "Development of the Colle-Salvetti correlation-energy formula into a functional of the electron density." *Phys. Rev. B*, 37(2), 785–789.
- Li, C., Li, Z., Liang, J., Luo, H., Liu, Y., Wei, J., and Wang, Y. (2018). "A twisted phenanthroimidazole based molecule with high triplet energy as a host material for high efficiency phosphorescent OLEDs." *J. Mater. Chem. C*, 6(47), 12888–12895.
- Li, G., Wang, S., Yang, S., Liu, G., Hao, P., Zheng, Y., Long, G., Li, D., Zhang, Y., Yang, W., Xu, L., Gao, W., Zhang, Q., Cui, G., and Tang, B. (2019). "Synthesis, photophysical properties and two-photon absorption study of tetraazachrysene-based N-heteroacenes." *Chem. – Asian J.*, 14(10), 1807–1813.

- Li, N., Wang, P., Lai, S. L., Liu, W., Lee, C. S., Lee, S. T., and Liu, Z. (2010). "Synthesis of multiaryl-substituted pyridine derivatives and applications in non-doped deep-blue oleds as electron-transporting layer with high hole-blocking ability." *Adv. Mater.*, 22(4), 527–530.
- Li, Q., Cui, L. S., Zhong, C., Yuan, X. D., Dong, S. C., Jiang, Z. Q., and Liao, L. S. (2014). "Synthesis of new bipolar host materials based on 1,2,4-oxadiazole for blue phosphorescent OLEDs." *Dyes Pigments*, 101, 142–149.
- Li, Y., Cao, Y., Gao, J., Wang, D., Yu, G., and Heeger, A. J. (1999). "Electrochemical properties of luminescent polymers and polymer light-emitting electrochemical cells." *Synth. Met.*, 99(3), 243–248.
- Liang, Y., Tao, Z., and Chen, J. (2012). "Organic electrode materials for rechargeable lithium batteries." *Adv. Energy Mater.*, 2(7), 742–769.
- Liaw, D. J., Wang, K. L., Pujari, S. P., Huang, Y. C., Tao, B. C., Chen, M. H., Lee, K. R., and Lai, J. Y. (2009). "A novel, conjugated polymer containing fluorene, pyridine and unsymmetric carbazole moieties: Synthesis, protonation and electrochemical properties." *Dyes Pigments*, 82(2), 109–117.
- Liu, C. K., Chen, Y. H., Long, Y. J., Sah, P. T., Chang, W. C., Chan, L. H., Wu, J. L., Jeng, R. J., Yeh, S. C., and Chen, C. T. (2018). "Bipolar 9-linked carbazole- π -dimesitylborane fluorophores for nondoped blue OLEDs and red phosphorescent OLEDs." *Dyes Pigments*, 157, 101–108.
- Liu, J., Yang, Y., Liu, X., and Zhen, Z. (2015). "Physical attachment of NLO chromophores to polymers for great improvement of long-term stability." *Mater. Lett.*, 142, 87–89.
- Liu, W., Zheng, C. J., Wang, K., Chen, Z., Chen, D. Y., Li, F., Ou, X. M., Dong, Y. P., and Zhang, X.-H. (2015). "Novel carbazol-pyridine-carbonitrile derivative as excellent blue thermally activated delayed fluorescence emitter for highly efficient organic light-emitting devices." *ACS Appl. Mater. Interfaces*, 7(34), 18930–18936.
- Maiman, T. H. (1960). "Stimulated optical radiation in ruby."
- Marghad, I., Bencheikh, F., Wang, C., Manolikakes, S., Rerat, A., Gosmini, C., Kim, D. hyeon, Ribierre, J. C., and Adachi, C. (2019). "Control of the dual emission from a thermally activated delayed fluorescence emitter containing phenothiazine units in organic light-emitting diodes." *RSC Adv.*, 9(8), 4336–4343.

- Martin, R. E., and Diederich, F. (1999). "Linear monodisperse π -conjugated oligomers: model compounds for polymers and more." *Angew. Chem. Int. Ed.*, 38(10), 1350–1377.
- Martsinovich, N., and Troisi, A. (2011). "Theoretical studies of dye-sensitised solar cells: from electronic structure to elementary processes." *Energy Environ. Sci.*, 4(11), 4473–4495.
- McCullough, R. D. (1998). "The chemistry of conducting polythiophenes." *Adv. Mater.*, 10(2), 93–116.
- McQuade, D. T., Pullen, A. E., and Swager, T. M. (2000). "Conjugated polymer-based chemical sensors." *Chem. Rev.*, 100(7), 2537–2574.
- Mi, Y., Liang, P., Yang, Z., Wang, D., Cao, H., He, W., Yang, H., and Yu, L. (2016). "Application of near-IR absorption porphyrin dyes derived from click chemistry as third-order nonlinear optical materials." *ChemistryOpen*, 5(1), 71–77.
- Mikroyannidis, J. A., Stylianakis, M. M., Dong, Q., Zhou, Y., and Tian, W. (2009). "New 4, 7-dithienebenzothiadiazole derivatives with cyano-vinylene bonds: synthesis, photophysics and photovoltaics." *Synth. Met.*, 159(14), 1471–1477.
- Mishra, A., and Bäuerle, P. (2012). "Small molecule organic semiconductors on the move: promises for future solar energy technology." *Angew. Chem. Int. Ed.*, 51(9), 2020–2067.
- Modelli, A., Jones, D., and Pshenichnyuk, S. A. (2010). "Electron attachment to dye-sensitized solar cell components: rhodanine and rhodanine-3-acetic acid." *J. Phys. Chem. C*, 114(3), 1725–1732.
- Mohan, M., N. Satyanarayan, M., and R. Trivedi, D. (2019). "Photophysics of proton transfer in hydrazides: a combined theoretical and experimental analysis towards OLED device application." *New J. Chem.*, 43(26), 10413–10428.
- Mohan, M., Pangannaya, S., Satyanarayan, M. N., and Trivedi, D. R. (2018). "Multicoloured thiophene based AIEgens: single crystal structure elucidation, spectral behaviour and DFT studies." *ChemistrySelect*, 3(13), 3803–3813.
- Moussalem, C., Segut, O., Gohier, F., Allain, M., and Frère, P. (2014). "Facile access via green procedures to a material with the benzodifuran moiety for organic photovoltaics." *ACS Sustain. Chem. Eng.*, 2(4), 1043–1048.
- Mulholland, M. E., Navarathne, D., Petrus, M. L., Dingemans, T. J., and Skene, W. G. (2014). "Correlating on-substrate prepared electrochromes with their solution

processed counterparts—towards validating polyazomethines as electrochromes in functioning devices.” *J. Mater. Chem. C*, 2(43), 9099–9108.

Murali, M. G., Dalimba, U., and Sridharan, K. (2012). “Synthesis, characterization, and nonlinear optical properties of donor–acceptor conjugated polymers and polymer/Ag nanocomposites.” *J. Mater. Sci.*, 47(23), 8022–8034.

Nalwa, H. S. (1997). *Handbook of Organic Conductive Molecules and Polymers, Conductive Polymers: Transport, Photophysics and Applications*. Wiley.

Nazim, M., Ameen, S., Akhtar, M. S., Lee, Y. S., and Shin, H. S. (2013). “Novel thiazolothiazole based linear chromophore for small molecule organic solar cells.” *Chem. Phys. Lett.*, 574, 89–93.

Nielsen, C. B., Turbiez, M., and McCulloch, I. (2013). “Recent advances in the development of semiconducting DPP-containing polymers for transistor applications.” *Adv. Mater.*, 25(13), 1859–1880.

Park, J. M., Park, S. K., Yoon, W. S., Kim, J. H., Kim, D. W., Choi, T. L., and Park, S. Y. (2016). “Designing thermally stable conjugated polymers with balanced ambipolar field-effect mobilities by incorporating cyanovinylene linker unit.” *Macromolecules*, 49(8), 2985–2992.

Park, S. S., Won, Y. S., Choi, Y. C., and Kim, J. H. (2009). “Molecular design of organic dyes with double electron acceptor for dye-sensitized solar cell.” *Energy Fuels*, 23(7), 3732–3736.

Pell, L. E., Schrickler, A. D., Mikulec, F. V., and Korgel, B. A. (2004). “Synthesis of amorphous silicon colloids by trisilane thermolysis in high temperature supercritical solvents.” *Langmuir*, 20(16), 6546–6548.

Peng, Q., Peng, J. B., Kang, E. T., Neoh, K. G., and Cao, Y. (2005). “Synthesis and electroluminescent properties of copolymers based on fluorene and 2,5-di(2-hexyloxyphenyl)thiazolothiazole.” *Macromolecules*, 38(17), 7292–7298.

Perepichka, I. F., and Perepichka, D. F. (2009). *Handbook of thiophene-based materials: applications in organic electronics and photonics, 2 volume set*. John Wiley & Sons.

Petrus, M. L., Bein, T., Dingemans, T. J., and Docampo, P. (2015). “A low cost azomethine-based hole transporting material for perovskite photovoltaics.” *J. Mater. Chem. A*, 3(23), 12159–12162.

Petrus, M. L., Bouwer, R. K., Lafont, U., Murthy, D. H. K., Kist, R. J., Bohm, M. L., Olivier, Y., Savenije, T. J., Siebbeles, L. D., and Greenham, N. C. (2013). “Conjugated poly (azomethine)s via simple one-step polycondensation chemistry: synthesis, thermal and optoelectronic properties.” *Polym. Chem.*, 4(15), 4182–4191.

Petrus, M. L., Bouwer, R. K. M., Lafont, U., Athanasopoulos, S., Greenham, N. C., and Dingemans, T. J. (2014). “Small-molecule azomethines: organic photovoltaics via Schiff base condensation chemistry.” *J. Mater. Chem. A*, 2(25), 9474–9477.

Poornesh, P., Umesh, G., Hegde, P. K., Manjunatha, M. G., Manjunatha, K. B., and Adhikari, A. V. (2009). “Studies on third-order nonlinear optical properties and reverse saturable absorption in polythiophene/poly (methylmethacrylate) composites.” *Appl. Phys. B*, 97(1), 117–124.

Prasad, P. N., and Williams, D. J. (1991a). *Introduction to nonlinear optical effects in molecules and polymers*. Wiley New York.

Qing, W., Liu, Z., Yang, S., Tan, L., Yang, Y., Zhang, D., and Li, J. (2015). “Modulating carrier transfer ability—linker effect on thieno [3, 4-*c*] pyrrole-4, 6-dione based conjugated polymers.” *RSC Adv.*, 5(69), 55619–55624.

Rajeshirke, M., Sreenath, M. C., Chitrambalam, S., Joe, I. H., and Sekar, N. (2018). “Enhancement of NLO properties in OBO fluorophores derived from carbazole-coumarin chalcones containing carboxylic acid at the N-alkyl terminal end.” *J. Phys. Chem. C.*, 122(26), 14313–14325.

Randell, N. M., Radford, C. L., Yang, J., Quinn, J., Hou, D., Li, Y., and Kelly, T. L. (2018). “Effect of acceptor unit length and planarity on the optoelectronic properties of isoindigo–thiophene donor–acceptor polymers.” *Chem. Mater.*, 30(14), 4864–4873.

Raynor, A. M., Gupta, A., Plummer, C. M., Jackson, S. L., Bilic, A., Patil, H., Sonar, P., and Bhosale, S. V. (2015). “Significant improvement of optoelectronic and photovoltaic properties by incorporating thiophene in a solution-processable D–A–D modular chromophore.” *Molecules*, 20(12), 21787–21801.

Reineke, S., Thomschke, M., Lussem, B., and Leo, K. (2013). “White organic light-emitting diodes: status and perspective.” *Rev. Mod. Phys.*, 85(3), 1245–1293.

Reinhardt, B. A., Brott, L. L., Clarson, S. J., Dillard, A. G., Bhatt, J. C., Kannan, R., Yuan, L., He, G. S., and Prasad, P. N. (1998). “Highly active two-photon dyes: Design, synthesis, and characterization toward application.” *Chem. Mater.*, 10(7), 1863–1874.

- Ren, S., Zeng, D., Zhong, H., Wang, Y., Qian, S., and Fang, Q. (2010). "Star-shaped donor- π -acceptor conjugated oligomers with 1,3,5-triazine cores: Convergent synthesis and multifunctional properties." *J. Phys. Chem. B*, 114(32), 10374–10383.
- Roncali, J. (1992). "Conjugated poly(thiophenes): Synthesis, functionalization, and applications." *Chem. Rev.*, 92(4), 711–738.
- Roncali, J. (1997). "Synthetic principles for bandgap control in linear π -conjugated systems." *Chem. Rev.*, 97(1), 173–206.
- Roncali, J. (1999). "Electrogenerated functional conjugated polymers as advanced electrode materials." *J. Mater. Chem.*, 9(9), 1875–1893.
- Roncali, J. (2007). "Molecular engineering of the band gap of π -conjugated systems: facing technological applications." *Macromol. Rapid Commun.*, 28(17), 1761–1775.
- Roquet, S., Cravino, A., Leriche, P., Aleveque, O., Frere, P., and Roncali, J. (2006). "Triphenylamine- thienylenevinylene hybrid systems with internal charge transfer as donor materials for heterojunction solar cells." *J. Am. Chem. Soc.*, 128(10), 3459–3466.
- Rustagi, K. C., and Ducuing, J. (1974). "Third-order optical polarizability of conjugated organic molecules." *Opt. Commun.*, 10(3), 258–261.
- Sahin, O., Osken, I., and Ozturk, T. (2011). "Investigation of electrochromic properties of poly(3,5-bis(4-methoxyphenyl)dithieno[3,2-*b*;2',3'-*d*]thiophene)." *Synth. Met.*, 161(1), 183–187.
- Schiff, H. (1864). "Information from the University Laboratory in Pisa: a new series of organic bases." *Justus Liebigs Ann. Chem.*, 131(1), 118–119.
- Sheik-Bahae, M., Said, A. A., Wei, T., Hagan, D. J., and Stryland, E. W. V. (1990). "Sensitive measurement of optical nonlinearities using a single beam." *IEEE J. Quantum Electron.*, 26(4), 760–769.
- Shen, Y. R. (1984). "The principles of nonlinear optics." *N. Y. Wiley-Intersci. 1984* 575.
- Shi, Q., Cheng, P., Li, Y., and Zhan, X. (2012). "A solution processable D-A-D molecule based on thiazolothiazole for high performance organic solar cells." *Adv. Energy Mater.*, 2(1), 63–67.
- Shirakawa, H., Louis, E. J., MacDiarmid, A. G., Chiang, C. K., and Heeger, A. J. (1977). "Synthesis of electrically conducting organic polymers: halogen derivatives of polyacetylene, (CH)_x." *J. Chem. Soc. Chem. Commun.*, (16), 578–580.

- Sicard, L., Navarathne, D., Skalski, T., and Skene, W. G. (2013). "On-substrate preparation of an electroactive conjugated polyazomethine from solution-processable monomers and its application in electrochromic devices." *Adv. Funct. Mater.*, 23(28), 3549–3559.
- Skabara, P. J. (2009). *Fused oligothiophenes*. Wiley: New York.
- Skotheim, T. A., Reynolds, J., and Reynolds, J. (2007). *Handbook of conducting polymers, 2 volume set*. CRC Press.
- Soileau, M. J. (1980). "Passive intensity limiter based on nonlinear optics (A)." *J Opt Soc Am*, 70, 1583.
- Song, S. Y., Jang, M. S., Shim, H. K., Hwang, D. H., and Zyung, T. (1999). "Highly efficient light-emitting polymers composed of both hole and electron affinity units in the conjugated main chain." *Macromolecules*, 32(5), 1482–1487.
- Sonntag, M., Kreger, K., Hanft, D., Stroehriegl, P., Setayesh, S., and Leeuw, D. de. (2005). "Novel star-shaped triphenylamine-based molecular glasses and their use in OFETs." *Chem. Mater.*, 17(11), 3031–3039.
- Stenger-Smith, J. D. (1998). "Intrinsically electrically conducting polymers. Synthesis, characterization, and their applications." *Prog. Polym. Sci.*, 23(1), 57–79.
- Su, S. J., Cai, C., and Kido, J. (2012). "Three-carbazole-armed host materials with various cores for RGB phosphorescent organic light-emitting diodes." *J. Mater. Chem.*, 22(8), 3447–3456.
- Su, S. J., Sasabe, H., Takeda, T., and Kido, J. (2008). "Pyridine-containing bipolar host materials for highly efficient blue phosphorescent OLEDs." *Chem. Mater.*, 20(5), 1691–1693.
- Sutherland, R. L. (1989). "Optical limiters, switches, and filters based on polymer dispersed liquid crystals." *Liq. Cryst. Chem. Phys. Appl.*, International Society for Optics and Photonics, 83–90.
- Sutherland, R. L. (2003). *Handbook of nonlinear optics*. CRC press.
- Tang, C. W., and VanSlyke, S. A. (1987). "Organic electroluminescent diodes." *Appl. Phys. Lett.*, 51(12), 913–915.
- Thakare, S. S., Sreenath, M. C., Chitrambalam, S., Joe, I. H., and Sekar, N. (2017). "Non-linear optical study of BODIPY-benzimidazole conjugate by solvatochromic, Z-scan and theoretical methods." *Opt. Mater.*, 64, 453–460.

- Thelakkat, M. (2002). “Star-Shaped, dendrimeric and polymeric triaryl amines as photoconductors and hole transport materials for electro-optical applications.” *Macromol. Mater. Eng.*, 287(7), 442–461.
- Tian, H., Yang, X., Chen, R., Zhang, R., Hagfeldt, A., and Sun, L. (2008). “Effect of different dye baths and dye-structures on the performance of dye-sensitized solar cells based on triphenylamine dyes.” *J. Phys. Chem. C*, 112(29), 11023–11033.
- Tong, Q. X., Lai, S. L., Chan, M. Y., Lai, K. H., Tang, J. X., Kwong, H. L., Lee, C. S., and Lee, S. T. (2007). “High T_g triphenylamine-based starburst hole-transporting material for organic light-emitting devices.” *Chem. Mater.*, 19(24), 5851–5855.
- Tutt, L. W., and Boggess, T. F. (1993). “A review of optical limiting mechanisms and devices using organics, fullerenes, semiconductors and other materials.” *Prog. Quantum Electron.*, 17(4), 299–338.
- Vellis, P. D., Ye, S., Mikroyannidis, J. A., and Liu, Y. (2008). “New divinylene trimers with triphenylpyridine segments: Synthesis, photophysics, electrochemical and electroluminescent properties.” *Synth. Met.*, 158(21), 854–860.
- Vintu, M., Unnikrishnan, G., Shiju, E., and Chandrasekharan, K. (2019). “Indolo[3,2-*b*]carbazole-based poly(arylene ethynylene)s through Sonogashira coupling for optoelectronic and sensing applications.” *J. Appl. Polym. Sci.*, 136(2), 46940.
- Vishnumurthy, K. A., Adhikari, A. V., Sunitha, M. S., Mary, K. A. A., and Philip, R. (2011). “Design and synthesis of a new thiophene based donor–acceptor type conjugated polymer with large third order nonlinear optical activity.” *Synth. Met.*, 161(15), 1699–1706.
- Vishnumurthy, K. A., Sunitha, M. S., and Adhikari, A. V. (2013). “Synthesis and characterization of thiophene-based donor–acceptor type polyimide and polyazomethines for optical limiting applications.” *Polym. Bull.*, 70(1), 147–169.
- Wan, Z., Jia, C., Wang, Y., and Yao, X. (2017). “A strategy to boost the efficiency of rhodanine electron acceptor for organic dye: from nonconjugation to conjugation.” *ACS Appl. Mater. Interfaces*, 9(30), 25225–25231.
- Wang, F., Zhao, Y., Xu, H., Zhang, J., Miao, Y., Guo, K., Shinar, R., Shinar, J., Wang, H., and Xu, B. (2019). “Two novel bipolar hosts based on 1,2,4-triazole derivatives for highly efficient red phosphorescent OLEDs showing a small efficiency roll-off.” *Org. Electron.*, 70, 272–278.

- Wang, J., Wang, S., Li, X., Zhu, L., Meng, Q., Xiao, Y., and Li, D. (2014). "Novel hole transporting materials with a linear π -conjugated structure for highly efficient perovskite solar cells." *Chem. Commun.*, 50(44), 5829–5832.
- White, W., Hudson, Z. M., Feng, X., Han, S., Lu, Z.-H., and Wang, S. (2009). "Linear and star-shaped benzimidazolyl derivatives: syntheses, photophysical properties and use as highly efficient electron transport materials in OLEDs." *Dalton Trans.*, 39(3), 892–899.
- Williams, D. J. (1983). "Nonlinear optical properties of organic and polymeric materials." *ACS Symp. Ser. 233*, ACS.
- Wu, D., Fang, B., Zhang, M., Du, W., Zhang, J., Tian, X., Zhang, Q., Zhou, H., Wu, J., and Tian, Y. (2018). "D-A type phenanthridine derivatives with aggregation-induced enhanced emission and third-order nonlinear optical properties for bioimaging." *Dyes Pigments*, 159, 142–150.
- Xu, L., Zhang, D., Zhou, Y., Zheng, Y., Cao, L., Jiang, X.-F., and Lu, F. (2017). "4-N, N-bis(4-methoxyphenyl) aniline substituted anthraquinone: X-ray crystal structures, theoretical calculations and third-order nonlinear optical properties." *Opt. Mater.*, 70, 131–137.
- Xu, Q., Li, Z., Liu, N., Jia, J., Yang, J., and Song, Y. (2019). "Third order nonlinear optical properties and transient dynamics of thiophene-contained pyrene derivatives: Effect of peripheral substituent group." *Opt. Laser Technol.*, 109, 666–670.
- Yang, C. J., and Jenekhe, S. A. (1991). "Conjugated aromatic poly (azomethines). 1. Characterization of structure, electronic spectra, and processing of thin films from soluble complexes." *Chem. Mater.*, 3(5), 878–887.
- Yook, K. S., and Lee, J. Y. (2014). "Small molecule host materials for solution processed phosphorescent organic light-emitting diodes." *Adv. Mater.*, 26(25), 4218–4233.
- You, J., Lai, S. L., Liu, W., Ng, T. W., Wang, P., and Lee, C. S. (2012). "Bipolar cyano-substituted pyridine derivatives for applications in organic light-emitting devices." *J. Mater. Chem.*, 22(18), 8922–8929.
- Yu, L. P., and Dalton, L. R. (1989). "Synthesis and characterization of new electroactive polymers." *Synth. Met.*, 29(1), 463–470.

Yu, X., Jia, J., Xu, S., Lao, K. U., Sanford, M. J., Ramakrishnan, R. K., Nazarenko, S. I., Hoye, T. R., Coates, G. W., and DiStasio, R. A. (2018). “Unraveling substituent effects on the glass transition temperatures of biorenewable polyesters.” *Nat. Commun.*, 9(1), 1–9.

Yuan, J. B., Zhang, Z. G., Leung, L. M., and Zhang, K. L. (2008). “Synthesis and characterization of novel star-shaped pyridine cored compounds with alternating carbazole and triphenylamine moieties.” *Chin. Chem. Lett.*, 19(6), 647–650.

Zawadzka, M., Wang, J., Blau, W. J., and Senge, M. O. (2013). “Nonlinear absorption properties of 5,10-A2B2 porphyrins – correlation of molecular structure with the nonlinear responses.” *Photochem. Photobiol. Sci.*, 12(6), 996–1007.

Zhan, Y., Peng, J., Ye, K., Xue, P., and Lu, R. (2013). “Pyrene functionalized triphenylamine-based dyes: synthesis, photophysical properties and applications in OLEDs.” *Org. Biomol. Chem.*, 11(39), 6814–6823.

Zhang, Q., Luo, J., Ye, L., Wang, H., Huang, B., Zhang, J., Wu, J., Zhang, S., and Tian, Y. (2014). “Design, synthesis, linear and nonlinear photophysical properties and biological imaging application of a novel A-type pyrimidine-based thiophene derivative.” *J. Mol. Struct.*, 1074, 33–42.

Zhang, X. L., Zhao, X., Liu, Z. B., Shi, S., Zhou, W. Y., Tian, J. G., Xu, Y. F., and Chen, Y. S. (2011). “Nonlinear optical and optical limiting properties of graphene oxide-Fe₃O₄ hybrid material.” *J. Opt.*, 13(7), 075202.

Zheng, M., Zhang, J., Wang, W., Gao, J., and Jia, J. (2019). “Facile synthesis of extended TPA-quinazolinone derivatives and the nonlinear optical properties.” *Dyes Pigments*, 162, 837–844.

Zhou, H., Yang, L., Stoneking, S., and You, W. (2010). “A weak donor- strong acceptor strategy to design ideal polymers for organic solar cells.” *ACS Appl. Mater. Interfaces*, 2(5), 1377–1383.

Zotti, G., Zecchin, S., Schiavon, G., Berlin, A., and Penso, M. (1999). “Ionochromic and potentiometric properties of the novel polyconjugated polymer from anodic coupling of 5,5'-bis(3,4-(ethylenedioxy)thien-2-yl)-2,2'-bipyridine.” *Chem. Mater.*, 11(11), 3342–3351.

LIST OF PUBLICATIONS

Papers published in international journals

- Viprabha K, Udaya Kumar D (2019). “Amelioration of opto–electronic response of thiophene-Imidazo [2, 1-*b*][1, 3, 4] thiadiazole based organic semiconductors.” *AIP Conference Proceedings*, AIP Publishing, 2057, 020030.
- Viprabha Kakekochi, Udaya Kumar D, Nikhil P P, Keloth Chandrasekharan (2019). “An investigation on photophysical and third–order nonlinear optical properties of novel thermally–stable thiophene–imidazo[2,1-*b*][1,3,4]thiadiazole based azomethines.” *Dyes and Pigments*, 167, 216-224.
- Viprabha Kakekochi, Udaya Kumar D, Nikhil P P, Keloth Chandrasekharan (2019). “Effects of substituents on enriching optical limiting action of novel imidazo[2,1-*b*][1,3,4]thiadiazole fused thiophene based small molecules.” *New Journal of Chemistry*, 43 (23), 9232-9242.
- Viprabha Kakekochi, Udaya Kumar D, Nikhil P P, Keloth Chandrasekharan (2020). “Impact of donor–acceptor alternation on optical power limiting behavior of H–Shaped thiophene–imidazo[2,1-*b*] [1,3,4]thiadiazole flanked conjugated oligomers.” *Dyes and Pigments*, 175, 108181.
- Viprabha Kakekochi, Sathish C.G., Udaya Kumar D, Nikhil P P, Keloth Chandrasekharan, Ezequiel Wolcan (2020). “Facile synthesis and exploration of excited state assisted two-photon absorption properties of D–A–D type thiophene–pyridine derivatives.” *Photochemical and Photobiological Sciences*, 19(5), 726–736.
- Viprabha Kakekochi, Sathish C.G., Udaya Kumar D, Nikhil P P, Keloth Chandrasekharan, Vibhu Darshan, Narayanan Unni K. N. (2020). “Butterfly-Shaped Thiophene-Pyridine Hybrids: Green Electroluminescence and Large Third-Order Optical Nonlinearities.” *ChemPlusChem*, 85 (8), 1762–1777.

CONFERENCES ATTENDED

- Viprabha K. and Udaya Kumar D. (2016). "Synthesis and characterization of donor-acceptor conjugated molecules containing 3,4-dialkoxy thiophene units." National conference on Recent Trends in Chemical Sciences (NCR TCS-2016), held at Manipal Institute of Technology, Manipal on 11-12 January, 2016.
- Viprabha K. and Udaya Kumar D. (2017). "3,4-dialkoxythiophene containing D-A conjugated molecule - alternate photoactive material for organic photovoltaics." International conference on Recent Advances in Material Chemistry (ICRAMC-2017), held at SRM University, Kattankulathur, Chennai, on 15-17 February, 2017.
- Viprabha K. and Udaya Kumar D. (2017). "A thiophene derivative for application in optoelectronic devices." International Conference on Emerging Trends in Chemical Sciences, held at Manipal Institute of Technology, Manipal on 14-16 September, 2017.
- Viprabha K. and Udaya Kumar D. (2018). "Thiophene Embedded Push-Pull Heterocyclic System: Efficient Candidate for Organic Electronics." International Conference on Sustainable Chemistry for Health, Environment and Materials held at IICT, Hyderabad on 5-7 August, 2018.
- Viprabha K. and Udaya Kumar D. (2018). "Amelioration of Opto – electronic Response of Thiophene - Imidazo[2,1-*b*][1,3,4]thiadiazole Based Organic Semiconductors." Second International Conference on Polymer Composites (ICPC-2018) held at Department of Mechanical Engineering, NITK, Surathkal on 15-16 December, 2018.
- Viprabha K. and Udaya Kumar D. (2018). "An Investigation on Photophysical Properties of Thiophene Based Small Molecules." 5th International Conference on Nanoscience and Nanotechnology, held at SRM institute of Science and Technology, Kattankulathur, Tamilnadu on 28-30 January, 2019.
- Viprabha K. and Udaya Kumar D. (2019). "A study on the synthesis and third-order nonlinear optical properties of thiophene based donor-acceptor optical materials." One day national seminar on Current Trends in Chemical Research and Development held at Vivekananda college of Arts, Science and Commerce, Puttur-574203 on 18-09-2019.

BIODATA

VIPRABHA K

Kakekochi House, Panaje post, Puttur-574259, INDIA| +91-8762921622|
viprabha.k@gmail.com

Personal details

Date of birth: 09.12.1992 | Gender: Female | Nationality: Indian

Education

Research Student | Department of Chemistry, National Institute of Technology Karnataka (NITK), India | Since July. 2015

Guide: Dr. Udaya Kumar Dalimba

Topic: Design, synthesis and investigation on optoelectronic properties of thiophene based heterocycles.

M.Sc. Chemistry | 2013-15 | National Institute of Technology Karnataka, Surathkal, India

CGPA: 9.24 out of 10, First Class with distinction

B.Sc. Physics, Chemistry and Mathematics | 2010-2013 | Vivekananda College of Arts, Science and Commerce Puttur, Mangalore University, India

Percentage: 87.10%, First Class with distinction

XIIth standard | 2010 | Vivekananda Pre-University College Puttur, Karnataka State Pre-University Board

Percentage: 72.33%, First Class

Xth standard | 2008 | Vivekananda Kannada Medium School, Karnataka Secondary Education Examination Board

Percentage: 85.12%, First Class with distinction

Research Publications

- Viprabha K, Kumar DU (2019). “Amelioration of opto–electronic response of thiophene-Imidazo [2, 1-*b*][1, 3, 4] thiadiazole based organic semiconductors.” *AIP Conference Proceedings*, AIP Publishing, 2057, 020030.

- Viprabha Kakekochi, Udaya Kumar D, Nikhil P P, Keloth Chandrasekharan (2019). “An investigation on photophysical and third-order nonlinear optical properties of novel thermally-stable thiophene-imidazo[2,1-*b*][1,3,4]thiadiazole based azomethines.” *Dyes and Pigments*, 167, 216-224.
- Viprabha Kakekochi, Udaya Kumar D, Nikhil P P, Keloth Chandrasekharan (2019). “Effects of substituents on enriching optical limiting action of novel imidazo[2,1-*b*][1,3,4]thiadiazole fused thiophene based small molecules.” *New Journal of Chemistry*, 43 (23), 9232-9242.
- Viprabha Kakekochi, Udaya Kumar D, Nikhil P P, Keloth Chandrasekharan (2020). “Impact of donor-acceptor alternation on optical power limiting behavior of H-Shaped thiophene-imidazo[2,1-*b*] [1,3,4]thiadiazole flanked conjugated oligomers.” *Dyes and Pigments*, 175, 108181.
- Viprabha Kakekochi, Sathish C.G., Udaya Kumar D, Nikhil P P, Keloth Chandrasekharan, Ezequiel Wolcan (2020). “Facile synthesis and exploration of excited state assisted two-photon absorption properties of D-A-D type thiophene-pyridine derivatives.” *Photochemical and Photobiological Sciences*, 19(5), 726-736.
- Viprabha Kakekochi, Sathish C.G., Udaya Kumar D, Nikhil P P, Keloth Chandrasekharan, Vibhu Darshan, Narayanan Unni K. N. (2020). “Butterfly-Shaped Thiophene-Pyridine Hybrids: Green Electroluminescence and Large Third-Order Optical Nonlinearities.” *ChemPlusChem*, 85 (8), 1762-1777.

“If you want to leave your footprints on the sands of time, do not drag your feet”

---A.P.J. Abdul Kalam
